IBM

Federal Systems Division, Space Systems Center, Huntsville, Alabama

Laser Aiming Simulation (LASIM) Final Report

Volume I Mathematical Formulation

20 May 1968

IBM No. 68-K10-0006
MSFC No. MA-004-1

IBM

Federal Systems Division, Space Systems Center, Huntsville, Alabama

Prepared for the
GEORGE C. MARSHALL
SPACE FLIGHT CENTER
Huntsville, Alabama

Laser Aiming Simulation (LASIM) Final Report

Volume I Mathematical Formulation
20 May 1968

Contract No. NAS 8-21033
IBM No. 68-K10-0006
MSFC No. MA-004-1

Classification and Content Approval E W Smyth

Data Manager Approval L. F. Shires Jr.

Program Office Approval R T Smith

FOREWORD

This report presents the results of a study undertaken under Contract No. NAS 8-21033 for the George C. Marshall Space Flight Center. These two volumes document the development of an all digital simulation of a laser communications system.

This is a final report and is submitted in fulfillment of the contractual effort begun in February of 1967 and completed in May 1968. Authors of this report were:

F. G. Milligan - Program Group Leader
R. L. Dobson
G. M. Groome

ABSTRACT

Laser communications systems hold great potential for use in future deep-space probes. Before this potential can be realized, however, the feasibility of such systems must be proven. To this end, consideration is being given to a laser communications system experiment mission for synchronous earth orbit. Of prime importance in this feasibility demonstration is investigation of the ability to point a diffraction limited laser beam, with beamwidth arc seconds or less, to sufficient accuracy for establishment of a communications link.

The experiment planner is faced with the problem of designing a spacecraft-communications system to satisfy mission requirements. Preliminary design of individual elements of the system can be performed by the groups responsible. When this is complete, a realistic evaluation of design elements in the total systems environment is then required. Use of prototype or engineering models for such evaluation is expensive and generally impractical. Simulation, on the other hand, provides a relatively inexpensive way of performing the required evaluation.

A configuration proposed for the experiment and chosen for simulation consists of: a docked CSM/LM, with an Apollo Telescope Mount (ATM) rack attached to the LM ascent stage, and a laser telescope attached to the ATM rack through gimbaled pivots.

A detailed digital simulation of the pointing performance of the spacecraft-laser communications system has been developed. This simulation is known as the Laser Aiming Simulation (LASIM). Digital simulation was chosen over analog or hybrid due to the complexity of the simulation problem, the accuracy requirements, and the simplicity afforded by non-real time operation.

The LASIM program is principally devoted to simulation of dynamics and control functions. Included under dynamics are math models of the vehicle's orbital motion and of the rotational motion of the spacecraft, control moment gyros, and the laser telescope. The control portion consists of the three tracking control systems and the point-ahead system. Capability is provided for assessment of the effects of hardware imperfection on total system performance. Imperfections resulting from component non-linearities and variations, and noise generation may be simulated.

The LASIM program serves as a tool for the system designer. As such it will be used not only for testing and verifying preliminary designs but also for establishing system performance requirements to aid in preliminary design.

This report describes the development, organization, and usage of the LASIM program. Volume I of this report addresses the mathematical formulations derived to depict the prototype hardware and system dynamics from which the digital program was written. Volume II of this report describes the actual LASIM program and provides the information required for its use.

TABLE OF CONTENTS

TABLE OF CONTENTS (Continued)

TABLE OF CONTENTS (continued)

LIST OF ILLUSTRATIONS

LIST OF ILLUSTRATIONS (Continued)

LIST OF ILLUSTRATIONS (Continued)

LIST OF ILLUSTRATIONS (Continued)

LIST OF TABLES

SECTION 1

LASER AIMING SIMULATION (LASIM) DESCRIPTION

The Laser Aiming Simulation (LASIM) is a digital computer program which simulates the tracking and pointing operation of a spaceborne laser communications system (designated the Laser Communications System Experiment, LCSE) in synchronous earth orbit. Operation of the system is simulated from the "initial acquisition" condition where the spaceborne laser telescope receiver has just acquired a ground based laser beacon within its coarse field-of-view. From this "initial acquisition" state, the performance of the tracking and pointing systems is digitally represented for nominal operating conditions. Simulation of the laser communications system hardware performance is accomplished by repeatedly solving the rigid-body dynamics and control equations which describe system operation.

The LASIM program depicts the operation of a specific hardware system design and configuration. The LASIM program may be used to investigate operation of this hardware configuration, allowing certain system parameters such as gains, time constants, inertias, etc. to change without program modification. This may be done by simple input instructions to the program. Investigation of the performance of different hardware configurations may be accomplished by making program modifications appropriate to describe the modified hardware. The LASIM program has been constructed in modular form to facilitate and simplify modifications to reflect hardware changes.

Capability has been provided within the LASIM program to generate certain perturbation effects, such as disturbance torques produced by astronaut motion and a form of uplink beacon intensity fluctuation. Determination of system response to many other anomalous conditions or disturbances may be made through program additions as these disturbances are defined. Typical examples are component non-linearities not presently modeled, hardware produced noise, or optical system parameter changes with environment.

The primary objective of the LASIM program development has been to provide an analysis tool which will determine very accurately the short term dynamic response of the laser tracking and pointing systems. To this end double precision arithmetic has been used throughout the program to allow accurate solution of the system equations. Also careful attention has been given to so-called "second order" dynamics effects which can affect the extremely accurate tracking and pointing required of the system.

A thorough description of the hardware systems simulated, and the manner in which the mathematical representations of this hardware were formulated, are presented in the sections which follow.

1.1 MISSION AND VEHICLE CONFIGURATION DESCRIPTION

The following paragraphs describe the mission considered in the LASIM program for the LCSE and the functional characteristics of the hardware used for the LASIM program development. Section 2 provides the detailed definition of the hardware component systems described in these paragraphs.

1.1.1 Mission Description

In order to determine realistic geometrical relationships between the space-borne LCSE and the ground based laser beacon, it is necessary to postulate a trajectory the spacecraft will follow during the simulated mission. The most pertinent quantities which must be determined to permit simulation of system operation are the line-of-sight vector from ground station to space-borne telescope and the line-of-sight rate. The line-of-sight vector defines the uplink laser beam direction and, combined with the line-of-sight rate, determines the direction of the downlink laser beam. This beam is offset from the uplink beam to account for transit time effects.

The LASIM program development assumes that the LCSE will follow an earth orbital trajectory in space. More specifically, it is assumed the trajectory will be a synchronous orbit inclined at 28 degrees with respect to the equatorial plane of the earth, with a mean spacecraft hover point at 104 degrees west longitude.

To complete the geometrical definition, the ground station is assumed to be located at 32 degrees north latitude and 104 degrees west longitude.

Provision is made as part of the LASIM program to generate the line-of-sight and line-of-sight rate as functions of time for the assumed satellite orbit and ground station location. These quantities serve as nominal system inputs, providing the hardware with the desired tracking and pointing directions.

It should be noted here that by proper initialization of the "trajectory generating" portion of the LASIM program (see Paragraph 2.7 for detailed discussion) any earth orbital trajectory may be simulated. However, the assumption of a synchronous orbit allows the rotational dynamics formulation for the satellite to be made without consideration of gravity gradient torques and atmospheric drag effects which become important at lower altitudes. Thus, to use the LASIM program for simulation of system operation in lower earth orbit (100=500 nm altitudes) the gravity gradient and drag effects at these altitudes must be added to the program.

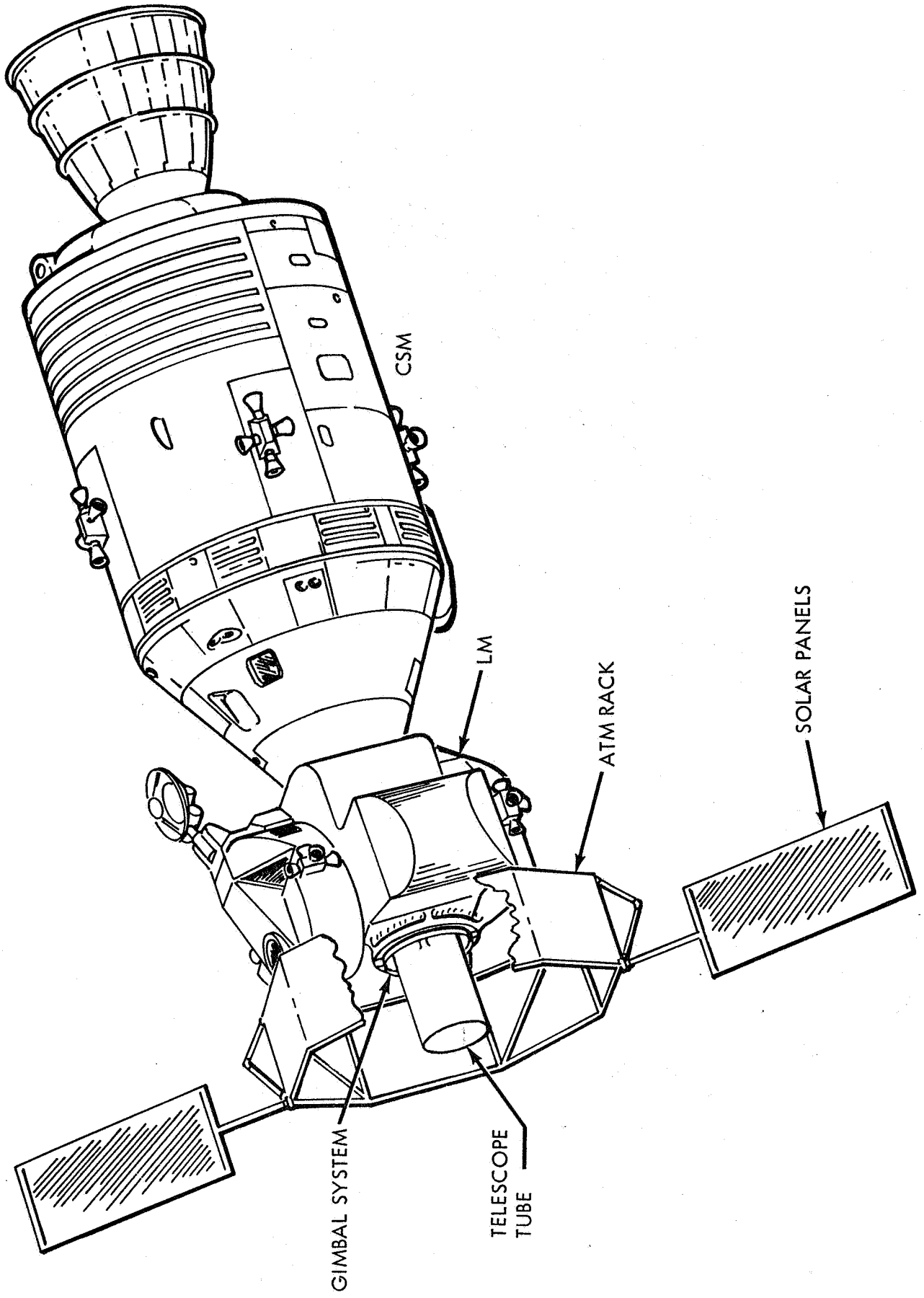

FIGURE 1-1 VEHICLE CONFIGURATION

1.1.2 Vehicle Description

The carrier vehicle, chosen for simulation consists of a Lunar Module (LM) ascent stage docked to a Command and Service Module (CSM). An Apollo Telescope Mount (ATM) rack replaces the LM descent stage. The LCSE hardware, consisting primarily of a laser telescope, is attached to the ATM rack through flexure pivot gimbals. This configuration is shown in Figure 1-1. The laser telescope and associated electronic equipment, together with equipment for non-LCSE experiments, are mounted within the inner gimbal structure and are collectively designated as the "Experiment Package" or "spar".

Three integrated control systems combine to provide LM/CSM/ATM vehicle attitude control, experiment package gimbal control, and optical direction control in order to accomplish the laser tracking function.

The objective of the combined control system operation is to align the telescope tracking optics with the uplink laser beam direction and align the telescope tube and the longitudinal axis of the LM/CSM/ATM vehicle with the uplink beam direction. This entire operation is called "tracking." Once this is performed, the pointing system, which operates through telescope optics only, offsets the downlink beam in the proper amount and direction to compensate for transit time effects in order to illuminate a receiver on the earth.

The laser telescope, through its optical sensor devices, provides the basic attitude reference for operation of the three tracking control systems. Figure 1-2 illustrates the range of the optical sensors in the laser telescope.

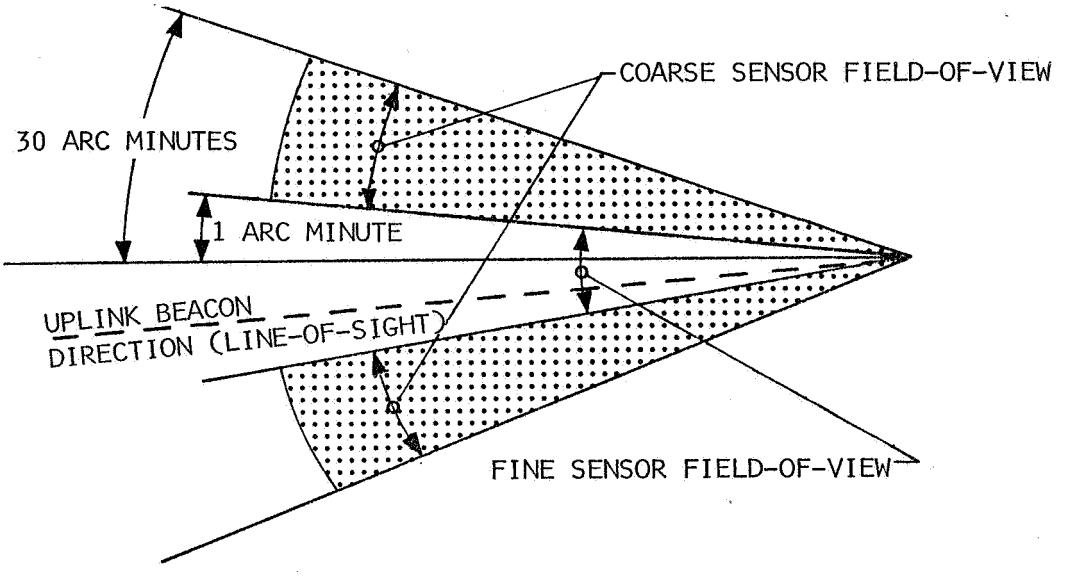

FIGURE 1-2 LASER TELESCOPE OPTICAL SENSING

During operation, light from the ground based laser will be collected in the telescope when its longitudinal axis is aligned to within ±30 arc minutes of the true-line-of-sight direction. Light cannot fall on both coarse and fine sensors simultaneously (except for a small transition region which is not modeled in the LASIM program). Figure 1-2 illustrates in a planar view the regions of illumination of the optical sensors. Operation of the optical sensing may be thought of as a "logical OR" operation, (since the ground beacon is focused in the fine or coarse sensors) a fact which is used to describe system operation in the following paragraphs.

Figure 1-3 depicts, functionally, the operation of the tracking control systems comprising the total Laser Communications System Experiment. Operation of the system is assumed to take place with acquisition of ground beacon within the coarse field-of-view of the telescope. The coarse sensor is a non-linear sensor which provides control signals to drive the experiment package gimbal torquers to align the telescope with the uplink beam. When this alignment has been accomplished to within ± 1 arc minute, the received light is transferred to the fine sensor and the fine tracking system is activated. This operation is denoted by the logical OR function in Figure 1-3. Signals from the fine sensor are used to position a movable lens in the fine tracking system so as to establish an optical path which is aligned with the uplink beam to within a fraction of an arc second. The speed of response of the fine tracking system in the linear region is considerably faster than that of the other two tracking control systems, a fact of importance as will be seen.

When the uplink beacon light is focused onto the fine sensor, no direct error signal is then provided the experiment package gimbal control system, since the coarse sensor no longer receives any light. This condition is not desirable since it results in a ± 1 arc minute deadband for the gimbal system. Thus an error signal is derived from the fine tracking system to provide position error control for the experiment package control system when the beacon light is focused in the "fine field-of-view." This is possible as implemented in the program because of the faster speed of response of the fine tracking system as previously mentioned. Detailed discussion of this coupling is given in Section 2.

The spacecraft (LM/CSM/ATM) control system is actuated to null the experiment package gimbal angles and thus align the longitudinal axis of the vehicle with the telescope axis. In addition, roll control is provided by the spacecraft system. Figure 1-3 illustrates the pitch and yaw (excluding roll) control operation of the spacecraft system. The experiment package gimbal angles are picked off through resolvers to serve as pitch and yaw position error signals. The required control torques are provided by three orthogonally-mounted, two-degree-of-freedom control-moment

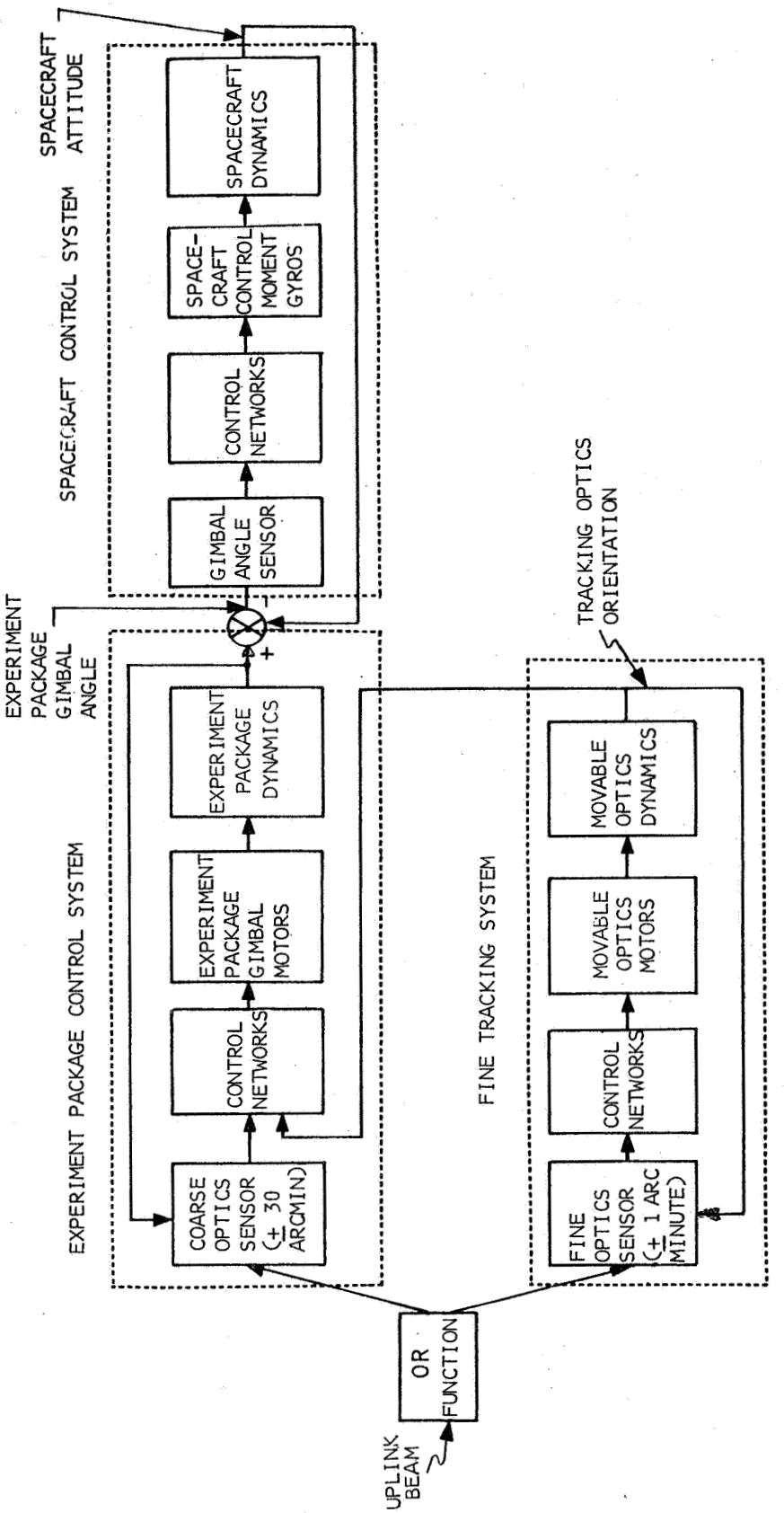

FIGURE 1-3 LCSE TRACKING SYSTEMS

FIGURE 1-4 LCSE POINTING CONTROL SYSTEM

gyros. Vehicle roll reference is provided by a rate-integrating gyro (not shown in the Figures) which feeds into the control system.

The pointing control system shown in Figure 1-4 operates to accomplish downlink beam spoiling to compensate for transit time effects as discussed previously. Commands are received from the ground which define the amount and direction of the downlink beam offset which is to be provided. A telescope mounted sun sensor is used to provide the system with a reference from which the beam offset direction is determined.

Figure 1-5 depicts the geometric axes and pointing directions which are controlled by the tracking and pointing control systems just described. As depicted in the figure, the axes will not, in general, be aligned.

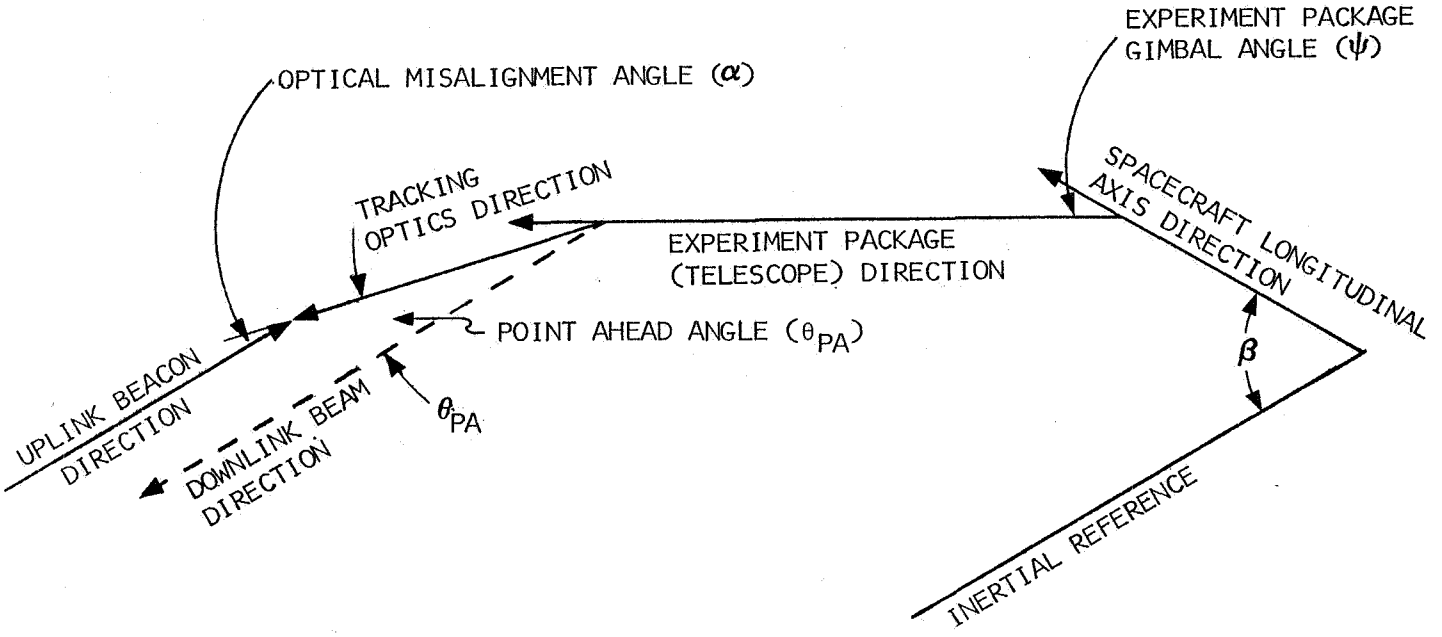

FIGURE 1-5 POINTING AND TRACKING GEOMETRY

SECTION 2

COMPONENT SYSTEM DESCRIPTION AND MATHEMATICAL REPRESENTATION

The following paragraphs define the hardware systems used as the basis for the LASIM program, and illustrate the mathematical representation of this hardware. Also presented are other mathematical formulations which are necessary for operation of the LASIM program.

In the dynamics and optics formulations to follow, references are made to various coordinate systems in which vector quantities are represented. Identification of these coordinate systems is fundamental to the mathematical formulations and their understanding. Figure 2.0-1 illustrates the basic coordinate systems to which reference will be made in the paragraphs to follow.

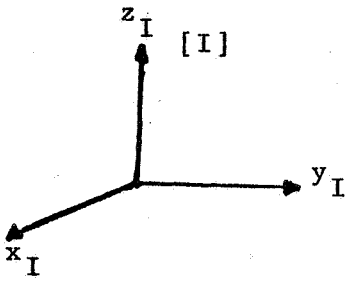

[I], Inertial frame:

- x_I - points in the direction of the Vernal Equinox
- y_I - lies in the equatorial plane 90° ahead of x_I
- z_I - points along earth north polar axis

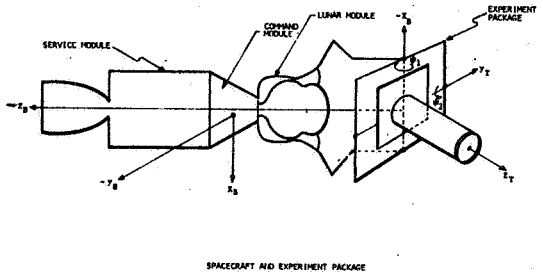

SPACECRAFT AND EXPERIMENT PACKAGE

[B], Body (Spacecraft) frame:

- z_B - points along the vehicle longitudinal axis
- x_B - points along the y axis of the LM coordinate system
- y_B - points along the negative Z axis of the LM coordinate system

[T], Telescope frame:

- z_T - points along telescope longitudinal axis, out of telescope
- y_T - points along telescope inner gimbal axis
- x_T - completes right-handed system

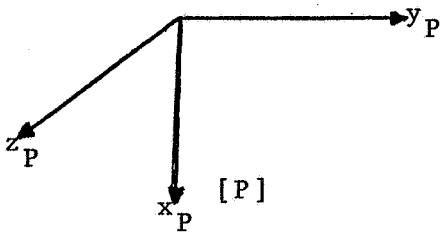

[P], Point Ahead frame:

- $\underline{z_P}$ - points in direction of $-\underline{L_s}$
- $\underline{x_P}$ - points in direction of $\underline{\dot{L}_s} \times -\underline{L_s}$
- y_P - points in direction of $\underline{z_P} \times \underline{x_P}$ to complete right-hand system

FIGURE 2.0-1 COORDINATE SYSTEM DEFINITIONS

2.1 SPACECRAFT SYSTEM

The LCSE has not yet been assigned to a specific vehicle. However, the following spacecraft system is a candidate system for LCSE and has been specified for simulation:

- Spacecraft - A LM ascent stage docked to a CSM, with an ATM rack replacing the LM descent stage.
- Experiment package - The ATM experiment package with the laser telescope attached. The package is connected to the ATM rack through gimbaled pivots.
- Experiment package control system - The ATM vernier control system.
- Spacecraft attitude control system - Three two-degree-of-freedom control moment gyros (CMGs).

Characteristics of the elements of the spacecraft system were defined to IBM in various meetings with NASA Astrionics Laboratory personnel and in the reference documents [1, 2, 3, 4, 5, 6].

Certain portions of the spacecraft system, as originally defined to IBM, were not suitable for the LCSE. In particular, the experiment package and CMG control systems were designed for the ATM solar astronomy mission. Modifications to the basic spacecraft system were made by IBM to complete a design for LCSE. Discussion of these modifications is to be found in Section 3. The system as used to develop the LASIM program is discussed here.

The spacecraft and experiment package are shown conceptually in Figure 2.1-1. The experiment package is gimbaled within the rack through roll, pitch, and yaw gimbals. The roll gimbal can be initialized, before starting an experiment, by an offset drive motor attached to the supporting ring of the experiment package. There is no capability for active roll control. For the LCSE, a roll gimbal is not required, and the roll angle is assumed zero. Pitch and yaw gimbals are "flex-pivot" gimbals, actuated by torque motors. The flex-pivot gimbals provide limited angular travel ($\pm 2°$).

The experiment package control system, as conceptualized for the LCSE and used in the simulation, is shown in Figure 2.1-2. The system controls the outer (pitch) and inner (yaw) telescope gimbals (ψ_1 and ψ_2, respectively); and operates in either a fine or coarse mode. The fine mode results when the upcoming laser beam is within the telescope fine field-of-view (2 arc minutes). In this mode, a signal proportional to the transfer lens position provides the error input, as discussed in Paragraph 2.3. In Figure 2.1-2, t_y and $-t_x$ are the outer and inner gimbal error signals,

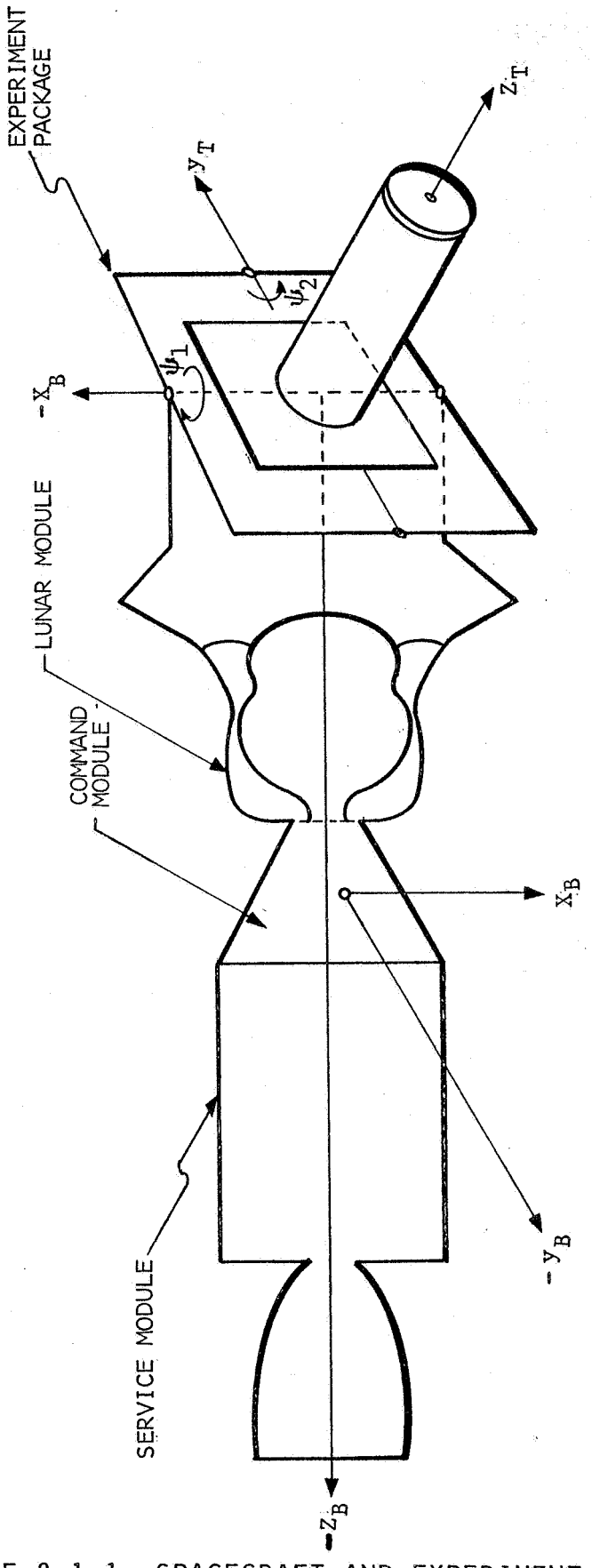

FIGURE 2.1-1 SPACECRAFT AND EXPERIMENT PACKAGE

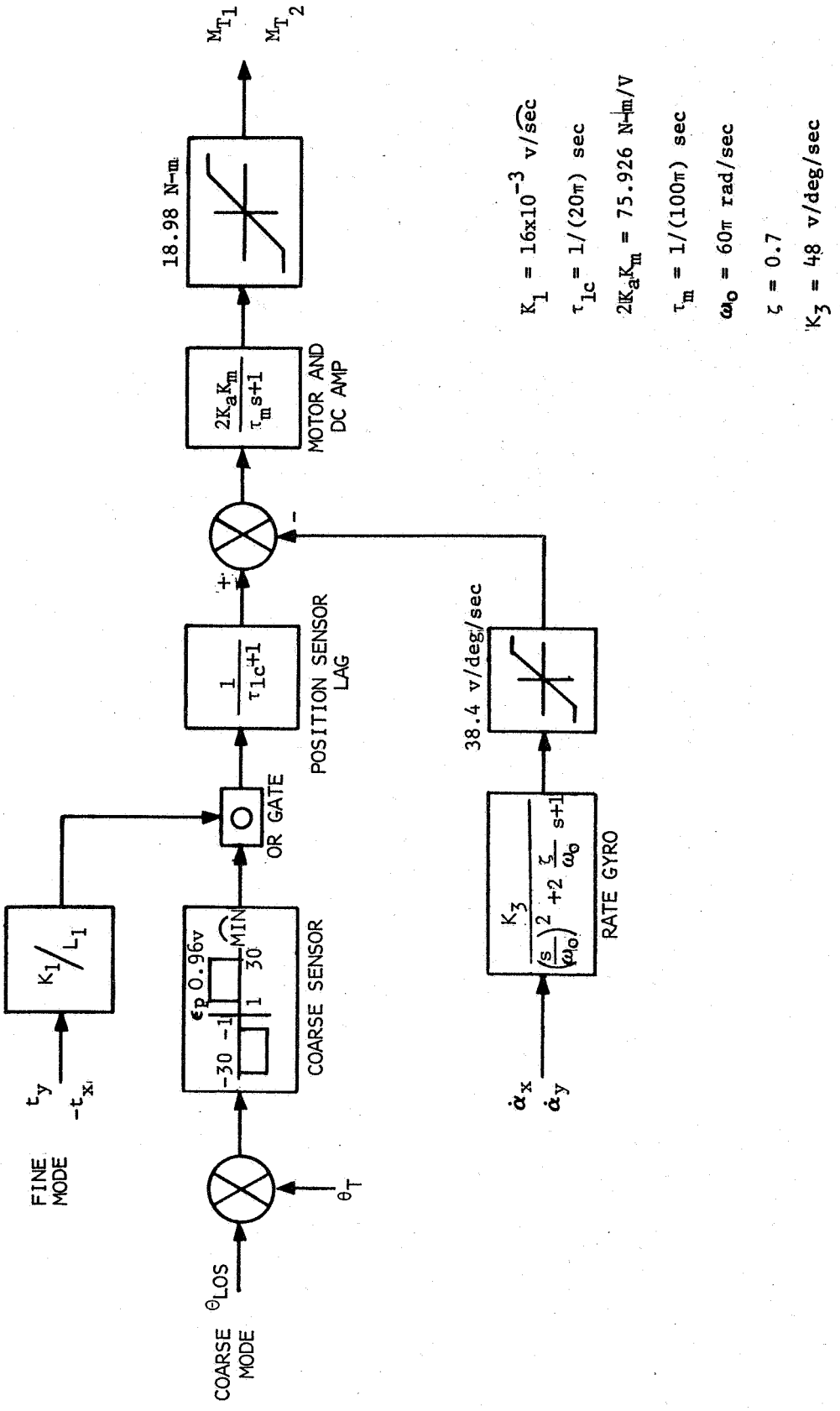

FIGURE 2.1-2 EXPERIMENT PACKAGE (TELESCOPE) CONTROL SYSTEM

respectively. If the ground beacon is in the telescope field-of-view but not in the fine field, the telescope control system is in the coarse mode. A nonlinear coarse sensor provides the error signal to the control system in this case. In the absence of specific definition of the coarse and fine sensor coupling into the telescope control system, it has been assumed that the significant dynamic effects of the sensors and associated electronics can be represented by a first order lag, as shown in Figure 2.1-2. Rate gyros on the gimbaled structure measure the rotation rates of the telescope relative to inertial space about the x_T and y_T axes ($\dot{\alpha}_x$ and $\dot{\alpha}_y$, respectively). These rates provide damping signals for the system as shown in Figure 2.1-2. The error minus rate signal is used to drive the gimbal torque motors. The motor torques, M_{T_1} and M_{T_2}, are fed into the experiment package and spacecraft dynamics equations.

The spacecraft attitude control system consists of three two-degree-of-freedom CMGs, mounted on the ATM rack. Each CMG consists of a spinning rotor held in a housing called the inner gimbal (see Figure 2.1-3). The inner gimbal is connected to the outer gimbal through a pivot perpendicular to the rotor spin axis. The outer gimbal is, in turn, connected to the ATM rack through a pivot perpendicular to the inner gimbal pivot. The CMG rotor spins at a constant angular rate relative to its inner gimbal. Varying rates are imparted to the inner and outer gimbals by geared D.C. motors. The CMGs are mounted on the ATM rack so that each rotor spin axis is parallel to a body axis (as defined in Section 2.0) of the LCSE vehicle when all CMG inner and outer gimbal angles are at their null positions. The CMGs are referred to as CMG 1, CMG 2, or CMG 3, with the numbers designating the body axis about which the rotor spins where: $1 \leftrightarrow x_B$, $2 \leftrightarrow y_B$, $3 \leftrightarrow z_B$.

During operation of the laser pointing experiment, the CMG system is required to position the vehicle in:

- Pitch and yaw so as to null the experiment package gimbals
- Roll so as to maintain the initial roll alignment

A detailed block diagram of the spacecraft control system hardware, as actually used in the simulation, is given in Figure 2.1-4. The input to CMGs 1 and 2 are ψ_1 (experiment package outer gimbal) and ψ_2 (experiment package inner gimbal), respectively. The input to CMG 3 is $-\int R dt$, or the negative integral of the z_B component of angular velocity of the [B] system relative to inertial space. The outputs from the CMG control system are the moments exerted on the inner and outer gimbals by the gimbal torque motors (after reflection through the gears).

With reference to Figure 2.1-4, it is seen that the vehicle control compensation is obtained through lead-lag networks with

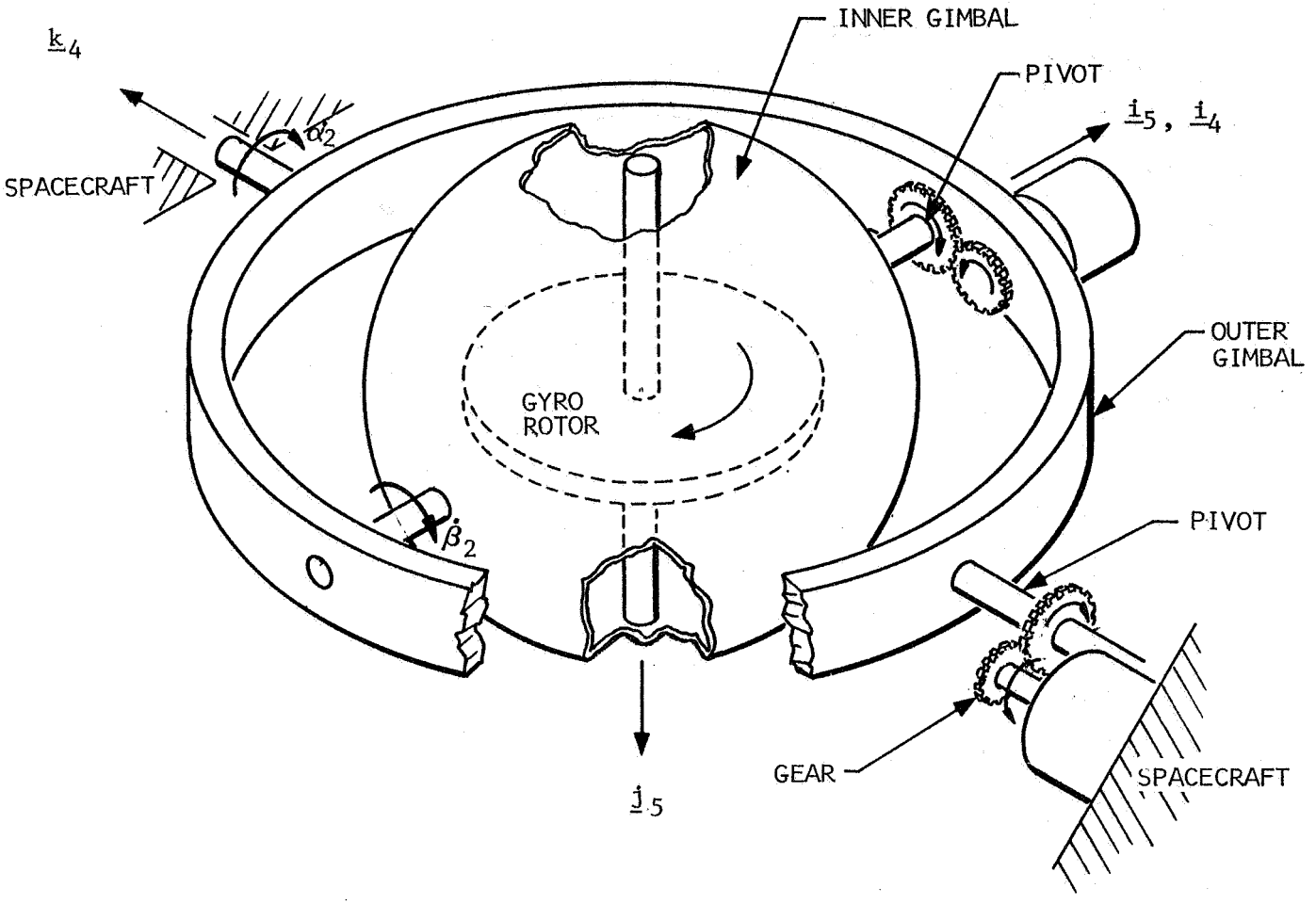

FIGURE 2.1-3 CONTROL MOMENT GYRO

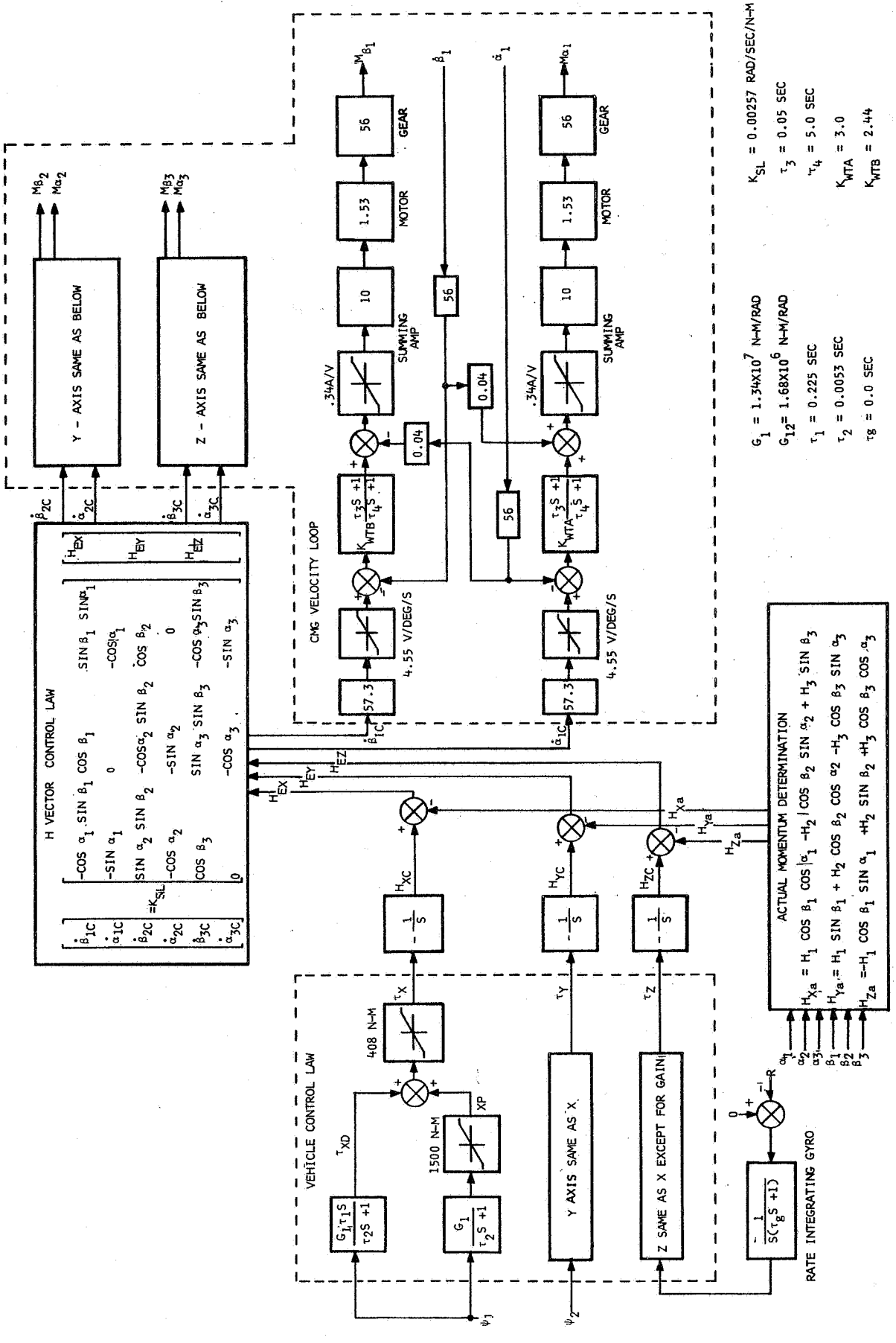

FIGURE 2.1-4 SPACECRAFT CONTROL SYSTEM

limiting, the outputs of which are the components of torque which the CMGs are to exert on the vehicle to null ψ_1, ψ_2, and $-\int R dt$. These commanded torque components (τ_x, τ_y, τ_z) are converted into commanded momentum components (in the body system) according to:

$$\dot{\underline{H}}_T \cong - \begin{bmatrix} \tau_x \\ \tau_y \\ \tau_z \end{bmatrix}$$

where:

$\dot{\underline{H}}_T$ = Time derivative with respect to inertial space of the total CMG momentum vector.

The closed loop H vector control law is then used to compute the difference between the commanded and actual momentum components and, from this, to find the desired CMG inner and outer gimbal rates, $\dot{\beta}_{ic}$ and $\dot{\alpha}_{ic}$ (i=1,2,3). The CMG gimbal velocity loops serve to drive the CMG gimbals at the desired rates. The outputs of these loops are the moments exerted on the gimbals by the torque motors. These outputs feed into the CMG and spacecraft dynamics.

Spacecraft and experiment package hardware is now defined. The next step is to develop the equations which must be solved to determine the transformation matrix from telescope to inertial coordinates, [T2I]. The relevant equations are:

- Dynamics equations - Equations which define the angular rates of the spacecraft, CMGs, and telescope, once the control torques acting on these bodies are known.
- Control equations - Equations used to represent the spacecraft and telescope control hardware and to compute the control torques acting on the spacecraft and telescope.
- Matrix transformation equations - These equations relate the spacecraft and telescope rates to [T2I] and $\frac{d}{dt}$ [T2I]. They are solved to yield [T2I].

Equation development for the dynamics and spacecraft control equations will now be discussed. Telescope control equation development is in Paragraph 2.4, while matrix transformation equations are developed in Paragraph 2.6.

2.1.1 Equation Development

2.1.1.1 Rotational Dynamics

Equations of rotational motion must be derived for the CMGs, the experiment package, and the spacecraft (LM/CSM plus ATM rack). To this end, the carrier vehicle configuration is conceptualized as a multi-part satellite, with each part a rigid body, as shown in Figure 2.1-5. Each part then has a relatively simple equation of motion, and the motion of the system can be found by combining motions of the parts.

The vector-dyadic equations basic to LASIM are quite similar to those found in the literature [7, 8]. Derivation of these equations will be discussed here, however, due to their fundamental importance. For the derivation, a system of N+1 moving parts will be assumed, with the 0^{th} part the spacecraft.

Newton's second law for rotational motion states that, for any rigid body,

$$\dot{\underline{h}}_0 = \underline{L}_0 \qquad (2.1\text{-}1)$$

where $\underline{h}_0$ is the angular momentum of the body about its mass centroid, 0, and $\underline{L}_0$ is the total moment about 0 of external forces acting on the body. It is also well known that:

$$\underline{h}_0 = [] \cdot \underline{\Omega} \qquad (2.1\text{-}2)$$

with [] the inertia dyadic of the body about its mass centroid and $\underline{\Omega}$ the angular velocity of the body in inertial space. Equations (2.1-1) and 2.1-2) can be applied to each of the N+1 bodies constituting the LCSE vehicle of Figure 2.1-5. If this is done, the following equation results for i=0,...,N:

$$\frac{d}{dt}\left[[]^i \cdot (\underline{\omega}+\underline{\omega}^i)\right] = \underline{L}^i_{0_i} + \sum_{j=0}^{N} \underline{L}^{ij}_{0_i} \qquad (2.1\text{-}3)$$

where

0_i = Mass centroid of i^{th} body

$[]^i$ = Inertia dyadic of i^{th} body about 0_i,

X = Coordinate system fixed in main body,

$\underline{\omega}$ = Angular velocity of X in inertial space,

$\underline{\omega}^i$ = Angular velocity of i^{th} part relative to main body ($\underline{\omega}^0 = \underline{0}$),

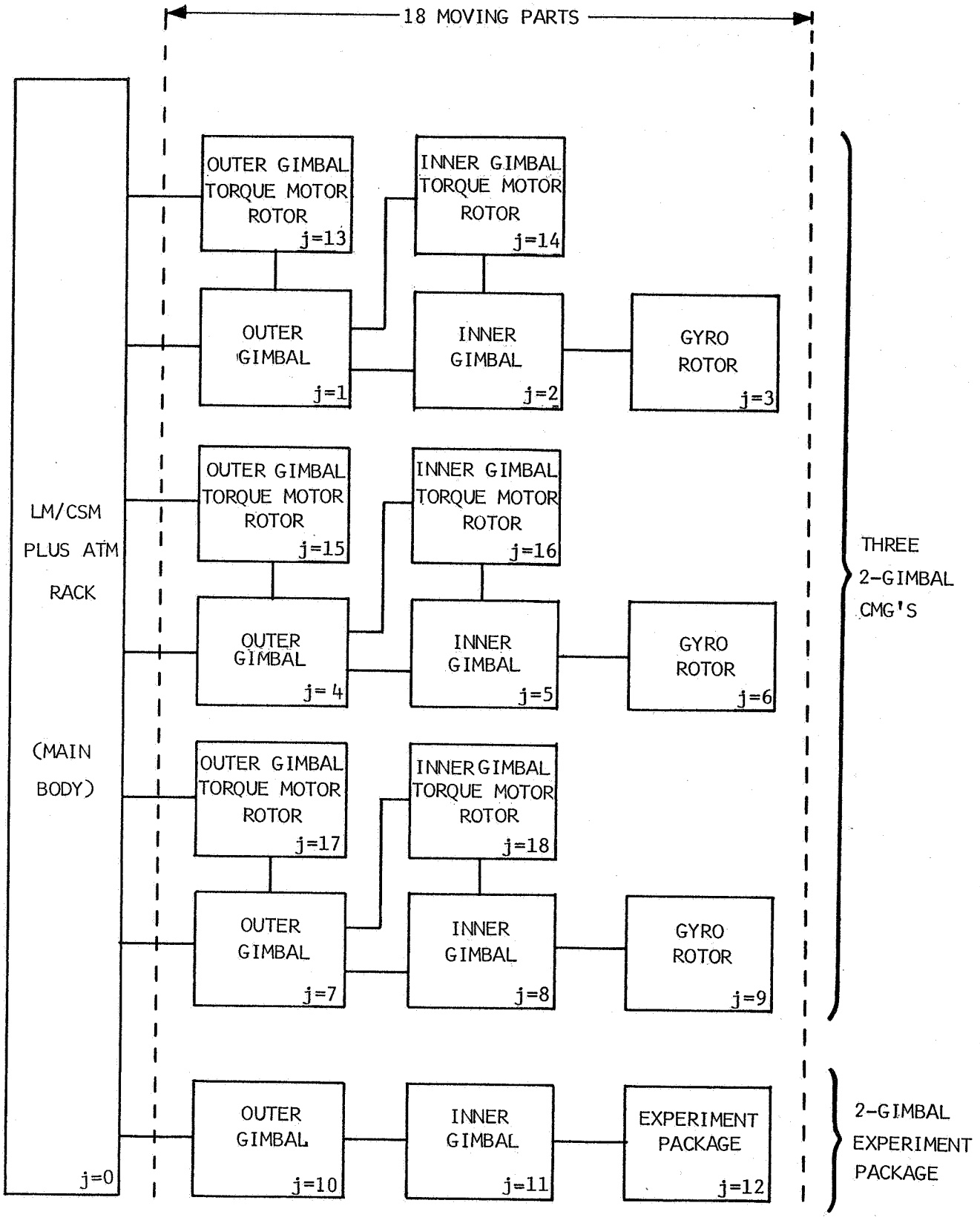

FIGURE 2.1-5 CARRIER VEHICLE CHARACTERIZATION

$\underline{L}^{i}_{O_i}$ = Moment about O_i of all forces external to the entire vehicle (e.g., gravity gradient, incident momentum),

$\underline{L}^{ij}_{O_i}$ = Moment about O_i of interaction force on $i^{\underline{th}}$ part due to $j^{\underline{th}}$ part. This torque is referred to as interaction torque.

Equation (2.1-3) provides the basic relationship required to determine the motion of each part relative to the main body (i.e., to find $\underline{\omega}^i$). In order to determine $\underline{\omega}$, however, it is convenient to eliminate the interaction torques, $\underline{L}^{ij}$. If the center of mass of the total system of bodies were fixed, the motion of all parts could be referred to that point and an equation for the computation of $\underline{\omega}$ derived. Unfortunately, the system center of mass is not fixed for the LCSE vehicle. The experiment package mass center is offset slightly from the experiment package hinge point (see Figure 2.1-6), thus leading to motion of the system center of mass.

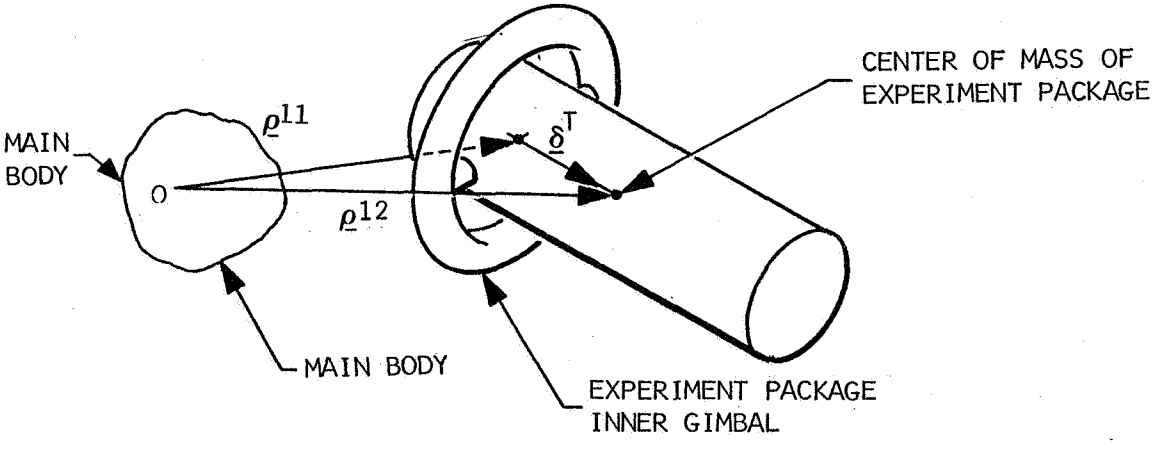

FIGURE 2.1-6 EXPERIMENT PACKAGE CENTER OF MASS OFFSET

The centers of mass of all other bodies are assumed fixed relative to the main body. This situation suggests using the center of mass of a system consisting of all parts (including the main body) except the experiment package as a basic reference point. This point, called O, is defined by the equation:

$$\underline{R} = \frac{1}{M}\left[\sum_{i=0}^{N}(\underline{R} + \underline{\rho}^i)M^i - M^{12}\underline{\rho}^{12}\right] \qquad (2.1\text{-}4)$$

or

$$\underline{0} = \sum_{i=0}^{N}\underline{\rho}^i M^i - M^{12}\underline{\rho}^{12}$$

where:

$$M = \sum_{i=0}^{N} M^i,$$

$\underline{R}$ = Radius vector to O from center of an inertial coordinate system (here assumed to be at Earth's center),

$\underline{\rho}^i$ = Vector from O to O_i,

M^i = Mass of $i^{\underline{th}}$ part

The X coordinate system is thus assumed centered at O, and its axes are assumed aligned with the x_B, y_B, z_B axes.

Motion of all parts except the experiment package can then be referred to O. Recall that the moment due to any force, $\underline{F}$, about a point, A, is related to the moment about another point, B, by:

$$\underline{L}_A = \underline{L}_B + \underline{\rho} \times \underline{F} \qquad (2.1\text{-}5)$$

where $\underline{\rho}$ is the vector from A to B. Thus, Equation (2.1-3) can be rewritten and summed over i=0,...,11,13...,N to yield:

$$\frac{d}{dt} \sum_{i=0}^{N}{}' \left[\underline{\underline{I}}^i \cdot (\underline{\omega}+\underline{\omega}^i) \right] = \sum_{i=0}^{N}{}' \underline{L}_O^i + \sum_{i=0}^{N}{}' \sum_{j=0}^{N} \underline{L}_O^{ij} - \sum_{i=0}^{N}{}' \underline{\rho}^i \times (\underline{F}^i + \sum_{j=0}^{N} \underline{F}^{ij}) \qquad (2.1\text{-}6)$$

where $\sum_{i=0}^{N}{}'$ denotes a sum over i=0,1,...,11,13,...,N.

But

$$\sum_{i=0}^{N} \sum_{j=0}^{N} \underline{L}_O^{ij} = \underline{0} = \sum_{i=0}^{N}{}' \sum_{j=0}^{N} \underline{L}_O^{ij} + \sum_{j=0}^{N} \underline{L}_O^{12,j} .$$

Also, for i=0,...,N,

$$M^i(\ddot{\underline{R}}+\ddot{\underline{\rho}}^i) = \underline{F}^i + \sum_{j=0}^{N} \underline{F}^{ij},$$

so that

$$\sum_{i=0}^{N}{}' \underline{\rho}^i \times (\underline{F}^i + \sum_{j=0}^{N} \underline{F}^{ij}) = \sum_{i=0}^{N}{}' \underline{\rho}^i \times M^i(\ddot{\underline{R}}+\ddot{\underline{\rho}}^i) = \sum_{i=0}^{N}{}' M^i \underline{\rho}^i \times \ddot{\underline{\rho}}^i. \qquad (2.1\text{-}7)$$

Equation (2.1-6) can, therefore, be rewritten as:

$$\frac{d}{dt}\left\{\sum_{i=0}^{N}{}' \left[\prod^{i} \cdot (\underline{\omega}+\underline{\omega}^{i}) + M^{i}\underline{\rho}^{i} \times \dot{\underline{\rho}}^{i}\right]\right\} = \sum_{i=0}^{N}{}' \underline{L}_{0}^{i} - \sum_{j=0}^{N} \underline{L}_{0}^{12,j}. \qquad (2.1\text{-}8)$$

For the telescope, Equation (2.1-3) yields:

$$\frac{d}{dt}\left[\prod^{12} \cdot (\underline{\omega}+\underline{\omega}^{12})\right] = \underline{L}_{O_{12}}^{12} + \sum_{j=0}^{N} \underline{L}_{0}^{12,j} - \underline{\rho}^{12} \times \sum_{j=0}^{N} \underline{F}^{12,j} \qquad (2.1\text{-}9)$$

Addition of Equations (2.1-8) and (2.1-9) gives:

$$\frac{d}{dt}\left[\sum_{i=0}^{N} \prod^{i} \cdot (\underline{\omega}+\underline{\omega}^{i}) + \sum_{i=0}^{N}{}' M^{i}\underline{\rho}^{i} \times \dot{\underline{\rho}}^{i}\right] = \sum_{i=0}^{N}{}' \underline{L}_{0}^{i} + \underline{L}_{O_{12}}^{12} - \underline{\rho}^{12} \times \sum_{j=0}^{N} \underline{F}^{12,j} \qquad (2.1\text{-}10)$$

Equation (2.1-10) is suitable for computation of $\underline{\omega}$, except for the presence of the $\underline{F}^{12,j}$ terms. These interaction forces can be eliminated by use of the equations of linear motion for the telescope and the LCSE vehicle without the telescope:

$$M^{12}(\ddot{\underline{R}} + \ddot{\underline{\rho}}^{12}) = \underline{F}^{12} + \sum_{j=0}^{N} \underline{F}^{12,j} \qquad (2.1\text{-}11)$$

$$(M-M^{12})\ddot{\underline{R}} = \sum_{i=0}^{N}{}' \underline{F}^{i} - \sum_{j=0}^{N} \underline{F}^{12,j} \qquad (2.1\text{-}12)$$

If Equation (2.1-11) is multiplied by $M-M^{12}$ and Equation (2.1-12) by $-M^{12}$ and the results added, the following equation is obtained:

$$[(M-M^{12}) + M^{12}] \sum_{j=0}^{N} \underline{F}^{12,j} = M^{12}(M-M^{12})\ddot{\underline{\rho}}^{12} - (M-M^{12})\underline{F}^{12} + M^{12} \sum_{i=0}^{N}{}' \underline{F}^{i}$$

$$\text{or} \quad \sum_{j=0}^{N} \underline{F}^{12,j} = \frac{1}{M}\left[M^{12}(M-M^{12})\ddot{\underline{\rho}}^{12} + M^{12} \sum_{i=0}^{N}{}' \underline{F}^{i} - (M-M^{12})\underline{F}^{12}\right] \qquad (2.1\text{-}13)$$

Let the external force on the system made up of all N+1 parts except the telescope be denoted by $\underline{F}^{S}$; i.e., let $\underline{F}^{S}$ be defined by

$$\underline{F}^{S} = \sum_{i=0}^{N}{}' \underline{F}^{i}. \qquad (2.1\text{-}14)$$

To further simplify the notation, define the moment $\underline{M}^E$ and the mass $\tilde{M}^{12}$ as follows:

$$\underline{M}^E = \underline{L}_O^S + \underline{L}_{O_{12}}^{12} - \frac{1}{M}\,\underline{\rho}^{12} \times [M^{12}\,\underline{F}^S - (M-M^{12})\underline{F}^{12}]$$

$$\tilde{M}^{12} = M^{12}(M-M^{12})/M \qquad (2.1\text{-}15)$$

where $\underline{L}^S$ is the moment resulting from $\underline{F}^S$. Then, from Equations (2.1-10, 13, 15), it follows that:

$$\frac{d}{dt}\left[\sum_{i=0}^{N} \underline{\underline{I}}^i \cdot (\underline{\omega}+\underline{\omega}^i) + \sum_{i=0}^{N}{}' M^i \underline{\rho}^i \times \dot{\underline{\rho}}^i + \tilde{M}^{12}\underline{\rho}^{12} \times \dot{\underline{\rho}}^{12}\right] = \underline{M}^E. \qquad (2.1\text{-}16)$$

Equations (2.1-3) and 2.1-16) are the basic equations for LASIM. They are quite general except for the assumption that all bodies except the experiment package have mass centers fixed in the main body. A rederivation of Equation (2.1-16) from Equation (2.1-3) can be made if this assumption becomes invalid due to changes in hardware specifications.

To provide a set of equations suitable for computer solution, the concise Equations (2.1-3) and (2.1-16) must be expanded. Each vector and dyadic must be expressed in an appropriate coordinate system and scalar equations derived which can be solved for:

- The components of $\underline{\omega}$
- Eight angles relating free parts to the main body

The three gyro rotors move with constant angular rate relative to the CMG inner gimbals, and equations for their motion need not be solved. The experiment package dynamics are incorporated with the inner gimbal structure dynamics since the two parts are rigidly attached. Although solar panels are shown in Figure 1-1, the spacecraft model received from NASA for simulation contained no definition for such parts.

Development of the scalar equations will now be discussed.

2.1.1.1.1 CMG Dynamics

The detailed scalar dynamics equations will first be developed for CMG 2. Equations of motion for the other two CMGs can then easily be derived by analogy. It is assumed here that all three CMGs have the same physical characteristics.

Three coordinate systems are used to derive the equations of motion of CMG 2 (see Figure 2.1-7). These are defined by their

unit vectors as follows:

- o $\underline{i}_5$, $\underline{j}_5$, $\underline{k}_5$ - $\underline{j}_5$ is along the gyro rotor spin axis and $\underline{i}_5$ is along the inner gimbal pivot.
- o $\underline{i}_4$, $\underline{j}_4$, $\underline{k}_4$ - $\underline{i}_4$ is coincident with $\underline{i}_5$ and $\underline{k}_4$ lies along the outer gimbal pivot.
- o $\underline{i}_B$, $\underline{j}_B$, $\underline{k}_B$ - Body axis set as previously defined.

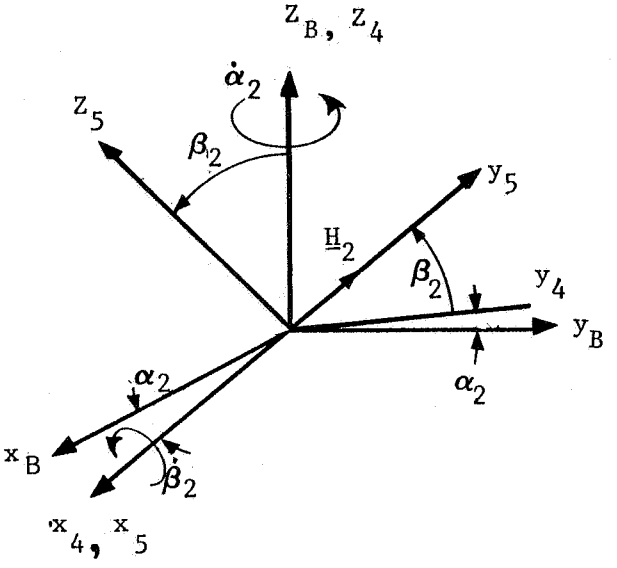

FIGURE 2.1-7 CMG COORDINATE SYSTEMS

The zero position of the CMG is defined when the vectors $\underline{i}_5$, $\underline{j}_5$, $\underline{k}_5$ are coincident with the vectors $\underline{i}_4$, $\underline{j}_4$, $\underline{k}_4$ and $\underline{i}_B$, $\underline{j}_B$, $\underline{k}_B$. The inner gimbal angle, β_2, and the outer gimbal angle, α_2, are shown in Figure 2.1-7. Components of vectors can be changed from one coordinate system to another by multiplying on the left by the following matrices:

$$[B24] = \begin{bmatrix} \cos\alpha_2 & \sin\alpha_2 & 0 \\ -\sin\alpha_2 & \cos\alpha_2 & 0 \\ 0 & 0 & 1 \end{bmatrix} \qquad [425] = \begin{bmatrix} 1 & 0 & 0 \\ 0 & \cos\beta_2 & \sin\beta_2 \\ 0 & -\sin\beta_2 & \cos\beta_2 \end{bmatrix}$$

where:

[B24] is matrix from body system to "4" system

[425] is matrix from "4" system to "5" system

Two scalar equations are required to define $\ddot{\alpha}_2$ and $\ddot{\beta}_2$ and thus to specify the motion of CMG 2 relative to the spacecraft. Equation (2.1-3), applied to CMG 2, yields:

$$\dot{\underline{h}}^4 = \frac{d}{dt}\left[\underline{\square}^4 \cdot (\underline{\omega} + \underline{\omega}^4)\right] = \underline{L}_{O_4}^{4,0} + \underline{L}_{O_4}^{4,5} + \underline{L}_{O_4}^{4,15} + \underline{L}_{O_4}^{4,16} \qquad (2.1\text{-}17)$$

$$\dot{\underline{h}}^5 = \frac{d}{dt}\left[\underline{\square}^5 \cdot (\underline{\omega} + \underline{\omega}^5)\right] = \underline{L}_{O_5}^{5,4} + \underline{L}_{O_5}^{5,6} + \underline{L}_{O_5}^{5,16} \qquad (2.1\text{-}18)$$

$$\dot{\underline{h}}^6 = \frac{d}{dt}\left[\underline{\square}^6 \cdot (\underline{\omega} + \underline{\omega}^6)\right] = \underline{L}_{O_6}^{6,5} \qquad (2.1\text{-}19)$$

$$\dot{\underline{h}}^{15} = \frac{d}{dt}\left[\underline{\square}^{15} \cdot (\underline{\omega} + \underline{\omega}^{15})\right] = \underline{L}_{O_{15}}^{15,0} + \underline{L}_{O_{15}}^{15,4} \qquad (2.1\text{-}20)$$

$$\dot{\underline{h}}^{16} = \frac{d}{dt}\left[\underline{\square}^{16} \cdot (\underline{\omega} + \underline{\omega}^{16})\right] = \underline{L}_{O_{16}}^{16,4} + \underline{L}_{O_{16}}^{16,5} \qquad (2.1\text{-}21)$$

where:

- $\dot{\underline{h}}^j$ = derivative in inertial space of the angular momentum of the j^{th} body about O_j
- All other $\underline{L}^{ij}$ terms are interaction torques as defined previously and include the electromagnetic moments which drive the two gimbal torque motor rotors.

For the CMG, it is assumed that the mass centroids of parts 4, 5, and 6 coincide; i.e., $O_4 = O_5 = O_6$. Then

$$\underline{L}_{O_4}^{4,5} = -\underline{L}_{O_5}^{5,4},$$
$$\underline{L}_{O_5}^{5,6} = -\underline{L}_{O_6}^{6,5}.$$

Thus, from Equations (2.1-18, 19, 21) and Figure 2.1-8,

$$(\dot{\underline{h}}^5 + \dot{\underline{h}}^6 + \dot{\underline{h}}^{16}) \cdot \underline{i}_5 = (\underline{L}_{O_5}^{5,4} + \underline{L}_{O_5}^{5,16} + \underline{L}_{O_{16}}^{16,4} + \underline{L}_{O_{16}}^{16,5}) \cdot \underline{i}_5$$
$$= \tau_2 + M_{ex} - \tau_1 \qquad (2.1\text{-}22)$$

where

- $\underline{L}_{O_5}^{5,4} \cdot \underline{i}_5$ = frictional torque on inner gimbal pivot, assumed zero,
- $\underline{L}_{O_5}^{5,16} \cdot \underline{i}_5 = \tau_2$ = torque exerted by inner gimbal torque motor on gear attached to inner gimbal,

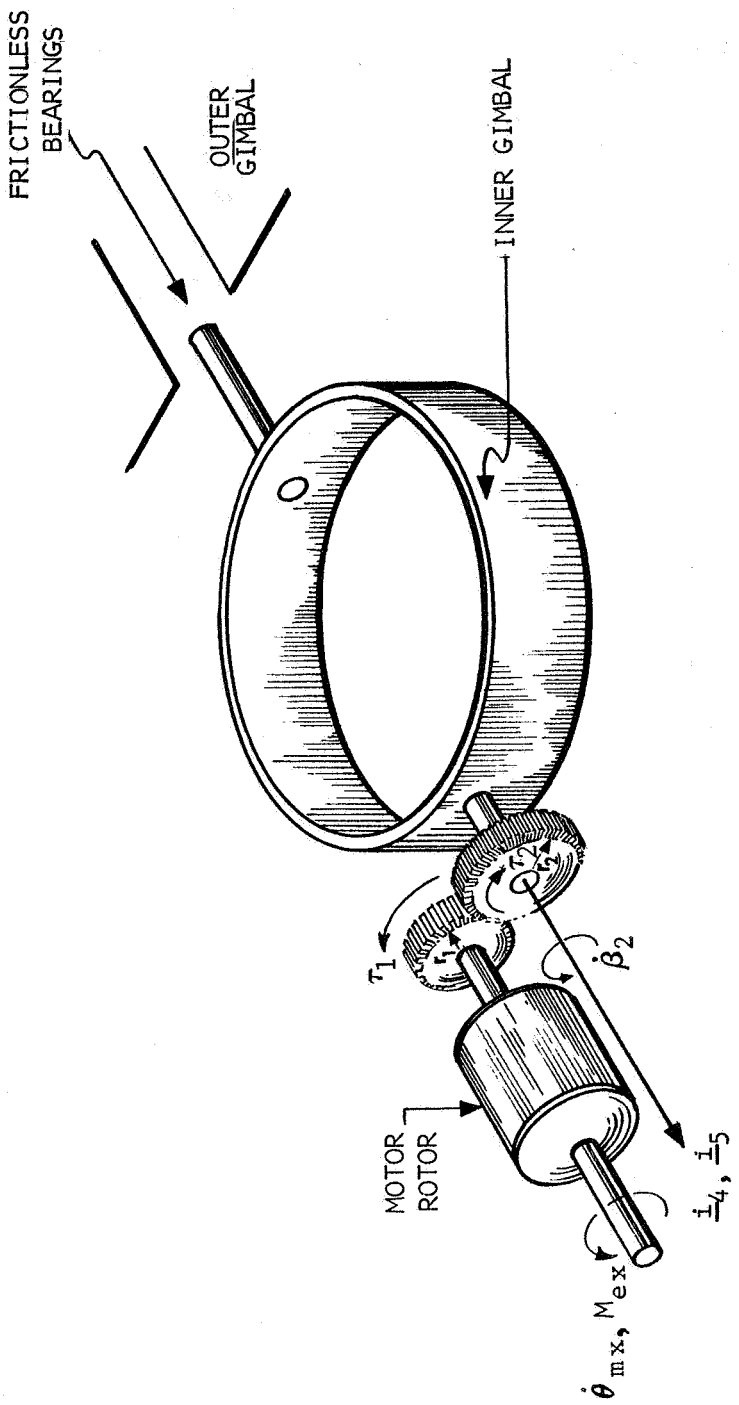

FIGURE 2.1-8 INNER GIMBAL TORQUE MOTOR

- $\underline{L}_{O_{16}}^{16,4} \cdot \underline{i}^5 = M_{ex}$ = Electromagnetic moment applied to inner gimbal torque motor rotor,
- $\underline{L}_{O_{16}}^{16,5} \cdot \underline{i}^5 = -\tau_1$ = Restraining torque exerted on gear attached to motor rotor by the inner gimbal.

The gear ratio of the inner and outer gimbal pivot is $N_G = r_2/r_1$. It is then known that

$$\tau_2 = N_G \tau_1, \tag{2.1-23}$$

$$\dot{\theta}_{mx} = N_G \dot{\beta}_2 \tag{2.1-24}$$

where $\dot{\theta}_{mx}$ is the rotation rate of the inner gimbal motor rotor. Let

$\underline{\omega}_2'$ = $\underline{\omega} + \underline{\omega}^4$

$\underline{\omega}_2$ = $\underline{\omega} + \underline{\omega}^5$

Ω_2 = Angular rate (constant) of the CMG 2 rotor relative to its inner gimbal.

Then the components of $\underline{\omega}$, $\underline{\omega}_2'$, $\underline{\omega}_2$, $\underline{\omega} + \underline{\omega}^6$, $\underline{\omega} + \underline{\omega}^{15}$, and $\underline{\omega} + \underline{\omega}^{16}$ are given as follows:*

$$\underline{\omega} \rightarrow \begin{bmatrix} P \\ Q \\ R \end{bmatrix}_B$$

$$\underline{\omega}_2' \rightarrow \begin{bmatrix} P \cos \alpha_2 + Q \sin \alpha_2 \\ -P \sin \alpha_2 + Q \cos \alpha_2 \\ R + \dot{\alpha}_2 \end{bmatrix}_4$$

$$\underline{\omega}_2 \rightarrow \begin{bmatrix} \omega_{2x}' + \dot{\beta}_2 \\ \omega_{2y}' \cos \beta_2 + \omega_{2z}' \sin \beta_2 \\ -\omega_{2y}' \sin \beta_2 + \omega_{2z}' \cos \beta_2 \end{bmatrix}_5$$

* The arrow symbol, $\rightarrow$, is used to denote a correspondence between a vector or dyadic and its components relative to some coordinate system.

$$\underline{\omega} + \underline{\omega}^{6} \rightarrow \begin{bmatrix} \omega_{2x} \\ \omega_{2y} + \Omega_2 \\ \omega_{2z} \end{bmatrix}_4$$

$$\underline{\omega} + \underline{\omega}^{15} \rightarrow \begin{bmatrix} P \cos \alpha_2 + Q \sin \alpha_2 \\ -P \sin \alpha_2 + Q \cos \alpha_2 \\ R + N_G \dot{\alpha}_2 \end{bmatrix}_4$$

$$\underline{\omega} + \underline{\omega}^{16} \rightarrow \begin{bmatrix} \omega_{2x}' + N_G \dot{\beta}_2 \\ \omega_{2y}' \cos \beta_2 + \omega_{2z}' \sin \beta_2 \\ -\omega_{2y}' \sin \beta_2 + \omega_{2z}' \cos \beta_2 \end{bmatrix}_5$$

where $[\ ]_j$ denotes the components of a vector relative to the coordinate system fixed in the j^{th} part, as previously defined (j=B means body system). Let inertia dyads $\mathbb{I}^4$, $\mathbb{I}^5$, $\mathbb{I}^6$, $\mathbb{I}^{15}$, and $\mathbb{I}^{16}$ have components as follows:

$$\mathbb{I}^4 \rightarrow \begin{bmatrix} C_a & 0 & 0 \\ 0 & A_a & 0 \\ 0 & 0 & B_a \end{bmatrix}_4$$

$$\mathbb{I}^5 \rightarrow \begin{bmatrix} C_b & 0 & 0 \\ 0 & A_b & 0 \\ 0 & 0 & B_b \end{bmatrix}_5$$

$$\mathbb{I}^6 \rightarrow \begin{bmatrix} B_g & 0 & 0 \\ 0 & A_g & 0 \\ 0 & 0 & B_g \end{bmatrix}_5$$

$$\boldsymbol{\mathcal{I}}^{15} \rightarrow \begin{bmatrix} 0 & 0 & 0 \\ 0 & 0 & 0 \\ 0 & 0 & J_{mr} \end{bmatrix}_4$$

$$\boldsymbol{\mathcal{I}}^{16} \rightarrow \begin{bmatrix} J_{mr} & 0 & 0 \\ 0 & 0 & 0 \\ 0 & 0 & 0 \end{bmatrix}_5$$

Then

$$\dot{\underline{h}}^5 + \dot{\underline{h}}^6 + \dot{\underline{h}}^{16} \rightarrow \frac{d}{dt} \begin{bmatrix} (C_b+B_g)(\omega_{2x}' + \dot{\beta}_2) + J_{mr}(\omega_{2x}' + N_G\dot{\beta}_2) \\ (A_b+A_g)\omega_{2y} + \Omega_2 A_g \\ (B_g + B_g)\omega_{2z} \end{bmatrix}_5 \qquad (2.1\text{-}25)$$

Thus, from Equations (2.1-22, 23, 25),

$$(\dot{\underline{h}}^5 + \dot{\underline{h}}^6 + \dot{\underline{h}}^{16}) \cdot \underline{i}_5 = (C_b+B_g)(\dot{\omega}_{2x}' + \ddot{\beta}_2) + J_{mr}(\dot{\omega}_{2x}'+N_G\ddot{\beta}_2)+ (B_b+B_g - A_b-A_g)\,\omega_{2y}\omega_{2z} - (\Omega_2 A_g)\,\omega_{2z}$$
$$= M_{EX} + (N_G-1)\tau_1 \qquad (2.1\text{-}26)$$

This equation can be solved for $\ddot{\beta}_2$ if τ_1 can be eliminated. Equation (2.1-21) can be used to do so:

$$\underline{i}_5 \cdot \underline{h}^{16} = \underline{i}_5 \cdot \frac{d}{dt}\left[\boldsymbol{\mathcal{I}}^{16} \cdot (\underline{\omega} + \underline{\omega}^{16})\right]$$
$$= J_{mr}\,(\dot{\omega}_{2x}' + N_G\ddot{\beta}_2) = M_{ex} - \tau_1$$

Thus

$$\tau_1 = -J_{mr}\,(\dot{\omega}_{2x}' + N_G\ddot{\beta}_2) + M_{ex}$$

From this relation and Equation (2.1-26), it follows that:

$$(C_b + B_g + N_G^2 J_{mr})\ddot{\beta}_2 + (C_b + B_g + N_G J_{mr})\dot{\omega}_{2x}'$$
$$+(B_b + B_g - A_b - A_g)\omega_{2y}\omega_{2z} - H_2\omega_{2z} = M_{\beta_2} \qquad (2.1\text{-}27)$$

where:

$H_2 = \Omega_2 A_g$, CMG 2 rotor angular momentum

$M_{\beta 2} = N_G M_{ex}$, N_G times torque produced by the inner gimbal torquer.

The scalar equation required to compute $\ddot{\alpha}_2$ can be found similarly. The procedure is to add Equations (2.1-17, 18, 19, 20, 21), compute the indicated $\dot{\underline{h}}$ terms, eliminate τ_1 and τ_2 by use of Equation (2.1-20), and solve for $\ddot{\alpha}_2$. The result is:

$$[B_a + J_{mr}N_G^2 + (A_b+A_g)\sin^2\beta_2 + (B_b+B_g)\cos^2\beta_2]\ddot{\alpha}_2 +$$

$$[B_a + N_G J_{mr} + (A_b+A_g)\sin^2\beta_2 + (B_b+B_g)\cos^2\beta_2]\dot{R}$$

$$-\dot{P}(A_b+A_g - B_b-B_g)\sin\alpha_2 \sin\beta_2 \cos\beta_2 + \dot{Q}(A_b+A_g - B_b-B_g)$$

$$\cos\alpha_2 \sin\beta_2 \cos\beta_2 = M_{\alpha 2} + J_{mr}(\omega_{2x}' + N_G\dot{\beta}_2)\omega_{2y}'$$

$$+(A_b+A_g)\sin\beta_2 [\cos\beta_2\, \omega_{2x}'\dot{\alpha}_2 + \sin\beta_2\, \omega_{2y}'\dot{\beta}_2$$

$$-(R+\dot{\alpha}_2)\dot{\beta}_2 \cos\beta_2] - (B_b+B_g)\cos\beta_2 [\sin\beta_2\, \omega_{2x}'\dot{\alpha}_2 -$$

$$\cos\beta_2\, \omega_{2y}'\dot{\beta}_2 - (R+\dot{\alpha}_2)\dot{\beta}_2 \sin\beta_2] - \omega_{2x} H_2 \cos\beta_2$$

$$-(A_a-C_a)\omega_{2x}'\omega_{2y}' + (B_b-C_b)\omega_{2x}\omega_{2z}\sin\beta_2$$

$$-(A_b+A_g - C_b-B_g)\omega_{2x}\omega_{2y}\cos\beta_2 \qquad (2.1\text{-}28)$$

where $M_{\alpha 2} = N_G M_{ez}$, N_G times the torque produced by the inner gimbal torquer.

Equations (2.1-27) and 2.1-28) can be used to compute $\ddot{\beta}_2$ and $\ddot{\alpha}_2$. Equations for $\ddot{\beta}_3$ and $\ddot{\alpha}_3$ can be obtained from these by making the following notational changes:

$\alpha_2 \rightarrow \alpha_3$	P → Q	2x → 3y
$\beta_2 \rightarrow \beta_3$	Q → R	2y → 3z
$H_2 \rightarrow H_3$	R → P	2z → 3x

The resulting equations are:

$$(C_b+B_g + N_G^2 J_{mr})\ddot{\beta}_3 + (C_b+B_g + N_G J_{mr})\dot{\omega}_{3y}' + (B_b+B_g - A_b-A_g)\omega_{3z}\omega_{3x}$$

$$-H_3\omega_{3x} = M_{\beta_3} \qquad (2.1\text{-}29)$$

$$[B_a + J_{mr}N_G^2 + (A_b+A_g)\sin^2\beta_3 + (B_b+B_g)\cos^2\beta_3]\ddot{\alpha}_3$$
$$+[B_a + N_G J_{mr} + (A_b+A_g)\sin^2\beta_3 + (B_b+B_g)\cos^2\beta_3]\dot{P}$$
$$-\dot{Q}(A_b+A_g - B_b-B_g)\sin\alpha_3 \sin\beta_3 \cos\beta_3$$
$$+\dot{R}(A_b+A_g - B_b-B_g)\cos\alpha_3 \sin\beta_3 \cos\beta_3 = M_{\alpha_3} + J_{mr}(\omega_{3y}' + N_G\dot{\beta}_2)\omega_{3z}'$$
$$+(A_b+A_g)\sin\beta_3 [\cos\beta_3 \omega_{3y}'\dot{\alpha}_3 + \sin\beta_3 \omega_{3z}'\dot{\beta}_3$$
$$-(P+\dot{\alpha}_3)\dot{\beta}_3 \cos\beta_3] - (B_b+B_g)\cos\beta_3[\sin\beta_3 \omega_{3y}'\dot{\alpha}_3 -$$
$$\cos\beta_3 \omega_{3z}'\dot{\beta}_3 - (P+\dot{\alpha}_3)\dot{\beta}_3 \sin\beta_3] - \omega_{3y} H_3 \cos\beta_3 - (A_a-C_a)\omega_{3y}'\omega_{3z}'$$
$$+(B_b-C_b)\omega_{3y}\omega_{3x}\sin\beta_3 - (A_b+A_g - C_b-B_g)\omega_{3y}\omega_{3z}\cos\beta_3$$

(2.1-30)

For the $\ddot{\beta}_1$, $\ddot{\alpha}_1$ equations, make the following substitutions in Equations (2.1-29) and (2.1-30):

α_3	$\rightarrow$	α_1	P $\rightarrow$ Q	3x	$\rightarrow$ 1y
β_3	$\rightarrow$	β_1	Q $\rightarrow$ R	3y	$\rightarrow$ 1z
H_3	$\rightarrow$	H_1	R $\rightarrow$ P	3z	$\rightarrow$ 1x

The resulting equations are:

$$(C_b+B_g + N_G^2 J_{mr})\ddot{\beta}_1 + (C_b+B_g + N_G J_{mr})\dot{\omega}_{1z}' + (B_b+B_g - A_b-A_g)\omega_{1x}\omega_{1y}$$
$$- H_1\omega_{1y} = M_{\beta_1},$$

(2.1-31)

$$[B_a+N_G^2 J_{mr} + (A_b+A_g)\sin^2\beta_1 + (B_b+B_g)\cos^2\beta_1]\ddot{\alpha}_1 +$$
$$[B_a+N_G J_{mr} + (A_b+A_g)\sin^2\beta_1 + (B_b+B_g)\cos^2\beta_1]\dot{Q}$$
$$-\dot{R}(A_b+A_g - B_b-B_g)\sin\alpha_1 \sin\beta_1 \cos\beta_1 + \dot{P}(A_b+A_g - B_b-B_g)\cos\alpha_1$$
$$\sin\beta_1 \cos\beta_1 = M_{\alpha_1} + J_{mr}(\omega_{1z}' + N_G\dot{\beta}_1)\omega_{1x}' + (A_b+A_g)\sin\beta_1 [\cos\beta_1$$
$$\omega_{1z}'\dot{\alpha}_1 + \sin\beta_1 \omega_{1x}'\dot{\beta}_1 - (Q+\dot{\alpha}_1)\dot{\beta}_1 \cos\beta_1] - (B_b+B_g)\cos\beta_1[\sin\beta_1$$
$$\omega_{1z}'\dot{\alpha}_1 - \cos\beta_1 \omega_{1x}'\dot{\beta}_1 - (Q+\dot{\alpha}_1)\dot{\beta}_1 \sin\beta_1] - \omega_{1z}H_1 \cos\beta_1 -$$
$$(A_a-C_a)\omega_{1z}'\omega_{1x}' + (B_b-C_b)\omega_{1z}\omega_{1y}\sin\beta_1 - (A_b+A_g - C_b-B_g)\omega_{1z}\omega_{1x}\cos\beta_1$$

(2.1-32)

Equations (2.1-27, 28, 29, 30, 31, 32) are the six equations which must be solved to determine the motion of the CMGs relative

to the spacecraft.

2.1.1.1.2 Experiment Package (Telescope) Dynamics

Due to the similarity of the telescope gimbal configuration with that of CMG 3, equation development for the telescope is roughly parallel to that followed for the CMGs. The correspondence between elements of the two systems is:

- o CMG outer gimbal - Telescope outer gimbal
- o CMB inner gimbal - Telescope inner gimbal
- o CMG gyro rotor - Experiment package (telescope)

There are, however, several important differences:

- o Torque motors on the telescope gimbals have gear ratio one. Inertias of the rotors are assumed to be included in the gimbal inertias.
- o When a flex-pivot gimbal is displaced through an angle ψ, a restoring torque $-K_f\psi$ is produced, where K_f is the flexure spring rate.
- o The center of mass of the telescope, O_{12}, is displaced a distance of δ^T along the z_T axis from the telescope hinge point.
- o The telescope, unlike the gyro rotor, is rigidly attached to its inner gimbal.

To describe the motion of the telescope, three coordinate systems will be used:

- o Telescope system, x_T, y_T, z_T, as previously defined
- o The "part 10" coordinate system - x_{10} along x_B, y_{10} along y_T.
- o Body system - x_B, y_B, z_B.

The zero position of the telescope gimbals, ψ_1, and ψ_2, is defined when the above three coordinate systems are coincident. Transformation of vector components from the body system to the "part 10" system can be achieved by multiplying by:

$$[B210] = \begin{bmatrix} 1 & 0 & 0 \\ 0 & \cos\psi_1 & \sin\psi_1 \\ 0 & -\sin\psi_1 & \cos\psi_1 \end{bmatrix}$$

Likewise, to transform from part 10 system to the telescope system, multiply by:

$$[102T] = \begin{bmatrix} \cos\psi_2 & 0 & -\sin\psi_2 \\ 0 & 1 & 0 \\ \sin\psi_2 & 0 & \cos\psi_2 \end{bmatrix}$$

The two scalar equations required to define $\ddot{\psi}_2$ and $\ddot{\psi}_1$, and thus the motion of the telescope relative to the spacecraft, can be obtained from Equation (2.1-3). The basic equations are:

$$\underline{\dot{h}}_{O_{10}}^{10} = \frac{d}{dt}\left[[\,]^{10} \cdot (\underline{\omega}+\underline{\omega}^{10})\right] = \underline{L}_{O_{10}}^{10,0} + \underline{L}_{O_{10}}^{10,11} \qquad (2.1\text{-}33)$$

$$\underline{\dot{h}}_{O_{11}}^{11} = \frac{d}{dt}\left[[\,]^{11} \cdot (\underline{\omega}+\underline{\omega}^{11})\right] = \underline{L}_{O_{11}}^{11,10} + \underline{L}_{O_{11}}^{11,12} \qquad (2.1\text{-}34)$$

$$\underline{\dot{h}}_{O_{12}}^{12} = \frac{d}{dt}\left[[\,]^{12} \cdot (\underline{\omega}+\underline{\omega}^{12})\right] = \underline{L}_{O_{12}}^{12,11} + \underline{L}_{O_{12}}^{12} \qquad (2.1\text{-}35)$$

where external torques on parts 10 and 11 are neglected. It is assumed that the mass centers of parts 10 and 11 coincide ($O_{10} = O_{11}$), but that $O_{11} \neq O_{12}$. Thus

$$\underline{L}_{O_{11}}^{11,12} = -\underline{L}_{O_{11}}^{12,11} = -\underline{L}_{O_{12}}^{12,11} - \underline{\delta}^T \times \underline{F}^{12,11}.$$

Since

$$M^{12}(\ddot{R} + \ddot{\underline{\rho}}^{11} + \ddot{\underline{\delta}}^T) = \underline{F}^{12} + \underline{F}^{12,11},$$

and

$$M^{11}(\ddot{R}+\ddot{\underline{\rho}}^{11}) = -\underline{F}^{10,11} - \underline{F}^{12,11} + \underline{F}^{11}$$

$$\underline{F}^{12,11} = (M^{11}M^{12}\,\ddot{\underline{\delta}}^T - M^{11}\underline{F}^{12} - M^{12}\underline{F}^{10,11} + M^{12}\underline{F}^{11}) / (M^{11} + M^{12})$$

Equation (2.1-35) therefore becomes

$$\frac{d}{dt}\left[[\,]^{12} \cdot (\underline{\omega}+\underline{\omega}^{12}) + \underline{\delta}^T \times \dot{\underline{\delta}}^T M^{11}M^{12}/(M^{11}+M^{12})\right] = \underline{L}_{O_{11}}^{12,11}$$

$$+ \underline{L}_{O_{12}}^{12} + \underline{\delta}^T \times (M^{11}\underline{F}^{12} - M^{12}\underline{F}^{11} + M^{12}\underline{F}^{10,11})/(M^{11}+M^{12}) \qquad (2.1\text{-}36)$$

In this equation

$$\underline{L}^{12}_{O_{12}} + \underline{\delta}^T \times (M^{11}\underline{F}^{12} - M^{12}\underline{F}^{11})/(M^{11}+M^{12})$$

is the moment due to external forces, which is negligible (see Paragraph 2.1.1.1.4 for further discussion). The net interaction force between parts 10 and 11, $\underline{F}^{10\,11}$, is zero since the parts do not translate relative to one another. Thus Equations (2.1-34) and (2.1-36) yield

$$\frac{d}{dt}\left[(\mathbb{I}^{11}+\mathbb{I}^{12})\cdot(\underline{\omega}+\underline{\omega}^{11}) + \underline{\delta}^T \times \dot{\underline{\delta}}^T M^{11} M^{12}/(M^{11}+M^{12})\right] = \underline{L}^{11,10}_{O_{11}} \quad (2.1\text{-}37)$$

since $\underline{\omega}^{12} = \underline{\omega}^{11}$. Only the y_T component of $\underline{L}^{11,10}_{O_{11}}$ is required for the motion of the inner gimbal:

$$\underline{j}_T \cdot \underline{L}^{11,10}_{O_{11}} = M_{T_2} - K_f\psi_2$$

where M_{T_2} = electromagnetic moment which drives the inner gimbal rotor.

To obtain a scalar representation for the momenta, let

$$\underline{\omega}_4' = \underline{\omega} + \underline{\omega}^{10}$$

$$\underline{\omega}_4 = \underline{\omega} + \underline{\omega}^{11}$$

The components of $\underline{\omega}_4'$ and $\underline{\omega}_4$ are:

$$\underline{\omega}_4' \rightarrow \begin{bmatrix} P + \dot{\psi}_1 \\ Q\cos\psi_1 + R\sin\psi_1 \\ -Q\sin\psi_1 + R\cos\psi_1 \end{bmatrix}_{10}$$

$$\underline{\omega}_4 \rightarrow \begin{bmatrix} \omega_{4x}'\cos\psi_2 - \omega_{4z}'\sin\psi_2 \\ \omega_{4x}' + \dot{\psi}_2 \\ \omega_{4x}'\sin\psi_2 + \omega_{4z}'\cos\psi_2 \end{bmatrix}_T$$

Let inertia dyadics $\mathbb{I}^{10}$, $\mathbb{I}^{11}$, and $\mathbb{I}^{12}$ have the following components:

$$\mathbb{I}^{10} \rightarrow \begin{bmatrix} A_O & 0 & 0 \\ 0 & B_O & 0 \\ 0 & 0 & C_O \end{bmatrix}_{10}$$

$$\square^{11} \rightarrow \begin{bmatrix} A_I & 0 & 0 \\ 0 & B_I & 0 \\ 0 & 0 & C_I \end{bmatrix}_T$$

$$\square^{12} \rightarrow \begin{bmatrix} A_T & 0 & 0 \\ 0 & B_T & 0 \\ 0 & 0 & C_T \end{bmatrix}_T$$

The term involving $\underline{\delta}^T \times \dot{\underline{\delta}}^T$ can be easily accounted for by noting that:

$$M^{12}\,\underline{\delta}^T \times \dot{\underline{\delta}}^T = M^{12}\underline{\delta}^T \times (\underline{\omega}_4 \times \underline{\delta}^T)$$

$$= M^{12}\,[\underline{\delta}^T \cdot \underline{\delta}^T E - \underline{\delta}^T\underline{\delta}^T] \cdot \underline{\omega}_4$$

where

E = unit dyadic.

Since $\underline{\delta}^T = \delta^T \underline{k}_T$,

$$\underline{\delta}^T \times \dot{\underline{\delta}}^T \rightarrow (\delta^T)^2 \begin{bmatrix} 1 & 0 & 0 \\ 0 & 1 & 0 \\ 0 & 0 & 0 \end{bmatrix} \begin{bmatrix} \omega_{4x} \\ \omega_{4y} \\ \omega_{4z} \end{bmatrix}$$

Thus it is convenient to define

$$\tilde{A}_T = A_T + (\delta^T)^2\, M^{11} M^{12} / (M^{11} + M^{12})$$

$$\tilde{B}_T = B_T + (\delta^T)^2\, M^{11} M^{12} / (M^{11} + M^{12})$$

Equation (2.1-37), upon dotting with $\underline{j}_T$, becomes:

$$[0\ 1\ 0]\,\frac{d}{dt}\left\{ \begin{bmatrix} A_I+\tilde{A}_T & 0 & 0 \\ 0 & B_I+\tilde{B}_T & 0 \\ 0 & 0 & C_I+C_T \end{bmatrix}_T \begin{bmatrix} \omega_{4x} \\ \omega_{4y} \\ \omega_{4z} \end{bmatrix}_T \right\} = M_{T_2} - K_f \psi_2$$

By carrying out the indicated differentiation, one obtains:

$$(B_I+\tilde{B}_T)(\ddot{\psi}_2+\dot{R}\sin\psi_1 + \dot{Q}\cos\psi_1 + \dot{\psi}_1\omega_{4z}') +$$

$$(A_I+\tilde{A}_T - C_I-C_T)\omega_{4z}\omega_{4x} = M_{T_2}-K_f\psi_2 \qquad (2.1\text{-}38)$$

To obtain a corresponding equation for $\ddot{\psi}_1$, add Equations (2.1-33, 34, 36) and dot with $\underline{i}_B$:

$$\underline{i}_B \cdot \frac{d}{dt}[\underline{h}^{10}_{O_{10}} + \underline{h}^{11}_{O_{11}} + \underline{h}^{12}_{O_{12}} + \underline{\delta}^T x \dot{\underline{\delta}}^T M^{11} M^{12}/(M^{11}+M^{12})] =$$

$$\underline{i}_B \cdot (\underline{L}^{10,0}_{O_{10}} + \underline{L}^{10,11}_{O_{10}} + \underline{L}^{11,10}_{O_{11}}) = M_{T_1} - K_f\psi_1$$

where M_{T_1} = electromagnetic moment which drives the outer gimbal motor rotor.

By substituting in the indicated inertia dyadics and angular velocities and carrying out the differentiation, the following equation is obtained:

$$A_O(\dot{P}+\ddot{\psi}_1) + (C_O-B_O)\omega_{4y}'\omega_{4z}' + (C_I+C_T - A_I-\tilde{A}_T)(\dot{R}\cos\psi_1 - \dot{Q}\sin\psi_1 - \dot{\psi}_1\omega_{4y}')$$
$$\sin\psi_2\cos\psi_2 + [(A_I+\tilde{A}_T)\cos^2\psi_2 + (C_I+C_T)\sin^2\psi_2](\dot{P}+\ddot{\psi}_1) +$$
$$[(C_I+C_T)\omega_{4x}\sin\psi_2 - (A_I+\tilde{A}_T)\omega_{4z}\cos\psi_2]\dot{\psi}_2 + [(C_I+C_T - B_I-\tilde{B}_T)\omega_{4z}\cos\psi_2 +$$
$$(B_I+\tilde{B}_T - A_I-\tilde{A}_T)\omega_{4x}\sin\psi_2]\omega_{4y} = M_{T_1} - K_f\psi_1 \qquad (2.1\text{-}39)$$

Equations (2.1-38) and (2.1-39) determine the motion of the telescope relative to the spacecraft.

2.1.1.1.3 Spacecraft Dynamics

The motion of all parts relative to the spacecraft has been determined. It remains to determine the motion of the spacecraft relative to inertial space (i.e., to find $\underline{\omega}$). Equation (2.1-16) is basic to the computation of $\underline{\omega}$. To make use of that equation, terms of the form

$$\frac{d}{dt}\{\square^i \cdot (\underline{\omega}+\underline{\omega}^i) + M^i \underline{\rho}^i x \dot{\underline{\rho}}^i\} \qquad (2.1\text{-}40)$$

must be evaluated, for i=0,...,18, in a common coordinate system. For this purpose, the body system will be used since its axes are parallel to those of the X system. The required evaluation will now be carried out.

First, note that for i=0,...,11,13,...,18,

$$\underline{\rho}^i \times \dot{\underline{\rho}}^i = \underline{\rho}^i \times (\underline{\rho}^i + \underline{\omega} \times \underline{\rho}^i) = \underline{\rho}^i \times (\underline{\omega} \times \underline{\rho}^i)$$

$$= (\underline{\rho}^i \cdot \underline{\rho}^i \, E - \underline{\rho}^i \underline{\rho}^i) \cdot \underline{\omega}$$

$$\rightarrow \begin{bmatrix} (\rho_2^i)^2 + (\rho_3^i)^2 & -\rho_1^i\rho_2^i & -\rho_1^i\rho_3^i \\ -\rho_1^i\rho_2^i & (\rho_1^i)^2 + (\rho_3^i)^2 & -\rho_2^i\rho_3^i \\ -\rho_1^i\rho_3^i & -\rho_2^i\rho_3^i & (\rho_1^i)^2 + (\rho_2^i)^2 \end{bmatrix}_B \begin{bmatrix} P \\ Q \\ R \end{bmatrix}_B \quad (2.1\text{-}41)$$

where ρ_1^i, ρ_2^i, and ρ_3^i are the components of $\underline{\rho}^i$ in the body and X system. Thus $\underline{\rho}^i \times \dot{\underline{\rho}}^i$ is a constant dyadic times $\underline{\omega}$ for i=0,...,11,13,...,18. For i=12 special consideration is required, since $\underline{\rho}^{12}$ is not fixed in the body. Thus

$$\underline{\rho}^{12} \times \dot{\underline{\rho}}^{12} = (\underline{\rho}^{10} + \underline{\delta}^T) \times (\dot{\underline{\rho}}^{10} + \dot{\underline{\delta}}^T)$$

$$= \underline{\rho}^{10} \times (\underline{\omega} \times \underline{\rho}^{10}) + \underline{\rho}^{10} \times \dot{\underline{\delta}}^T + \underline{\delta}^T \times \dot{\underline{\rho}}^{10} + \underline{\delta}^T \times \dot{\underline{\delta}}^T. \quad (2.1\text{-}42)$$

Two of these terms can be handled easily:

- $\underline{\rho}^{10} \times (\underline{\omega} \times \underline{\rho}^{10})$ is a constant dyadic times $\underline{\omega}$. It can be grouped with $[]^0 \cdot \underline{\omega}$.
- $\underline{\delta}^T \times \dot{\underline{\delta}}^T$ was shown in Paragraph 2.1.1.2 to be a constant dyadic times $\underline{\omega}_4$. This term can be grouped with $[]^{12} \cdot (\underline{\omega} + \underline{\omega}^{12})$.

The remaining two terms will be treated below.

Based on the above discussion, a constant dyadic $[]_V$ can be defined by:

$$[]_V \cdot \underline{\omega} = []^0 \cdot \underline{\omega} + \sum_{i=0}^{11} M^i \underline{\rho}^i \times \dot{\underline{\rho}}^i + \tilde{M}^{12} \underline{\rho}^{10} \times \dot{\underline{\rho}}^{10} \quad (2.1\text{-}43)$$

Let $[]_V$ have components in the body system given by

$$[]_V \rightarrow \begin{bmatrix} I_{xx} & -I_{xy} & -I_{xz} \\ -I_{xy} & I_{yy} & -I_{yz} \\ -I_{xa} & -I_{yz} & I_{zz} \end{bmatrix}_B$$

The elements of $[]_V$ can be computed from the components of $[]^0$

and $\underline{\rho}^i$ by applying Equations (2.1-41, 43).

Computation of the terms

$$\frac{d}{dt}\{[]^i \cdot (\underline{\omega} + \underline{\omega}^i)\} \quad , i=1...,18,$$

has already been discussed in Paragraphs 2.1.1.1.1 and 2.1.1.1.2. There, use was made of part centered coordinate systems due to the simplicity of $[]^i$ in such systems. For application to the problem of determining $\underline{\omega}$, these terms must be computed in the body system. To illustrate, consider the following:

$$\frac{d}{dt}\left[[]^4 \cdot (\underline{\omega}+\underline{\omega}^4) + []^5 \cdot (\underline{\omega}+\underline{\omega}^5) + []^6 \cdot (\underline{\omega}+\underline{\omega}^6) + []^{15} \cdot (\underline{\omega}+\underline{\omega}^{15}) + []^{16} \cdot (\underline{\omega}+\underline{\omega}^{16})\right] \rightarrow$$

$$\frac{d}{dt}\left[[B24]^T\left\{\begin{bmatrix} C_a & \omega_{2x}' \\ A_a & \omega_{2y}' \\ B_a & \omega_{2z}' \end{bmatrix}_4 + [425]^T \begin{bmatrix} (C_b+B_g)\omega_{2x} \\ (A_b+B_g)\omega_{2y} \\ (B_b+B_g)\omega_{2z} \end{bmatrix}_5 + \begin{bmatrix} 0 \\ 0 \\ J_{mr}N_G\dot{\alpha}_2 \end{bmatrix}_4 + [425]^T \begin{bmatrix} J_{mr}N_G\dot{\beta}_2 \\ 0 \\ 0 \end{bmatrix}_5\right\}\right]$$

where products of body rates with J_{mr} have been neglected. Performance of the indicated calculations will yield components of five of the required 18 terms in the body system. The other 13 terms are computed similarly. Results of the calculations are found in Paragraph 2.1.2.

All of the elements of Expression (2.1.40) have now been accounted for except the following two items:

- $M^i\underline{\rho}^i \times \dot{\underline{\rho}}^i$ for i=13,...,18
- The derivative of the two unexplained terms of Equation (2.1-42).

To eliminate the first of these, assume that $M^i = 0$ for i = 13,..., 18 since the motor rotors have very small mass. For the other terms, it can be shown that

$$\frac{d}{dt}(\underline{\rho}^{10} \times \underline{\dot{\delta}}^T + \underline{\delta}^T \times \underline{\dot{\rho}}^{10}) \rightarrow A^{T1} \begin{bmatrix} \dot{P} \\ \dot{Q} \\ \dot{R} \end{bmatrix}_B + A^{T2} \begin{bmatrix} \ddot{\psi}_1 \\ \ddot{\psi}_2 \end{bmatrix}_B \qquad (2.1\text{-}44)$$

where

$$A^{T1} = \begin{bmatrix} 2(\rho_2^{10}\delta_2 + \rho_3^{10}\delta_3) & -\rho_1^{10}\delta_2 - \rho_2^{10}\delta_1 & -\rho_1^{10}\delta_3 - \rho_3^{10}\delta_1 \\ -\rho_1^{10}\delta_2 - \rho_2^{10}\delta_1 & 2(\rho_1^{10}\delta_1 + \rho_3^{10}\delta_3) & -\rho_2^{10}\delta_3 - \rho_3^{10}\delta_2 \\ -\rho_1^{10}\delta_3 - \rho_3^{10}\delta_1 & -\rho_2^{10}\delta_3 - \rho_3^{10}\delta_2 & 2(\rho_1^{10}\delta_1 + \rho_2^{10}\delta_2) \end{bmatrix}_B$$

$$A^{T2} = \begin{bmatrix} \rho_2^{10}\delta_2 + \rho_3^{10}\delta_3 - \delta_1(\rho_2^{10}\cos\psi_1 + \rho_3^{10}\sin\psi_1) \\ -\rho_1^{10}\delta_2 \qquad (\rho_1^{10}\delta_1 + \rho_3^{10}\delta_3)\cos\psi_1 - \rho_3^{10}\delta_2 \sin\psi_1 \\ -\rho_1^{10}\delta_3 \qquad -\rho_2^{10}\delta_3 \cos\psi_1 + (\rho_1^{10}\delta_1 + \rho_2^{10}\delta_2)\sin\psi_1 \end{bmatrix}_B$$

δ_1, δ_2, δ_3 are the components of $\underline{\delta}^T$ in the body system, and terms involving products of rates with $\tilde{\delta}^T \times \rho^{10}$ have been neglected.

The sum of the 19 expressions of the type (2.1-40), required for Equation (2.1-16), can now be rewritten as follows:

$$\frac{d}{dt}\left[\sum_{i=0}^{18} \left[\right]^i \cdot (\omega + \underline{\omega}^i) + \sum_{i=0}^{18}{}' M^i \underline{\rho}^i \times \dot{\underline{\rho}}^i + \tilde{M}^{12} \underline{\rho}^{12} \times \dot{\underline{\rho}}^{12}\right] =$$

$$\frac{d}{dt}\left[\left[\right]_V \cdot \underline{\omega} + \sum_{i=1}^{18}{}' \left[\right]^i \cdot (\underline{\omega} + \underline{\omega}^i) + \overline{\left[\right]}^{12} \cdot (\underline{\omega} + \underline{\omega}^{12})\right]$$

$$+ \tilde{M}^{12} \frac{d}{dt}\left[\underline{\rho}^{10} \times \underline{\dot{\delta}}^T + \underline{\delta}^T \times \underline{\dot{\rho}}^{10}\right] = \underline{M}^E \qquad (2.1\text{-}45)$$

with

- o $\left[\right]_V$ computed as previously indicated (it is a constant for a given set of vehicle characteristics).
- o $\overline{\left[\right]}^{12} = \left[\right]^{12} + (\underline{\delta}^T \cdot \underline{\delta}^T E - \underline{\delta}^T \underline{\delta}^T)\tilde{M}^{12} \rightarrow \begin{bmatrix} \overline{A}_T & 0 & 0 \\ 0 & \overline{B}_T & 0 \\ 0 & 0 & C_T \end{bmatrix}_T$

- $\overline{A}_T = A_T + \tilde{M}^{12} (\delta^T)^2$
- $\overline{B}_T = B_T + \tilde{M}^{12} (\delta^T)^2$
- $\frac{d}{dt} [\underline{\rho}^{10} \times \dot{\underline{\delta}}^T + \underline{\delta}^T \times \dot{\underline{\rho}}^{10}]$ defined by Equation (2.1-44)

If the indicated operations of Equation (2.1-45) are carried out, three scalar equations result. These equations can be put in the form:

$$\begin{bmatrix} a_{11} & a_{12} & a_{13} & a_{14} & a_{15} & a_{16} & a_{17} & 0 & a_{19} & a_{1,10} & a_{1,11} \\ a_{12} & a_{22} & a_{23} & 0 & a_{25} & a_{26} & a_{27} & a_{28} & a_{29} & a_{2,10} & a_{2,11} \\ a_{13} & a_{23} & a_{33} & a_{34} & a_{35} & 0 & a_{37} & a_{38} & a_{39} & a_{3,10} & a_{3,11} \end{bmatrix}_B$$

$$[\dot{P} \quad \dot{Q} \quad \dot{R} \quad \ddot{\beta}_1 \quad \ddot{\alpha}_1 \quad \ddot{\beta}_2 \quad \ddot{\alpha}_2 \quad \ddot{\beta}_3 \quad \ddot{\alpha}_3 \quad \ddot{\psi}_2 \quad \ddot{\psi}_1]^T = \begin{bmatrix} M_{EX} + b_1 \\ M_{EY} + b_2 \\ M_{EZ} + b_3 \end{bmatrix} \qquad (2.1\text{-}46)$$

where b_1, b_2, and b_3 consist of all of the terms which involve products of angular rates and M_{EX} M_{EY} and M_{EZ} are the components in the body system of $\underline{M}^E$ defined by Equation (2.1-15). Equations for a_{ij} and b_i are given in Paragraph 2.1.2; computation of M_{EX} M_{EY} and M_{EZ} is discussed in Paragraph 2.1.1.1.4. Matrix Equation (2.1-46) provides the three required equations to compute $\dot{P}$, $\dot{Q}$, and $\dot{R}$ and thus find $\underline{\omega}$.

2.1.1.1.4 External Forces and Torques

In order to complete the definition of equations for computation of $\underline{\omega}$, the external torques, $\underline{L}_O^S$ and $\underline{L}_{O_{12}}^{12}$, and the external forces, $\underline{F}^S$ and $\underline{F}^{12}$, must be made explicit and M^E computed. External torques acting on the LCSE vehicle are due to [7]:

- Gravitational gradient
- Aerodynamic pressure
- Electromagnetic field
- Incident momentum (solar radiation, micrometeorites, cosmic rays, etc.)
- Astronaut motion (Astronauts should theoretically be

considered as moving "parts" within the vehicle. A simplified model has, however, been employed which idealizes astronaut motion torque as external torque and neglects changes in the vehicle's inertia due to the motion.)

However, at synchronous altitudes, all of these torques except those induced by astronaut motion, are of small magnitude and low frequencey and can be neglected. Thus, except for astronaut induced torques, external torques have been assumed zero for simulation purposes. Moments of the forces $\underline{F}^S$ and $\underline{F}^{12}$, as they appear in Equation (2.1-15), have also been neglected (again except for astronaut motion) since they essentially cancel.

To illustrate the correctness of the above remarks, consider the torque induced by the gravitational attraction of the earth (the dominant external force acting on the body). The torque acting on the system, S (all parts except the telescope), due to a spherical earth is, to the first order in the ratio of maximum satellite dimensions to orbit radius [9],

$$G\underline{L}_O^S \cong -\frac{3\mu}{R^3}\frac{\underline{\underline{R}}}{R} \cdot \underline{\underline{I}}^S \times \frac{\underline{\underline{R}}}{R}$$

where

μ = Gravitational constant times mass of the earth = 3.986032×10^{14} m^3/sec^2

$\underline{\underline{I}}^S$ = Inertia dyadic of S about mass centroid, O.

Thus,

$$\left| G\underline{L}_O^S \right| < \frac{3 \times 4 \times 10^{14}}{(4 \times 10^7)^3} \times 4 \times 10^5 = 0.75 \times 10^{-2} \text{ n-m}$$

since $R \cong 42{,}000{,}000$ meters and the maximum component of $\underline{\underline{I}}^S$ is less than 400,000 kg-m^2. Clearly, the gravitational gradient torque on the telescope is even smaller. Also appearing in the definition of $\underline{M}^E$ are the terms:

$$\frac{1}{M}\underline{\rho}^{12} \times [M^{12}\underline{F}^S - (M-M^{12})\underline{F}^{12}].$$

For the earth's gravitation

$$G\underline{F}^S = -\frac{\mu(M-M^{12})}{R^3}\underline{R},$$

$$G\underline{F}^{12} = -\frac{\mu M^{12}}{|\underline{R}+\underline{\rho}^{12}|^3}(\underline{R}+\underline{\rho}^{12}) \cong -\frac{\mu M^{12}}{R^3}\left(1-3\frac{\underline{R}\cdot\underline{\rho}^{12}}{R^2}\right)(\underline{R}+\underline{\rho}^{12})$$

to the first order in $\underline{\rho}^{12}/R$. Thus

$$\frac{1}{M}\,\underline{\rho}^{12}\times\left[M^{12}\,{}_{G}\underline{F}^{S}-(M-M^{12})\,{}_{G}\underline{F}^{12}\right]\cong-\frac{\mu(M-M^{12})M^{12}}{MR^{3}}\,\underline{\rho}^{12}\times\frac{3\underline{R}\cdot\underline{\rho}^{12}}{R^{2}}\,\underline{R}$$

The magnitude of this torque is less than

$$\frac{4\times10^{14}\times2\times10^{3}}{(4\times10^{7})^{3}}\times10\times3\times10=0.325\times10^{-2}\ \text{n-m.}$$

since $(M-M^{12})/M<1$, $M^{12}=2000$ kg, $\rho^{10}\leq 10$ meters.
Thus, gravitational gradient effects are negligible at synchronous altitudes.

Torques due to astronaut motion, unlike the other external torques, can be of appreciable magnitude and frequency. Torques from this source are not, however, amenable to analytical development and are greatly dependent on the type of crew activities performed during the laser pointing experiment. Thus, no general purpose model of astronaut induced torque has been included in the simulation. Rather, available emperical data [1] has been used to simulate torques due to a particular astronaut maneuver (see Figure 2.1-9). In addition, sinusoidal torques of varying frequency and amplitude have been applied to the vehicle during analysis runs to simulate hypothetical external torques.

2.1.1.2 Spacecraft Control

Hardware elements of the spacecraft control system were discussed earlier in this section and shown in Figure 2.1-4. Transfer functions shown in Figure 2.1-4 which contain the Laplace operator, s, must be transformed to difference equations using the Tustin Method (see Paragraph 2.3) to facilitate digital representation of the system. Since the method can only be applied to linear elements, combination of the transfer functions is not possible in most cases. Table 2.1-1 shows the transfer functions as grouped and the corresponding difference equation representation. Formulas for the difference equation coefficients are to be found in Table 2.1-2 with nominal values for the control parameters given in Figure 2.1-4. The remaining elements of the spacecraft control system of Figure 2.1-4 are already suitable for implementation on the digital computer.

In the simulation solution of the spacecraft control equations is performed at 100 cycles per second.

2.1.2 Math Flow

Calculations for the Spacecraft System can be categorized as follows:

1. Calculation of constants for the dynamics and spacecraft

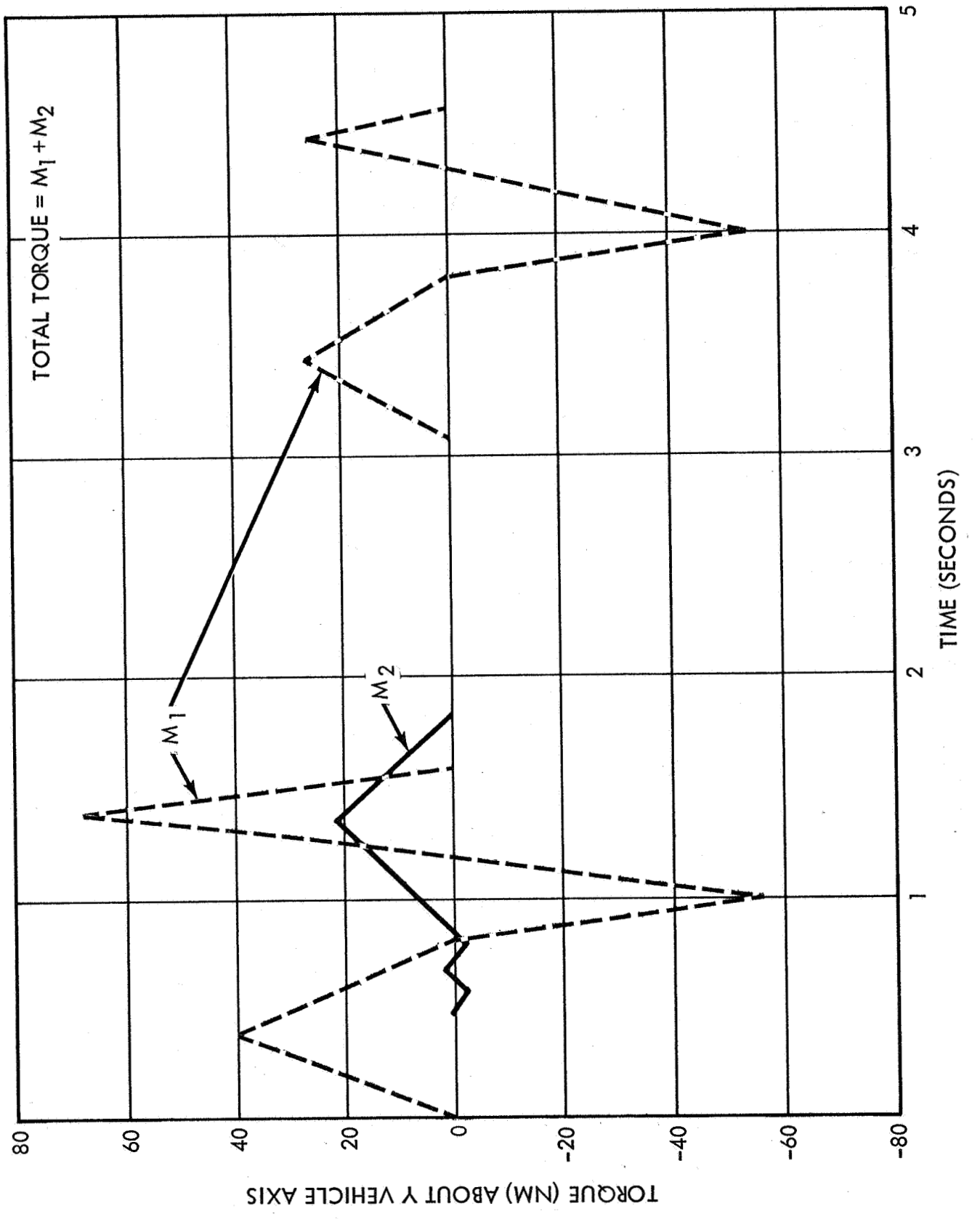

FIGURE 2.1-9 ASTRONAUT MOTION TORQUE

TABLE 2.1-1

SPACECRAFT CONTROL TRANSFER FUNCTION REPRESENTATIONS

TRANSFER FUNCTION	DIFFERENCE EQUATION REPRESENTATION
$\tau_{xp}'/\psi_1 = G_1/(\tau_2 S+1)$	$\tau_{xp}'(nT_S) = C_{10p}[\psi_1(nT_S)+\psi_1((n-1)T_S)]+d_{11}\tau_{xp}'((n-1)T_S)$
$\tau_{yp}'/\psi_2 = G_1/(\tau_2 S+1)$	$\tau_{yp}'(nT_S) = C_{10p}[\psi_2(nT_S)+\psi_2((n-1)T_S)]+d_{11}\tau_{yp}'((n-1)T_S)$
$\tau_{xd}/\psi_1 = G_1\tau_1 S/(\tau_2 S+1)$	$\tau_{xd}(nT_S) = C_{10d}[\psi_1(nT_S)-\psi_1((n-1)T_S)]+d_{11}\tau_{xd}((n-1)T_S)$
$\tau_{yd}/\psi_2 = G_1\tau_1 S/(\tau_2 S+1)$	$\tau_{yd}(nT_S) = C_{10d}[\psi_2(nT_S)-\psi_2((n-1)T_S)]+d_{11}\tau_{xd}((n-1)T_S)$
$\tau_{zp}'/-R = G_{1z}/(\tau_2 S^2+S)$	$\tau_{zp}'(nT_S) = C_{10pz}[R(nT_S)+2R((n-1)T_S)+R((n-2)T_S)]$ $+d_{31}\tau_{zp}'((n-1)T_S)+d_{32}\tau_{zp}'((n-2)T_S)$
$\tau_{zd}/-R = G_{1z}\tau_1/(\tau_2 S+1)$	$\tau_{zd}(nT_S) = C_{10dz}[R(nT_S)+R(n-1)T_S)]+d_{11}\tau_{zd}((n-1)T_S)$
$H_{XBC}/\tau_x = -1/S$	$H_{XBC}(nT_S) = H_{XBC}((n-1)T_S)-[\tau_x(nT_S)+\tau_x((n-1)T_S)]T_S/2$
$H_{YBC}/\tau_y = -1/S$	$H_{YBC}(nT_S) = H_{YBC}((n-1)T_S)-[\tau_y(nT_S)+\tau_y((n-1)T_S)]T_S/2$
$H_{ZBC}/\tau_z = -1/S$	$H_{ZBC}(nT_S) = H_{ZBC}((n-1)T_S)-[\tau_z(nT_S)+\tau_z((n-1)T_S)]T_S/2$
$T_{M\alpha_i}/\dot{\alpha}_{\varepsilon i} = K_{WTA}(\tau_3 S+1)/(\tau_4 S+1)$	$T_{M\alpha_i}(nT_S) = C_{40}\dot{\alpha}_{\varepsilon i}(nT_S)+C_{41}\dot{\alpha}_{\varepsilon i}((n-1)T_S)+d_{41}T_{M\alpha_i}((n-1)T_S)$
$T_{M\beta_i}/\dot{\beta}_{\varepsilon i} = K_{WTB}(\tau_3 S+1)/(\tau_4 S+1)$	$T_{M\beta_i}(nT_S) = C_{50}\dot{\beta}_{\varepsilon i}(nT_S)+C_{51}\dot{\beta}_{\varepsilon i}((n-1)T_S)+d_{41}T_{M\beta_i}((n-1)T_S)$

TABLE 2.1-2

SPACECRAFT CONTROL DIFFERENCE EQUATION COEFFICIENTS

$$C_{10p} = G_1 T_S/(T_S+2\tau_2)$$

$$C_{10d} = 2\tau_1 G_1/(T_S+2\tau_2)$$

$$C_{10pz} = -T_S^2 G_{1z}/(2(T_S+2\tau_2)$$

$$c_{10dz} = -T_S G_{1z}\tau_1/(T_S+2\tau_2)$$

$$d_{11} = (2\tau_2-T_S)/(T_S+2\tau_2)$$

$$d_{31} = 4\tau_2/(T_S+2\tau_2)$$

$$d_{32} = (T_S-2\tau_2)/(T_S+2\tau_2)$$

$$C_{40} = K_{WTA}(2\tau_3+T_S)/(2\tau_4+T_S)$$

$$C_{41} = K_{WTA}(T_S-2\tau_3)/(2\tau_4+T_S)$$

$$C_{50} = K_{WTB}(2\tau_3+T_S)/(2\tau_4+T_S)$$

$$C_{51} = K_{WTB}(T_S-2\tau_3)/(2\tau_4+T_S)$$

$$d_{41} = (2\tau_4-T_S)/(2\tau_4+T_S)$$

control equations which are a function of vehicle configuration-dependent data.

2. Evaluation of spacecraft control equations (find the motor torques which drive the CMG gimbals).

3. Evaluation of CMG dynamics equations (find the angular accelerations, velocities, and positions of the CMG gimbals).

4. Evaluation of telescope dynamics equations (find the angular accelerations, velocities, and positions of the telescope and its gimbals).

5. Evaluation of spacecraft dynamics equations (find the angular acceleration and velocity of the spacecraft),

Figure 2.1-10 illustrates functionally the calculations under Category 1. The detailed equations are shown in Table 2.1-3. The quantities computed have been discussed previously in this section.

Figure 2.1-11 shows functionally the calculations required for spacecraft control simulation. The corresponding equations are given in Table 2.1-4.

The CMG, telescope, and spacecraft dynamics calculations are shown in Figures 2.1-12, 13, 14. The detailed equations comprising the math models appear in Tables 2.1-5, 6, 7. The notation employed in the math model requires some explanation.

Equations 2.1-27, 28, 29, 30, 31, 32, 38, 39, 46 provide the eleven differential equations which must be solved to find β_i, α_i, ψ_2, ψ_1, P, Q, and R. To obtain these quantities in the digital simulation, the accelerations $\ddot{\beta}_i$, $\ddot{\alpha}_i$, $\ddot{\psi}_2$, $\ddot{\psi}_1$, $\dot{P}$, $\dot{Q}$, and $\dot{R}$ are computed for each time step, and then the required angular rates and positions are obtained by integration. Thus, the eleven fundamental differential equations are rewritten in the form*:

*Note that the matrix structure reflects symmetry in the equations of motion wherever applicable.

$$\begin{bmatrix} a_{11} & a_{12} & a_{13} & a_{14} & a_{15} & a_{16} & a_{17} & 0 & a_{19} & a_{1,10} & a_{1,11} \\ a_{12} & a_{22} & a_{23} & 0 & a_{25} & a_{26} & a_{27} & a_{28} & a_{29} & a_{2,10} & a_{2,11} \\ a_{13} & a_{23} & a_{33} & a_{34} & a_{35} & 0 & a_{37} & a_{38} & a_{39} & a_{3,10} & a_{3,11} \\ a_{14} & 0 & a_{34} & a_{44} & 0 & 0 & 0 & 0 & 0 & 0 & 0 \\ a_{15} & a_{25} & a_{35} & 0 & a_{55} & 0 & 0 & 0 & 0 & 0 & 0 \\ a_{16} & a_{26} & 0 & 0 & 0 & a_{44} & 0 & 0 & 0 & 0 & 0 \\ a_{17} & a_{27} & a_{37} & 0 & 0 & 0 & a_{77} & 0 & 0 & 0 & 0 \\ 0 & a_{28} & a_{38} & 0 & 0 & 0 & 0 & a_{44} & 0 & 0 & 0 \\ a_{19} & a_{29} & a_{39} & 0 & 0 & 0 & 0 & 0 & a_{99} & 0 & 0 \\ 0 & a_{10,2} & a_{10,3} & 0 & 0 & 0 & 0 & 0 & 0 & a_{10,10} & 0 \\ a_{11,1} & a_{11,2} & a_{11,3} & 0 & 0 & 0 & 0 & 0 & 0 & 0 & a_{11,1} \end{bmatrix} \begin{bmatrix} \dot{P} \\ \dot{Q} \\ \dot{R} \\ \ddot{\beta}_1 \\ \ddot{\alpha}_1 \\ \ddot{\beta}_2 \\ \ddot{\alpha}_2 \\ \ddot{\beta}_3 \\ \ddot{\alpha}_3 \\ \ddot{\psi}_2 \\ \ddot{\psi}_1 \end{bmatrix}$$

$$= [b_1+M_{EX},\ b_2+M_{EY},\ b_3+M_{EZ},\ B_4,\ B_5,\ B_6,\ B_7,\ B_8,\ B_9,\ B_{10},\ B_{11}]^T \qquad (2.1\text{-}46)$$

where

$$B_4 = b_4+M_{\beta_1}$$

$$B_5 = b_5+M_{\alpha_1}$$

$$B_6 = b_6+M_{\beta_2}$$

$$B_7 = b_7+M_{\alpha_2}$$

$$B_8 = b_8+M_{\beta_3}$$

$$B_9 = b_9+M_{\alpha_3}$$

$$B_{10} = b_{10}+M_{T_2} - K_f\psi_2$$

$$B_{11} = b_{11}+M_{T_1} - K_f\psi_1$$

with b_i representing the cross-coupling torques. The accelerations can be obtained by inversion of the 11 by 11 matrix, A.

To reduce computational requirements, an alternate solution approach, which provides the required accuracy, has been adopted.

Note that the last eight rows of the matrix in Equation (2.1-46) lead to equations which can be solved for $\ddot{\beta}_i$, $\ddot{\alpha}_i$ $\ddot{\psi}_2$, $\ddot{\psi}_1$ in terms of $\dot{P}$, $\dot{Q}$, $\dot{R}$. For example,

$$\ddot{\beta}_2 = (B_6 - a_{16}\dot{P} - a_{26}\dot{Q})/a_{44}$$

$$\ddot{\psi}_1 = (B_{11} - a_{11,2}\dot{Q} - a_{11,3}\dot{R})/a_{11,1} - \dot{P} \qquad (2.1\text{-}47)$$

This process is carried out for each of the eight accelerations $\ddot{\beta}_1$, $\ddot{\alpha}_1$, $\ddot{\beta}_2$, $\ddot{\alpha}_2$, $\ddot{\beta}_3$, $\ddot{\alpha}_3$, $\ddot{\psi}_2$, $\ddot{\psi}_1$. The results are substituted into the first three equations derived from Equation (2.1-46). This yields three equations of which the following is one:

$$\begin{aligned}
&(a_{11} - a_{14}^2/a_{44} - a_{15}^2/a_{55} - a_{16}^2/a_{44} - a_{17}^2/a_{77} - a_{19}^2/a_{99} - a_{1,11})\dot{P} \\
&+ (a_{12} - a_{15}a_{25}/a_{55} - a_{16}a_{26}/a_{44} - a_{17}a_{27}/a_{77} - a_{29}a_{19}/a_{99} \\
&- a_{1,10}a_{10,2}/a_{10,10} - a_{1,11}a_{11,2}/a_{11,1})\dot{Q} + (a_{13} - a_{14}a_{34}/a_{44} \\
&- a_{15}a_{35}/a_{55} - a_{37}a_{17}/a_{77} - a_{19}a_{39}/a_{99} - a_{1,10}a_{10,3}/a_{10,10} \\
&- a_{1,11}a_{11,3}/a_{11,1})\dot{R} = M_{EX} + b_1 - [B_4 a_{14}/a_{44} + B_5 a_{15}/a_{55} \\
&+ B_6 a_{16}/a_{44} + B_7 a_{17}/a_{77} + B_9 a_{19}/a_{99} + B_{10} a_{1,10}/a_{10,10} + B_{11} a_{1,11}/a_{11,1}]
\end{aligned}$$

The three equations so derived can be rewritten as

$$\begin{bmatrix} a'_{11} & a'_{12} & a'_{13} \\ a'_{21} & a'_{22} & a'_{23} \\ a'_{31} & a'_{32} & a'_{33} \end{bmatrix} \begin{bmatrix} \dot{P} \\ \dot{Q} \\ \dot{R} \end{bmatrix} = \begin{bmatrix} B_1 \\ B_2 \\ B_3 \end{bmatrix} \qquad (2.1\text{-}48)$$

The method of solution of the dynamics equations involves the following steps:

1. Solve Equation (2.1-48) for $\dot{P}$, $\dot{Q}$, $\dot{R}$, by inverting the 3 x 3 Matrix A'.

2. Substitute values of $\dot{P}$, $\dot{Q}$, $\dot{R}$, obtained in Step 1 into equations of the type (2.1-47) to obtain values for $\ddot{\beta}_i$, $\ddot{\alpha}_i$, $\ddot{\psi}_2$, $\ddot{\psi}_1$.

3. Integrate the angular accelerations from Steps 1 and 2 to obtain the necessary velocities and positions.

Dynamics equations for the CMG, telescope, and spacecraft are all solved at 100 cycles per second.

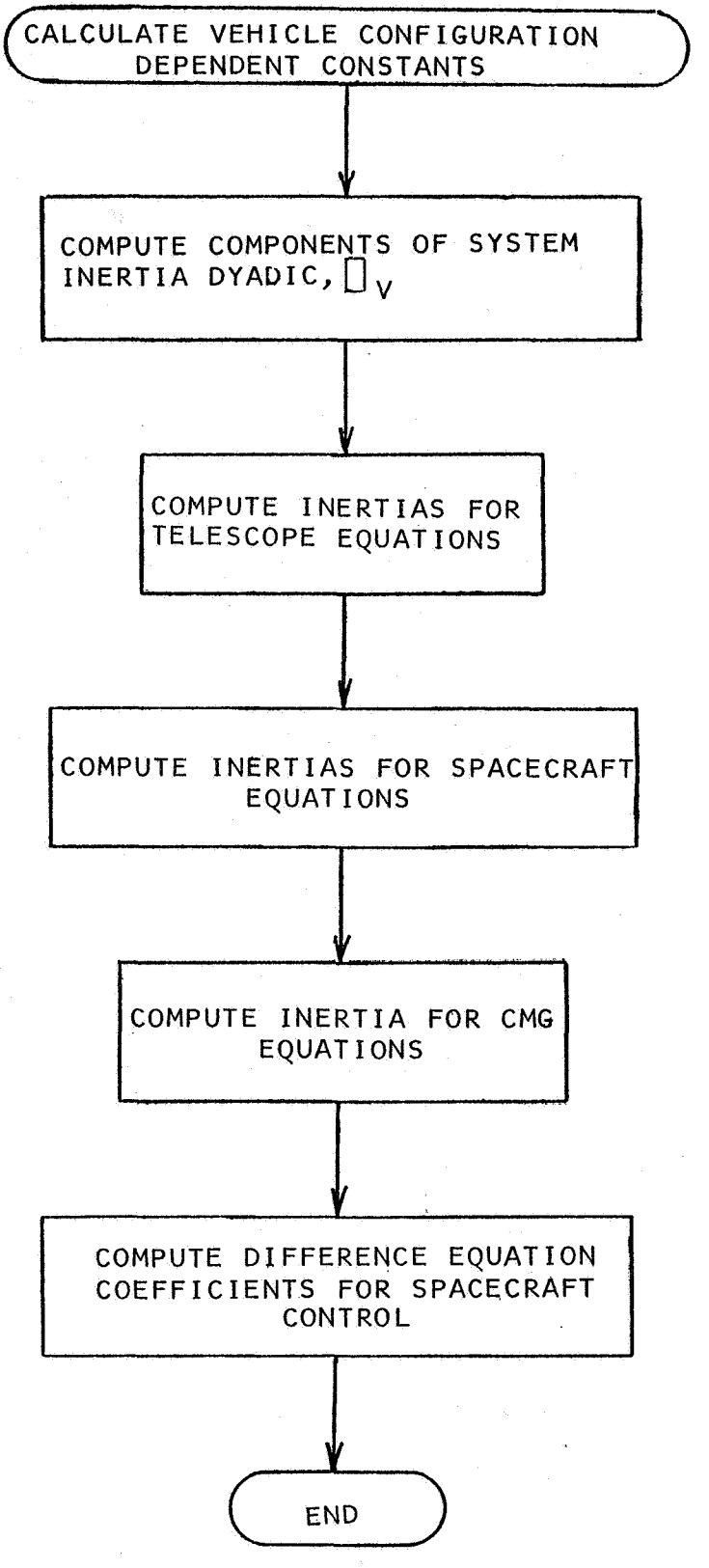

FIGURE 2.1-10 SPACECRAFT SYSTEM INITIALIZATION MATH FLOW

TABLE 2.1-3

SPACECRAFT SYSTEM INITIALIZATION - DETAILED EQUATIONS

Compute Components of System Inertia Dyadic, $\Box_V$

$$I_{xx} = I'_{xx} + \sum_{i=0}^{11} M^i[(\rho_2^i)^2+(\rho_3^i)^2]+\tilde{M}^{12}[(\rho_2^{10})^2+(\rho_3^{10})^2]$$

$$I_{yy} = I'_{yy} + \sum_{i=0}^{11} M^i[(\rho_1^i)^2+(\rho_3^i)^2]+\tilde{M}^{12}[(\rho_1^{10})^2+(\rho_3^{10})^2]$$

$$I_{zz} = I'_{zz} + \sum_{i=0}^{11} M^i[(\rho_1^i)^2+(\rho_2^i)^2]+\tilde{M}^{12}[(\rho_1^{10})^2+(\rho_2^{10})^2]$$

$$I_{xy} = I'_{xy} + \sum_{i=0}^{11} M^i\rho_1^i\rho_2^i + \tilde{M}^{12}\rho_1^{10}\rho_2^{10}$$

$$I_{xz} = I'_{xz} + \sum_{i=0}^{11} M^i\rho_1^i\rho_3^i + \tilde{M}^{12}\rho_1^{10}\rho_3^{10}$$

$$I_{yz} = I'_{yz} + \sum_{i=0}^{11} M^i\rho_2^i\rho_3^i + \tilde{M}^{12}\rho_2^{10}\rho_3^{10}$$

Compute Inertias for Telescope Equation

$$\tilde{A}_T = A_T + (\delta^T)^2 M^{11} M^{12}/(M^{11}+M^{12})$$

$$\tilde{B}_T = B_T + (\delta^T)^2 M^{11} M^{12}/(M^{11}+M^{12})$$

$$a_{10,10} = \tilde{B}_T + B_I$$

Compute Inertias for Spacecraft Equations

$$\bar{A}_T = A_T + \tilde{M}^{12}(\delta^T)^2$$

$$\bar{B}_T = B_T + \tilde{M}^{12}(\delta^T)^2$$

Compute Inertia for CMG Equations

$$a_{44} = B_g + C_b + N_G^2 J_{mr}$$

Compute Difference Equation Coefficients for Spacecraft Control

See Table 2.1-2 for equations.

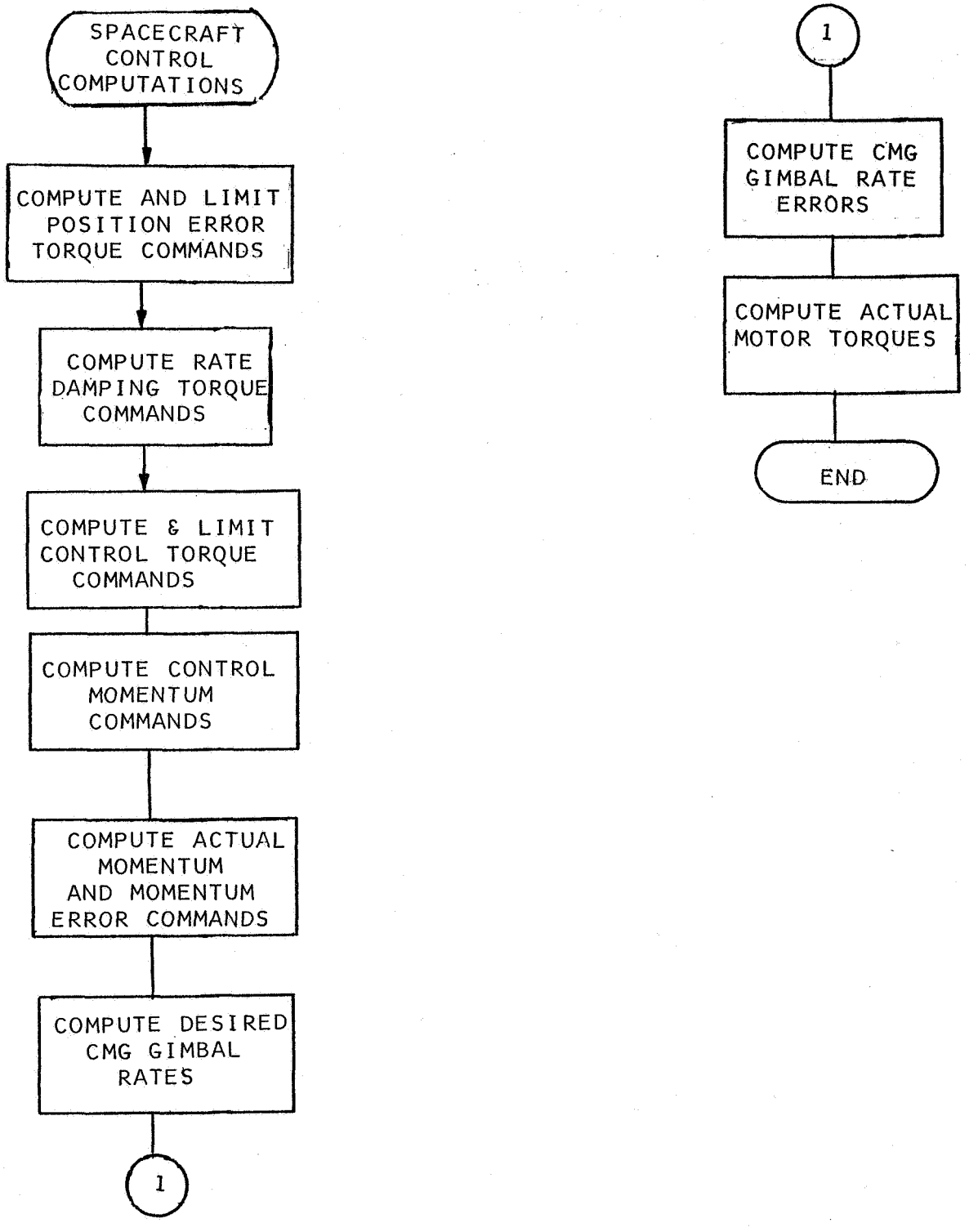

FIGURE 2.1-11 SPACECRAFT CONTROL MATH FLOW

TABLE 2.1-4

SPACECRAFT CONTROL SYSTEM - DETAILED MATH FLOW

Compute and Limit Position Error Torque Commands

$$\tau'_{xp}(nT_s) = C_{10p}[\psi_1(nT_s) + \psi_1((n-1)T_s)] + d_{11}\,\tau'_{xp}((n-1)T_s)$$

$$\tau_{xp}(nT_s) = \text{sgn}[\tau'_{xp}(nT_s)]\ \min\{|\tau'_{xp}(nT_s)|,\ \text{CMGPLM}\}$$

$$\tau'_{yp}(nT_s) = C_{10p}[\psi_2(nT_s) + \psi_2((n-1)T_s)] + d_{11}\,\tau'_{yp}((n-1)T_s)$$

$$\tau_{yp}(nT_s) = \text{sgn}[\tau'_{yp}(nT_s)]\ \min\{|\tau'_{yp}(nT_s)|,\ \text{CMGPLM}\}$$

$$\tau'_{zp}(nT_s) = C_{10pz}[R(nT_s) + 2R((n-1)T_s) + R((n-2)T_s)] + d_{31}\,\tau'_{zp}((n-1)T_s) + d_{32}\,\tau'_{zp}((n-2)T_s)$$

$$\tau_{zp}(nT_s) = \text{sgn}[\tau'_{zp}(nT_s)]\ \min\{|\tau'_{zp}(nT_s)|,\ \text{CMGPLM}\}$$

Compute Rate Damping Torque Commands

$$\tau_{xd}(nT_s) = C_{10d}[\psi_1(nT_s) - \psi_1((n-1)T_s)] + d_{11}\,\tau_{xd}((n-1)T_s)$$

$$\tau_{yd}(nT_s) = C_{10d}[\psi_2(nT_s) - \psi_2((n-1)T_s)] + d_{11}\,\tau_{yd}((n-1)T_s)$$

$$\tau_{zd}(nT_s) = C_{10dz}[R(nT_s) + R((n-1)T_s)] + d_{11}\,\tau_{zd}((n-1)T_s)$$

TABLE 2.1-4

SPACECRAFT CONTROL SYSTEM - DETAILED MATH FLOW (CONT.)

Compute and Limit Control Torque Commands

$$\tau'_x(nT_s) = \tau_{xp}(nT_s) + \tau_{xd}(nT_s)$$

$$\tau_x(nT_s) = \text{sgn}[\tau'_x(nT_s)]\ \min\{\tau'_x(nT_s),\ CMGCLM\}$$

$$\tau'_y(nT_s) = \tau_{yp}(nT_s) + \tau_{yd}(nT_s)$$

$$\tau_y(nT_s) = \text{sgn}[\tau'_y(nT_s)]\ \min\{\tau'_y(nT_s),\ CMGCLM\}$$

$$\tau'_z(nT_s) = \tau_{zp}(nT_s) + \tau_{zd}(nT_s)$$

$$\tau_z(nT_s) = \text{sgn}[\tau_z(nT_s)]\ \min\{\tau'_z(nT_s),\ CMGCLM\}$$

Compute Control Momentum Commands

$$H_{xBC}(nT_s) = H_{xBC}((n-1)T_s) - T_S/2[\tau_x(nT_s) + \tau_x((n-1)T_s)]$$

$$H_{yBC}(nT_s) = H_{yBC}((n-1)T_s) - T_S/2[\tau_y(nT_s) + \tau_y((n-1)T_s)]$$

$$H_{zBC}(nT_s) = H_{zBC}((n-1)T_s) - T_S/2[\tau_z(nT_s) + \tau_z((n-1)T_s)]$$

Compute Actual Momentum and Momentum Error Commands

$$H_{xBA}(nT_s) = H_1\cos\beta_1\cos\alpha_1 - H_2\cos\beta_2\sin\alpha_2 + H_3\sin\beta_3$$

$$H_{yBA}(nT_s) = H_1\sin\beta_1 + H_2\cos\beta_2\cos\alpha_2 - H_3\cos\beta_3\sin\alpha_3$$

$$H_{zBA}(nT_s) = -H_1\cos\beta_1\sin\alpha_1 + H_2\sin\beta_2 + H_3\cos\beta_3\cos\alpha_3$$

$$H_{ExB}(nT_s) = H_{xBC}(nT_s) - H_{xBA}(nT_s)$$

$$H_{EyB}(nT_s) = H_{yBC}(nT_s) - H_{yBA}(nT_s)$$

$$H_{EzB}(nT_s) = H_{zBC}(nT_s) - H_{zBA}(nT_s)$$

TABLE 2.1-4

SPACECRAFT CONTROL SYSTEM - DETAILED MATH FLOW (CONT.)

Compute and Limit Desired CMG Gimbal Rates

$$\dot{\alpha}'_{c1}(nT_s) = K_{SL}[-\sin\alpha_1 H_{ExB}(nT_s) - \cos\alpha_1 H_{EzB}(nT_s)]$$

$$\dot{\alpha}'_{c2}(nT_s) = K_{SL}[-\cos\alpha_2 H_{ExB}(nT_s) - \sin\alpha_2 H_{EyB}(nT_s)]$$

$$\dot{\alpha}'_{c3}(nT_s) = K_{SL}[-\cos\alpha_3 H_{EyB}(nT_s) - \sin\alpha_3 H_{EzB}(nT_s)]$$

$$\dot{\beta}'_{c1}(nT_s) = K_{SL}[-\cos\alpha_1 \sin\beta_1 H_{ExB}(nT_s) + \cos\beta_1 H_{EyB}(nT_s) + \sin\beta_1 \sin\alpha_1 H_{EzB}(nT_s)]$$

$$\dot{\beta}'_{c2}(nT_s) = K_{SL}[\sin\beta_2 \sin\alpha_2 H_{ExB}(nT_s) - \cos\alpha_2 \sin\beta_2 H_{EyB}(nT_s) + \cos\beta_2 H_{EzB}(nT_s)]$$

$$\dot{\beta}'_{c3}(nT_s) = K_{SL}[\cos\beta_3 H_{ExB}(nT_s) + \sin\beta_3 \sin\alpha_3 H_{EyB}(nT_s) - \cos\alpha_3 \sin\beta_3 H_{EzB}(nT_s)]$$

$$\left.\begin{aligned}\dot{\alpha}_{ci}(nT_s) &= \operatorname{sgn}[\dot{\alpha}'_{ci}(nT_s)] \min\{4.55, |57.3\,\dot{\alpha}'_{ci}(nT_s)|\} \\ \dot{\beta}_{ci}(nT_s) &= \operatorname{sgn}[\dot{\beta}'_{ci}(nT_s)] \min\{4.55, |57.3\,\dot{\beta}'_{ci}(nT_s)|\}\end{aligned}\right\} \quad i = 1,2,3$$

Compute CMG Gimbal Rate Errors

$$\left.\begin{aligned}\dot{\alpha}_{\varepsilon i}(nT_s) &= \dot{\alpha}_{ci}(nT_s) - G_{CMG2}\,\dot{\alpha}_i(nT_s) \\ \dot{\beta}_{\varepsilon i}(nT_s) &= \dot{\beta}_{ci}(nT_s) - G_{CMG2}\,\dot{\beta}_i(nT_s)\end{aligned}\right\} \quad i = 1,2,3$$

TABLE 2.1-4

SPACECRAFT CONTROL SYSTEM - DETAILED MATH FLOW (CONT.)

Compute Actual Motor Torques

$$
\left.
\begin{aligned}
T_{M\alpha_i}(nT_s) &= C_{40}\,\dot{\alpha}_{\varepsilon i}(nT_s) + C_{41}\,\dot{\alpha}_{\varepsilon i}((n-1)T_s) + d_{41}\,T_{M\alpha_i}((n-1)T_s) \\
T_{M\beta_i}(nT_s) &= C_{50}\,\dot{\beta}_{\varepsilon_i}(nT_s) + C_{51}\,\dot{\beta}_{\varepsilon_i}((n-1)T_s) + d_{41}\,T_{M\beta_i}((n-1)T_s) \\
M'_{\alpha i}(nT_s) &= T_{M\alpha_i}(nT_s) + G_{cc}\,\dot{\beta}_i\,((n-1)T_s) \\
M'_{\beta i}(nT_s) &= T_{M\beta_i}(nT_s) - G_{CC}\,\dot{\alpha}_i\,((n-1)T_s) \\
M_{\alpha_i} &= G_{CMG3}\,\mathrm{sgn}[M'_{\alpha_i}(nT_s)]\,\min\{0.34,\ |M'_{\alpha_i}(nT_s)|\} \\
M_{\beta_i} &= G_{CMG3}\,\mathrm{sgn}[M'_{\beta_i}(nT_s)]\,\min\{0.34,\ |M'_{\beta_i}(nT_s)|\}
\end{aligned}
\right\} \quad i=1,2,3
$$

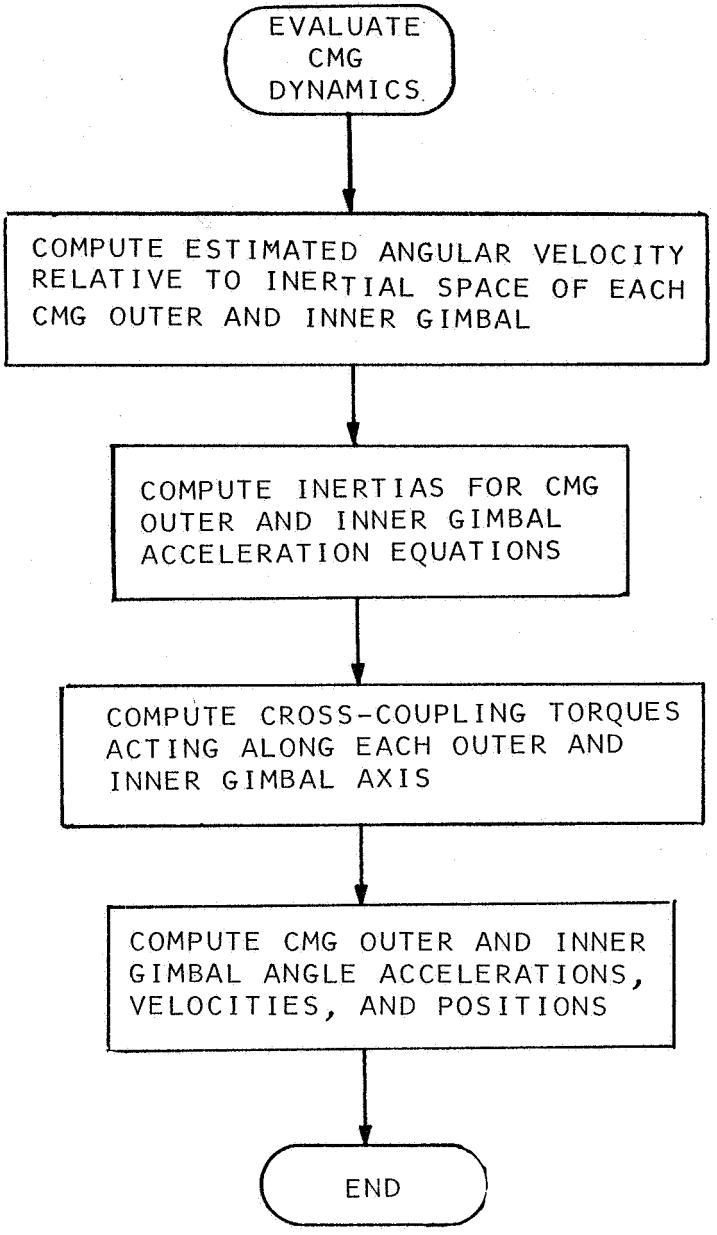

FIGURE 2.1-12 CMG DYNAMICS MATH FLOW

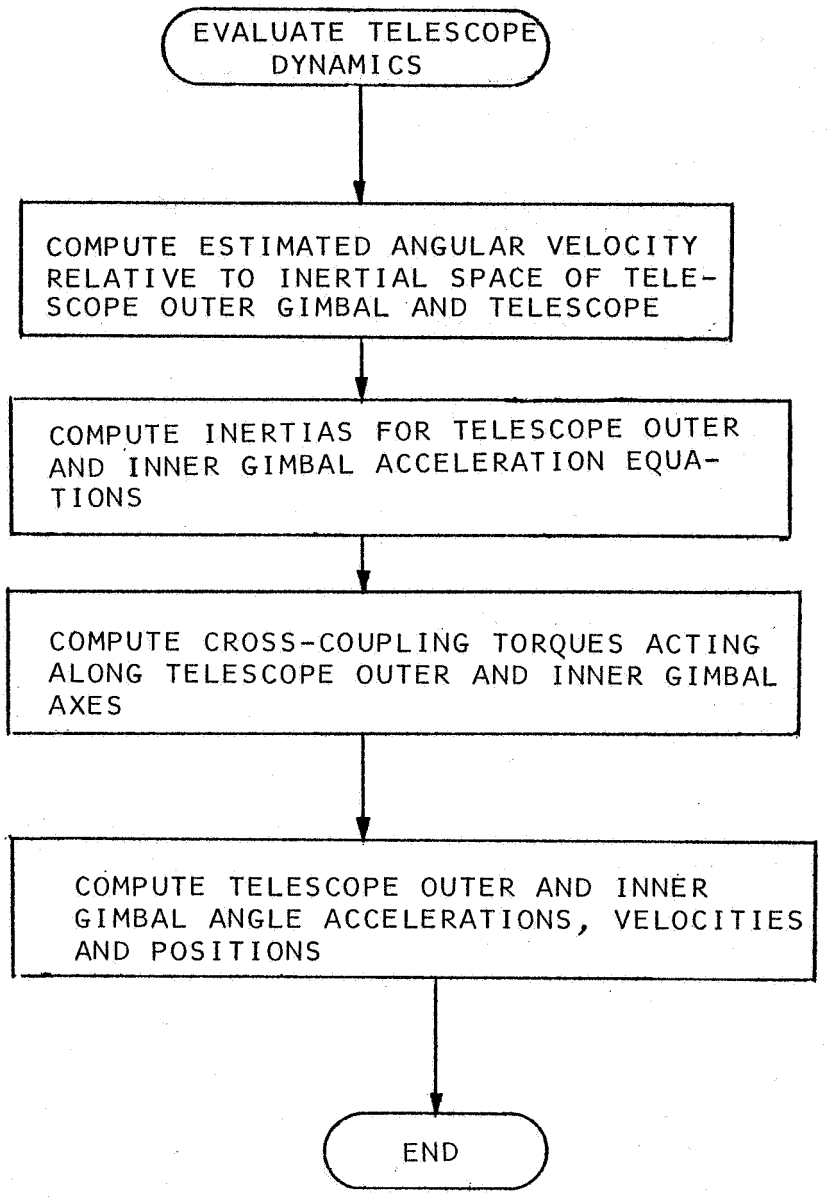

FIGURE 2.1-13 EXPERIMENT PACKAGE (TELESCOPE) DYNAMICS MATH FLOW

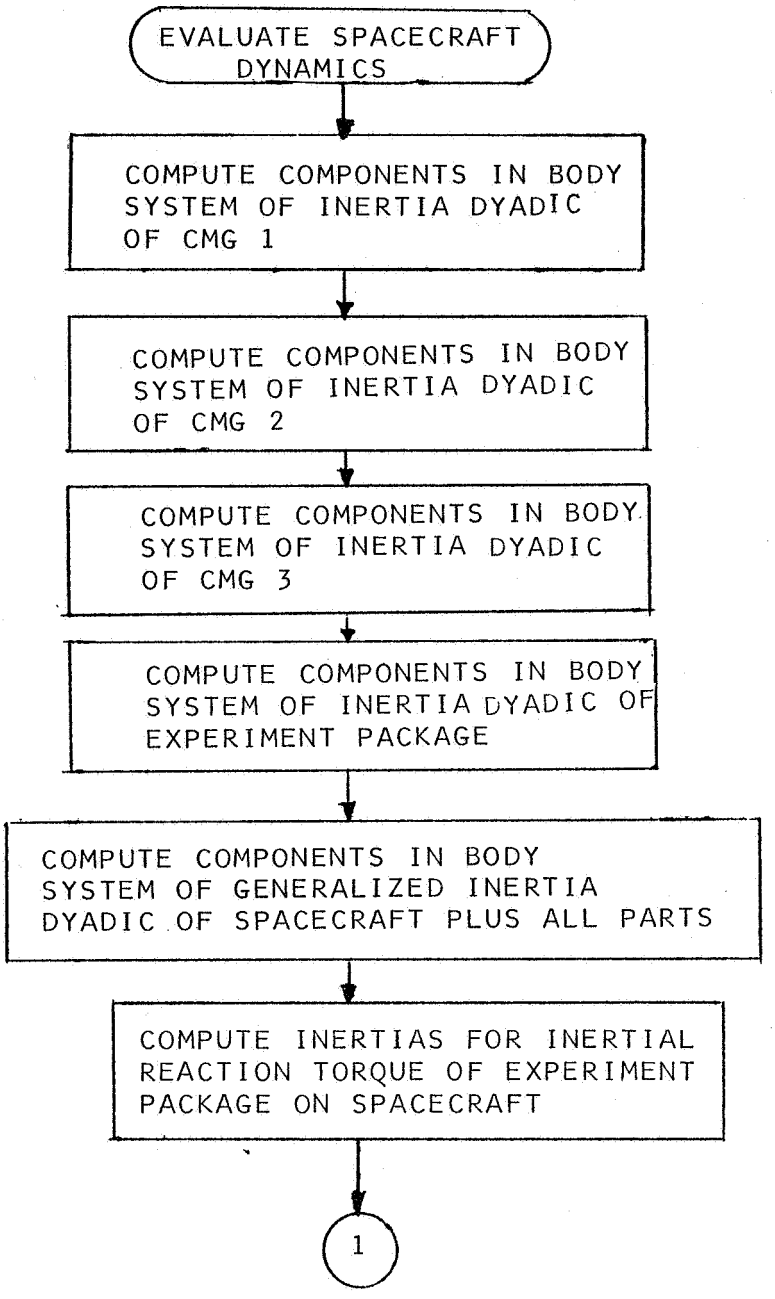

FIGURE 2.1-14 SPACECRAFT DYNAMICS MATH FLOW

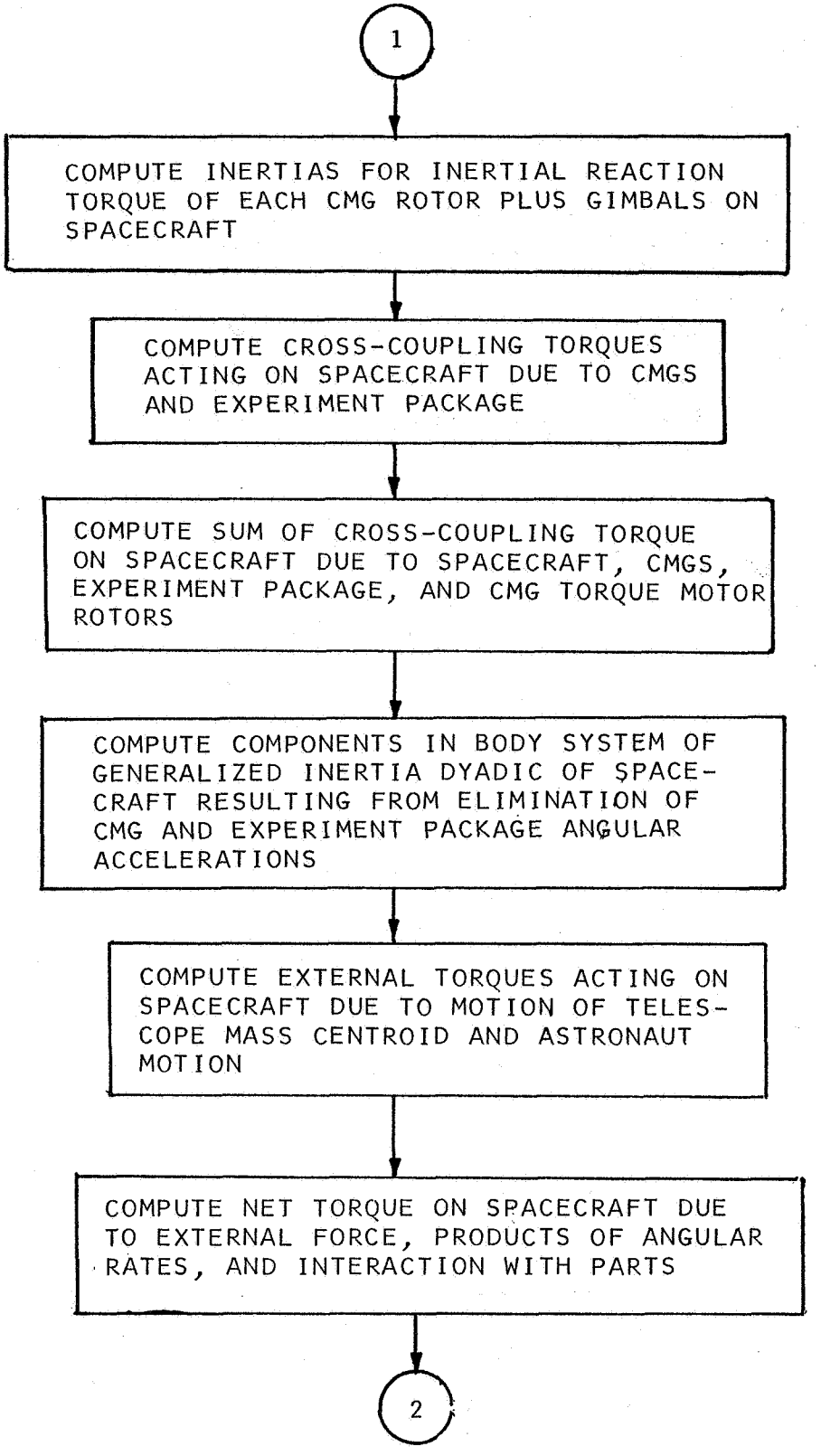

FIGURE 2.1-14 (CONT.) SPACECRAFT DYNAMICS MATH FLOW

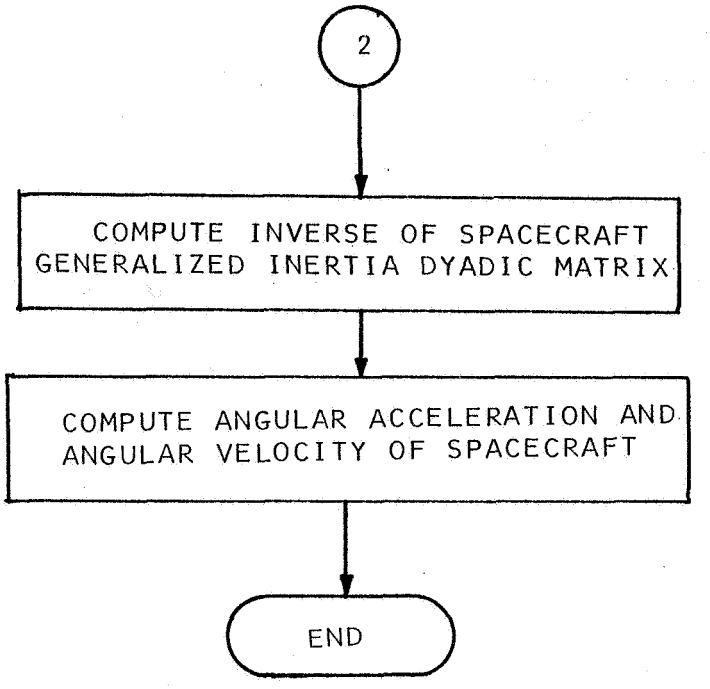

FIGURE 2.1-14 (CONT.) SPACECRAFT DYNAMICS MATH FLOW

TABLE 2.1-5 CMG DYNAMICS - DETAILED MATH FLOW

COMPUTE ESTIMATED ANGULAR VELOCITY RELATIVE TO INERTIAL SPACE OF EACH CMG OUTER AND INNER GIMBAL

$$\omega_{1x}' = P\cos\alpha_1 - R\sin\alpha_1$$

$$\omega_{1y}' = Q + \dot{\alpha}_1$$

$$\omega_{1z}' = P\sin\alpha_1 + R\cos\alpha_1$$

$$\omega_{2x}' = P\cos\alpha_2 + Q\sin\alpha_2$$

$$\omega_{2y}' = -P\sin\alpha_2 + Q\cos\alpha_2$$

$$\omega_{2z}' = R + \dot{\alpha}_2$$

$$\omega_{3x}' = P + \dot{\alpha}_3$$

$$\omega_{3y}' = Q\cos\alpha_3 + R\sin\alpha_3$$

$$\omega_{3z}' = -Q\sin\alpha_3 + R\cos\alpha_3$$

$$\omega_{1x} = \omega_{1x}' \cos\beta_1 + \omega_{1y}' \sin\beta_1$$

$$\omega_{1y} = -\omega_{1x}' \sin\beta_1 + \omega_{1y}' \cos\beta_1$$

$$\omega_{1z} = \omega_{1z}' + \dot{\beta}_1$$

$$\omega_{2x} = \omega_{2x}' + \dot{\beta}_2$$

$$\omega_{2y} = \omega_{2y}' \cos\beta_2 + \omega_{2z}' \sin\beta_2$$

$$\omega_{2z} = -\omega_{2y}' \sin\beta_2 + \omega_{2z}' \cos\beta_2$$

$$\omega_{3x} = \omega_{3x}' \cos\beta_3 - \omega_{3z}' \sin\beta_3$$

$$\omega_{3y} = \omega_{3y}' + \dot{\beta}_3$$

$$\omega_{3z} = \omega_{3x}' \sin\beta_3 + \omega_{3z}' \cos\beta_3$$

TABLE 2.1-5 (CONTINUED)

COMPUTE INERTIAS FOR CMG OUTER AND INNER GIMBAL ACCELERATION EQUATIONS

$$a_{25} = (A_b+A_g)\sin^2\beta_1 + (B_b+B_g)\cos^2\beta_1 + B_a+N_GJ_{mr}$$

$$a_{37} = (A_b+A_g)\sin^2\beta_2 + (B_b+B_g)\cos^2\beta_2 + B_a+N_GJ_{mr}$$

$$a_{19} = (A_b+A_g)\sin^2\beta_3 + (B_b+B_g)\cos^2\beta_3 + B_a+N_GJ_{mr}$$

$$a_{14} = (C_b+B_g+N_GJ_{mr})\sin\alpha_1$$

$$a_{34} = (C_b+B_g+N_GJ_{mr})\cos\alpha_1$$

$$a_{15} = (A_b+A_g - B_b-B_g)\cos\alpha_1 \sin\beta_1 \cos\beta_1$$

$$a_{35} = -(A_b+A_g - B_b-B_g)\sin\alpha_1 \sin\beta_1 \cos\beta_1$$

$$a_{16} = (B_g+C_b+N_GJ_{mr})\cos\alpha_2$$

$$a_{26} = (B_g+C_b+N_GJ_{mr})\sin\alpha_2$$

$$a_{17} = -(A_g+A_b - B_g-B_b)\sin\alpha_2 \sin\beta_2 \cos\beta_2$$

$$a_{27} = (A_g+A_b - B_g-B_b)\cos\alpha_2 \sin\beta_2 \cos\beta_2$$

$$a_{28} = (B_g+C_b+N_GJ_{mr})\cos\alpha_3$$

$$a_{38} = (B_g+C_b+N_GJ_{mr})\sin\alpha_3$$

$$a_{29} = -(A_g+A_b - B_g-B_b)\sin\alpha_3 \sin\beta_3 \cos\beta_3$$

$$a_{39} = (A_g+A_b - B_g-B_b)\cos\alpha_3 \sin\beta_3 \cos\beta_3$$

$$a_{55} = a_{25} + N_GJ_{mr}(N_G-1)$$

$$a_{77} = a_{37} + N_GJ_{mr}(N_G-1)$$

$$a_{99} = a_{19} + N_GJ_{mr}(N_G-1)$$

TABLE 2.1-5 (CONTINUED)

COMPUTE CROSS-COUPLING TORQUES ACTING ALONG EACH OUTER AND INNER GIMBAL AXIS

$$B_4 = M_{\beta_1} - (B_g+C_b+N_G J_{mr})\dot{\alpha}_1\,\omega_{1x}' + [(A_g+A_b - B_g-B_b)\omega_{1x} + H_1]\omega_{1y}$$

$$B_5 = M_{\alpha_i} + (C_a-A_a)\omega_{1x}'\,\omega_{1z}' + (\omega_{1z}'+N_G\dot{\beta}_1)\omega_{1x}'\,J_{mr}$$
$$+(A_b+A_g)\,(\dot{\alpha}_1\omega_{1z}'\sin\beta_1\cos\beta_1 - \dot{\beta}_1\,\omega_{1y}\sin\beta_1 - \omega_{1x}\,\omega_{1z}\cos\beta_1)$$
$$+(B_g+B_b)\,(-\dot{\alpha}_1\omega_{1z}'\sin\beta_1\cos\beta_1 + \omega_{1x}\,\dot{\beta}_1\cos\beta_1)$$
$$+(B_b-C_b)\,\omega_{1y}\omega_{1z}\sin\beta_1 + [(B_g+C_b)\omega_{1x} - H_1]\omega_{1z}\cos\beta_1$$

$$B_6 = M_{\beta_2} - (B_g+C_b+N_G J_{mr})\dot{\alpha}_2\,\omega_{2y}' + [(A_g+A_b - B_g-B_b)\omega_{2y} + H_2]\omega_{2z}$$

$$B_7 = M_{\alpha_2} + (C_a-A_a)\,\omega_{2x}'\,\omega_{2y}' + (A_b+A_g)\,(\dot{\alpha}_2\,\omega_{2x}'\sin\beta_2\cos\beta_2$$
$$-\dot{\beta}_2\,\omega_{2z}\sin\beta_2 - \omega_{2y}\,\omega_{2x}\cos\beta_2) + (B_g+B_b)\,(\omega_{2y}\dot{\beta}_2\cos\beta_2$$
$$-\dot{\alpha}_2\,\omega_{2x}'\sin\beta_2\cos\beta_2) + (B_b-C_b)\,\omega_{2z}\,\omega_{2x}\sin\beta_2$$
$$+[(B_g+C_b)\,\omega_{2y} - H_2]\,\omega_{2x}\cos\beta_2 + (\omega_{2x}' + N_G\,\dot{\beta}_2)\,\omega_{2y}'\,J_{mr}$$

$$B_8 = M_{\beta_3} - (B_g+C_b+N_G J_{mr})\dot{\alpha}_3\omega_{3z}' + [(A_g+A_b - B_g-B_b)\omega_{3z} + H_3]\omega_{3x}$$

$$B_9 = M_{\alpha_3} + (C_a-A_a)\,\omega_{3z}'\,\omega_{3y}' + (A_g+A_b)\,(\dot{\alpha}_3\,\omega_{3y}'\sin\beta_3\cos\beta_3$$
$$-\dot{\beta}_3\,\omega_{3x}\sin\beta_3 - \omega_{3z}\omega_{3y}\cos\beta_3) + (\omega_{3y}'+N_G\dot{\beta}_3)\omega_{3z}'\,J_{mr}$$
$$+(B_g+B_b)\,(-\dot{\alpha}_3\,\omega_{3y}'\sin\beta_3\cos\beta_3 + \omega_{3z}\,\dot{\beta}_3\cos\beta_3)$$
$$+(B_b-C_b)\,\omega_{3x}\omega_{3y}\sin\beta_3 + [(B_g+C_b)\,\omega_{3z} - H_3]\,\omega_{3y}\cos\beta_3$$

TABLE 2.1-5 (CONTINUED)

COMPUTE CMG OUTER AND INNER GIMBAL ANGLE ACCELERATIONS, VELOCITIES, AND POSITIONS

$$\ddot{\beta}_1(nT_s) = (B_4 - a_{14}\dot{P} - a_{34}\dot{R})/a_{44}$$

$$\ddot{\alpha}_1(nT_s) = (B_5 - a_{15}\dot{P} - a_{25}\dot{Q} - a_{35}\dot{R})/a_{55}$$

$$\ddot{\beta}_2(nT_s) = (B_6 - a_{16}\dot{P} - a_{26}\dot{Q})/a_{44}$$

$$\ddot{\alpha}_2(nT_s) = (B_7 - a_{17}\dot{P} - a_{27}\dot{Q} - a_{37}\dot{R})/a_{77}$$

$$\ddot{\beta}_3(nT_s) = (B_8 - a_{28}\dot{Q} - a_{38}\dot{R})/a_{44}$$

$$\ddot{\alpha}_3(nT_s) = (B_9 - a_{19}\dot{P} - a_{29}\dot{Q} - a_{39}\dot{R})/a_{99}$$

$$\left.\begin{aligned}
\dot{\beta}_i(nT_s) &= \dot{\beta}_i((n-1)T_s) + \int_{(n-1)T_s}^{nT_s} \ddot{\beta}_i \, dt \\
\dot{\alpha}_i(nT_s) &= \dot{\alpha}_i((n-1)T_s) + \int_{(n-1)T_s}^{nT_s} \ddot{\alpha}_i \, dt \\
\beta_i(nT_s) &= \beta_i((n-1)T_s) + \int_{(n-1)T_s}^{nT_s} \dot{\beta}_i \, dt \\
\alpha_i(nT_s) &= \alpha_i((n-1)T_s) + \int_{(n-1)T_s}^{nT_s} \dot{\alpha}_i \, dt
\end{aligned}\right\} \quad i = 1,2,3$$

TABLE 2.1-6 TELESCOPE DYNAMICS - DETAILED MATH FLOW

Compute Estimated Angular Velocity Relative to Inertial Space of Telescope Outer Gimbal and Telescope

$$\omega_{4x}' = P + \dot{\psi}_1$$

$$\omega_{4y}' = Q\cos\psi_1 + R\sin\psi_1$$

$$\omega_{4z}' = -Q\sin\psi_1 + R\cos\psi_1$$

$$\omega_{4x} = \omega_{4x}' \cos\psi_2 - \omega_{4z}' \sin\psi_2$$

$$\omega_{4y} = \omega_{4y}' + \dot{\psi}_2$$

$$\omega_{4z} = \omega_{4x}' \sin\psi_2 + \omega_{4z}' \cos\psi_2$$

Compute Inertias for Telescope Outer and Inner Gimbal Acceleration Equations

$$a_{10\,2} = (\tilde{B}_T + B_I) \cos \psi_1$$

$$a_{10\,3} = (\tilde{B}_T + B_I) \sin \psi_1$$

$$a_{11\,1} = (\tilde{A}_T + A_I) \cos^2 \psi_2 + (C_T + C_I) \sin^2 \psi_2 + A_O$$

$$a_{11\,2} = (\tilde{A}_T + A_I - C_T - C_I) \sin \psi_1 \sin \psi_2 \cos \psi_2$$

$$a_{11\,3} = (C_T + C_I - \tilde{A}_T - A_I) \cos \psi_1 \sin \psi_2 \cos \psi_2$$

Compute Cross-Coupling Torques Acting Along Telescope Outer and Inner Gimbal Axes

$$b_{10} = [(\tilde{B}_T + B_I) \dot{\psi}_1 \omega_{4z}' + (\tilde{A}_T + A_I - C_T - C_I) \omega_{4z} \omega_{4x}]$$

$$\begin{aligned} b_{11} = -\{&(C_O - B_O) \omega_{4z}' \omega_{4y}' - (C_T + C_I - \tilde{A}_T - A_I)\dot{\psi}_1 \omega_{4y}' \\ &\sin \psi_2 \cos \psi_2 + [(C_T + C_I) \omega_{4x} \sin \psi_2 - \\ &(\tilde{A}_T + A_I) \omega_{4z} \cos \psi_2]\dot{\psi}_2 + [(C_T + C_I - \tilde{B}_T - B_I)\omega_{4z} \cos \psi_2 \\ &+(\tilde{B}_T + B_I - \tilde{A}_T - A_I)\omega_{4x} \sin \psi_2]\omega_{4y}\} \end{aligned}$$

TABLE 2.1-6 (CONTINUED)

Compute Telescope Outer and Inner Gimbal Angles Accelerations, Velocities and Positions

$$\ddot{\psi}_2(kT_T) = [-a_{10,2}\dot{Q} - a_{10,3}\dot{R} - K_f\psi_2 + M_{T_2} + b_{10}]/a_{10,10}$$

$$\ddot{\psi}_1(kT_T) = -\dot{P} + [-a_{11,2}\dot{Q} - a_{11,3}\dot{R} - K_f\psi_1 + M_{T_1} + b_{11}]/a_{11,1}$$

$$\dot{\psi}_2(kT_T) = \dot{\psi}_2((k-1)T_T) + \int_{(k-1)T_T}^{kT_T} \ddot{\psi}_2 dt$$

$$\dot{\psi}_1(kT_T) = \dot{\psi}_1((k-1)T_T) + \int_{(k-1)T_T}^{kT_T} \ddot{\psi}_1 dt$$

$$\psi_2(kT_T) = \psi_2((k-1)T_T) + \int_{(k-1)T_T}^{kT_T} \dot{\psi}_2 dt$$

$$\psi_1(kT_T) = \psi_1((k-1)T_T) + \int_{(k-1)T_T}^{kT_T} \dot{\psi}_1 dt$$

TABLE 2.1-7 SPACECRAFT DYNAMICS - DETAILED MATH FLOW

Compute Components in Body System of Inertia Dyad of CMG 1

$$AA1_{11} = [(A_g+A_b)\cos^2\beta_1 + (B_g+B_b)\sin^2\beta_1 + A_a]\cos^2\alpha_1 + (B_g+C_b+C_a)\sin^2\alpha_1$$

$$AA1_{12} = (A_g+A_b - B_g-B_b)\sin\beta_1 \cos\beta_1 \cos\alpha_1$$

$$AA1_{13} = -[(A_g+A_b)\cos^2\beta_1 + (B_g+B_b)\sin^2\beta_1 + A_a-C_a - B_g-C_b]\sin\alpha_1 \cos\alpha_1$$

$$AA1_{22} = (A_g+A_b)\sin^2\beta_1 + (B_g+B_b)\cos^2\beta_1 + B_a$$

$$AA1_{23} = -(A_g+A_b - B_g-B_b)\sin\alpha_1 \sin\beta_1 \cos\beta_1$$

$$AA1_{33} = [(A_g+A_b)\cos^2\beta_1 + (B_g+B_b)\sin^2\beta_1]\sin^2\alpha_1 + (B_g+C_b)\cos^2\alpha_1 + A_a \sin^2\alpha_1 + C_a \cos^2\alpha_1$$

Compute Components in Body System of Inertia Dyad of CMG 2

$$AA2_{11} = [(A_g+A_b)\cos^2\beta_2 + (B_g+B_b)\sin^2\beta_2]\sin^2\alpha_2 + (B_g+C_b)\cos^2\alpha_2 + A_a \sin^2\alpha_2 + C_a \cos^2\alpha_2$$

$$AA2_{12} = -[(A_g+A_b)\cos^2\beta_2 + (B_g+B_b)\sin^2\beta_2 - B_g-C_b + A_a-C_a]\sin\alpha_2 \cos\alpha_2$$

$$AA2_{13} = -(A_g+A_b - B_g-B_b)\sin\beta_2 \cos\beta_2 \sin\alpha_2$$

$$AA2_{22} = [(A_g+A_b)\cos^2\beta_2 + (B_g+B_b)\sin^2\beta_2]\cos^2\alpha_2 + (B_g+C_b)\sin^2\alpha_2 + A_a \cos^2\alpha_2 + C_a \sin^2\alpha_2$$

$$AA2_{23} = (A_g+A_b - B_g-B_b)\sin\beta_2 \cos\beta_2 \cos\alpha_2$$

$$AA2_{33} = (A_g+A_b)\sin^2\beta_2 + (B_g+B_b)\cos^2\beta_2 + B_a$$

TABLE 2.1-7 (CONTINUED)

Compute Components in Body System of Inertia Dyad of CMG 3

$$AA3_{11} = (A_g+A_b)\sin^2\beta_3 + (B_g+B_b)\cos^2\beta_3 + B_a$$

$$AA3_{12} = -(A_g+A_b - B_g-B_b)\sin\alpha_3 \sin\beta_3 \cos\beta_3$$

$$AA3_{13} = (A_g+A_b - B_g-B_b)\cos\alpha_3 \sin\beta_3 \cos\beta_3$$

$$AA3_{22} = [(A_g+A_b)\cos^2\beta_3 + (B_g+B_b)\sin^2\beta_3]\sin^2\alpha_3 + (B_g+C_b)\cos^2\alpha_3 + A_a \sin^2\alpha_3 + C_a \cos^2\alpha_3$$

$$AA3_{23} = -[(A_g+A_b)\cos^2\beta_3 + (B_g+B_b)\sin^2\beta_3 - B_g-C_b+A_a-C_a]\sin\alpha_3 \cos\alpha_3$$

$$AA3_{33} = [(A_g+A_b)\cos^2\beta_3 + (B_g+B_b)\sin^2\beta_3]\cos^2\alpha_3 + (B_g+C_b)\sin^2\alpha_3 + A_a \cos^2\alpha_3 + C_a \sin^2\alpha_3$$

Compute Components in Body System of Inertia Dyad of Experiment Package

$$AA4_{11} = A_0+(\bar{A}_T+A_I)\cos^2\psi_2 + (C_T+C_I)\sin^2\psi_2$$

$$AA4_{12} = (\bar{A}_T+A_I - C_T-C_I)\sin\psi_1 \sin\psi_2 \cos\psi_2$$

$$AA4_{13} = (C_T+C_I - \bar{A}_T-A_I)\cos\psi_1 \sin\psi_2 \cos\psi_2$$

$$AA4_{22} = B_0 \cos^2\psi_1 + C_0 \sin^2\psi_1 + (\bar{B}_T+B_I)\cos^2\psi_1 + [(\bar{A}_T+A_I)\sin^2\psi_2 + (C_T+C_I\cos^2\psi_2] \sin^2\psi_1$$

$$AA4_{23} = [B_0-C_0 +\bar{B}_T+B_I - (\bar{A}_T+A_I)\sin^2\psi_2 - (\bar{C}_T+C_I)\cos^2\psi_2]\cos\psi_1 \sin\psi_1$$

$$AA4_{33} = B_0 \sin^2\psi_1 + C_0 \cos^2\psi_1 + (\bar{B}_T+B_I)\sin^2\psi_1 + [(\bar{A}_T+A_I)\sin^2\psi_2 + (C_T+C_I)\cos^2\psi_2] \cos^2\psi_1$$

TABLE 2.1-7 (CONTINUED)

Compute Components in Body System of Generalized Inertia Dyad of Spacecraft Plus All Parts

$$a_{11} = I_{xx} + AA1_{11} + AA2_{11} + AA3_{11} + AA4_{11} + 2(\delta_2\rho_2^{10} + \delta_3\rho_3^{10})\tilde{M}^{12}$$

$$a_{12} = -I_{xy} + AA1_{12} + AA2_{12} + AA3_{12} + AA4_{12} - (\delta_2\rho_1^{10} + \delta_1\rho_2^{10})\tilde{M}^{12}$$

$$a_{13} = -I_{xz} + AA1_{13} + AA2_{13} + AA3_{13} + AA4_{13} - (\delta_3\rho_1^{10} + \delta_1\rho_3^{10})\tilde{M}^{12}$$

$$a_{22} = I_{yy} + AA1_{22} + AA2_{22} + AA3_{22} + AA4_{22} + 2(\delta_1\rho_1^{10} + \delta_3\rho_3^{10})\tilde{M}^{12}$$

$$a_{23} = -I_{yz} + AA1_{23} + AA2_{23} + AA3_{23} + AA4_{23} - (\delta_3\rho_2^{10} + \delta_2\rho_3^{10})\tilde{M}^{12}$$

$$a_{33} = I_{zz} + AA1_{33} + AA2_{33} + AA3_{33} + AA4_{33} + 2(\delta_1\rho_1^{10} + \delta_2\rho_2^{10})\tilde{M}^{12}$$

Compute Inertias for Inertial Reaction Torque of Experiment Package on Spacecraft

$$a_{1,10} = -\delta_1(\rho_2^{10}\cos\psi_1 + \rho_3^{10}\sin\psi_1)\tilde{M}^{12}$$

$$a_{2,10} = +[(\delta_1\rho_1^{10} + \delta_3\rho_3^{10})\cos\psi_1 - \delta_2\rho_3^{10}\sin\psi_1]\tilde{M}^{12} + (\bar{B}_T + B_I)\cos\psi_1$$

$$a_{3,10} = -[\delta_3\rho_2^{10}\cos\psi_1 - (\delta_1\rho_1^{10} + \delta_2\rho_2^{10})\sin\psi_1]\tilde{M}^{12} + (\bar{B}_T + B_I)\sin\psi_1$$

$$a_{1,11} = +(\delta_2\rho_2^{10} + \delta_3\rho_3^{10})\tilde{M}^{12} + A_O + (\bar{A}_T + A_I)\cos^2\psi_2 + (C_T + C_I)\sin^2\psi_2$$

$$a_{2,11} = -\delta_2\rho_1^{10}\tilde{M}^{12} + (\bar{A}_T + A_I - C_T - C_I)\sin\psi_1\sin\psi_2\cos\psi_2$$

$$a_{3,11} = -\delta_3\rho_1^{10}\tilde{M}^{12} + (C_T + C_I - \bar{A}_T - A_I)\cos\psi_1\sin\psi_2\cos\psi_2$$

Compute Inertias for Inertial Reaction Torque of Each CMG Rotor Plus Gimbals on Spacecraft

The required inertias are a_{14}, a_{15}, a_{16}, a_{17}, a_{19}, a_{25}, a_{26}, a_{27}, a_{28}, a_{29}, a_{34}, a_{35}, a_{37}, a_{38}, and a_{39}. All were computed previously for the CMG dynamics.

TABLE 2.1-7 (CONTINUED)

Compute Cross-Coupling Torques Acting on Spacecraft Due to CMGs and Experiment Package

Define functions F_1, F_2, F_3 by:

$$F_1(CA, CB, SA, SB, \dot{A}, \dot{B}, C_x, C_y, C_z, D_x, D_y, D_z, H) =$$

$$[(A_g+A_b)CB^2 + (B_g+B_b)SB^2]\dot{A}\, D_z\, CA - [(A_g+A_b)C_y CB +$$

$$(B_g+B_b)C_x SB]\dot{B}\, CA + \{(B_b-C_b)C_y\, CB + [(A_b+A_g - B_b-B_g)C_x+H]SB\}\, C_z\, CA$$

$$+(A_a\, D_z\, CA - C_a\, D_x\, SA)\dot{A} + [(B_a-C_a)D_z\, CA + (A_a-B_a)D_x\, SA]D_y$$

$$-(B_g+C_b)\dot{A}\, D_x\, SA + [(A_g+A_b - B_g-B_b)C_x+H]C_y\, SA$$

$$F_2(CA, CB, SA, SB, \dot{A}, \dot{B}, C_x, C_y, C_z, D_x, D_y, D_z, H)=$$

$$-\{(A_a-C_a)D_x\, D_z + (B_b+B_g - A_b-A_g)\dot{A}\, D_z\, SB\, CB$$

$$+[(A_g+A_b)C_y\, SB - (B_g+B_b)C_x\, CB]\dot{B} + (C_b-B_b)C_z\, C_y\, SB$$

$$+ [(A_g+A_b - B_g-C_b)C_x+H]CB\, C_z\}$$

$$F_3(CA, CB, SA, SB, \dot{A}, \dot{B}, C_x, C_y, C_z, D_x, D_y, D_z, H)=$$

$$-\{(A_a\, DZ\, SA + C_a\, D_x\, CA)\dot{A} + [(B_a-C_a)D_z\, SA + (B_a-A_a)D_x\, CA]D_y$$

$$+ [(A_g+A_b)CB^2 + (B_g+B_b)SB^2]\dot{A}\, D_z\, SA - [(A_g+A_b)C_y\, CB$$

$$+ (B_g+B_b)C_x\, SB]\dot{B}\, SA + (B_b-C_b)C_y\, C_z\, CB\, SA$$

$$- [(B_g+C_b - A_g-A_b)C_x - H]C_z\, SA\, SB + (B_g+C_b)\dot{A}\, D_x\, CA$$

$$+ [(B_a+B_b - A_g-A_b)C_x - H]C_y\, CA\}$$

Then

$$A_1^1 = F_1(\cos\alpha_1, \cos\beta_1, \sin\alpha_1, \sin\beta_1, \dot{\alpha}_1, \dot{\beta}_1, \omega_{1x}, \omega_{1y}, \omega_{1z},$$
$$\omega_{1x}', \omega_{1y}', \omega_{1z}', H_1)$$

$$A_2^1 = F_2(\text{Argument same as } A_1^1)$$

$$A_3^1 = F_3(\text{Argument same as } A_1^1)$$

$$A_1^2 = F_3(\cos\alpha_2, \cos\beta_2, \sin\alpha_2, \sin\beta_2, \dot{\alpha}_2, \dot{\beta}_2, \omega_{2y}, \omega_{2z}, \omega_{2x},$$
$$\omega_{2y}', \omega_{2z}', \omega_{2x}', H_2)$$

TABLE 2.1-7 (CONTINUED)

$$A_2^2 = F_1(\text{Argument same as } A_1^2)$$

$$A_3^2 = F_2(\text{Argument same as } A_1^2)$$

$$A_1^3 = F_2(\cos\alpha_3,\ \cos\beta_3,\ \sin\alpha_3,\ \sin\beta_3,\ \dot{\alpha}_3,\ \dot{\beta}_3,\ \omega_{3z},\ \omega_{3x},\ \omega_{3y},\ \omega_{3z}',\ \omega_{3x}'\ \omega_{3y}',\ H_3)$$

$$A_2^3 = F_3(\text{Argument same as } A_1^3)$$

$$A_3^3 = F_1(\text{Argument same as } A_1^3)$$

$$A_1^4 = -\{(C_O-B_O)\omega_{4z}'\ \omega_{4y}' - (C_T+C_I - \bar{A}_T-A_I)\dot{\psi}_1\ \omega_{4y}'\ \sin\psi_2\ \cos\psi_2 + [(C_T+C_I)\omega_{4x}\ \sin\psi_2 - (\bar{A}_T+A_I)\omega_{4z}\ \cos\psi_2]\dot{\psi}_2 + [(C_T+C_I - \bar{B}_T-B_I)\ \omega_{4z}\ \cos\psi_2 + (\bar{B}_T+B_I - \bar{A}_T-A_I)\omega_{4x}\sin\psi_2]\omega_{4y}\}$$

$$A_2^4 = -\{(B_O\ \omega_{4z}'\ \cos\psi_1 + C_O\ \omega_{4y}'\ \sin\psi_1)\dot{\psi}_1 + [(A_O-C_O)\omega_{4z}'\ \cos\psi_1 + (A_O-B_O)\omega_{4y}'\ \sin\psi_1]\omega_{4x}' + (\bar{B}_T+B_I)\dot{\psi}_1\ \omega_{4z}'\ \cos\psi_1 + (\bar{A}_T+A_I - C_T-C_I)\omega_{4z}\ \omega_{4x}\ \cos\psi_1 + [(\bar{A}_T+A_I)\sin^2\psi_2 + (C_T+C_I)\cos^2\psi_2]\dot{\psi}_1\ \omega_{4y}'\ \sin\psi_1 - [(C_T+C_I)\omega_{4x}\ \cos\psi_2 + (\bar{A}_T+A_I)\omega_{4z}\ \sin\psi_2]\dot{\psi}_2\ \sin\psi_1 + [(\bar{A}_T+A_I\ -\bar{B}_T-B_I)\omega_{4x}\ \cos\psi_2 + (C_T+C_I - \bar{B}_T-B_I)\omega_{4z}\ \sin\psi_2]\omega_{4y}\ \sin\psi_1\}$$

$$A_3^4 = -\{(B_O\ \omega_{4z}'\ \sin\psi_1 - C_O\ \omega_{4y}'\ \cos\psi_1)\dot{\psi}_1 + [(A_O-C_O)\omega_{4z}'\ \sin\psi_1 + (B_O-A_O)\omega_{4y}'\ \cos\psi_1]\ \omega_{4x}' + (\bar{B}_T+B_I)\dot{\psi}_1\ \omega_{4z}'\ \sin\psi_1 + (\bar{A}_T+A_I - C_T-C_I)\omega_{4z}\ \omega_{4x}\ \sin\psi_1 - (\bar{A}_T+A_I)\sin^2\psi_2 + (C_T+C_I)\cos^2\psi_2]\dot{\psi}_1\ \omega_{4y}'\ \cos\psi_1 + [(C_T+C_I)\omega_{4x}\ \cos\psi_2 + (\bar{A}_T+A_I)\omega_{4z}\ \sin\psi_2]\dot{\psi}_2\ \cos\psi_1 + [(\bar{B}_T+B_I - \bar{A}_T-A_I)\omega_{4x}\ \cos\psi_2 + (\bar{B}_T+B_I - C_T-C_I)\omega_{4z}\ \sin\psi_2]\omega_{4y}\ \cos\psi_1\}$$

TABLE 2.1-7 (CONTINUED)

Compute Sum of Cross-Coupling Torques on Spacecraft Due to Spacecraft, CMGs, Experiment Package, and CMG Torque Motor Rotors

$$b_1 = -\{I_{yz}(R^2-Q^2) + (I_{zz}-I_{yy})QR + (I_{xy}R-I_{xz}Q)P\} + \sum_{i=1}^{4} A_1^i + J_{mr}$$
$$\{[(Q+N_G\dot{\alpha}_1)\omega_{1z}' - (\omega_{1z}'+N_G\dot{\beta}_1)\omega_{1y}']\cos\alpha_1 - [Q+(N_G+1)\dot{\alpha}_1]\omega_{1x}' \sin\alpha_1$$
$$+ [-(R+N_G\dot{\alpha}_2)\omega_{2x}' + (\omega_{2x}'+N_G\dot{\beta}_2)\omega_{2z}']\sin\alpha_2$$
$$- [R+(N_G+1)\dot{\alpha}_2]\omega_{2y}' \cos\alpha_2 + (\omega_{3y}'+N_G\dot{\beta}_3)\omega_{3z}'\}$$

$$b_2 = -\{I_{xz}(P^2-R^2) + (I_{xx}-I_{zz})PR + (I_{yz}P-I_{xy}R)Q\} + \sum_{i=1}^{4} A_2^i +$$
$$J_{mr}\{(\omega_{1z}'+N_G\dot{\beta}_1)\omega_{1x}' - [R+(N_G+1)\dot{\alpha}_2]\omega_{2y}' \sin\alpha_2 +$$
$$[(R+N_G\dot{\alpha}_2)\omega_{2x}' - (\omega_{2x}'+N_G\dot{\beta}_2)\omega_{2z}']\cos\alpha_2 +$$
$$[(\omega_{3y}'+N_G\dot{\beta}_3)\omega_{3x}' - (P+N_G\dot{\alpha}_3)\omega_{3y}']\sin\alpha_3 -$$
$$[P+(N_G+1)\dot{\alpha}_3]\omega_{3z}' \cos\alpha_3\}$$

$$b_3 = -\{I_{xy}(Q^2-P^2) + (I_{yy}-I_{xx})PQ + (I_{xz}Q-I_{yz}P)R\} + \sum_{i=1}^{4} A_3^i +$$
$$J_{mr}\{[(Q+N_G\dot{\alpha}_1)\omega_{1z}' + (\omega_{1z}'+N_G\dot{\beta}_1)\omega_{1y}']\sin\alpha_1 -$$
$$[Q+(N_G+1)\dot{\alpha}_1]\omega_{1x}' \cos\alpha_1 + (\omega_{2x}'+N_G\dot{\beta}_2)\omega_{2y}'$$
$$+[(P+N_G\dot{\alpha}_3)\omega_{3y}' - (\omega_{3y}'+N_G\dot{\beta}_3)\omega_{3x}']\cos\alpha_3$$
$$-[P+(N_G+1)\dot{\alpha}_3]\omega_{3z}' \sin\alpha_3\}$$

Compute Components in Body System of Generalized Inertia Dyad of Spacecraft Resulting from Elimination of CMG and Experiment Package Angular Accelerations

$$a_{11}' = a_{11} - \frac{a_{19}^2}{a_{99}} - a_{1,11} - a_{15}^2/a_{55} - a_{17}^2/a_{77} - (a_{14}^2 + a_{16}^2)/a_{44}$$

$$a_{12}' = a_{12} - \frac{a_{15}a_{25}}{a_{55}} - \frac{a_{29}a_{19}}{a_{99}} - a_{16}a_{26}/a_{44} - a_{17}a_{27}/a_{77} - a_{1,10}a_{10,2}/a_{10\,10} - a_{1,11}a_{11,2}/a_{11,1}$$

$$a_{13} \quad a_{13} - \frac{a_{17}a_{37}}{a_{77}} - \frac{a_{39}a_{19}}{a_{99}} - a_{14}a_{34}/a_{44} - a_{15}a_{35}/a_{55} - a_{1,10}a_{10,3}/a_{10,10} - a_{1,11}a_{11,3}/a_{11,1}$$

TABLE 2.1-7 (CONTINUED)

$$a'_{21} = a'_{12} + a_{1,10}a_{10,2}/a_{10,10} + a_{1,11}a_{11,2}/a_{11,1} - a_{2,11}$$

$$a'_{22} \quad a_{22} - \frac{a_{25}^2}{a_{55}} - (a_{26}^2 + a_{28}^2)/a_{44} - a_{27}^2/a_{77} - a_{29}^2/a_{99}$$
$$-a_{2,10}a_{10,12}/a_{10,10} - a_{2,11}a_{11,2}/a_{11,1}$$

$$a'_{23} = a_{23} - \frac{a_{35}a_{25}}{a_{55}} - \frac{a_{27}a_{37}}{a_{77}} - a_{28}a_{38}/a_{44} - a_{29}a_{39}/a_{99}$$
$$-a_{2,10}a_{10,3}/a_{10,10} - a_{2,11}a_{11,3}/a_{11,1}$$

$$a'_{31} \quad a_{13}' + a_{1,10}a_{10,3}/a_{10,10} + a_{1,11}a_{11,3}/a_{11,1} - a_{3,11}$$

$$a_{32}' = a_{23}' + (a_{2,10}a_{10,3} - a_{3,10}a_{10,2})/a_{10\,10} + (a_{2,11}a_{11,3} - a_{11,2}a_{3,11})/a_{11\,1}$$

$$a_{33}' = a_{33} - (a_{34}^2 + a_{38}^2)/a_{44} - a_{35}^2/a_{55} - \frac{a_{37}^2}{a_{77}} - a_{39}^2/a_{99}$$
$$- a_{3,10}a_{10,3}/a_{10,10} - a_{3,11}a_{11,3}/a_{11,1}$$

Compute External Torques Acting on Spacecraft

$$\begin{bmatrix} M_{EX} \\ M_{EY} \\ M_{EZ} \end{bmatrix} = \underline{L}_O^S + \underline{L}_{O_{12}}^{12} - \frac{1}{M}\underline{\rho}^{12} \times [M^{12}\underline{F}^S - (M-M^{12})\underline{F}^{12}]$$

with moments and forces given by empirical astronaut motion data.

Compute Net Torque on Spacecraft Due to External Force, Products of Angular Rates, and Interaction with Parts

$$B_1 = M_{EX} + b_1 - \{[a_{14}B_4 + a_{16}B_6]/a_{44} + \frac{a_{15}}{a_{55}}B_5$$
$$+a_{17}/a_{77}\,B_7 + \frac{a_{19}}{a_{99}}B_9 + a_{1,10}/a_{10,10}(M_{T_2} - K_f\psi_2 + b_{10})$$
$$+a_{1,11}/a_{11,1}\,(M_T - K_f\psi_1 + b_{11})\}$$

TABLE 2.1-7 (CONTINUED)

$$B_2 = M_{EY} + b_2 - \{\frac{a_{25}}{a_{55}} B_5 + [a_{26} B_6 + a_{28} B_8]/a_{44} + a_{27}/a_{77} B_7 + a_{29}/a_{99} B_9 + a_{2,10}/a_{10,10} (M_{T_2} - K_f \psi_2 + b_{10}) + a_{2,11}/a_{11} (M_{T_1} - K_f \psi_1 + b_{11})\}$$

$$B_3 = M_{EZ} + b_3 - \{[a_{34} B_4 + a_{38} B_8]/a_{44} + a_{35}/a_{55} B_5 + \frac{a_{37}}{a_{77}} B_7 + a_{39}/a_{99} B_9 + a_{3,10}/a_{10,10} (M_{T_2} - K_f \psi_2 + b_{10}) + a_{3,11}/a_{11,1} (M_T - K_f \psi_1 + b_{11})\}$$

Compute Inverse of Spacecraft Generalized Inertia Dyad Matrix

$$[APINV] = \begin{bmatrix} a'_{11} & a'_{12} & a'_{13} \\ a'_{21} & a'_{22} & a'_{23} \\ a'_{31} & a'_{32} & a'_{33} \end{bmatrix}^{-1}$$

Compute Angular Acceleration and Angular Velocity of Spacecraft

$$\begin{bmatrix} \dot{P}(nT_s) \\ \dot{Q}(nT_s) \\ \dot{R}(nT_s) \end{bmatrix} = [APINV] \begin{bmatrix} B_1 \\ B_2 \\ B_3 \end{bmatrix}$$

$$P(nT_s) = P((n-1)T_s) + \int_{(n-1)T_s}^{nT_s} \dot{P}\, dt$$

$$Q(nT_s) = Q((n-1)T_s) + \int_{(n-1)T_s}^{nT_s} \dot{Q}\, dt$$

$$R(nT_s) = R((n-1)T_s) + \int_{(n-1)T_s}^{nT_s} \dot{R}\, dt$$

2.2 OPTICAL SYSTEM MODEL

The laser telescope configuration assumed for the LASIM program development is illustrated in Figure 2.2-1. This configuration was taken from Perkin-Elmer Report No. 8631, dated 31 December 1966.

Of importance to the tracking system simulation is the optics model used for focusing the received light onto the coarse and fine sensors shown in Figure 2.2-1, and the characteristics of the sensors themselves.

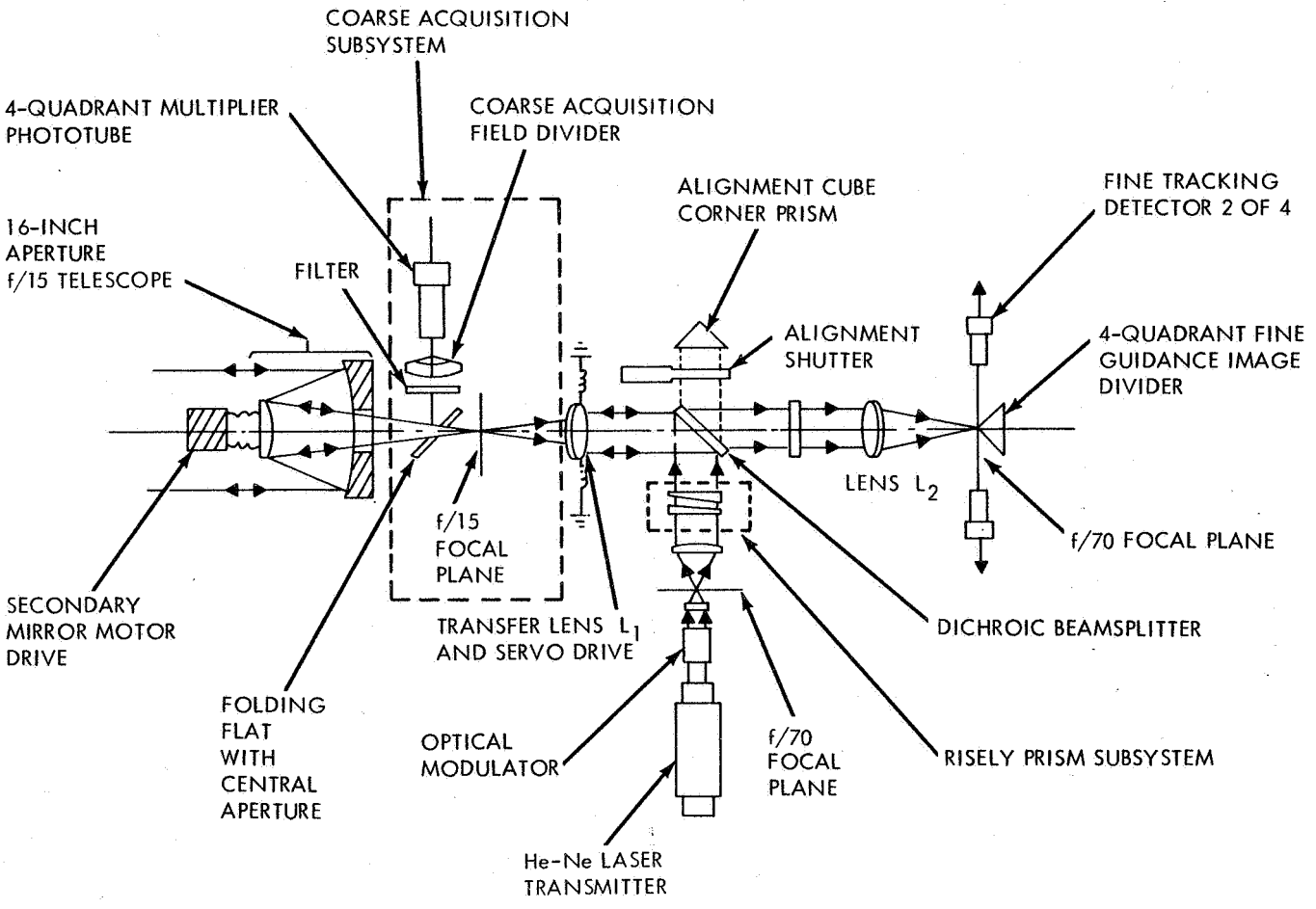

FIGURE 2.2-1 LASER TELESCOPE CONFIGURATION

It has been assumed in the equation development representing telescope optics that lenses L_1 and L_2 in Figure 2.2-1 introduce no aberrations, nor do the telescope primary and secondary mirrors. Geometric optics formulations are used to determine the image

position in the fine and coarse focal planes from which the sensor output signals are obtained. The following paragraphs describe the optics formulations made and the sensor characteristics used for the LASIM program.

2.2.1 Uplink Beam Input

From a determination of the relative positions of the ground station and target satellite (discussed in Paragraph 2.7), a vector is computed in inertial coordinates representing the line-of-sight from ground to target. No atmospheric refraction is considered in the calculation of the line-of-sight vector since once the satellite laser telescope has acquired the beacon, the refraction may be ignored (except for high frequency dynamic refraction, discussed in Section 3).

The line-of-sight vector is transformed into the telescope coordinate frame and normalized prior to the optical calculations. The normalized line-of-sight vector is designated as $\underline{L}$. The origin of the telescope or [T] frame is, for the optical calculations, assumed to be located at the center of a lens, equivalent to the telescope primary and secondary mirror system. Figure 2.2-2 illustrates, in a plane, the geometric equivalent of the telescope used for the optics calculations.

The angle which the normalized line-of-sight vector, $\underline{L}$, makes with the z_T axis (telescope longitudinal axis) or θ_z in Figure 2.2-2, is the quantity used to determine whether or not the ground beacon is in the telescope field-of-view.

If 1 arc minute $< \theta_z \leq$ 30 arc minutes, it is known that the ground beacon will be focused onto the coarse system photomultiplier tube, assumed to be located at an equivalent f/15 focal plane. Generation of the coarse sensor output in this case is described in Paragraph 2.2.2.

If $\theta_z \leq$ 1 arc minute, the image of the ground beacon will be formed in the f/70 focal plane; and reflected from the "fine guidance image divider" into the fine system photomultiplier tubes as shown in Figure 2.2-1. The edge widths of the image divider prisms are small in comparison to the size of the diffraction pattern formed in the f/70 plane. For this reason it is assumed that the plane is divided into the four symmetric quadrants separated by knife edge boundaries. It is further assumed that the fine system detectors are located in the f/70 plane itself, rather than being removed somewhat as they actually are. The optical calculations next proceed to a determination of the geometric image location in the f/70 focal plane. The y coordinate of the image is designated as p_y on Figure 2.2-2.

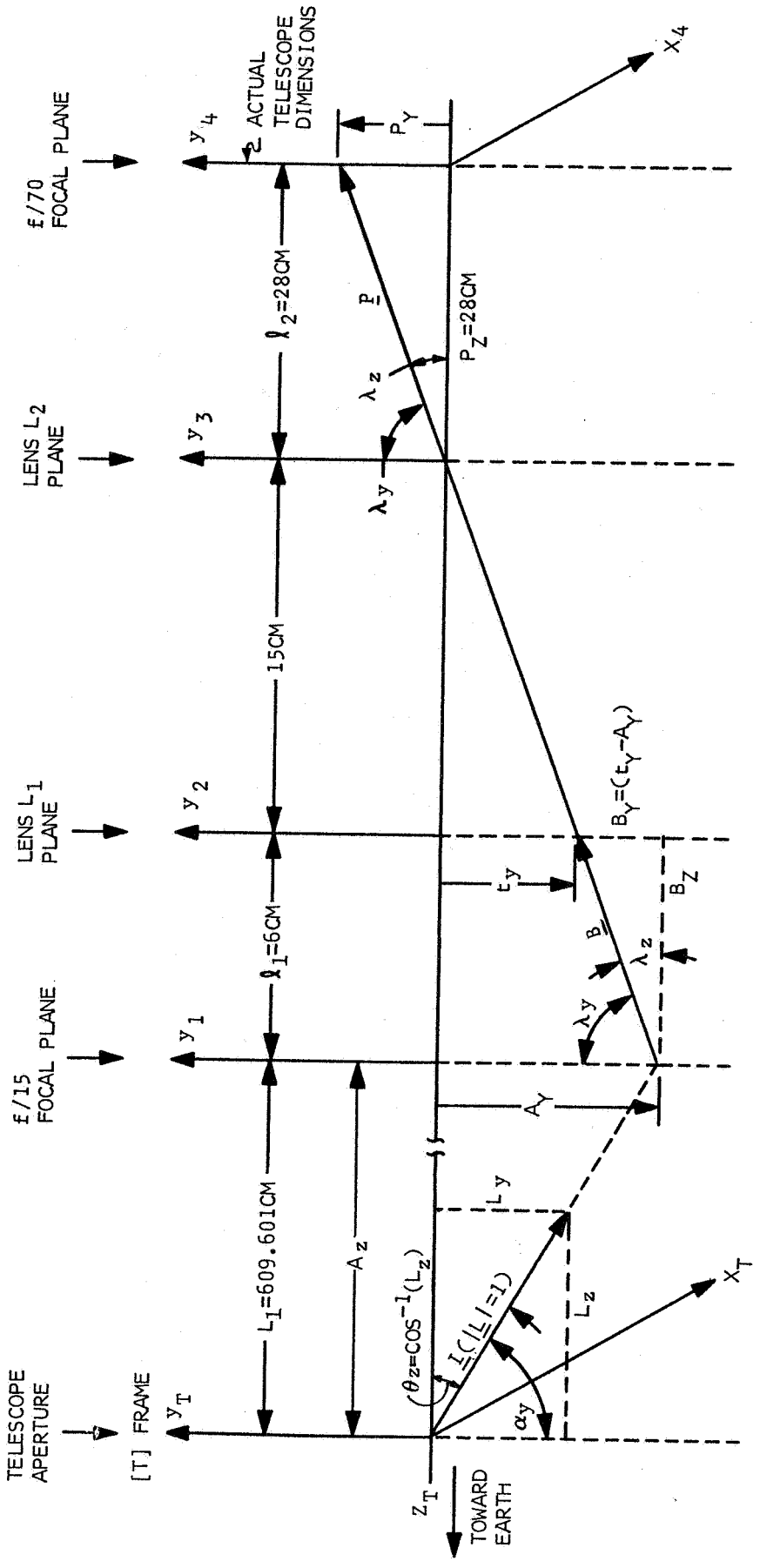

IN GENERAL:

$$\underline{L} = L_x \underline{X_T} + L_y \underline{Y_T} + L_z \underline{Z_T}$$

FOR THIS FIGURE:

$$\underline{L} = (0)\,\underline{X_T} + L_Y \underline{Y_T} + L_Z \underline{Z_T}$$

FIGURE 2.2-2 LASER TELESCOPE GEOMETRIC MODEL

To calculate p_y, the vector $\underline{B}$ in Figure 2.2-2 is first determined.

$$\underline{B} = B_y \underline{y_1} + B_Z \underline{Z_1}, \text{ where } y_1 \text{ and } Z_1 \text{ are unit vectors} \qquad (2.2\text{-}1)$$

From the geometry in Figure 2.2-2:

$$B_y = |\underline{B}| \cos \lambda_y = t_y - A_y,$$

$$B_z = |\underline{B}| \cos \lambda_z = 6 \text{ cm}, \text{ where } t_y = \text{transfer lens y position coordinate}$$

$$A_y = \text{image y position coordinate in the f/15 focal plane.}$$

from which

$$\cos \lambda_y = \left(\frac{t_y - A_y}{6} \right) \cos \lambda_z \qquad (2.2\text{-}2)$$

The vector $\underline{B}$ defines the direction of a ray of light from the image center in the f/15 plane through the center of transfer lens L_1. The direction of the ray along $\underline{B}$ is parallel to all rays between lenses L_1 and L_2 since, in this region, the light is collimated. A ray in this direction then passes through the center of lens L_2, establishing the focal point in the f/70 plane.

The vector $\underline{p}$ is a vector from the center of lens L_2 to the focal point in the f/70 plane, in the direction of $\underline{B}$. The components, p_x and p_y, of $\underline{p}$ define the image position in the f/70 plane. From the geometry of Figure 2.2-2:

$$\underline{p} = p_y \underline{y_3} + p_z \underline{z_3}; \text{ where } \underline{y3} \text{ and } \underline{Z3} \text{ are unit vectors,} \qquad (2.2\text{-}3)$$

$$p_z = |\underline{p}| \cos \lambda_z = 28 \text{ cm},$$

from which

$$|p| = \frac{28}{\cos \lambda_z},$$

and

$$p_y = |p| \cos \lambda_y = \left(\frac{28}{\cos \lambda_z} \right) \cos \lambda_y. \qquad (2.2\text{-}4)$$

Combining Equations 2.2-2 and 2.2-4:

$$p_y = (\frac{28}{6})(t_y - A_y). \qquad (2.2\text{-}5)$$

To complete the derivation, A_y must be related to the components L_y and L_z of the normalized vector $\underline{L}$. Again by geometry, considering the vector $\underline{A}$ which is parallel to $\underline{L}$ and intersects the f/15 plane:

$$A_y = |A| \cos \alpha_y \qquad (2.2\text{-}6)$$

where

$$|A| = \frac{A_Z}{\cos \theta_z} = \frac{609.601}{L_z} \qquad (2.2\text{-}7)$$

$$\cos \alpha_y = \frac{L_y}{|\underline{L}|} = L_y,$$

from which is obtained: $A_y = 609.601(\frac{L_y}{L_z})$. (2.2-8)

Substituting into Equation 2.2-5 yields,

$$p_y = (\frac{28}{6})t_y - (\frac{28}{6})(609.601)(\frac{L_y}{L_z}) \qquad (2.2\text{-}9)$$

In similar manner, the x coordinate of the image in the f/70 plane, p_x, may be obtained as:

$$p_x = (\frac{28}{6})t_x - (\frac{28}{6})(609.601)(\frac{L_x}{L_z}). \qquad (2.2\text{-}10)$$

Equations 2.2-9 and 2.2-10 are of fundamental importance in determining fine tracking system operation. The manner in which the image position coordinates, p_x and p_y, are used to determine the fine sensor output is shown in Paragraph 2.2.3.

2.2.2 Coarse Sensor Model

The coarse optics sensor provides on-off signals in the x and y telescope gimbal control system channels as a function of the image location in the f/15 focal plane. Figure 2.2-3 depicts the image plane divided into four quadrants with the orientation of the telescope control axes indicated. The normalized line-of-sight vector $\underline{L}$ is shown in the figure to illustrate the manner in which the coarse sensor is simulated. For the situation shown in Figure 2.2-3, control signals should be generated by the coarse sensor to align the Z_T axis with the $\underline{L}$ direction; that is, telescope rotations (ψ_1 and $-\psi_2$) about the x_T and y_T axes should be as shown. The coarse sensor can be adequately simulated by simply providing step position error commands (with the proper polarity to align

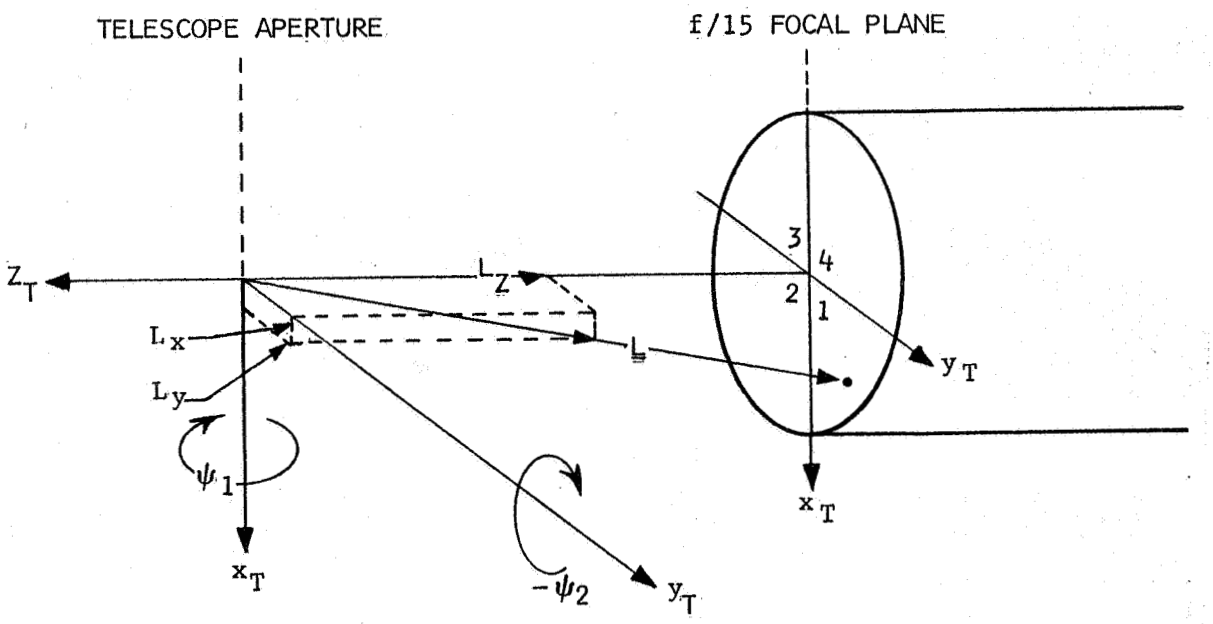

FIGURE 2.2-3 COARSE SENSOR GEOMETRY

the telescope with $\underline{L}$) to the telescope control system. The appropriate polarity can be determined by testing the sign of the $\underline{L}$ components, L_x and L_y. The following table defines the simulation of the coarse sensor in the program.

TABLE 2.2-1 COARSE SENSOR DEFINITION

L_x	L_y	Image in Quadrant # in f/15 focal plane	ψ_1 command	ψ_2 command
+	+	1	+	-
+	-	2	-	-
-	-	3	-	+
-	+	4	+	+

Figure 2.2-4 illustrates the coarse sensor characteristic which results from the simulation mechanization discussed above. The abcissa of the curve shown in Figure 2.2-4 represents the angular misalignment between telescope longitudinal axis and line-of-sight, about either the x_T or y_T axes. The value of e in Figure 2.2-4, representing the output voltage of the photo-multiplier tube and associated preamplifiers, is determined by control system position gain requirements and is discussed in Paragraph 2.4.1.

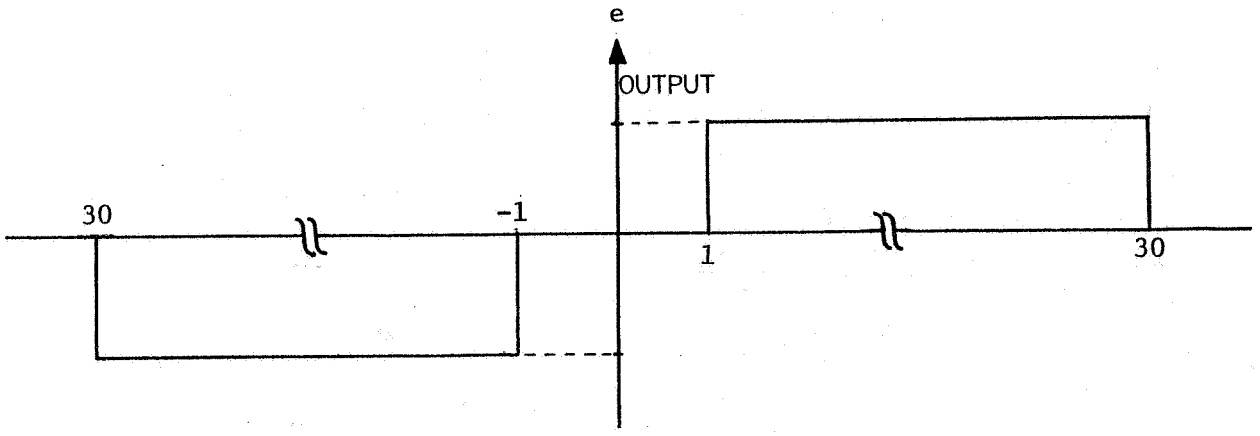

FIGURE 2.2-4 COARSE SENSOR CHARACTERISTIC

2.2.3 Fine Sensor Model

It is recognized that light focused onto the f/70 focal plane will form an image, or diffraction pattern, rather than a point of light. To a first approximation, the image will appear as the classical Airy diffraction pattern. The intensity, for a clear circular aperture, with the light source being an infinite point source of quasi monochromatic or coherent light, is determined as:

$$I(f) = I_1\left[\frac{2\ J_1(f)}{f}\right]^2, \qquad (2.2\text{-}11)$$

where:

$f = Ka\omega$

ω = sine of the angle of deviation

a = aperture radius

$K = \frac{2\pi}{\lambda}$, λ = wavelength

J_1 = first order Bessel function of the first kind

I_o = intensity at the center of the circularly symmetric image.

Figure 2.2-5 illustrates the normalized intensity function versus f.

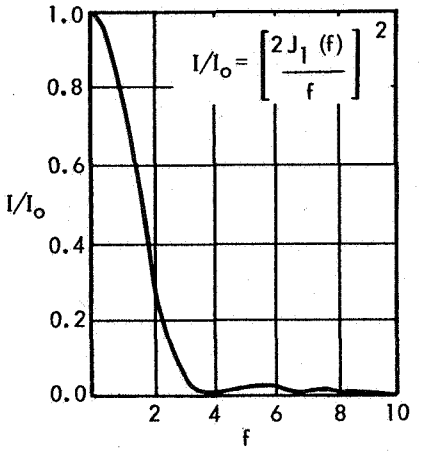

FIGURE 2.2-5 INTENSITY IN THE AIRY PATTERN FOR A CLEAR CIRCULAR APERTURE

In the dynamic tracking situation, the image in the f/70 plane will not remain centered exactly. The object of the tracking system is to maintain centering to an equivalent 0.1 arc second or less, which means the center of the image must be kept within 10^{-3} cm of the center of the plane. Figure 2.2-6 illustrates the situation which obtains when the image is off center.

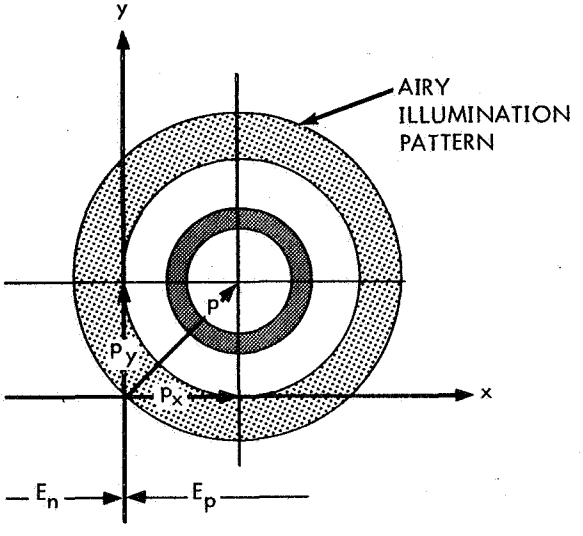

FIGURE 2.2-6 IMAGE IN THE f/70 FOCAL PLANE

The coordinates specifying the image center p_x and p_y are those derived previously. The quantities E_n and E_p on Figure 2.2-6 represent the actual light energy falling in the half planes $p_x < 0$, $p_x > 0$ respectively. It is assumed that the photomultiplier tubes collect all light falling in each quadrant of

the plane and inhomogenieties across photomultiplier light sensitive surfaces are ignored. The input signals from the 4 photomultipliers located in each quadrant are combined in such a way (see Figure 2.3-1, Paragraph 2.3) as to generate a control signal, e_x, which is proportional to the difference in energies E_p and E_n shown in Figure 2.2-6. Thus, consideration need not be given each photomultiplier tube; but only the difference between energies E_p and E_n determined. Simulation of the fine sensor becomes a problem of determining $(E_p - E_n)$ as a function of the image coordinates p_x and p_y. To this end, the normalized intensity function of Equation 2.2-11 may be integrated over the f/70 focal plane, leaving the p_x coordinate implicit in the process, to produce an energy fraction μ which represents the fraction of total energy falling in the $p_x > 0$ half plane as a function of the p_x coordinate. This energy fraction is illustrated in Figure 2.2-7 as curve 1. The energy E_p is determined as μE_T, where E_T is the total light energy incident on the plane.

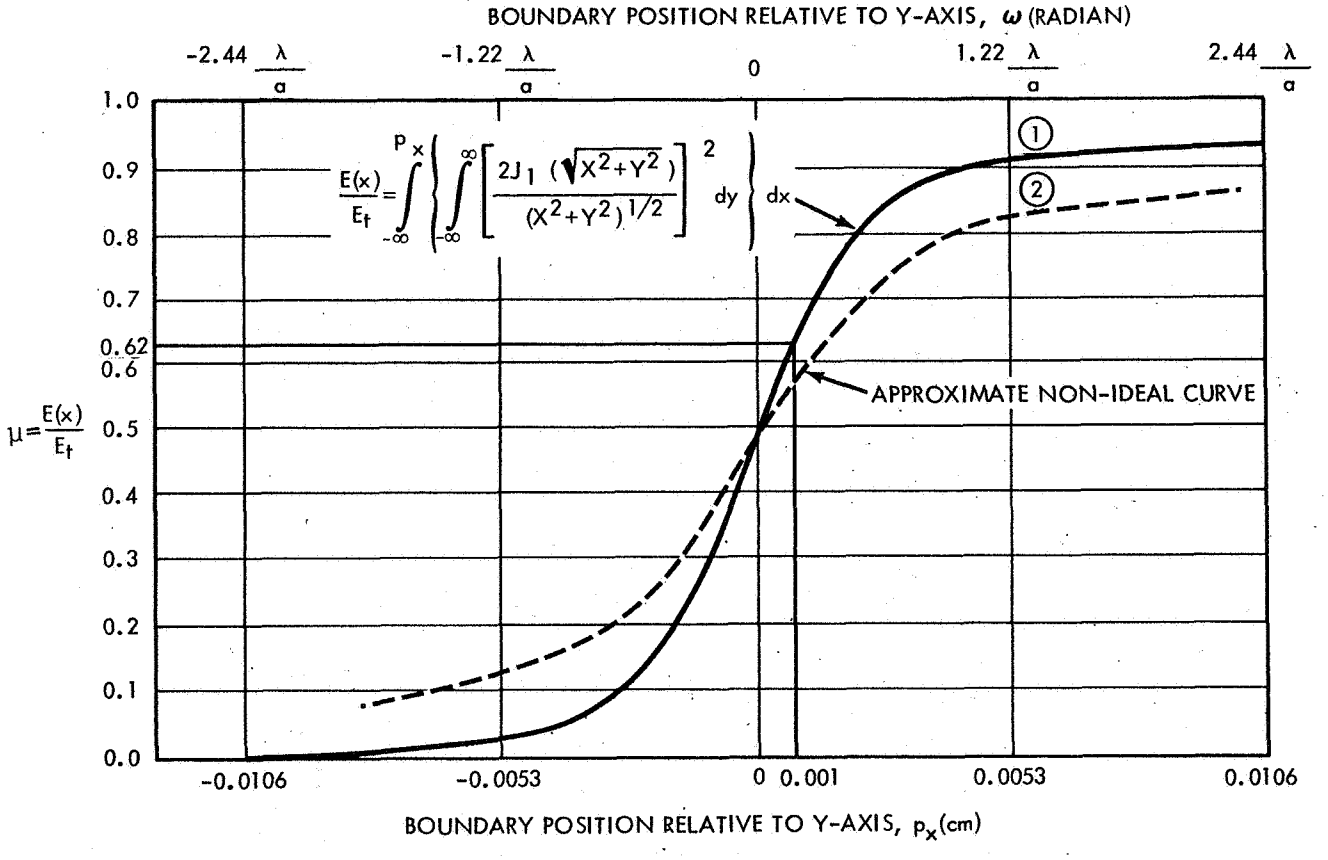

FIGURE 2.2-7 ENERGY FRACTION ON ONE SIDE OF A KNIFE-EDGE BOUNDARY

The output signal from the combined photomultipliers, e_x, is determined as:

$$e_x = K_o(E_p - E_n) = K_o[\mu E_T - E_T(1-\mu)] = K_o E_T(2\mu - 1) \qquad (2.2\text{-}12)$$

where K_o = optical system gain.

Relations for the y channel output from the photomultipliers may be expressed in similar manner.

Curve 2 on Figure 2.2-7 represents an energy fraction curve which considers the central obscuration of the telescope aperture and mirror surface anomalies. Curve 2 is approximate; however it represents a more realistic relation than curve 1 and is used in the LASIM program. A separate routine is used in the LASIM program to compute μ versus p_x and p_y, and with small modification, any curve desired can be accommodated.

The relation of Equation 2.2-12, along with the curve of μ versus p_x and p_y, is used in the LASIM program to simulate the fine system optical sensor. A nominal value of E_T used in the program is 10^{11} photons/second. (E_T is actually expressed in "power" units; references to "light energy" in this section imply energy per unit time, or power.) The optical system gain K_o in Equation 2.2-12 is set equal to 7.92×10^{-10} volts/photons per second. This value was derived from information contained in Perkin-Elmer Report No. 8387, dated 29 April 1966 and assumes an operating current level for the individual photomultipliers of 25 μa. Figure 2.2-8 illustrates the elements combined in the optical system gain K_o.

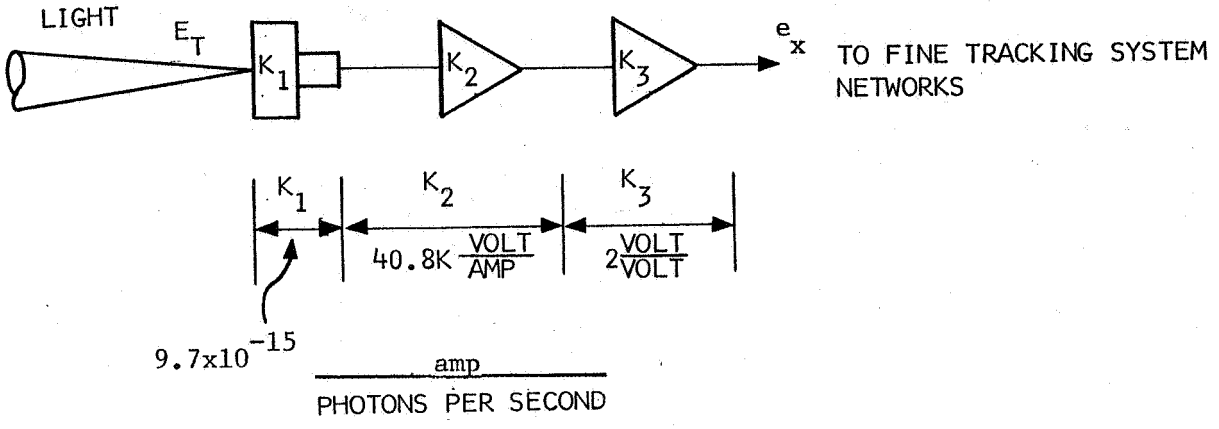

K_1 = COMBINED PHOTOMULTIPLIER CURRENT GAIN

K_2 = PRE AMP TRANSRESISTANCE

K_3 = DEMOD AND SUMMING AMP VOLTAGE GAIN

$$K_O = K_1 K_2 K_3 = 7.92 \times 10^{-10} \ \frac{\text{VOLT}}{\text{PHOTONS PER SECOND}}$$

FIGURE 2.2-8 OPTICAL SYSTEM GAIN

2.2.4 Downlink Beam

The downlink laser beam originates from the Ne-He laser shown on Figure 2.2-1 and passes through two Risely prisms which perform the beam deflection, or "point ahead" operation, previously referred to. The Risely prisms are rotated independently and beam deflection is accomplished in two directions as seen in Figure 2.2-9. The angle θ_{PA1} is the amount the beam is deflected, at the prisms, from the nominal beam direction. The nominal direction corresponds to the line-of-sight. The angle θ_R in Figure 2.2-9 determines the direction in which the beam will be deflected. In terms of prisms rotation angles θ_{P1} and θ_{P2} shown on Figure 2.2-9, the relations:

$$\theta_R = \frac{\theta_{P_1} - \theta_{P_2}}{2} \qquad (2.2\text{-}13)$$

$$\theta_{PA1} = M\sin\left(\frac{\theta_{P1}+\theta_{P2}}{2}\right) \qquad (2.2\text{-}14)$$

M = 10 arc minutes

define the beam deflection angles θ_R and θ_{PA1}. Thus the Risely prisms deflect the downward beam, at the prisms, from the line-of-sight direction by 10 arc minutes maximum.

The amount which the downlink beam is deflected from the line-of-sight at the telescope aperature, θ_{PA}, (as opposed to θ_{PA1} which is valid at the prisms) is given as

$$\theta_{PA} = \left(\frac{PA1}{L_1/\ell_1}\right). \qquad (2.2\text{-}15)$$

L_1 = f/15 focal length of telescope = 609.601 cm

ℓ_1 = focal length of lens L_1 = 6 cm

The angle θ_R undergoes no change from prism location to telescope aperture. Then, at the telescope aperture, the downlink beam deflection angles are:

$$\theta_{PA} = 5.9055 \sin\left(\frac{\theta_{P1}+\theta_{P2}}{2}\right) \text{ (arc seconds)}, \qquad (2.2\text{-}16)$$

$$\theta_R = \left(\frac{\theta_{P1}-\theta_{P2}}{2}\right) 2.06 \times 15 \text{ (arc seconds)} \qquad (2.2\text{-}17)$$

The prism rotations θ_{P1} and θ_{P2} are forced by the pointing control system discussed in Paragraph 2.5.

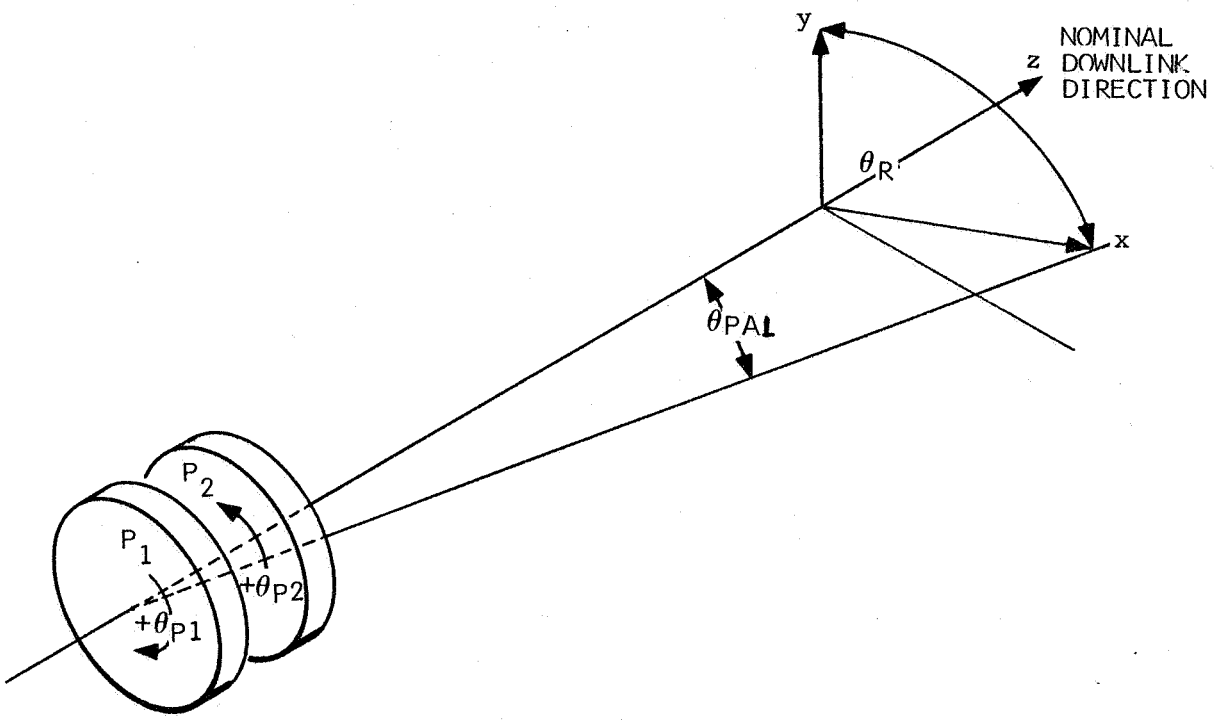

FIGURE 2.2-9 RISELY PRISMS

2.3 FINE TRACKING SYSTEM

Definition of the fine tracking system hardware was obtained from Perkin-Elmer Report No. 8387, dated 29 April 1966. Figure 2.3-1 illustrates the model used for the fine tracking system. Both the x and y channels of the system are assumed to conform to Figure 2.3-1. No dynamical coupling between channels is considered.

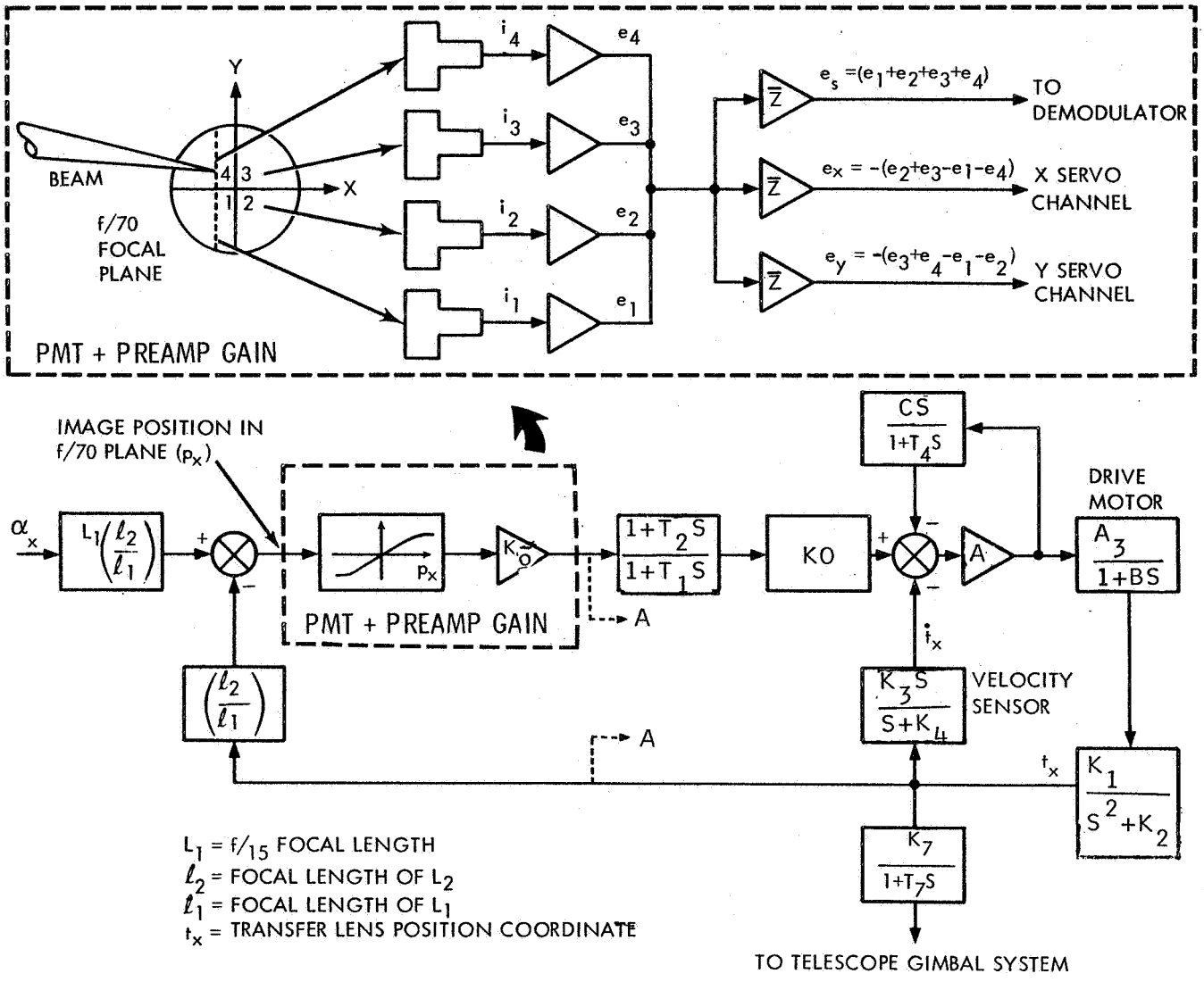

FIGURE 2.3-1 FINE TRACKING SYSTEM BLOCK DIAGRAM

The fine tracking system operates to position the transfer lens so as to center the beacon image in the f/70 focal plane of the telescope. The x coordinate of the image center, p_x, is related to the transfer lens position, t_x, as described by Equation 2.2-10, repeated here.

$$p_x = \left(\frac{28}{6}\right) t_x - \left(\frac{28}{6}\right)(609.601)\left(\frac{L_x}{L_z}\right) \qquad (2.3\text{-}1)$$

From the geometry of Figure 2.2-2 (Paragraph 2.2), it can be seen that the quantity (L_x/L_z) is equal to tan α_x which, for small angles, is approximately equal to α_x, or the misalignment angle between telescope x axis and line-of-sight. The quantity α_x is shown on Figure 2.3-1 as representing the input to the control system for illustrative purposes. (In the actual program the approximation is <u>not</u> made and the quantity L_x/L_z used in the computation for p_x.)

One element shown in Figure 2.3-1 is not directly a part of the fine tracking system. A position sensor is used to pick off the transfer lens position, t_x, to serve as an error signal for the telescope gimbal system, during the time the system operates in the fine-field-of-view, ($\theta_z \leq 1$ arc minute). This was mentioned in Paragraph 1.1.2.1. From Equation 2.3-1 it is seen that if $p_x=0$, then:

$$t_x = (609.601)\left(\frac{L_x}{L_z}\right) \approx 609.601\alpha_x \qquad (2.3\text{-}2)$$

using the approximation $\alpha_x \approx \frac{L_x}{L_z}$.

Thus, the transfer lens position is linearily related to the misalignment angle, α_x, and may be used to provide a linear region of control input for the coarse system. This is possible <u>only</u> if p_x is equal or approximately equal to zero. Because the fine tracking system operates much faster, in the linear region, than does the gimbal system, p_x will be quite small and this procedure will work.

Of importance to the success of the method just described is the sensitivity, linearity, and saturation of the transfer lens position sensor. No information on this device, except a linear model, is known. Consequently a linear representation has been used in the LASIM program, as shown on Figure 2.3-1.

2.3.1 <u>Fine System Equation Development</u>

The elements comprising the fine tracking system shown to the right of section A-A in Figure 2.3-1 are characterized as linear elements which allows transfer function representation. The

elements in Figure 2.3-1 to the right of section A-A may be combined, using block diagram manipulations, to give a single transfer function, G(s), which relates transfer lens position t_x to the error signal e_x. Figure 2.3-2 illustrates the resulting fine tracking system block diagram. Formulation of G(s) is straightforward and will not be illustrated. The resulting G(s) has the form,

$$G(s) = \frac{T_x(s)}{E_x(s)} = \frac{a_o+a_1s+a_2s^2+a_3s^3}{b_o+b_1s+b_3s^2+b_3s^3+b_4s^4+b_5s^5+b_6s^6} \qquad (2.3\text{-}3)$$

where the coefficients $a_o, \ldots, a_3$; $b_o, \ldots, b_6$ are functions of the gains and time constants in Figure 2.3-1. These relations are shown in Table 2.3-1 at the end of this section.

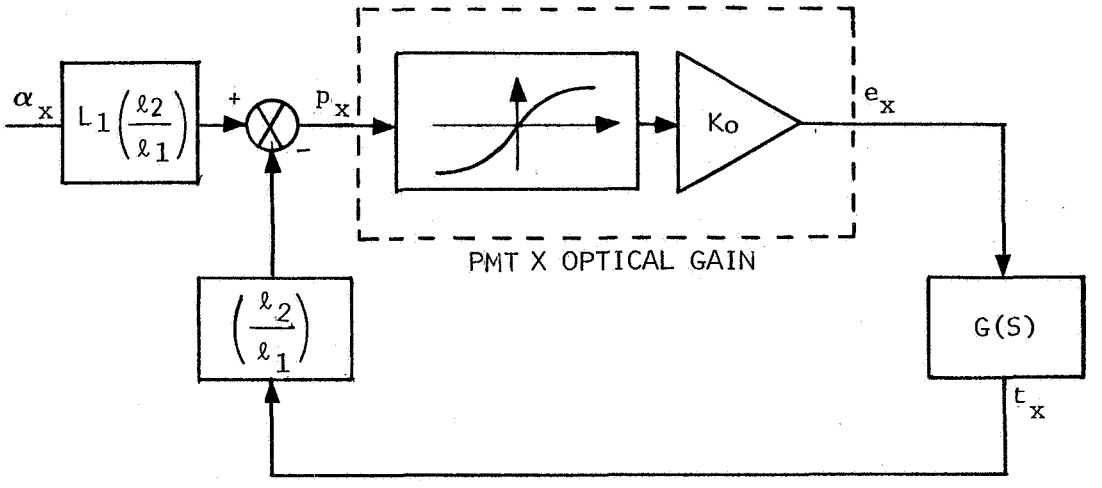

FIGURE 2.3-2 FINE TRACKING SYSTEM EQUIVALENT BLOCK DIAGRAM

Digital simulation of the fine tracking system requires solving the system equations in the time domain, rather than the frequency domain in which Equation 2.3-3 is written. There are various methods of accomplishing this as indicated in References [10, 11, 12, 13, 14]. The method selected for the LASIM program is the most straightforward and has proved to work satisfactorily. The method chosen is called the Tustin Method [14] and proceeds as follows. The variable s in Equation 2.3-3 is replaced by

$$s = \frac{2}{T}\left(\frac{1-\Delta}{1+\Delta}\right), \qquad (2.3\text{-}4)$$

where: T = sampling time = .002 sec for fine equations only and

$$\Delta = \frac{1}{Z} = \epsilon^{-ST}$$

Higher powers of s in Equation 2.3-3 are replaced by the corresponding power of the "Tustin Substitution" indicated in Equation 2.3-4. The variable T equals 1/f where f is the sampling frequency, or the number of times the equations will be solved per second in the simulation. Solution of the fine system equations is performed 500 times per second. The value of f is dependent upon the bandwidth of the networks being solved. In general, for good accuracy f is 5 to 10 times the highest frequency of significance in the network. In the linear region, the fine tracking system has a bandwidth of approximately 30 cps. Because of the extreme accuracy desired in the LASIM program, f was chosen 500, or approximately 17 times the break frequency of the system.

Making the substitution of Equation 2.3-4 into Equation 2.3-3, results in a ratio of polynomials in Δ, shown as $G(\Delta)$.

$$G(\Delta) = \frac{T_x(\Delta)}{E_x(\Delta)} = \frac{c_o+c_1\Delta+c_2\Delta^2+c_3\Delta^3+c_4\Delta^4+c_5\Delta^5+c_6\Delta^6}{d_o+d_1\Delta+d_2\Delta^2+d_3\Delta^3+d_4\Delta^4+d_5\Delta^5+d_6\Delta^6} \qquad (2.3\text{-}5)$$

The coefficients $c_o, \ldots, c_6$; $d_o, \ldots, d_6$ are functions of the a's and b's in Equation 2.3-3 and are tabulated in Table 2.3-1. Solution of Equation 2.3-5 for the time domain, transfer lens position, $t_x(t)$ at time $t=t_1=nT$ is made by recalling the definition of Δ,

$$(\Delta = \varepsilon^{-ST})$$

and taking the inverse Laplace transform indicated in Equation 2.3-6.

$$t_x(t_1) = \frac{1}{d_o} \left\{ \mathcal{L}^{-1} \left[\sum_{i=0}^{6} c_i E(\Delta) \varepsilon^{-isT} - \sum_{j=1}^{6} d_j T(\Delta) \varepsilon^{-jsT} \right] \right\}. \qquad (2.3\text{-}6)$$

The inverse transform of the individual terms of Equation 2.3-7 such as i=3 yields:

$$\mathcal{L}^{-1}[c_3 E_x(\Delta)\varepsilon^{-3ST}] \Big|_{t=t_1} = c_3 e_x(t_1-3T). \qquad (2.3\text{-}7)$$

The equation which results from performing the indicated operations on Equation 2.3-6 yields a difference equation ideally suited to mechanization on a digital computer.

$$t_{x(nT)} = \frac{1}{d_o} \left\{ \sum_{i=0}^{6} c_i e_x[(n-i)T] - \sum_{j=1}^{6} d_j t_x[(n-j)T] \right\} \quad (2.3\text{-}8)$$

The notation $t_x(nT)$ denotes the time domain value of the variable $t_x(t)$ at $t=nT$. The quantity $e_x[(n-3)T]$ denotes the time domain value of $e_x(t)$ at $t=(n-3)T$, or a past value of e_x. Equation 2.3-8 is evaluated 500 times per second in the LASIM program to determine a train of impulses for the transfer lens position, t_x, which approximates the continuous response of the fine tracking system. The foregoing applies also to the solution of the y transfer lens position coordinate, t_y.

Paragraph 2.3.2 discusses the sequence of mathematical operations implemented in the LASIM program to solve the equations derived in this section and thereby simulate the fine tracking system.

TABLE 2.3-1

COEFFICIENT AND PARAMETER DEFINITION FOR FINE TRACKING SYSTEM

$$a_0 = KOK_1A_3AK_4$$

$$a_1 = KOK_1A_3A(K_4T_4+1+T_2K_4)$$

$$a_2 = KOK_1A_3A[T_2+T_4(1+T_2K_4)]$$

$$a_3 = KOK_1A_3AT_4T_2$$

$$b_0 = K_2K_4$$

$$b_1 = T_1K_2K_4+K_2K_4B+K_2(1+T_6K_4)+K_1A_3AK_3$$

$$b_2 = K_4+K_2B(1+T_6K_4)+K_2T_6+T_1[K_2K_4B+K_2(1+T_6K_4)+K_1AA_3K_3]+K_1A_3AK_3T_4$$

$$b_3 = BK_4+1+T_6K_4+K_2BT_6+T_1[K_4+K_2B(1+T_6K_4)+K_2T_6+K_1AA_3K_3T_4]$$

$$b_4 = B(1+T_6K_4)+T_6+T_1(BK_4+1+T_6K_4+K_2BT_6)$$

$$b_5 = BT_6+T_1[B(1+T_6K_4)+T_6]$$

$$b_6 = T_1BT_6$$

$$c_0 = a_0+\frac{2a_1}{T} \quad \frac{4a_2}{T^2} + \frac{8a_3}{T^3}$$

$$c_1 = 6a_0+ \frac{8a_1}{T} + \frac{8a_2}{T^2}$$

$$c_2 = 15a_0 + \frac{10a_1}{T} - \frac{4a_2}{T^2} - \frac{24a_3}{T^3}$$

$$c_3 = 20a_0 -\frac{16a_2}{T^2}$$

$$c_4 = 15a_0 -\frac{10a_1}{T} - \frac{4a_2}{T^2} + \frac{24a_3}{T^3}$$

$$c_5 = 6a_0 -\frac{8a_1}{T} + \frac{8a_2}{T^2}$$

$$c_6 = a_0 -\frac{2a_1}{T} + \frac{4a_2}{T^2} - \frac{8a_3}{T^3}$$

$$d_0 = b_0 + \frac{2b_1}{T} + \frac{4b_2}{T^2} + \frac{8b_3}{T^3} + \frac{16b_4}{T^4} + \frac{32b_5}{T^5} + \frac{64b_6}{T^6}$$

$$d_1 = 6b_0 + \frac{8b_1}{T} + \frac{8b_2}{T^2} - \frac{32b_4}{T^4} \quad \frac{128b_5}{T^5} - \frac{384b_6}{T^6}$$

$$d_2 = 15b_0 + \frac{10b_1}{T} - \frac{4b_2}{T^2} - \frac{24b_3}{T^3} - \frac{16b_4}{T^4} + \frac{160b_5}{T^5} + \frac{960b_6}{T^6}$$

TABLE 2.3-1 (CONTINUED)

$$d_3 = 20b_0 - \frac{16b_2}{T^2} + \frac{64b_4}{T^4} - \frac{1280b_6}{T^6}$$

$$d_4 = 15b_0 - \frac{10b_1}{T} - \frac{4b_2}{T^2} + \frac{24b_3}{T^3} - \frac{16b_4}{T^4} - \frac{160b_5}{T^5} + \frac{960b_6}{T^6}$$

$$d_5 = 6b_0 - \frac{8b_1}{T} + \frac{8b_2}{T^2} - \frac{32b_4}{T^4} + \frac{128b_5}{T^5} - \frac{384b_6}{T^6}$$

$$d_6 = b_0 - \frac{2b_1}{T} + \frac{4b_2}{T^2} - \frac{8b_3}{T^3} + \frac{16b_4}{T^4} - \frac{32b_5}{T^5} + \frac{64b_6}{T^6}$$

$$K_0 = 1/R_{in} = 1/2 \ .4 \times 10^5$$

$$T_2 = \frac{1}{2\pi(7)}$$

$$T_1 = \frac{1}{2\pi(.466)}$$

$$C = 3.3 \times 10^{-8}$$

$$A = 10^6$$

$$T_4 = RC = (2.4 \times 10^5)(3.3 \times 10^{-8}) = \frac{1}{2\pi(20.1)}$$

$$T_6 = AC + T$$

$$K_1 = 1/250$$

$$K_2 = \frac{35.4 \times 10^3}{250} = 141.4$$

$$K_3 = .0167 = 1/60$$

$$K_4 = 240\pi$$

$$A_3 = 2.67 \times 10^4$$

$$B = 2 \times 10^{-4}$$

2.3.2 Fine Tracking System Math Flow

This paragraph will summarize the equations derived previously, which are solved in simulating the fine tracking system; and indicate the sequence of solution necessary for simulation. Figure 2.3-3 illustrates the order of the indicated computations mechanized in the LASIM program.

The equations solved in each block of computations indicated in Figure 2.3-3 are illustrated in Table 2.3-1.

TABLE 2.3-2 FINE TRACKING SYSTEM MATH FLOW

- Compute Image Coordinates in the f/70 Focal Plane -

$$p_x(nT) = \left(\frac{28}{6}\right) t_x[(n-1)T] - \left(\frac{28}{6}\right)(609.601)\left(\frac{L_x(nT)}{L_z(nT)}\right)$$

$$p_y(nT) = \left(\frac{28}{6}\right) t_x[(n-1)T] - \left(\frac{28}{6}\right)(609.601)\left(\frac{L_y(nT)}{L_z(nT)}\right)$$

- Determine Energy Fractions -

$$\left.\begin{aligned} \mu_x(nT) &= f_{(p_x(nT))} \\ \mu_y(nT) &= f_{(p_y(nT))} \end{aligned}\right\}$$ As determined from the function illustrated in Figure 2.2-7.

- Determine Error Voltages -

$$e_x(nT) = K_o E_T (2\mu_x(nT) - 1)$$

$$e_y(nT) = K_o E_T (2\mu_y(nT) - 1)$$

- Compute New Transfer Lens Position -

$$t_x(nT) = \frac{1}{d_o}\left\{\sum_{i=0}^{6} C_i C_x[(n-i)T] - \sum_{j=1}^{6} d_j t_x[(n-j)]\right\}$$

$$t_y(nT) = \frac{1}{d_o}\left\{\sum_{i=0}^{6} C_i C_y[(n-i)T] - \sum_{j=1}^{6} d_j t_x[n-j)T]\right\}$$

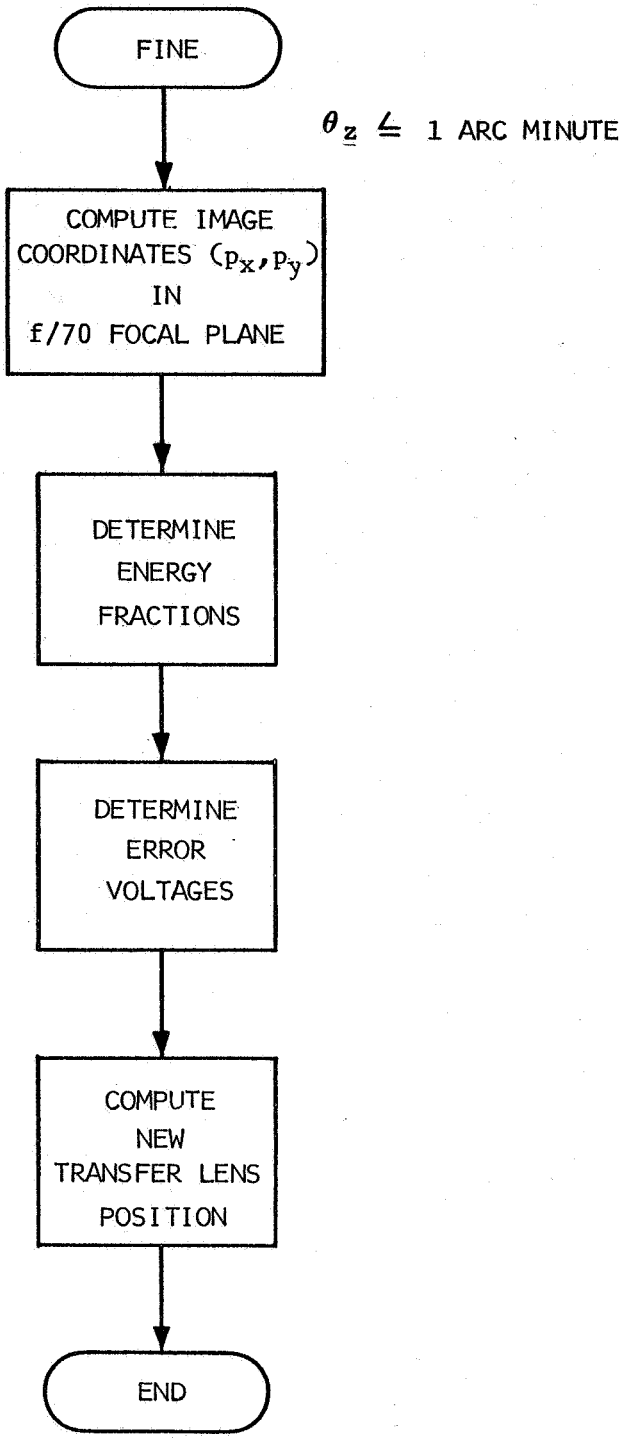

FIGURE 2.3-3 FINE TRACKING SYSTEM MATH FLOW

2.4 TELESCOPE CONTROL SYSTEM

The telescope control system hardware was described in Paragraph 2.1. The mathematical representation of the hardware will now be developed.

2.4.1 Equation Development

Figure 2.1-2 depicts the telescope control system, with inputs and outputs for both outer (pitch) and inner (yaw) gimbal control. As indicated by the figure, the control hardware is functionally the same for both ψ_1 and ψ_2 control.

In the coarse mode, the y_T and x_T components of the line of sight, L_y and L_x, feed into the coarse sensor. The idealized coarse sensor, as discussed in Paragraph 2.2.2, can be modeled as follows:

$$\text{POSEX} = \begin{cases} 0 & \text{if } \Theta_z \leq 1 \text{ min} \\ 0 & \text{if } \Theta_z > 30 \text{ min} \\ 0.96 \text{ sgn } (L_y) & \text{if } 1 \text{ min} < \Theta_z \leq 30 \text{ min} \end{cases}$$

$$\text{POSEY} = \begin{cases} 0 & \text{if } \Theta_z \leq 1 \text{ min} \\ 0 & \text{if } \Theta_z > 30 \text{ min} \\ 0.96 \text{ sgn } (-L_x) & \text{if } 1 \text{ min} < \Theta_z \leq 30 \text{ min} \end{cases}$$

where POSEX and POSEY are the position error commands from an ideal sensor. In the fine mode, a position sensor is used to pick off the transfer lens positions, t_y and t_x, for use by the telescope control system. An idealized sensor is modeled as follows:

$$\text{POSEX} = \begin{cases} 0 & \text{if } \Theta_z > 1 \text{ min} \\ K_1 t_y / L_1 & \text{if } \Theta_z \leq 1 \text{ min} \end{cases}$$

$$\text{POSEY} = \begin{cases} 0 & \text{if } \Theta_z > 1 \text{ min} \\ -K_1 t_x / L_1 & \text{if } \Theta_z \leq 1 \text{ min} \end{cases}$$

The position sensor lag, shown in Figure 2.1-2 and discussed in Paragraph 2.1, is simulated, using Tustin's Method, by the difference equation

$$POSXL(nH_c) = T_{ao}\ POSEX(nH_c) + T_{a1}\ POSEX((n-1)H_c)$$

$$-T_{a2}\ POSXL((n-1)H_c), \qquad (2.4\text{-}1)$$

where H_c = time step for telescope control equations = .01 seconds, for the x channel with an analogous equation used for the y channel. Coefficients T_{ao}, T_{a1}, and T_{a2} are defined in Table 2.4-1.

For program implementation the OR gate of Figure 2.1-2 is replaced by a test on cos Θ_z. If $|\cos\Theta_z|$ is greater than the cosine of 1 arc minute, the coarse sensor model provides POSEX for use in Equation (2.4-1). If $\cos\Theta_z$ is less than the cosine of 1 arc minute, the fine sensor model provides the required input.

The rate gyros used to measure the telescope rates, $\dot{\alpha}_x$ and $\dot{\alpha}_y$, about the x_T and y_T axes are represented as second order systems. The difference equation used for simulation of the x channel rate gyro is:

$$RATEX(nH_c) = T_{do}\ \dot{\alpha}_x(nH_c) + T_{d1}\ \dot{\alpha}_x((n-1)H_c) +$$

$$T_{d2}\ \dot{\alpha}_x((n-2)H_c) - T_{c1}\ RATEX((n-1)H_c) -$$

$$T_{c2}\ RATEX((n-2)H_c) \qquad (2.4\text{-}2)$$

with coefficients defined in Table 2.4-1. The y channel rate gyro is simulated analogously. The gyro output, given by Equation (2.4-2), must be limited to 38.4 volts/degree/second.

The position minus rate signals are used to drive the gimbal torque motors. For use in LASIM, it has been shown that the dynamics of the motor are negligible. Thus the motor is represented as $2\ K_a K_m$, with the motor output limited to 18.98 n-m (14 ft. lbs.)

TABLE 2.4-1 TELESCOPE CONTROL DIFFERENCE EQUATION COEFFICIENTS

$$T_{ao} = H_c/(H_c + \tau_{1c})$$

$$T_{a1} = H_c/(H_c + \tau_{1c})$$

$$T_{a2} = (H_c - \tau_{1c})/(H_c + \tau_{1c})$$

$$T_{co} = 4/H_c^2 + 4\zeta\omega_o/H_c + \omega_o^2$$

$$T_{c1} = (-8/H_c^2 + 2\omega_o^2)/T_{co}$$

$$T_{c2} = (4/H_c^2 - 4\zeta\omega_o/H_c + \omega_o^2)/T_{co}$$

$$T_{do} = (180\omega_o^2 K_3/\pi)/T_{co}$$

$$T_{d1} = 2\ T_{do}$$

$$T_{d2} = T_{do}$$

2.4.2 Math Flow

Figure 2.4-1 illustrates functionally the calculations performed in the LASIM program every H_c seconds to simulate the telescope control system. The detailed simulation equations are shown in Table 2.4-2. Difference equation coefficients are defined by Table 2.4-1, with nominal control system parameters given in Figure 2.1-2.

The telescope control equations are solved at 100 cycles per second (i.e., H_c = 0.01 seconds).

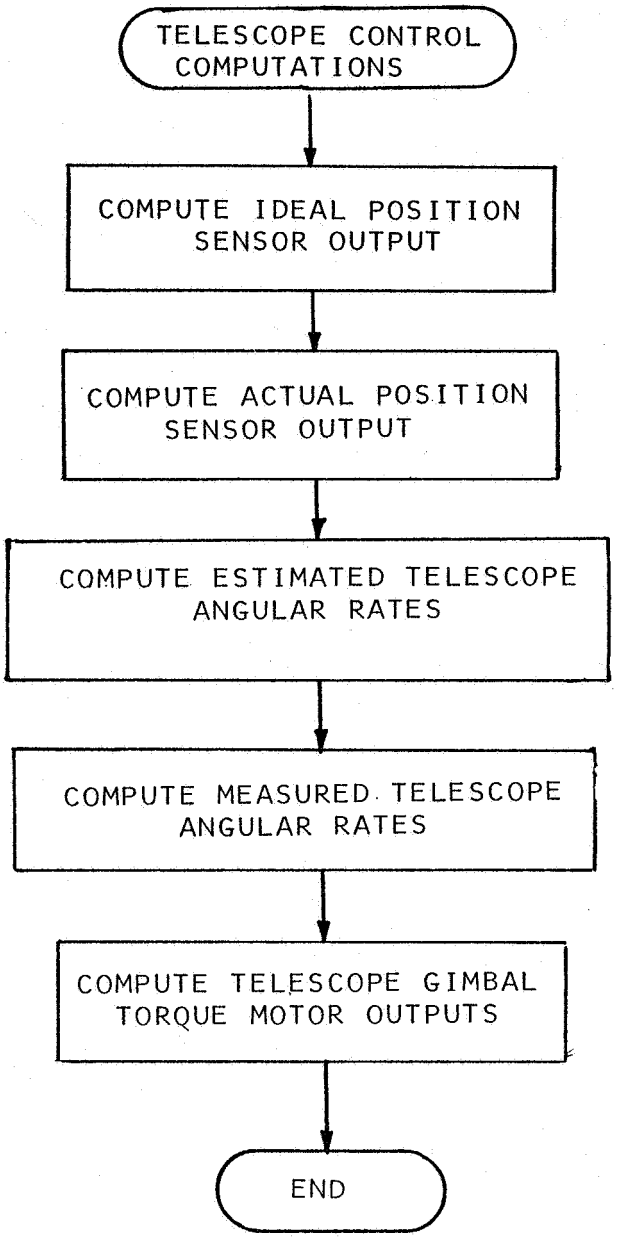

FIGURE 2.4-1 TELESCOPE CONTROL MATH FLOW

TABLE 2.4-2 TELESCOPE CONTROL - DETAILED MATH FLOW

Compute Ideal Position Sensor Output

If $|\cos\Theta_z| \geq \cos(1\ \widehat{\text{min}})$,

$$POSEX(nH_c) = K_1 t_y / L_1$$

$$POSEY(nH_c) = -K_1 t_x / L_1$$

If $\cos(30\ \widehat{\text{min}}) \leq |\cos\Theta_z| < \cos(1\ \widehat{\text{min}})$,

$$POSEX(nH_c) = 0.96\ \text{sgn}(L_y)$$

$$POSEY(nH_c) = 0.96\ \text{sgn}(-L_x)$$

If $|\cos(\Theta_z)| > \cos(30\ \widehat{\text{min}})$,

$$POSEX(nH_c) = 0$$

$$POSEY(nH_c) = 0$$

Compute Actual Position Sensor Output

$$POSXL(nH_c) = T_{ao}\ POSEX(nH_c) + T_{a1}\ POSEX((n-1)H_c) - T_{a2}\ POSXL((n-1)H_c)$$

$$POSYL(nH_c) = T_{ao}\ POSEY(nH_c) + T_{a1}\ POSEY((n-1)H_c) - T_{a2}\ POSYL((n-1)H_c)$$

Compute Estimated Telescope Angular Rates

$$\dot{\psi}_1(nH_c) = \dot{\psi}_1((n-1)H_c) + H_c\ \ddot{\psi}_1((n-1)H_c)$$

$$\dot{\psi}_2(nH_c) = \dot{\psi}_2((n-1)H_c) + H_c\ \ddot{\psi}_2((n-1)H_c)$$

$$\underline{\omega}(nH_c) = \underline{\omega}((n-1)H_c) + H_c\ \dot{\underline{\omega}}((n-1)H_c)$$

$$\psi_1(nH_c) = \psi_1((n-1)H_c) + H_c\ \dot{\psi}_1(nH_c)$$

$$\psi_2(nH_c) = \psi_2((n-1)H_c) + H_c\ \dot{\psi}_2(nH_c)$$

$$\dot{\alpha}_x(nH_c) = [P(nH_c)+\dot{\psi}_1(nH_c)]\cos\psi_2 + [Q(nH_c)\sin\psi_1 - R(nH_c)\cos\psi_1]\sin\psi_2$$

$$\dot{\alpha}_y(nH_c) = Q(nH_c)\cos\psi_1 + R(nH_c)\sin\psi_1 + \dot{\psi}_2(nH_c)$$

TABLE 2.4-2 (continued)

Compute Measured Telescope Angular Rates

$$RATEX(nH_c) = T_{do}\,\dot{\alpha}_x(nH_c) + T_{d1}\,\dot{\alpha}_x((n-1)H_c) + T_{d2}\,\dot{\alpha}_x((n-2)H_c) - T_{c1}\,RATEX((n-1)H_c) - T_{c2}\,RATEX((n-2)H_c)$$

$$RATEY(nH_c) = T_{do}\,\dot{\alpha}_y(nH_c) + T_{d1}\,\dot{\alpha}_y((n-1)H_c) + T_{d2}\,\dot{\alpha}_y((n-2)H_c) - T_{c1}\,RATEY((n-1)H_c) - T_{c2}\,RATEY((n-2)H_c)$$

$$RATEXI(nH_c) = sgn[RATEX(nH_c)]\ \min\{38.4,\ |RATEX(nH_c)|\}$$

$$RATEYI(nH_c) = sgn[RATEY(nH_c)]\ \min\{38.4,\ |RATEY(nH_c)|\}$$

Compute Telescope Gimbal Torque Motor Outputs

$$M_{T_1}'(nH_c) = 2K_aK_m[POSXL(nH_c) - RATEXI(nH_c)]$$

$$M_{T_2}'(nH_c) = 2K_aK_m[POSYL(nH_c) - RATEYI(nH_c)]$$

$$M_{T_1}(nH_c) = sgn[M_{T_1}'(nH_c)]\ \min\{18.98,\ M_{T_1}'(nH_c)\}$$

$$M_{T_2}(nH_c) = sgn[M_{T_2}'(nH_c)]\ \min\{18.98,\ M_{T_2}'(nH_c)\}$$

2.5 POINTING CONTROL SYSTEM

Definition of the pointing control system was obtained from Perkin-Elmer Report No. 8631, dated 31 December 1966. As mentioned previously, the pointing control system implements deflection of the downlink beam from the actual line-of-sight in order that the ground station receiver be illuminated.

In simulating the pointing control function, two distinct groups of calculations are required. The amount and direction of the beam offset is computed on the ground and telemetered to the spacecraft. Then the spaceborne hardware implements the offset commands through the Risely prism servos, in conjunction with a vehicle mounted sun-sensor. These two separate operations must be represented in the LASIM program to simulate the dynamic performance of the pointing control system.

Figure 2.5-1 illustrates the hardware representation used in the LASIM program for the Risely prism servos. The servo elements themselves are characterized as linear elements as seen in the figure. Bias or dc type errors associated with the control transformer (CT) and tachometer have been ignored in representing the pointing control system, since dynamic performance analysis is the desired objective of the LASIM program. It is assumed that bias errors can be compensated for.

The ground command input indicated on Figure 2.5-1 is computed in the LASIM program and discussed in Paragraph 2.5.1. The other system input, the sun sensor roll gimbal angle, is also computed in the LASIM program and discussed in Paragraph 2.5.1. The mechanism of accomplishing the actual downlink beam deflection by actuating the Risely prisms was discussed in Paragraph 2.2.4.

2.5.1 Pointing Control Equation Development

2.5.1.1 Risely Prism Servos

The block diagram of Figure 2.5-1 is easily combined into a single transfer function, $G_p(s)$, relating $\Theta_{P1}(s)$, or the resultant prism rotation angle, to $\Theta_{1C}(s)$, the prism command angle.

$$G_p(s) = \frac{\Theta_{P1}(s)}{\Theta_{1G}(s)} = \frac{a_{po}}{S^2+b_{p1}S+b_{po}} \qquad (2.5\text{-}1)$$

Coefficients a_{po}, b_{po}, and b_{p1} are functions of network parameters and are tabulated in Table 2.5-1. The solution of Equation 2.5-1 is obtained digitally by solving a difference equation formed by using the Tusin substitution discussed in Paragraph 2.3.1. The resulting difference equation is:

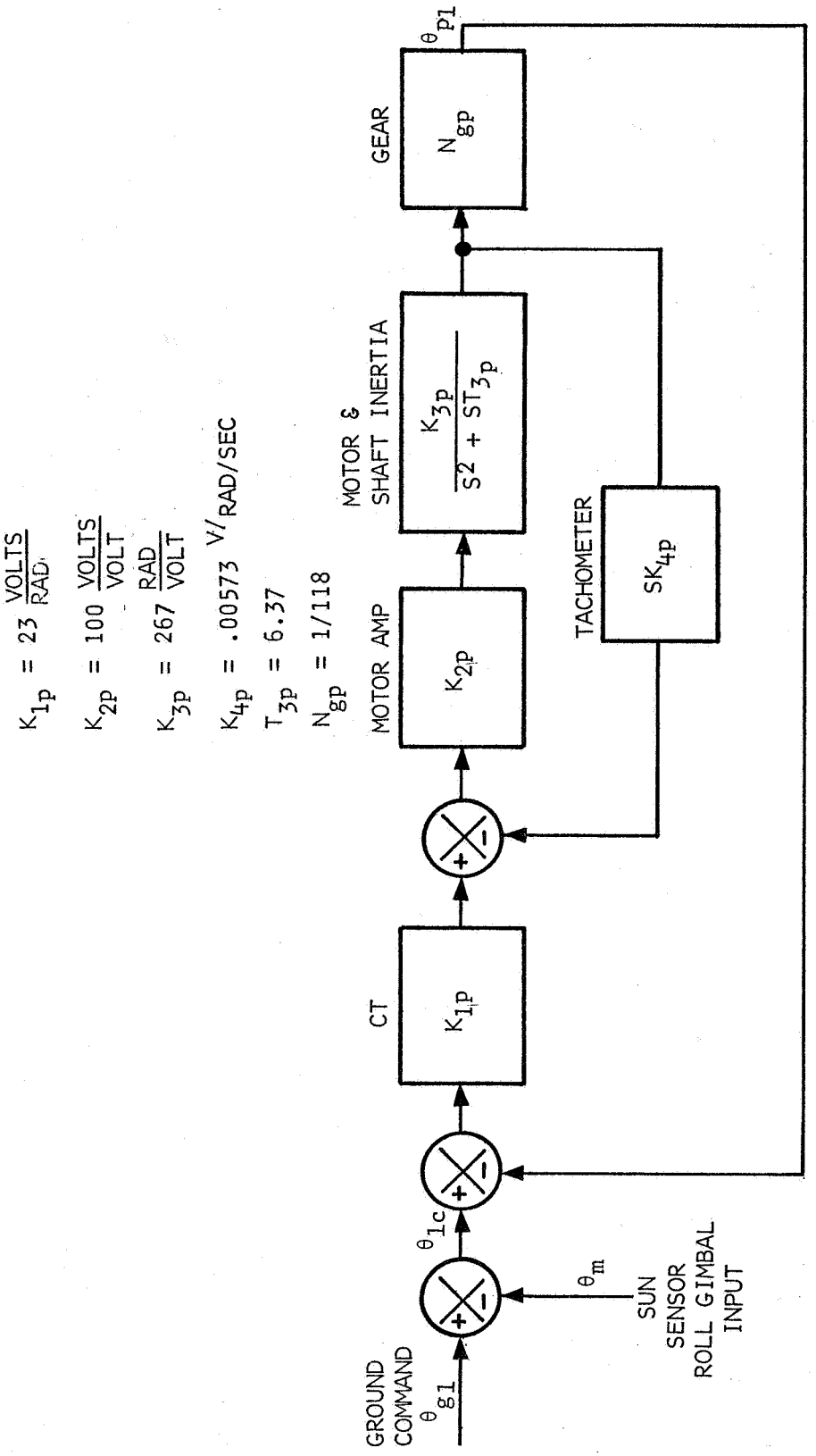

FIGURE 2.5-1 POINT AHEAD SYSTEM BLOCK DIAGRAM

$$\Theta_{P1}(nT) = \frac{1}{d_{op}} \left\{ c_{op}\Theta_{1C}(nT) + c_{1p}\Theta_{1C}[(n-1)T] + c_{2p}\Theta_{1C}[(n-2)T] - d_{1p}\Theta_{P1}[(n-1)T] - d_{2p}\Theta_{P_2}[(n-2)T] \right\} \qquad (2.5\text{-}2)$$

Coefficients c_{op}, ..., d_{op}, ..., d_{2p} are functions of the a_p and b_p coefficients in Equation 2.5-1 and are listed in Table 2.5-1.

2.5.1.2 Ground Computation and Sun Sensor Gimbal Angle Equation Development

In order to point the down-going beam so that the ground receiver is illuminated, compensation is required for the apparent change in position of the ground station during the time interval required for the laser beam to travel from ground station to satellite and return. The apparent change in position of the ground station is a function of the component of relative velocity, between ground station and satellite, normal to the line-of-sight. The phenomenon is most easily considered from a coordinate frame whose origin is at the satellite. Figure 2.5-2 illustrates the quantities under discussion.

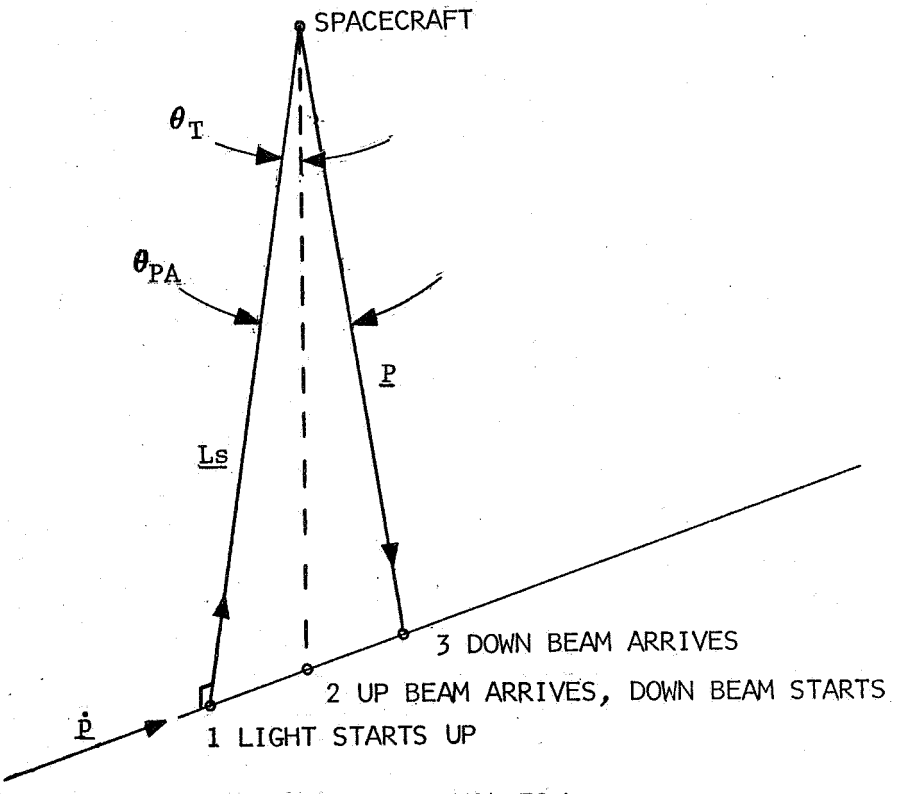

$\dot{P}$ = RELATIVE VELOCITY OF GROUND STATION NORMAL TO Ls
L = UNIT VECTOR IN DIRECTION OF Ls
P = OFFSET, DOWNLINK POINTING VECTOR

FIGURE 2.5-2 TRANSIT TIME EFFECTS

TABLE 2.5-1 POINT-AHEAD DIFFERENCE EQUATION COEFFICIENTS

$$\omega = \sqrt{K_{jp}\, n_{gp}\, K_{2p}\, K_{3p}}$$

$$\zeta = \frac{T_{3p} + K_{2p}\, K_{3p}\, K_{4p}}{2\omega}$$

Not calculated in Pointing Control program

$$a_{po} = \omega^2$$

$$b_{po} = \omega^2$$

$$b_{p1} = 2\zeta\omega$$

$$\lambda = \frac{4}{T^2} + \frac{4}{T}\zeta\omega + \omega^2$$

$$\beta = \frac{4}{T^2\lambda}$$

$$\gamma = \frac{4\zeta\omega}{T\lambda}$$

$$c_{op}/d_{op} = \omega^2/\lambda$$

$$c_{1p}/d_{op} = 2\omega^2/\lambda$$

$$c_{2p}/d_{op} = \omega^2/\lambda$$

$$-d_{1p}/d_{op} = 2\beta - \omega^2/\lambda$$

$$-d_{2p}/d_{op} = 2\gamma - 1$$

The time required for light to travel from the ground at position 1 to the spacecraft is:

$$t = \frac{|\underline{L}_s|}{c}, \qquad (2.5\text{-}3)$$

$\underline{L}_s$ = line-of-sight vector from ground to spacecraft at position 1 on Figure 2.5-2.

c = speed of light

During time t, the ground station has moved to position 2 on Figure 2.5-2. The angular offset is:

$$\Theta_T = \frac{|\dot{\underline{p}}|t}{|\underline{L}_s|} \text{ (radians)}, \qquad (2.5\text{-}4)$$

where $|\dot{\underline{p}}|$ is the component of relative velocity normal to $\underline{L}_s$ or

$$|\dot{\underline{p}}| = \left|\dot{\underline{L}}_s \times \underline{L}\right|$$

$\dot{L}_s$ = line of sight rate or total relative velocity vector,

$\underline{L}$ = unit vector in direction of $\underline{L}_s$.

It is considered that the downgoing beam leaves the satellite when the uplink beam arrives. If it is assumed that $|\underline{L}_s|$ does not change during time t and continues to remain constant, and that $|\dot{\underline{p}}|$ remains constant, the time required for the return beam to travel from satellite to position 3, on Figure 2.5-2, is also t as given by Equation 2.5-3. Since t is about .1 second, the above assumptions are valid, and the total angular offset from "apparent line-of-sight" $\underline{L}_s$ to "desired pointing direction" $\underline{P}$ is $2\Theta_T$ or,

$$\theta_{PA} = \frac{2|\dot{\underline{p}}|}{c}, \qquad (2.5\text{-}5)$$

where θ_{PA} is called the "point-ahead angle". The pointing control system offsets the downlink beam from the line-of-sight by θ_{PA} radians.

In Figure 2.5-2, it is indicated that the beam deflection is made in the plane formed by the relative velocity component $\dot{\underline{p}}$ and the line-of-sight vector $\underline{L}_s$. Since the spaceborne system cannot determine the orientation of this plane, a means is required by which the proper direction of the beam offset will be assured. Figure 2.5-3 illustrates the quantities used to provide a reference, from which the pointing control system can determine the correct orientation of the pointing vector $\underline{P}$.

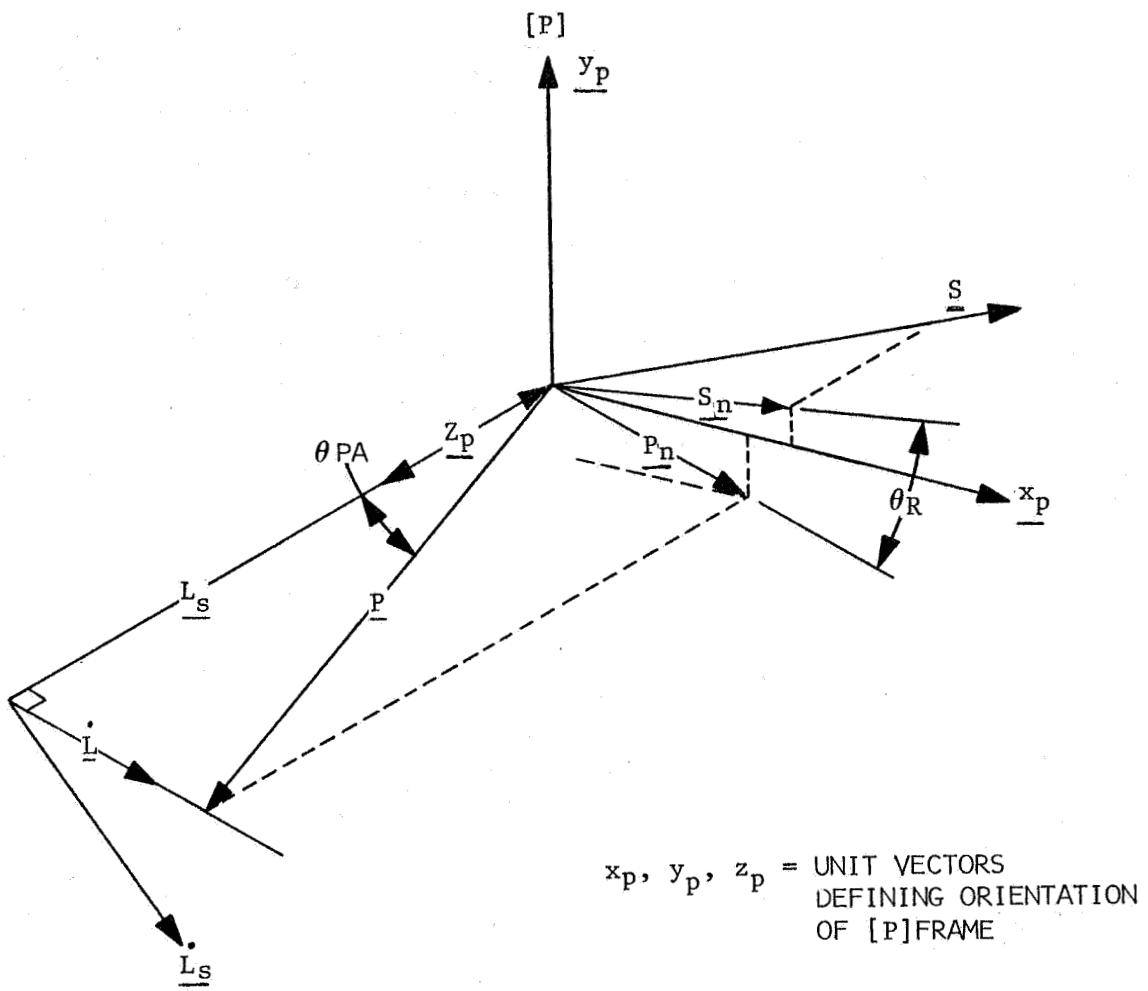

FIGURE 2.5-3 POINT AHEAD GEOMETRY

From spacecraft and sun ephemeris, ground computations are made to establish the components of a vector ($\underline{S}$) from the satellite to the sun (or other stellar reference) in an orthogonal coordinate frame shown as the [P] frame in Figure 2.5-3. The [P] frame has one axis (z_p) along the line-of-sight vector, L_s, and the other axes normal to L_s. The desired pointing vector $\underline{P}$ is also computed in this frame. The angle θ_R in Figure 2.5-3 is determined between S_n and P_n, the components of the sun vector $\underline{S}$ and pointing vector $\underline{P}$ respectively, which are normal to the line-of-sight direction. The angle θ_R establishes the "roll reference angle" of the downlink beam offset from the sun vector component S_n.

By using a telescope mounted sun sensor in the spaceborne system, the angle θ_m between the vector S_n and the telescope y_T axis, may be determined as shown in Figure 2.5-4. This angle

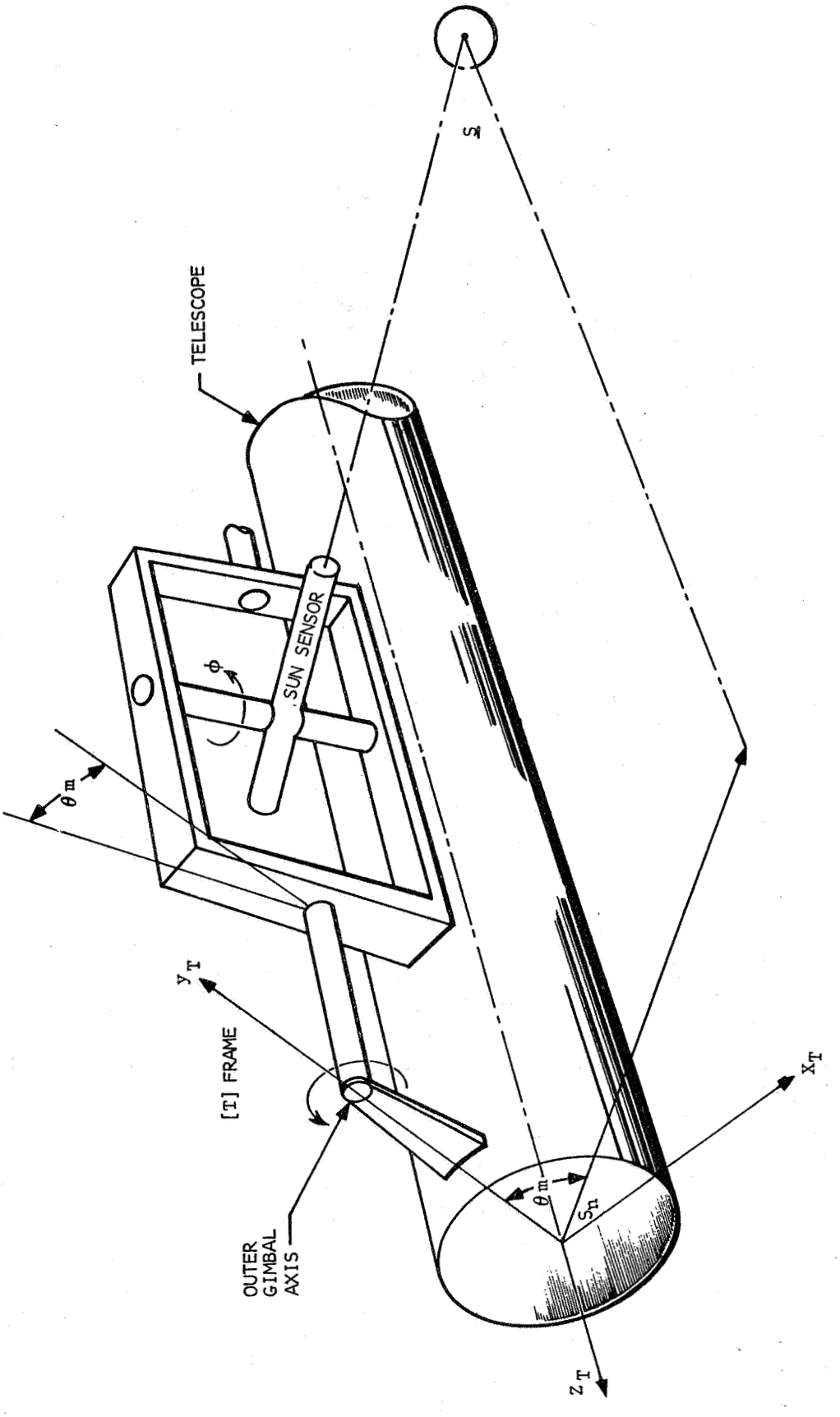

FIGURE 2.5-4 SUN SENSOR ORIENTATION

provides rotational information from a physical reference on the telescope, to the sun line projection S_n, from which the pointing control system can effect the downlink beam roll offset Θ_R. It is seen that the sun vector, which can be computed on the ground and also detected in space, provides the necessary reference link to allow correct pointing. It should be noted that detailed hardware simulation of sun sensor operation is not represented in the LASIM program.

Figure 2.5-5 summarizes the information combined to generate the Risely prism servo command angle θ_{1C} as shown on Figure 2.5-1. The roll angle, with reference the z_T axis, which the Risely prisms are commanded to produce, is denoted θ_{RC} in Figure 2.5-5. The [T] coordinate frame shown in the figure is that defined earlier where z_T points down along the telescope longitudinal axis and the y_T axis is aligned with the telescope inner gimbal axis.

To summarize the preceding, θ_{PA} and θ_R shown on Figure 2.5-3 are computed on the ground and the following combinations of these angles are telemetered to the spacecraft:

$$\left.\begin{aligned} \theta_{g1} &= \theta_R + \sin^{-1}(\theta_{PA1}/m) \\ \theta_{g2} &= \theta_R - \sin^{-1}(\theta_{PA1}/m) \end{aligned}\right\} \qquad (2.5\text{-}6)$$

where θ_{PA_1} is in prism units as opposed to "aperture units."

The sun sensor mounted to the telescope measures the angle θ_m shown on Figure 2.5-4 and 2.5-5. This angle is combined with θ_{g1} and θ_{g2} to produce the servo commands,

$$\left.\begin{aligned} \theta_{1c} &= \theta_{g1} + \theta_m \\ \theta_{2c} &= \theta_{g2} + \theta_m \end{aligned}\right\} \qquad (2.5\text{-}7)$$

indicated on Figure 2.5-1.

It is to be noted that the frame in which θ_m is measured ([T] frame) is not exactly aligned with the [P] frame in which θ_R and θ_{PA} are determined. The degree to which the [T] frame is parallel to the [P] frame is a function of how well the telescope gimbal control system works to align the z_T axis with the line-of-sight. The pointing error calculations in the LASIM program reflect the contribution of this error source.

The actual ground computations which will be made in support of the LCSE mission are not defined; however the basic quantities illustrated in the foregoing will be determined. The simulation of the ground computations used in the LASIM program is intended to provide an input for the pointing control system only. For

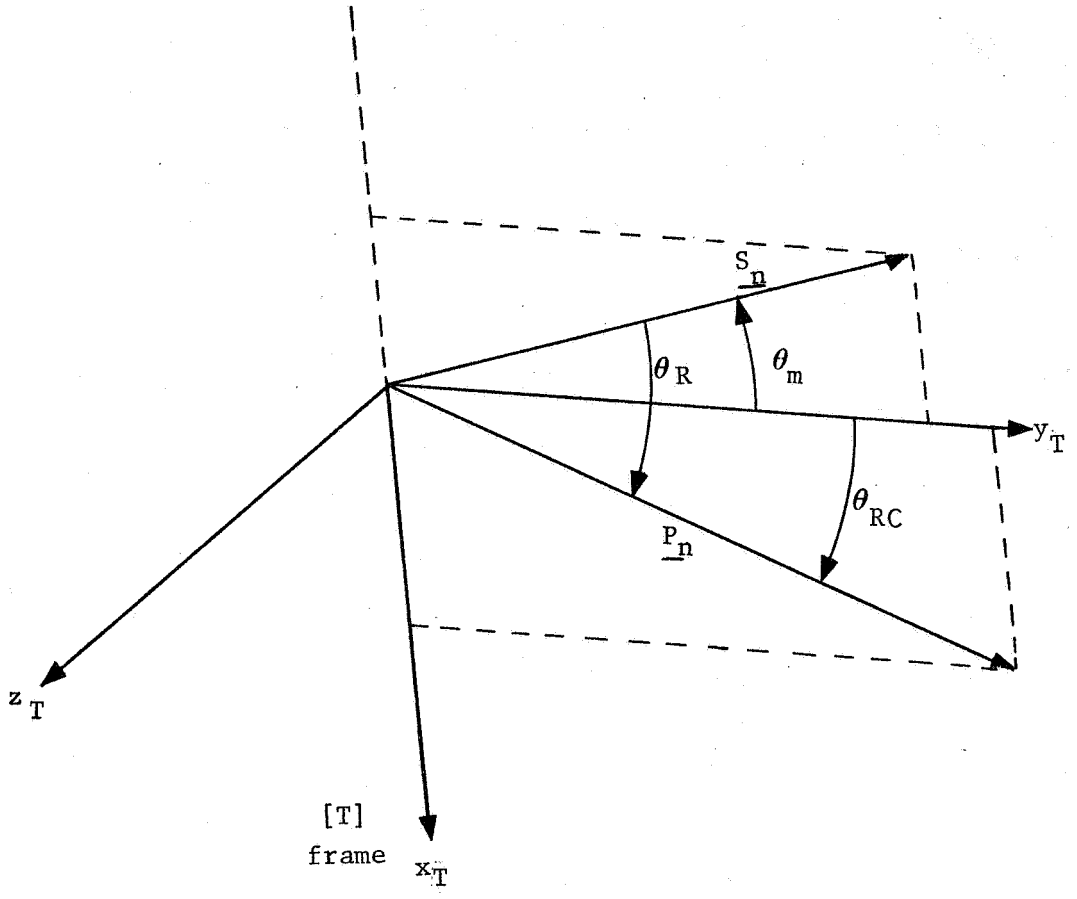

$$\theta_{RC} = \theta_R + \theta_m$$

FIGURE 2.5-5 ROLL REFERENCE ANGLES FOR POINT AHEAD

this reason, consideration has not been given to refraction of the actual line-of-sight and other non-ideal effects. Also, the accuracy with which the satellite's position and velocity may be determined, from tracking data, will affect the overall accuracy of the pointing operation. Consideration of these effects is beyond the scope of the current LASIM development effort.

The basis for determination of the various angles required to generate the Risely prism servo commands has been illustrated in this paragraph. These angles are determined by solving straightforward vector equations in terms of the vectors illustrated on Figures 2.5-2, 2.5-3, and 2.5-4. The actual equations solved, and the solution sequence, are indicated in Paragraph 2.5.2.

The final calculations made in the LASIM program related to the pointing operation determine the "pointing error" or the angular difference, in telescope aperture space, between the desired pointing direction and the actual pointing direction. Since the accuracy with which the tracking system can align with line-of-sight affects the pointing error, the final error calculations reflect the combined errors of the tracking and pointing systems. These pointing error equations are also shown in Paragraph 2.5.2.

2.5.2 Pointing Simulation Math Flow

Figure 2.5-6 illustrates, functionally, the calculations performed in the LASIM program to simulate the following pointing operations:

1. Ground computations to determine Θ_{g1}, Θ_{g2}
2. Generation of the sun sensor gimbal angle, Θ_m
3. Risely prism servo operation
4. Final pointing error evaluation.

A brief word is given here to explain the sun vector, $\underline{S}$, used in the LASIM simulation. Since the sun vector remains essentially constant during the period of time for which a simulation run will be made, and since the sun vector is used only as a reference quantity, an arbitrary vector is chosen. Further, since only the orientation of the sun vector is of interest, a unit vector is selected for $\underline{S}$. The sun vector is defined such that it has the following components in the [T] frame initially:

$$\underline{S}'_{[T]} = -\frac{1}{\sqrt{2}}\underline{x}_T + \frac{1}{\sqrt{2}}y_T + (0)\,Z_T. \qquad (2.5\text{-}8)$$

The vector $\underline{S}'$ is next transformed into inertial coordinates and remains fixed in inertial space. Notice that as the [T] frame axes move with the telescope during the course of a simulation,

the components of the vector $\underline{S}$ in the [T] frame will change from the initial values indicated in Equation 2.5-8.

The equations solved in each block on Figure 2.5-6 are illustrated in Table 2.5-1. Paragraph 2.6 discusses the various coordinate transformations and the manner in which they are determined.

TABLE 2.5-2 POINTING CONTROL MATH FLOW

- Initialize Sun Vector in Inertial Coordinates -

$$\underline{S} = [T2I][\underline{S}'_{[T]}]$$

- Compute [P] Frame Orientation -

$$\underline{z}_P = -\underline{L}_s / |\underline{L}_s|$$

$$\underline{y}_P = \dot{\underline{L}}_S \times -\underline{L}_S / |\dot{\underline{L}}_S \times -\underline{L}_S|$$

$$\underline{x}_P = \underline{z}_P \times \underline{y}_P$$

- Compute Point Ahead Angle -

$$\Theta_{PA} = \frac{2}{C} |\dot{\underline{L}}_S \times \underline{L}|$$

- Compute Unit Vectors in P_n, S_n Directions -

$$\underline{P}_u = \frac{\underline{P}_n}{|\underline{P}_n|} = \underline{x}_P$$

$$\underline{b} = \underline{S} \times -\underline{L}$$

$$\underline{S}_n = -\underline{L} \times \underline{b}$$

$$\underline{S}_u = \frac{\underline{S}_n}{|\underline{S}_n|}$$

Compute Roll Reference Angle -

$$\Theta_R = \cos^{-1}\left[\frac{\underline{S}_u \cdot \underline{P}_u}{|\underline{S}_u| \; |\underline{P}_u|}\right] = \cos^{-1}(\underline{S}_u \cdot \underline{P}_u)$$

- Compute Sun Sensor Gimbal Angle -

$$\underline{S}| = [I2T]\,\underline{S}| = S_x \underline{x}_T + S_y \underline{y}_T + S_z \underline{z}_T$$
[T] frame [I] frame

$$\Theta_m = \tan^{-1}\left(\frac{S_x}{S_y}\right)$$

- Compute Risely Prism Servo Commands -

$$\Theta'_{PA} = \text{Sin}^{-1}(\Theta_{PA} \frac{609.601}{6M}) \text{ (conversion to prism rotation)}$$

$$\Theta_{g1} = \Theta_R + \Theta'_{PA}$$

$$\Theta_{g2} = \Theta_R - \Theta'_{PA}$$

$$\Theta_{1C} = \Theta_m + \Theta_{g1}$$

$$\Theta_{2C} = \Theta_m + \Theta_{g2}$$

- Simulate Risely Prism Servo Operation -

$$\Theta_{P1}(nT) = \frac{1}{d_{op}} \left\{ c_{op} \Theta_{1C}(nT) + c_{1p}\Theta_{1C}[(n-1)T] + c_{2p}\Theta_{1C}[(n-2)T] - d_{1p}\Theta_{P1}[(n-1)T] - d_{2p}\Theta_{P1}[(n-2)T] \right\}$$

$$\Theta_{P2}(nT) = \frac{1}{d_{op}} \left\{ c_{op}\Theta_{2C}(nT) + c_{1p}\Theta_{2C}[(n-1)T] + C_{2p}\Theta_{2C}[(n-2)T] - d_{1p}\Theta_{P2}[(n-1)T] - d_{2p}\Theta_{P2}[(n-2)T] \right\}$$

- Compute Actual Pointing Vector -

$$\Theta_{PA \text{ actual}} = .00291 \text{ Sin}(\frac{\Theta_{P1} + \Theta_{P2}}{2}) = \Theta_{PAa} \text{ (in prism units)}$$

$$\Theta_{R \text{ actual}} = \frac{\Theta_{P1} - \Theta_{P2}}{2} = \Theta_{Ra}$$

$$\underline{P_a} = P_{ax}\,\underline{x_T} + P_{ay}\,\underline{y_T} + P_{az}\,\underline{z_T}$$

$$P_{ax} = [t_x + 6 \cos \Theta_{Ra} \tan \Theta_{PAa}] \frac{1}{609.601}$$

$$P_{ay} = [t_y + 6 \sin \Theta_{Ra} \tan \Theta_{PAa}] \frac{1}{609.601}$$

- Compute Desired Pointing Vector -

$$\left| \frac{\underline{P}}{|\underline{P}|} = \underline{L} \cos \Theta_{PA} + \underline{X_p} \sin \Theta_{PA} = \underline{P_1} \right| = \text{unit vector in } \underline{P} \text{ direction}$$

[I] frame [I] frame

$$\underline{P_1}\Big|_{[T]} = [I2T]\ \underline{P_1}\Big|_{[I]} = P_{1x}\ \underline{X_T} + P_{1y}\ \underline{y_T} + P_{1z}\ \underline{z_T}$$

- Compute Total Pointing Errors -

$$\varepsilon_x = P_{1x}/609.601 - P_{ax} \text{ (radians)}$$

$$\varepsilon_y = P_{1y}/609.601 - P_{ay} \text{ (radians)}$$

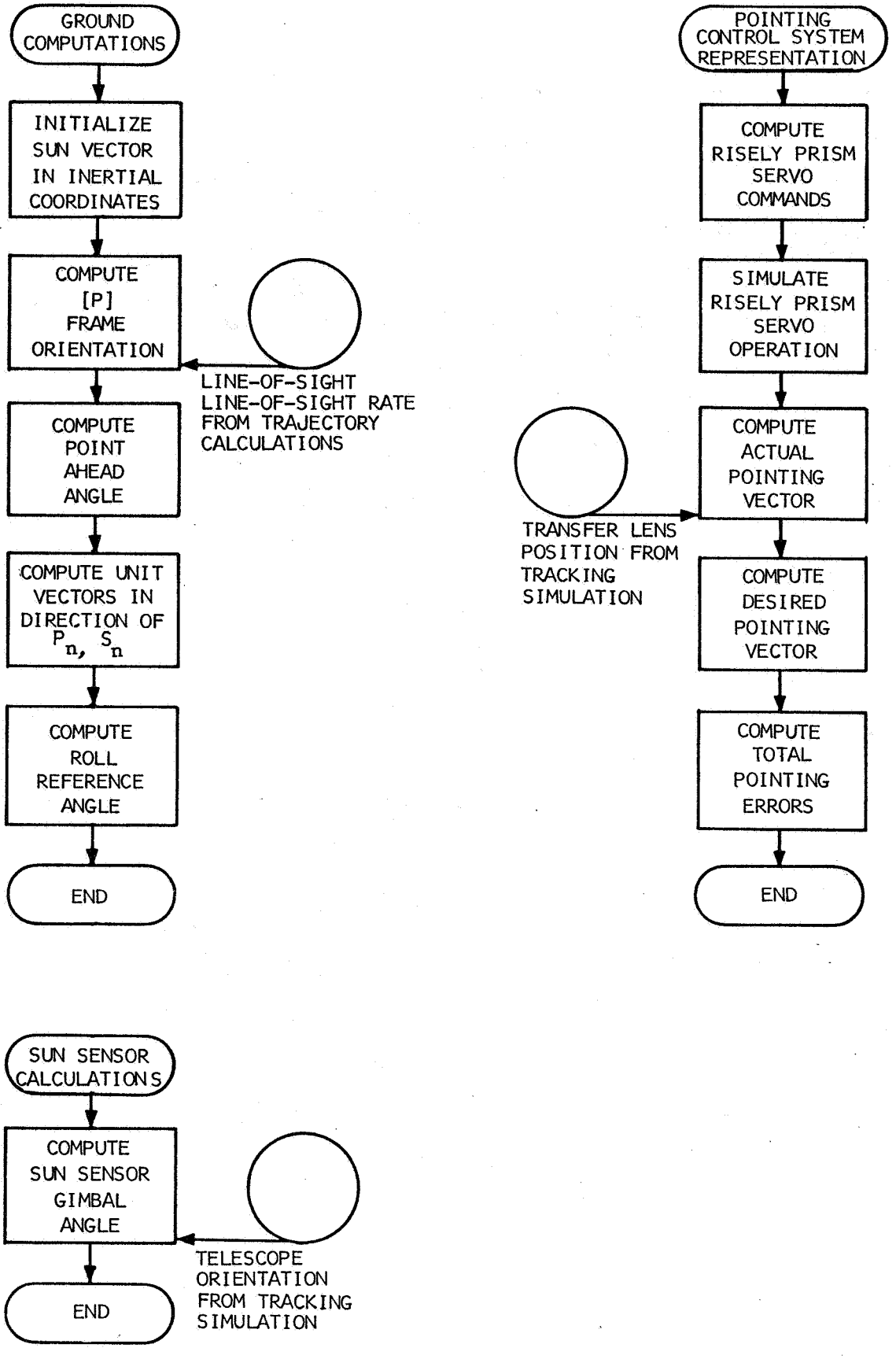

FIGURE 2.5-6 POINTING CONTROL MATH FLOW

2.6 MATRIX TRANSFORMATION FORMULATION

Two problems are to be addressed here. First, the equations which must be solved to determine the transformation matrix from telescope to inertial coordinates [T2I], as a function of time will be derived. The basic equations are differential equations relating derivatives of elements of [T2I] (direction cosine rates) to the inertial rate of the telescope, $\underline{\omega}+\underline{\omega}^{12}=\underline{\omega}_4$. The other problem addressed is that of computing the initial attitude of the telescope and body, given initial values for ψ_1, ψ_2, and the pitch and yaw telescope offset angles, α_x and α_y.

2.6.1 Equation Development

2.6.1.1 Computation of [T2I]

Let $B=[b_{ij}]$ be the matrix which transforms components of vectors from some rotating coordinate frame to an inertial frame; i.e., if vector $\underline{V}$ has components $[x\ y\ z]^T$ in rotating coordinates and $[u\ v\ w]^T$ in inertial coordinates, then

$$\begin{bmatrix} u \\ v \\ w \end{bmatrix} = B \begin{bmatrix} x \\ y \\ z \end{bmatrix}$$

Let $\underline{\Omega}$ be the angular velocity of the rotating coordinate system with respect to inertial coordinates. Let $\underline{\Omega}$ have components $[\omega_x\ \omega_y\ \omega_z]^T$ relative to the rotating system. Then it is known that, for i=1,2,3,

$$\left.\begin{aligned} \dot{b}_{i1} &= \omega_z b_{i2} - \omega_y b_{i3} \\ \dot{b}_{i2} &= \omega_x b_{i3} - \omega_z b_{i1} \\ \dot{b}_{i3} &= \omega_y b_{i1} - \omega_x b_{i2} \end{aligned}\right\} \qquad (2.6\text{-}1)$$

These are the basic equations needed to find [T2I] as a function of time.

Equations (2.6-1) can be written equivalently as

$$\dot{\underline{b}}_i = \Omega \underline{b}_i \qquad (2.6\text{-}2)$$

where $\underline{b}_i$ is a row vector of B with components $[b_{i1}\ b_{i2}\ b_{i3}]^T$ and

$$\Omega = \begin{bmatrix} 0 & \omega_z & -\omega_y \\ -\omega_z & 0 & \omega_x \\ \omega_y & \omega_x & 0 \end{bmatrix}$$

A numerical technique must be employed to solve the differential equations (2.6-1) or (2.6-2) on a digital computer. For LASIM the standard fourth order Runge-Kutta method was chosen. It was assumed that $\underline{\Omega}$, the angular velocity vector, was constant over each time step, H_C. Under this assumption the Runge-Kutta method yields, for i=1, 2, 3 and n=0, 1, ...,

$$\underline{b}_i((n+1)H_C) = \underline{b}_i(nH_C) + (\underline{k}_{i1}+2\underline{k}_{i2}+2\underline{k}_{i3}+\underline{k}_{i4})/6 \qquad (2.6\text{-}3)$$

where

$$\underline{k}_{i1} = H_C\Omega\underline{b}_i(nH_C), \qquad (2.6\text{-}4)$$

$$\underline{k}_{i2} = H_C\Omega[\underline{b}_i(nH)+\tfrac{1}{2}\underline{k}_{i1}] = \underline{k}_{i1}+\frac{H_C}{2}\Omega\underline{k}_{i1}, \qquad (2.6\text{-}5)$$

$$\underline{k}_{i3} = H_C\Omega[\underline{b}_i(nH_C)+\tfrac{1}{2}\underline{k}_{i2}] = \underline{k}_{i1}+\frac{H_C}{2}\Omega\underline{k}_{i2}, \qquad (2.6\text{-}6)$$

$$\underline{k}_{i4} = H_C\Omega[\underline{b}_i(nH_C)+\underline{k}_{i3}] = \underline{k}_{i1}+H_C\Omega\underline{k}_{i3}. \qquad (2.6\text{-}7)$$

The above method can be applied to computation of [T2I] by replacing b_{ij} by T2I (i,j) and $\underline{\Omega}$ By $\underline{\omega}_4$. To improve the accuracy of the method, the evaluation of Equations (2.6-3) through (2.6-7) for $\underline{b}_i((n+1)H_C$ is made using

$$[\omega_{4_x}((n+1)H_C)+\omega_{4_x}(nH_C)]/2,\ [\omega_{4_y}((n+1)H_C)+\omega_{4_y}(nH_C)]/2,$$

and $[\omega_{4_z}((n+1)H_C)+\omega_{4_z}(nH_C)]/2$ for ω_x, ω_y, and ω_z (recall that ω_x, ω_y, and ω_z were assumed constant over each time step).

A new value for [T2I] is computed every H_C=0.01 seconds using the Runge-Kutta method. However, [T2I] must be updated for each fine step, T, where T = .002 seconds. Satisfactory results have been obtained by using a first order extrapolation procedure within the 0.01 second intervals.

That is,

$$[T2I]((m+1)T) = [T2I](mT)+T\frac{d}{dt}[T2I](nH_C) \qquad (2.6\text{-}8)$$

where $(n+1)H_C<(m+1)T\leq(n+2)H_C$. Each time [T2I] is recomputed using the Runge-Kutta method, [T2I](mT) is reinitialized. Finally, from Equations (2.6-2) and (2.6-4) it is seen that $\underline{k}_{11}/H_C$ is a row of $\frac{d}{dt}[T2I](nH_C)$. Thus a special computation for $\frac{d}{dt}[T2I]$ is not required.

2.6.1.2 Initialization of Body and Telescope Attitudes

The initial body and telescope attitude orientations are determined in the LASIM program by computation of the telescope to inertial matrix, [T2I], and the telescope to body matrix, [T2B]. In order to provide flexibility to the user, these matrix computations are based upon input values for the telescope gimbal angles, ψ_1 and ψ_2, and pitch and yaw telescope offset angles, α_x and α_y. The additional degree of freedom (in roll) is removed by assuming that the x_B and x_T axes "nominally" are along $\underline{V} \times \underline{L}_M$, where $\underline{V}$ is the vehicle inertial velocity vector and $\underline{L}_M$ is the normalized line-of-sight <u>from</u> ground <u>to</u> spacecraft.

To derive the required initialization equations, it is first necessary to find the nominal [T2I] matrix, [T2IN], which specifies the telescope attitude for $\alpha_x = \alpha_y = 0$. For this case z_T is along $-\underline{L}_M$, x_T is along $\underline{V} \times \underline{L}_M$, and y_T is perpendicular to x_T and z_T.

It is known that the columns of [T2IN], $\underline{C}_1$, $\underline{C}_2$, and $\underline{C}_3$ must be given by:

$$\underline{C}_3 = -\underline{L}_M$$

$$\underline{C}_1 = \underline{V} \times \underline{L}_M / |\underline{V} \times \underline{L}_M|$$

$$\underline{C}_2 = C_3 \times \underline{C}_1.$$

Then

$$[T2IN] = [\underline{C}_1\ \underline{C}_2\ \underline{C}_3] \qquad (2.6\text{-}9)$$

where it is understood that, in Equation (2.6-9), $\underline{C}_1$, $\underline{C}_2$, and $\underline{C}_3$ stand for the 3 x 1 matrices made up of components of $\underline{C}_1$, $\underline{C}_2$, and $\underline{C}_3$ relative to the [I] frame.

The angles, α_x and α_y, are defined in Figure 2.6-1. It is seen that their effect is to misalign the z_T axis in pitch and yaw from the line of sight.

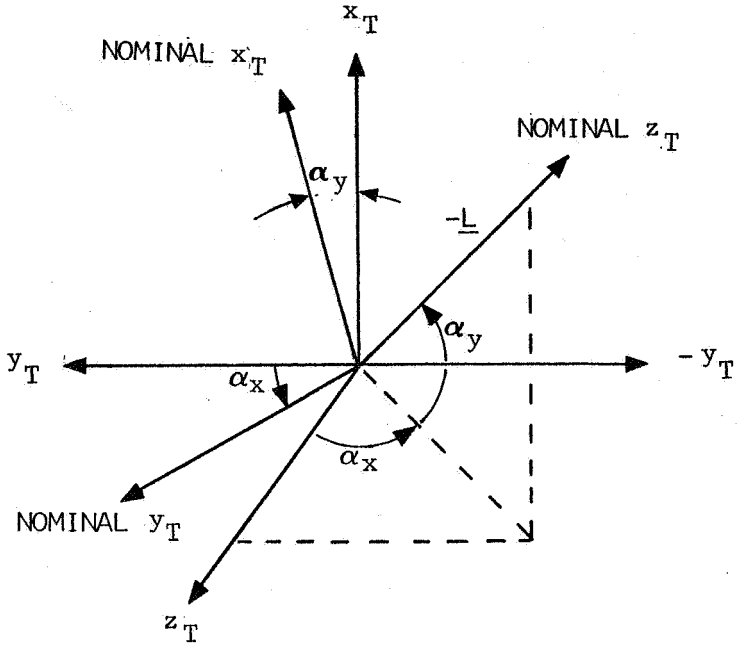

FIGURE 2.6-1 DEFINITION OF TELESCOPE OFFSET ANGLES

Based on the definition of α_x and α_y, the matrix, [OFF], which relates the actual telescope frame to the nominal frame is given by:

$$[OFF] = \begin{bmatrix} \cos\alpha_y & 0 & -\sin\alpha_y \\ 0 & 1 & 0 \\ \sin\alpha_y & 0 & \cos\alpha_y \end{bmatrix} \begin{bmatrix} 1 & 0 & 0 \\ 0 & \cos\alpha_x & \sin\alpha_x \\ 0 & -\sin\alpha_x & \cos\alpha_x \end{bmatrix}$$

Moreover, from the definitions,

$$[T2I] = [T2IN][OFF].$$

The body attitude matrix can now be specified, given ψ_1 and ψ_2, by computing:

$$[T2B] = \begin{bmatrix} \cos\psi_2 & 0 & \sin\psi_2 \\ \sin\psi_1 \sin\psi_2 & \cos\psi_1 & -\sin\psi_1 \cos\psi_2 \\ -\cos\psi_1 \sin\psi_2 & \sin\psi_1 & \cos\psi_1 \cos\psi_2 \end{bmatrix}$$

The body to inertial matrix can be computed as $[B2I] = [T2I][T2B]^T$.

2.6.2 Math Flow

2.6.2.1 [T2I] Computation Math Flow

Figure 2.6-2 illustrates functionally the calculations performed in the LASIM program every H_C seconds to compute $[T2I]((n+1)H_C)$

and $\frac{d}{dt}[T2I](nH_C)$ given $[T2I](nH_C)$ and $[\underline{\omega}_4((n+1)H_C) + \underline{\omega}_4(nH_C)]/2$.

It also illustrates the calculations performed every T seconds to compute $[T2I]((m+1)T)$ given $[T2I](mT)$ and

$\frac{d}{dt}[T2I](nH_C)$. Detailed mathematical expressions, corresponding to the descriptions of Figure 2.6-2, are found in Table 2.6-1. The notation of Table 2.6-1 is defined as follows:

$$\underline{k}_{ij} = [C_{ij}\ D_{ij}\ E_{ij}]^T,\ i=1,\ 2,\ 3;\ j=1,\ 2,\ 3,\ 4.$$

$$\frac{d}{dt}[T2I](nH_C)=[DT2I].$$

$$[T2I] = [B]$$

$$[\omega_{4_x}((n+1)H_C) + \omega_{4_x}(nH_C)]/2 = \omega_x$$

$$[\omega_{4_y}((n+1)H_C) + \omega_{4_y}(nH_C)]/2 = \omega_y$$

$$[\omega_{4_z}((n+1)H_C) + \omega_{4_z}(nH_C)]/2 = \omega_z$$

2.6.2.2 Attitude Initialization Math Flow

The computations which must be performed to initialize the telescope and body attitudes are indicated generally in Figure 2.6-3 and in detail in Table 2.6-2.

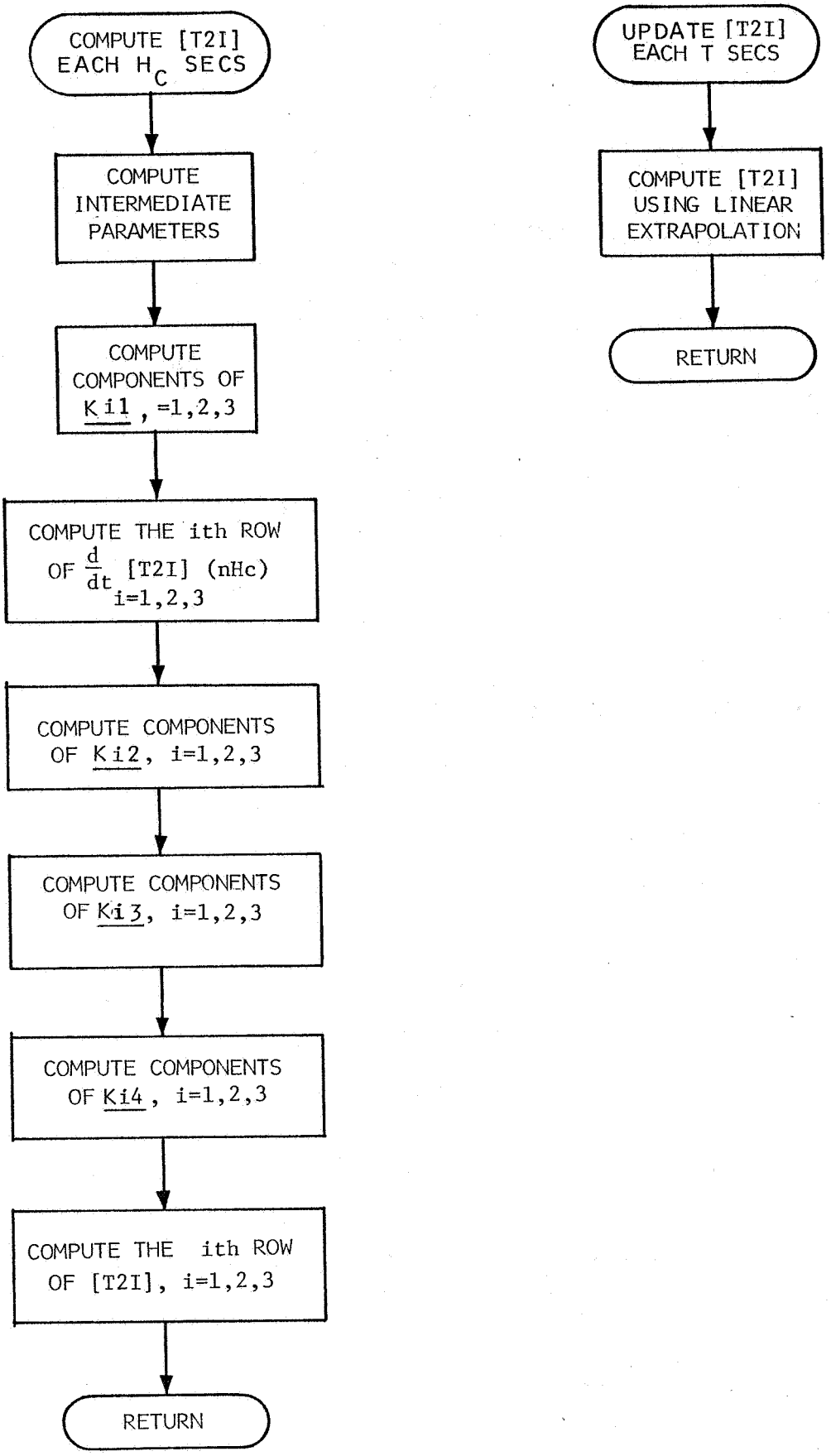

FIGURE 2.6-2 [T2I] COMPUTATION MATH FLOW

TABLE 2.6-1 [T2I] COMPUTATION-DETAILED MATH FLOW

Compute Intermediate Parameters

$T_1 = \omega_x H_c$

$T_2 = \omega_y H_c$

$T_3 = \omega_z H_c$

$T_{H1} = T_1/2$

$T_{H2} = T_2/2$

$T_{H3} = T_{3/2}$

Compute Components of K_{i1}, i=1, 2, 3

$C_{i1} = B_{i2}T_3 - B_{i3}T_2$

$D_{i1} = B_{i3}T_1 - B_{i1}T_3$

$E_{i1} = B_{i1}T_2 - B_{i2}T_1$

Compute the ith Row of $\frac{d}{dt}$[T2I], i=1, 2, 3

$DA_{i1} = C_{i1}/H_C$

$DA_{i2} = D_{i1}/H_C$

$DA_{i3} = E_{i1}/H_C$

Compute Components of k_{i2}, i=1, 2, 3

$C_{i2} = C_{i1} + D_{i1}T_{H3} - E_{i1}T_{H2}$

$D_{i2} = D_{i1} + E_{i1}T_{H1} - C_{i1}T_{H3}$

$E_{i2} = E_{i1} + C_{i1}T_{H2} - D_{i1}T_{H1}$

Table 2.6-1 (Continued)

Compute Components of k_{i3}, i=1, 2, 3

$$C_{i3} = C_{i1}+D_{i2}T_{H3}-E_{i2}T_{H2}$$

$$D_{i3} = D_{i1} + E_{i2}T_{H1}-C_{i2}T_{H3}$$

$$E_{i3} = E_{i1}+C_{i2}T_{H2}-D_{i2}T_{H1}$$

Compute Components of k_{i4}, i=1, 2, 3

$$C_{i4} = C_{i1}+D_{i3}T_{3}-E_{i3}T_{2}$$

$$D_{i4} = D_{i1}+E_{i3}T_{1}-C_{i3}T_{3}$$

$$E_{i4} = E_{i1}+C_{i3}T_{2}-D_{i3}T_{1}$$

Compute ith Row of [T2I], i=1, 2, 3

$$B_{i1}((n+1)H_C)=B_{i1}(nH_C)+(C_{i1}+2(C_{i2}+C_{i3}+C_{i4})/6$$

$$B_{i2}((n+1)H_C)=B_{i2}(nH_C)+(D_{i1}+2(D_{i2}+D_{i3})+D_{i4})/6$$

$$B_{i3}((n+1)H_C) = B_{i3}(nH_C)+(E_{i1}+2(E_{i2}+E_{i3})+E_{i4})/6$$

Compute [T2I] Using Linear Extrapolation

$$[T2I]((m+1)T) = [T2I](mT) + T[DT2I](mH_C)$$

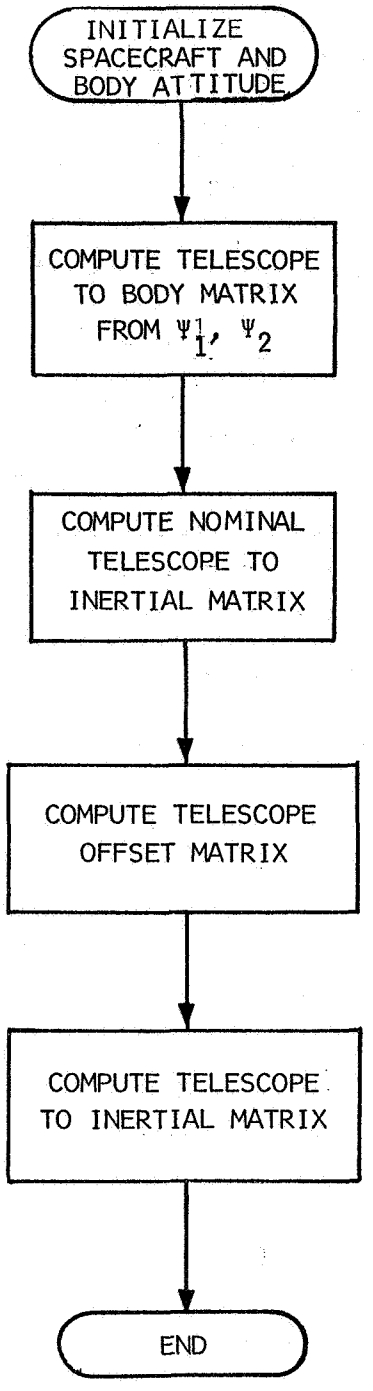

FIGURE 2.6-3 ATTITUDE INITIALIZATION COMPUTATION

TABLE 2.6-2 ATTITUDE INITIALIZATION - DETAILED MATH FLOW

Compute [T2B] from ψ_1, ψ_2.

$T2B(1,1) = \cos \psi_2$

$T2B(1,2) = 0$

$T2B(1,3) = \sin \psi_2$

$T2B(2,1) = \sin \psi_1 \sin \psi_2$

$T2B(2,2) = \cos \psi_1$

$T2B(2,3) = -\sin \psi_1 \cos \psi_2$

$T2B(3,1) = -\cos \psi_1 \sin \psi_2$

$T2B(3,2) = \sin \psi_1$

$T2B(3,3) = \cos \psi_1 \cos \psi_2$

Compute Nominal [T2B], [T2IN].

$T2IN(1,3) = -L_{Mx}$

$T2IN(2,3) = -L_{My}$

$T2IN(3,3) = -L_{Mz}$

$T2IN(1,1) = (V_y L_{Mz} - V_z L_{My}) / |\underline{V} \times \underline{L}_M|$

$T2IN(2,1) = (V_z L_{Mx} - V_x L_{Mz}) / |\underline{V} \times \underline{L}_M|$

$T2IN(3,1) = (V_x L_{My} - V_y L_{Mx}) / |\underline{V} \times \underline{L}_M|$

$T2IN(1,2) = L_{Mz}\, T2IN(2,3) - L_{My} T2IN(3,3)$

$T2IN(2,2) = L_{Mx} T2IN(3,3) - L_{Mz}\, T2IN(1,3)$

$T2IN(3,2) = L_{My} T2IN(1,3) - L_{Mx} T2IN(2,3)$

TABLE 2.6-2 (CONTINUED)

Compute Telescope Offset Matrix, [OFF]

$OFF(1,1) = \cos \alpha_y$

$OFF(1,2) = \sin \alpha_x \sin \alpha_y$

$OFF(1,3) = -\cos \alpha_x \sin \alpha_y$

$OFF(2,1) = 0$

$OFF(2,2) = \cos \alpha_x$

$OFF(2,3) = \sin \alpha_x$

$OFF(3,1) = \sin \alpha_y$

$OFF(3,2) = -\sin \alpha_x \cos \alpha_y$

$OFF(3,3) = \cos \alpha_x \cos \alpha_y$

Compute [T2I]

[T2I] = [T2IN][OFF]

2.7 ORBIT GENERATION

The LASIM program, at the user's selection, will determine the line-of-sight and line-of-sight rate between a ground station and the satellite in an actual, specified earth orbit. These quantities serve as inputs to the tracking system simulation and the poining control computations. For the synchronous orbit mission, the line-of-sight rate is slow relative to the tracking system capability. For purely dynamic response evaluations with the program, a fixed line-of-sight vector may be used, eliminating the requirement to determine the satellite's motion in orbit relative to the ground station. The capability to use actual orbit data is included in the program primarily to provide the flexibility for evaluations in other than synchronous orbits where the line-of-sight rate may not be small.

The so-called orbit generator determines satellite and ground station position in inertial space and from these, the line-of-sight and line-of-sight rate as functions of time. The satellite position is determined by solution of the translational equations of motion of a point mass in a central force field. Only earth's gravitation is considered; drag and other effects are neglected. The gravitational potential model includes the effects of the second through fourth zonal harmonics. The earth is modeled as an ellipsoid, giving a more realistic estimate of satellite altitude over a ground station than would result from a spherical model.

Initialization quantities are required to define trajectory geometry and ground station location. The following quantities are required to permit solution of the system equations.

- Satellite Orbit Parameters:

  Longitude of the ascending node, Ω
  Argument of perifocus, ω'
  Inclination, i
  Semimajor axis, a
  Eccentricity, e
  Time of perifocal passage, T.

- Ground Station Parameters:

  Latitude of ground station
  Longitude of ground station.

2.7.1 Equation Development

The assumption is made that only gravitational attraction acts on the satellite point mass in the development of the orbital equations of motion. The earth's gravitation potential function

is modeled as:

$$\mathcal{J}(R_s, Z_s) = \frac{\mu}{R_s}\left[1 + \frac{K_1}{R_s^2}(1-3r^2) + \frac{K_2}{R_s^3}(3-5r^2) - \frac{K_3}{R_s^4}(3-30r^2+35r^4)\right] \quad (2.7\text{-}1)$$

where: R_s = satellite radius vector magnitude.

Z_s = Z component of satellite radius vector (along North polar axis).

$$K_1 = \frac{JR_E^2}{3}$$

$$K_2 = \frac{HR_E^3}{5}$$

$$K_3 = \frac{-DR_E^4}{35}$$

R_E = earth equatorial radius.

J, H, D - are the coefficients of the zonal harmonics

$$r = \frac{Z_S}{R_S} = \sin\phi$$

ϕ = geocentric latitude.

The spacecraft vector equation of motion is:

$$\ddot{\underline{R}}_S = \frac{\partial \mathcal{J}}{\partial \underline{R}_S} \quad (2.7\text{-}2)$$

where the right hand side of Equation 2.7-2 denotes the gradient of $\mathcal{J}$ with respect to $\underline{R}_S$. Expanding Equation 2.7-2 by performing the indicated differentiation produces the following:

$$\ddot{X}_s = -\frac{\mu X_s}{R_s^3}\left[1 + \frac{3K_1}{R_s^2}(1-5r^2) + \frac{5K_2}{R_s^3}r(3-7r^2) - \frac{5K_3}{R_s^4}(3-42r^2+63r^4)\right] \quad (2.7\text{-}3)$$

$$\ddot{Y}_s = -\frac{\mu Y_s}{R_s^3}\left[1 + \frac{3K_1}{R_s^2}(1-5r^2) + \frac{5K_2}{R_s^3}\, r(3-7r^2) - \frac{5K_3}{R_s^4}(3-42r^2+63r^4)\right] \qquad (2.7\text{-}4)$$

$$\ddot{Z}_s = \frac{\mu}{R_s^3}\left[Z_s\left[1 + \frac{3K_1}{R_s^2}(3-5r^2) + \frac{5K_2}{R_s^3}\, r(6-7r^2) - \frac{5K_3}{R_s^4}(15-70r^2+63r^4)\right] - \frac{3K_2}{R_s^2}\right] \qquad (2.7\text{-}5)$$

These constitute the spacecraft orbital equations of motion. The coordinate system in which the X_s, Y_s and Z_s parameters are defined and computed is an inertially fixed, polar-equatorial frame with Z along the north polar axis and X, Y in the equatorial plane. The X axis points toward the vernal equinox and Y completes the right hand system.

The position and velocity of the ground station in inertial space is simply calculated from knowledge of the station location on the earth's surface and earth rate.

From the position and velocity vectors of the satellite and ground station and their differences, the line-of-sight and line-of-sight rate are easily determined.

2.7.1.1 Cowell Integration

In this section a brief discussion of the method employed for determination of the orbit by numerical integration is presented. To integrate from current time t_n over a time step Δt using Cowell integration one first calculates a set of first points x_1, y_1, z_1, r_1 given by:

$$\left.\begin{aligned} x_1 &= x_n + \frac{\Delta t}{2}\dot{x}_n + \frac{\Delta t^2}{8}\ddot{x}_n \\ y_1 &= y_n + \frac{\Delta t}{2}\dot{y}_n + \frac{\Delta t^2}{8}\ddot{y}_n \\ z_1 &= z_n + \frac{\Delta t}{2}\dot{z}_n + \frac{\Delta t 2}{8}\ddot{z}_n \\ r_1 &= \sqrt{x_1^2 + y_1^2 + z_1^2} \end{aligned}\right\} \qquad (2.7\text{-}6)$$

where x_n, y_n, z_n are current vehicle position coordinates in inertial space, $\dot{x}_n$, $\dot{y}_n$, $\dot{z}_n$ are current vehicle velocity coordinates in inertial space, $\ddot{x}_n$, $\ddot{y}_n$, $\ddot{z}_n$ are current vehicle acceleration coordinates in inertial space.

Using the vehicle acceleration coordinates $\ddot{x}$, $\ddot{y}$, $\ddot{z}$, corresponding to an intermediate time step

$$t = t_n + \frac{\Delta t}{2} ,$$

a set of second points x_2, y_2, z_2, r_2 is calculated.

$$\left.\begin{aligned} x_2 &= x_n + \Delta t\, \dot{x}_n + \frac{\Delta t^2}{2} \ddot{x}_1 \\ y_2 &= y_n + \Delta t\, \dot{y}_n + \frac{\Delta t^2}{2} \ddot{y}_1 \\ z_2 &= z_n + \Delta t\, \dot{z}_n + \frac{\Delta t^2}{2} \ddot{z}_1 \\ r^2 &= \sqrt{x_2^2 + y_2^2 + z_2^2} \end{aligned}\right\} \qquad (2.7\text{-}7)$$

The updated vehicle position coordinates x_{n+1}, y_{n+1}, z_{n+1}, are then calculated by

$$\left.\begin{aligned} x_{n+1} &= x_n + \Delta t[\dot{x}_n + (\tfrac{\Delta t}{6})\ (\ddot{x}_n + 2\ddot{x}_1)] \\ y_{n+1} &= y_n + \Delta t[\dot{y}_n + (\tfrac{\Delta t}{6})\ (\ddot{y}_n + 2\ddot{y}_1)] \\ z_{n+1} &= z_n + \Delta t[\dot{z}_n + (\tfrac{\Delta t}{6})\ (\ddot{z}_n + 2\ddot{z}_1)] \\ r_{n+1} &= \sqrt{x_{n+1}^2 + y_{n+1}^2 + z_{n+1}^2} \end{aligned}\right\} \qquad (2.7\text{-}8)$$

Using the vehicle acceleration coordinates x_2, y_2, z_2 corresponding to the time $t = t_n + t$, the updated vehicle velocity coordinates $\dot{x}_{n+1}$, $\dot{y}_{n+1}$, $\dot{z}_{n+1}$, are given by

$$\left.\begin{aligned}
\dot{x}_{n+1} &= \dot{x}_n + \left(\frac{\Delta t}{6}\right)\left(\ddot{x}_n + 4\ddot{x}_1 + \ddot{x}_2\right) \\
\dot{y}_{n+1} &= \dot{y}_n + \left(\frac{\Delta t}{6}\right)\left(\ddot{y}_n + 4\ddot{y}_1 + \ddot{y}_2\right) \\
\dot{z}_{n+1} &= \dot{z}_n + \left(\frac{\Delta t}{6}\right)\left(\ddot{z}_n + 4\ddot{z}_1 + \ddot{z}_2\right) \\
r_{n+1} &= \sqrt{\dot{x}_{n+1}^2 + \dot{y}_{n+1}^2 + \dot{z}_{n+1}^2}
\end{aligned}\right\} \qquad (2.7\text{-}9)$$

2.7.2 Orbit Generator Math Flow

Figure 2.7-1 illustrates the sequence of calculations performed in the orbit generator subroutine. Table 2.7-2 enumerates the equations evaluated in the blocks shown in Figure 2.7-1.

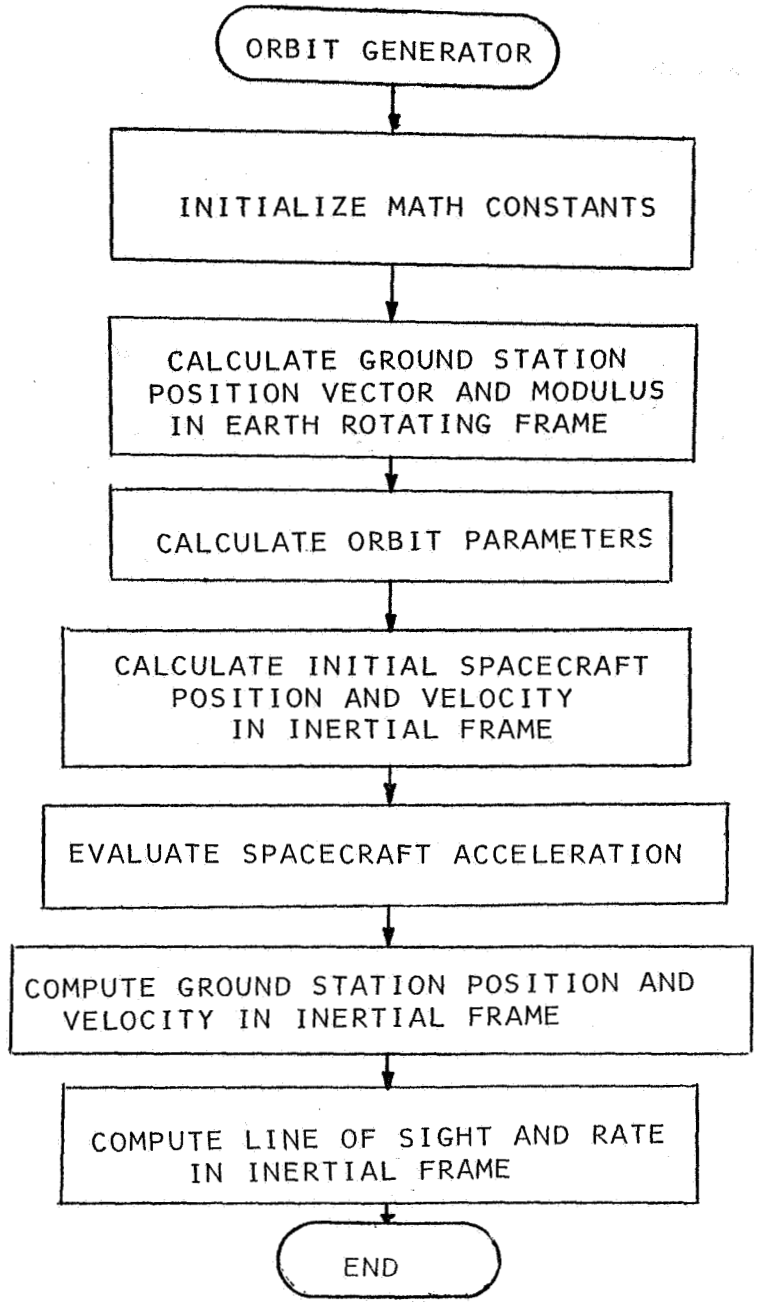

FIGURE 2.7-1 ORBIT GENERATOR MATH FLOW

TABLE 2.7-1 ORBIT GENERATOR MATH FLOW

Calculate Ground Station Position Vector and Modulus in Earth Rotating Frame

$$ERV = \frac{(ERP)(ERE)}{\sqrt{(ERE)^2(\sin\lambda_g)^2 + (ERP)^2(\cos\lambda_g)^2}}$$

$$R_{TX} = (ERV)(\cos\lambda_g)(\cos\phi_g)$$

$$R_{TY} = (ERV)(\cos\lambda_g)(\sin\phi_g)$$

$$R_{TZ} = (ERV)(\sin\lambda_g)$$

$$R_{TM} = \sqrt{R_{TX}^2 + R_{TY}^2 + R_{TZ}^2}$$

Calculate Orbit Parameters

$$a = \left(\frac{\tau\sqrt{\mu}}{2\pi}\right)^{\frac{2}{3}}$$

$$\tau = \frac{2\pi a^{\frac{3}{2}}}{\sqrt{\mu}}$$

$$e = 1 - \frac{R_P + R_E}{a} \quad \text{or} \quad e = \frac{R_A + R_E}{a} - 1$$

$$\omega' = \text{Arcsin}\left(\frac{\sin(\lambda s)}{\sin(i)}\right) \quad \text{for launch direction North}$$

$$\omega' = (\pi - |\omega'|)\,\text{sign}(\omega') \quad \text{for launch direction South}$$

$$\Omega = \text{Arctan}\left(\frac{\cos(\omega')\cos(\lambda s)\sin(\phi s) - \sin(\omega')\cos(i)\cos(\lambda s)\cos(\phi s)}{\cos(\omega')\cos(\lambda s)\cos(\phi_s) + \sin(\omega')\cos(i)\sin(\phi_s)}\right)$$

$$\Theta_s = \omega' - \omega$$

TABLE 2.7-1 ORBIT GENERATOR MATH FLOW (CONT.)

$$\sin(E_s) = \frac{\sin(\Theta s)\sqrt{1-e^2}}{1+e\cos(\Theta_s)}$$

$$\cos(E_s) = \frac{e+\cos(\Theta_s)}{1+e\cos(\Theta_s)}$$

$$E_s = \text{Arctan}\left(\frac{\sin(E_s)}{\cos(E_s)}\right) \text{ modulo } 2\pi \text{ radians}$$

$$T = t - \frac{\tau}{2\pi}\left[(E_s - 2\pi) - e\sin(\Theta_s)\right]$$

$$M = \left[(t-T)\sqrt{\mu/a}\right]/a$$

$$E_1 = E_o - \frac{(E_o - e\sin(E_o) - M}{1-e\cos(E_o)} \quad \text{Iterate to obtain}$$

$$E = E_n = E_{n-1} - \frac{E_{n-1} - e\sin(E_{n-1}) - M}{1-e\cos(E_{n-1})}$$

Calculate Initial Spacecraft Position and Velocity in Inertial Frame

$$X = a(\cos(E)-e)(\cos(\omega)\cos(\Omega)-\sin(\omega)\cos(i)\sin(\Omega)) + a\sqrt{1-e^2}\sin(E)(-\sin(\omega)\cos(\Omega)-\cos(\omega)\cos(i)\sin(\Omega))$$

$$Y = a(\cos(E)-e)(\cos(\omega)\sin(\Omega)+\sin(\omega)\cos(i)\cos(\Omega)) + a\sqrt{1-e^2}\sin(E)(-\sin(\omega)\sin(\Omega)+\cos(\omega)\cos(i)\cos(\Omega))$$

$$Z = a(\cos(E)-e)(\sin(\omega)\sin(i)) + a\sqrt{1-e^2}\sin(E)(\cos(\omega)\sin(\omega))$$

TABLE 2.7-1 ORBIT GENERATOR MATH FLOW (CONT.)

$$\dot{X} = \frac{\sqrt{1-e^2}\cos(E)(-\sin(\omega)\cos(\Omega)-\cos(\omega)\cos(i)\sin(\Omega)}{(1-e\cos(E))\sqrt{a/\mu}} -$$

$$\frac{\sin(E)(\cos(\omega)\cos(\Omega)-\sin(\omega)\cos(i)\sin(\Omega))}{(1-e\cos(E))\sqrt{a/\mu}}$$

$$\dot{Y} = \frac{\sqrt{1-e^2}\cos(E)(-\sin(\omega)\sin(\Omega)+\cos(\omega)\cos(i)\cos(\Omega))}{(1-e\cos(E))\sqrt{a/\mu}} -$$

$$\frac{\sin(E)(\cos(\omega)\sin(\Omega)+\sin(\omega)\cos(i)\cos(\Omega))}{(1-e\cos(E))\sqrt{a/\mu}}$$

$$\dot{Z} = \frac{\sqrt{1-e^2}\cos(E)\cos(\omega)\sin(i)-\sin(E)\sin(\omega)\sin(i)}{(1-e\cos(E))\sqrt{a/\mu}}$$

$$R = \sqrt{X^2 + Y^2 + Z^2}$$

$$V = \sqrt{\dot{X}^2 + \dot{Y}^2 + \dot{Z}^2}$$

Evaluate Spacecraft Acceleration

$$\ddot{X} = \frac{\mu}{R^3}\left[1+JR_E^2\left(1-5\frac{Z^2}{R^2}\right)/R^2 + HR_E^3\left(3-7\frac{Z^2}{R^2}\right)\frac{Z}{R^4} - DR_E^4\left(3-42\frac{Z^2}{R^2}+63\frac{Z^4}{R^4}\right)/7R^4\right]X$$

TABLE 2.7-1 ORBIT GENERATOR MATH FLOW (CONT.)

Compute Ground Station Position and Velocity in Inertial Frame

$$\alpha = \omega_E \, t \bmod 2\pi$$

$$R_{T1X} = R_{TX} \cos(\alpha) - R_{TY} \sin(\alpha)$$

$$R_{T1Y} = R_{TX} \sin(\alpha) + R_{TY} \cos(\alpha)$$

$$R_{T1Z} = R_{TZ}$$

$$V_{T1X} = -\omega_E \, R_{TY} \cos(\alpha) - \omega_E \, R_{TX} \sin(\alpha)$$

$$V_{T1Y} = -\omega_E \, R_{TY} \sin(\alpha) + \omega_E \, R_{TX} \cos(\alpha)$$

$$V_{T1Z} = 0.0$$

Compute Line of Sight and Velocity in Inertial Frame

$$L_X = R_{T1X} - X$$

$$L_Y = R_{T1Y} - Y$$

$$L_Z = R_{T1Z} - Z$$

$$\dot{L}_X = V_{T1X} - \dot{X}$$

TABLE 2.7-1 ORBIT GENERATOR MATH FLOW (CONT.)

$$r_1 = \sqrt{X_1^2 + Y_1^2 + Z_1^2}$$

$$X_2 = X_n + \Delta t \dot{X}_n + \frac{\Delta t^2}{2} \ddot{X}_1$$

$$Y_2 = Y_n + \Delta t \dot{Y}_n + \frac{\Delta t^2}{2} \ddot{Y}_1$$

$$Z_2 = Z_n + \Delta t \dot{Z}_n + \frac{\Delta t^2}{2} \ddot{Z}_1$$

$$r_2 = \sqrt{X_2^2 + Y_2^2 + Z_2^2}$$

$$X_{n+1} = X_n + \Delta t [\dot{X}_n + \frac{\Delta t}{6} (\ddot{X}_n + 2\ddot{X}_1)]$$

$$Y_{n+1} = Y_n + \Delta t [\dot{Y}_n + \frac{\Delta t}{6} (\ddot{Y}_n + 2\ddot{Y}_1)]$$

$$Z_{n+1} = Z_n + \Delta t [\dot{Z}_n + \frac{\Delta t}{6} (\ddot{Z}_n + 2\ddot{Z}_1)]$$

$$\dot{X}_{n+1} = \dot{X}_n + \frac{\Delta t}{6} (\ddot{X}_n + 4\ddot{X}_1 + \ddot{X}_2)$$

$$\dot{Y}_{n+1} = \dot{Y}_n + \frac{\Delta t}{6} (\ddot{Y}_n + 4\ddot{Y}_1 + \ddot{Y}_2)$$

$$\dot{Z}_{n+1} = \dot{Z}_n + \frac{\Delta t}{6} (\ddot{Z}_n + 4\ddot{Z}_1 + \ddot{Z}_2)$$

$$r_{n+1} = \sqrt{X_{n+1}^2 + Y_{n+1}^2 + Z_{n+1}^2}$$

$$V_{n+1} = \sqrt{\dot{X}_{n+1}^2 + \dot{Y}_{n+1}^2 + \dot{Z}_{n+1}^2}$$

TABLE 2.7-1 ORBIT GENERATOR MATH FLOW (CONT.)

$$\ddot{Y} = -\frac{\mu}{R^3}\left[1+JR_E^2\left(1-5\frac{Z^2}{R^2}\right)/R^2 + HR_E^3\left(3-7\frac{Z^2}{R^2}\right)\frac{Z}{R^4} - DR_E^4\left(3-42\frac{Z^2}{R^2}+63\frac{Z^4}{R^4}\right)/7R^4\right]Y$$

$$\ddot{Z} = -\frac{\mu}{R^3}\left\{\left[1+JR_E^2\left(3-5\frac{Z^2}{R^2}\right)/R^2 + HR_E^3\left(6-7\frac{Z^2}{R^2}\right)\frac{Z}{R^4} - DR_E^4\left(15-70\frac{Z^2}{R^2}+63\frac{Z^4}{R^4}\right)/7R^4\right]Z - 3HR_E^3/5R^2\right\}$$

Compute Spacecraft Position and Velocity for Next Time Step

$$X_1 = X_n+\frac{\Delta t}{2}\dot{X}_n+\frac{\Delta t^2}{8}\ddot{X}_n$$

$$Y_1 = Y_n+\frac{\Delta t}{2}\dot{Y}_n+\frac{\Delta t^2}{8}\ddot{Y}_n$$

$$Z_1 = Z_n+\frac{\Delta t}{2}\dot{Z}_n+\frac{\Delta t^2}{8}\ddot{Z}_n$$

$$\dot{L}_Y = V_{T1Y} - \dot{Y}$$

$$\dot{L}_Z = V_{T1Z} - \dot{Z}$$

SECTION 3

LCSE ANALYSIS

In the course of the LASIM program development effort, certain analysis tasks have been undertaken to:

1. Define portions of the spacecraft control system to allow simulation thereof,

2. Modify existing ATM Experiment Package (Telescope) Control System gains to produce compatibility with the Fine Tracking System.

3. Use the developed LASIM program for investigation of system performance for selected inputs.

This section will summarize the analysis effort undertaken and present the results obtained. This section will also present areas for further study which have bearing upon the ultimate feasibility of LCSE operation.

3.1 SPACECRAFT CONTROL SYSTEM SYNTHESIS

Contained within the ATM rack are the CMG devices discussed extensively in Paragraph 2.1. The attitude control system, utilizing the ATM CMG's, was originally designed for a solar observation experiment consisting of solar telescopes which are gimbal mounted to the ATM rack, which, in turn, is attached to an S-IVB workshop, cluster-configured spacecraft [1]. For the solar observation mission, the telescope gimbal control system, and the spacecraft attitude control system (employing the ATM CMG's), were designed to operate independently. By this is meant, the spacecraft is oriented to point at the sun by using so-called coarse sun sensors mounted on the vehicle to provide position errors to the spacecraft control system. The gimbal mounted experiment package, consisting of the solar telescopes, is oriented more precisely in the direction of the sun through the gimbal control system using fine sun sensors mounted on the gimbaled structure to provide position error signals for the gimbal torquers. In this way the spacecraft is oriented toward the sun independent of telescope orientation; and the gimbal system orients the telescopes in the direction of the sun within the deadband of the spacecraft system to accomplish the precision pointing required for the experiment.

The Laser Communications System Experiment differs from the solar observation experiment in the important respect that the observation reference is a relatively low power laser beam emanating from a luminescent earth background. Only through the precision optics of the laser telescope, mounted on the gimbaled structure, can this laser beam be detected. Furthermore, the coarse sensor of the laser telescope does not provide proportional output signals which might be used to provide position reference for the spacecraft attitude control system.

Thus, to provide independent spacecraft and telescope gimbal system control, as in the solar mission, requires mounting a laser telescope on the spacecraft, with a coarse detector which provides linear position error signals.

The series approach requires that the telescope gimbal system utilize the telescope coarse and fine sensors to provide error signals to the gimbal torquers, which then drive against the spacecraft inertia to orient the telescope in the line-of-sight direction. The spacecraft system derives position error signals from resolvers mounted on the gimbal pivots, which sense the telescope gimbal angles. The spacecraft is then oriented to align itself with the telescope. In other words, the spacecraft control law requires that the spacecraft operate only to null the telescope gimbal angles, which indirectly orients the spacecraft toward the observation reference, since the telescope will orient itself in the direction of the uplink laser beam. The spacecraft system in this case is said to be in series with the telescope gimbal system.

In the course of the LASIM program development, it became necessary to conceptualize the series coupling approach discussed above, in order to have a feasible system which could be simulated. The reason for this was, and is, that a firm decision has not been reached on the spacecraft configuration for the LCSE mission nor on the complete control system design to be employed for spacecraft control. Thus, the approach taken on the LASIM project, prior to any digital simulation, was to postulate a control system configuration which would work, using the basic hardware elements of the existing ATM rack and experiment package. After this step, the system as postulated was simulated. Paragraph 2.1 defines, explicitly, the spacecraft control system arrived at in the design effort. No attempt was made to optimize the response of the spacecraft system in the design effort which preceded the simulation. However, in subsequent simulation of vehicle rigid body response with the LASIM program, the design parameters selected appeared adequate.

3.2 TELESCOPE CONTROL SYSTEM PARAMETERS

Initially, it was assumed that the telescope gimbal control system as designed for the ATM solar observation experiment could be used in the LCSE mission. This system is basically a second order system with 3db bandwidth of approximately 5 cps, damping ratio (ζ) of 1.35, and is rate limited at .25 degree per second (900 arc seconds per second). Figure 3.2-1 illustrates the basic ATM experiment package (EPS) or telescope gimbal control system as defined to IBM. The system of Figure 3.2-1 is used for both x (outer) and y (inner) gimbal axes control.

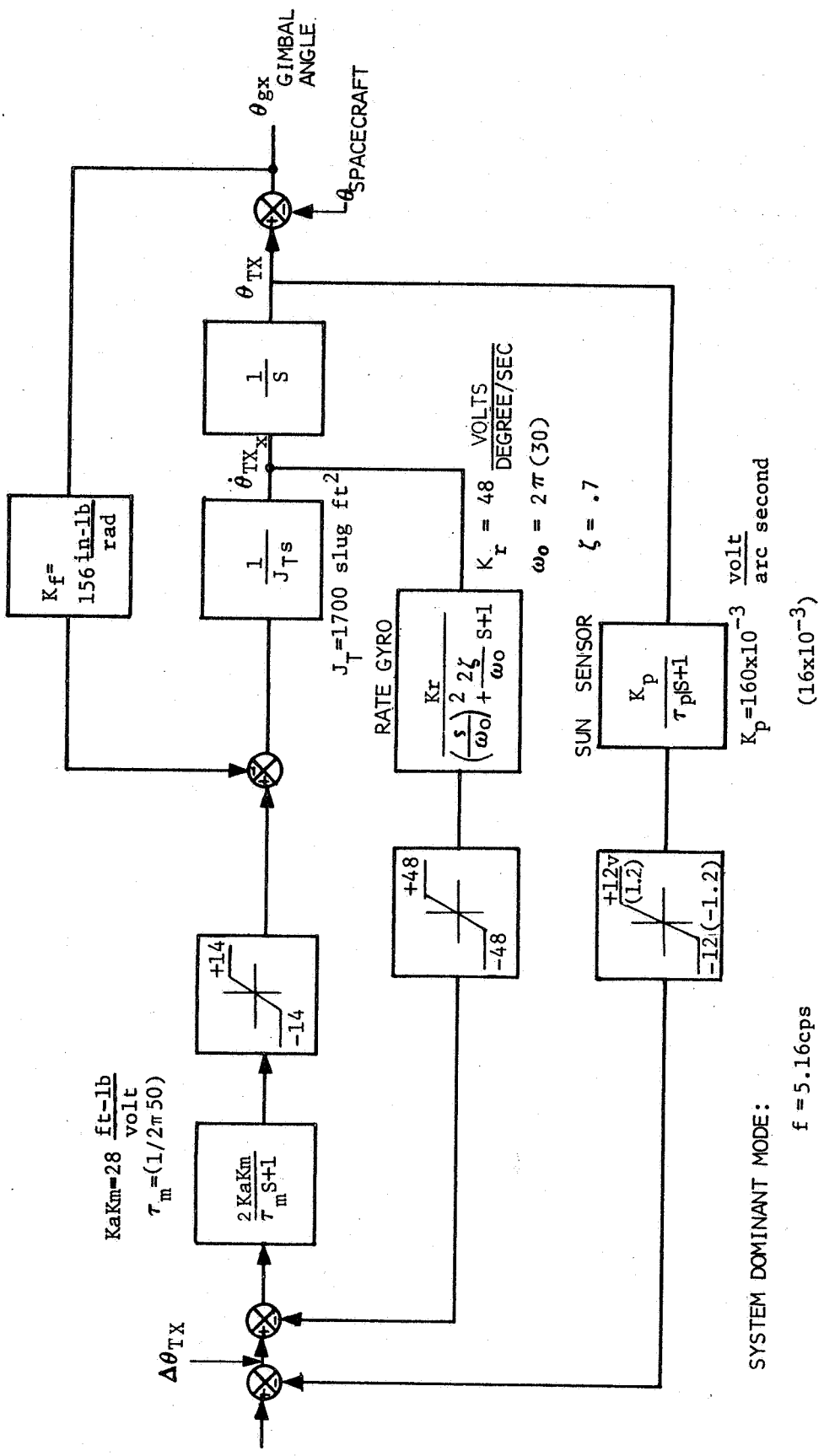

FIGURE 3.2-1 ATM EXPERIMENT PACKAGE (TELESCOPE) CONTROL SYSTEM

A two axis simulation of telescope dynamic response to a step input, in both channels, using the control system of Figure 3.2-1, was made during early LASIM development efforts. Figures 3.2-2 through 3.2-6 illustrate the results; where the initial errors were $\Delta\theta_{Tx}$ = 900 arc seconds, $\Delta\theta_{Ty}$ = -500 arc seconds. From the results shown, it appears that the system is somewhat underdamped.

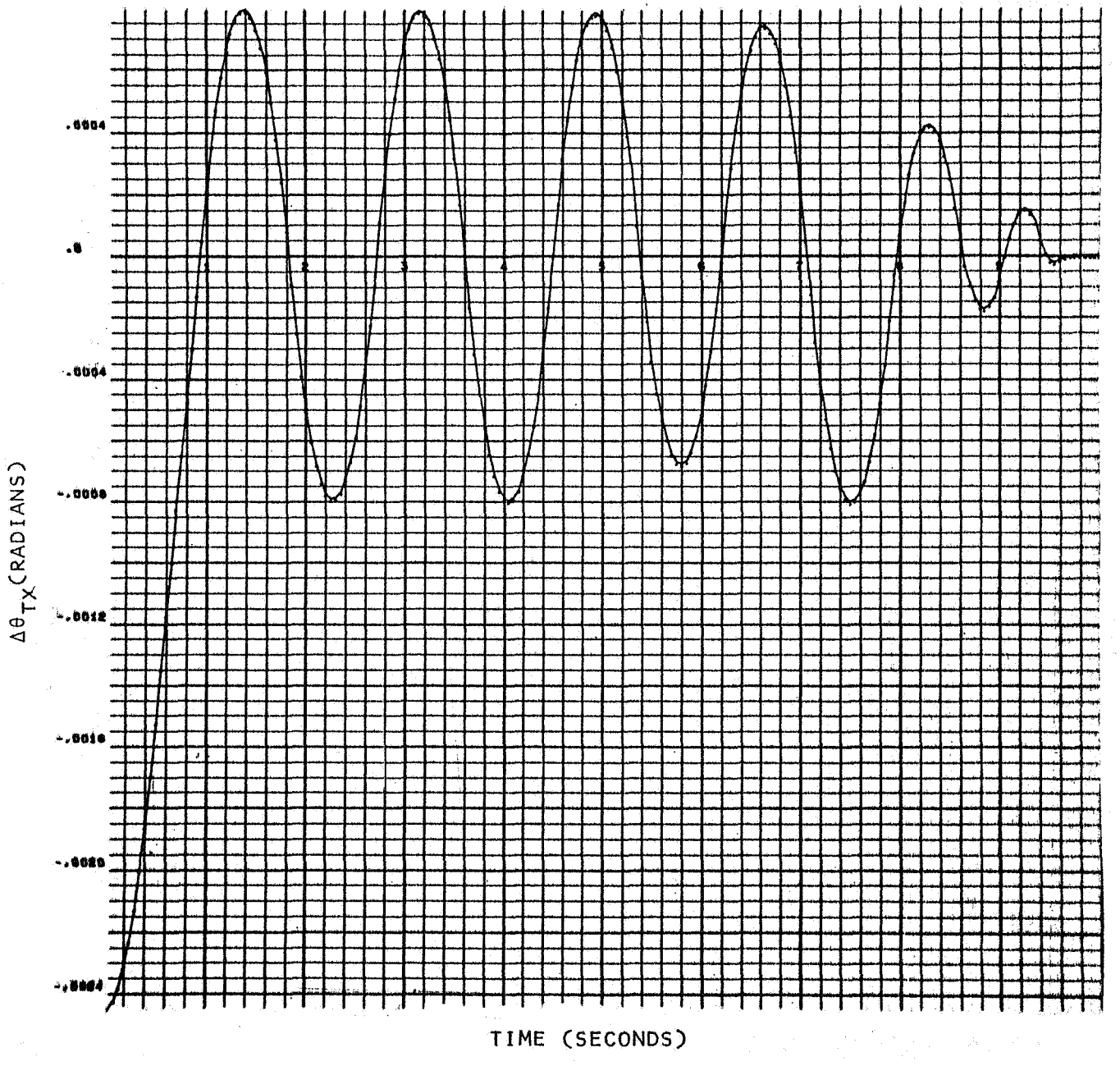

FIGURE 3.2-2 X CHANNEL STEP RESPONSE

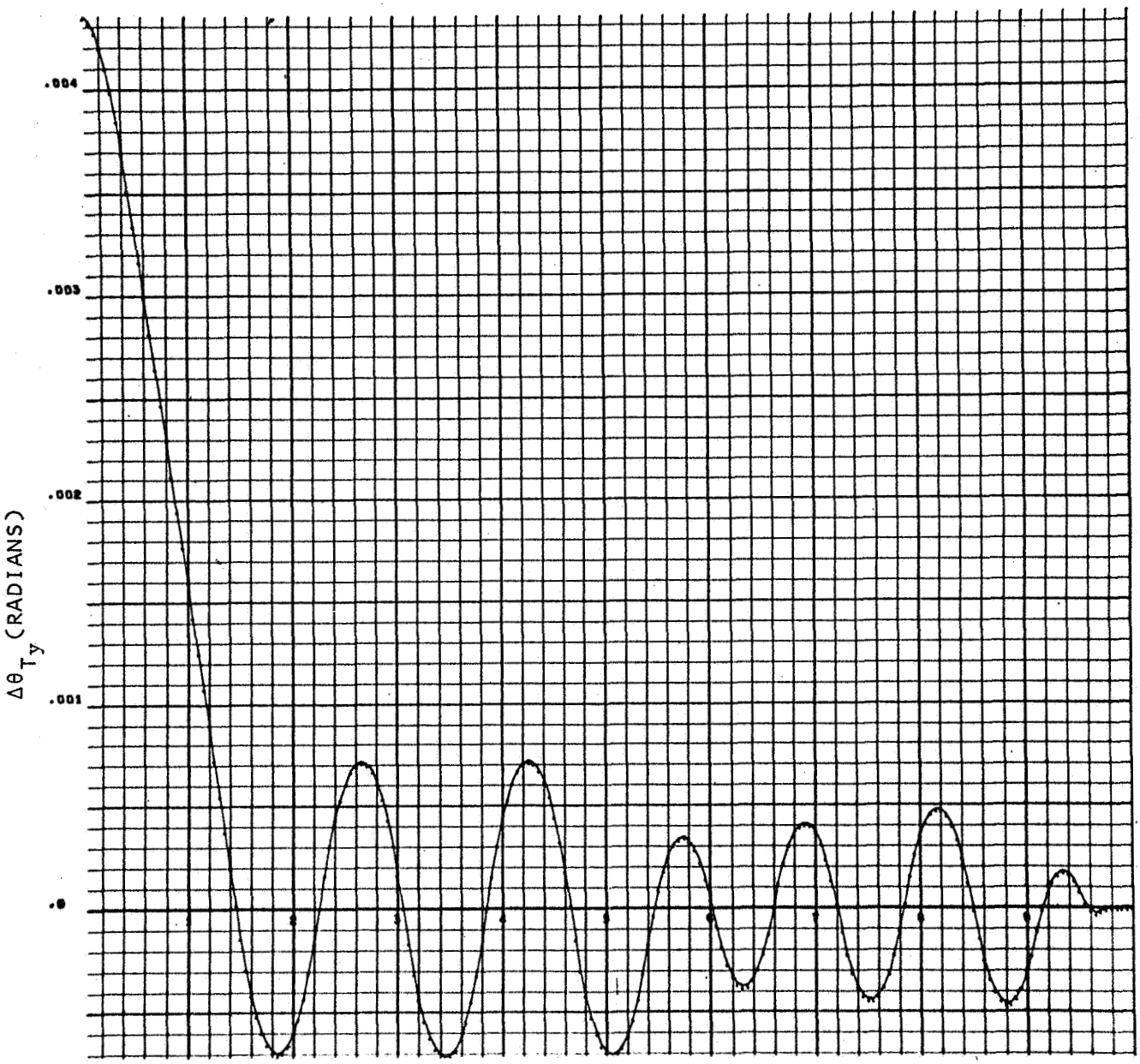

FIGURE 3.2-3 Y CHANNEL STEP RESPONSE

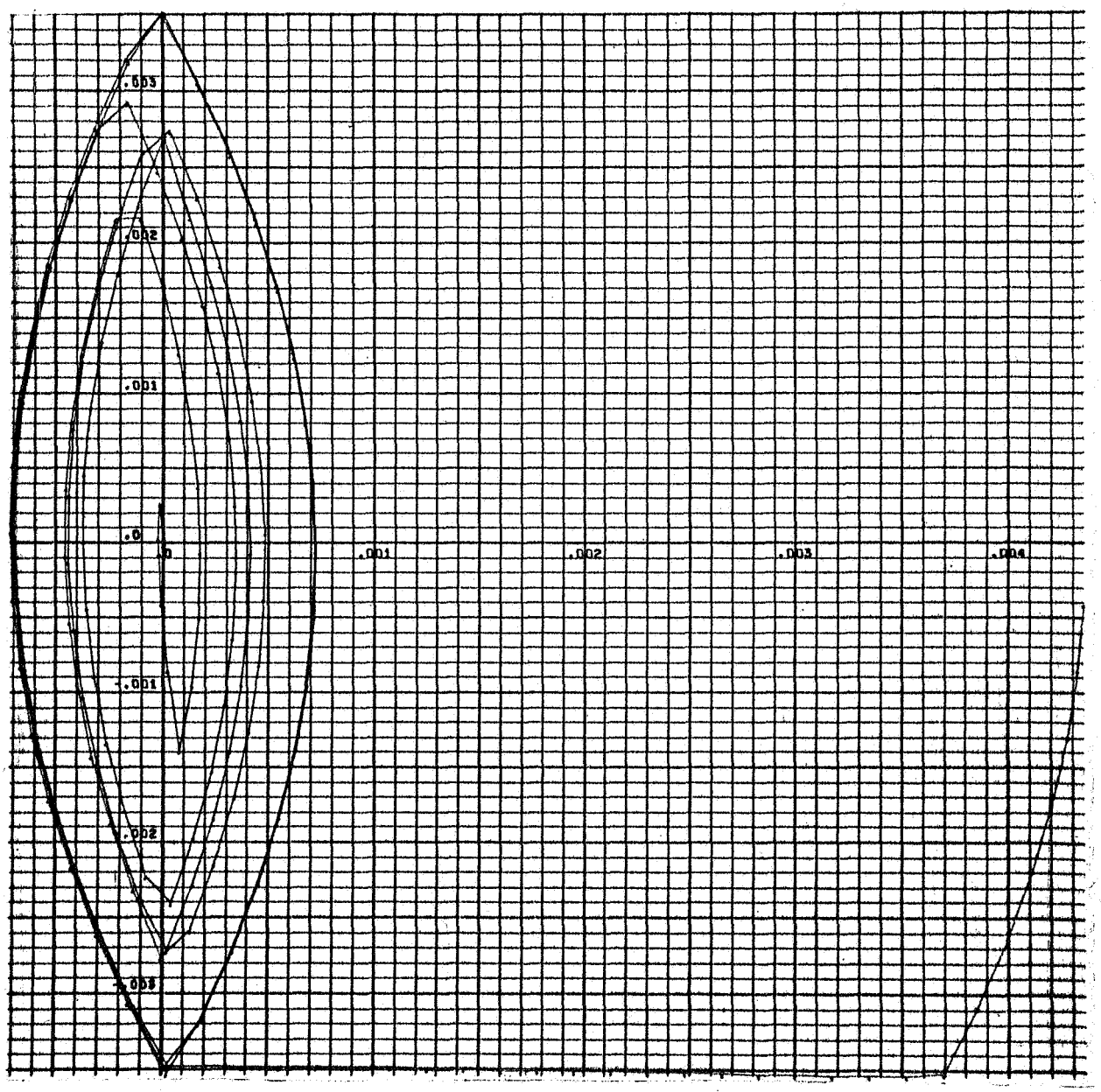

FIGURE 3.2-4 X CHANNEL PHASE PLANE PLOT

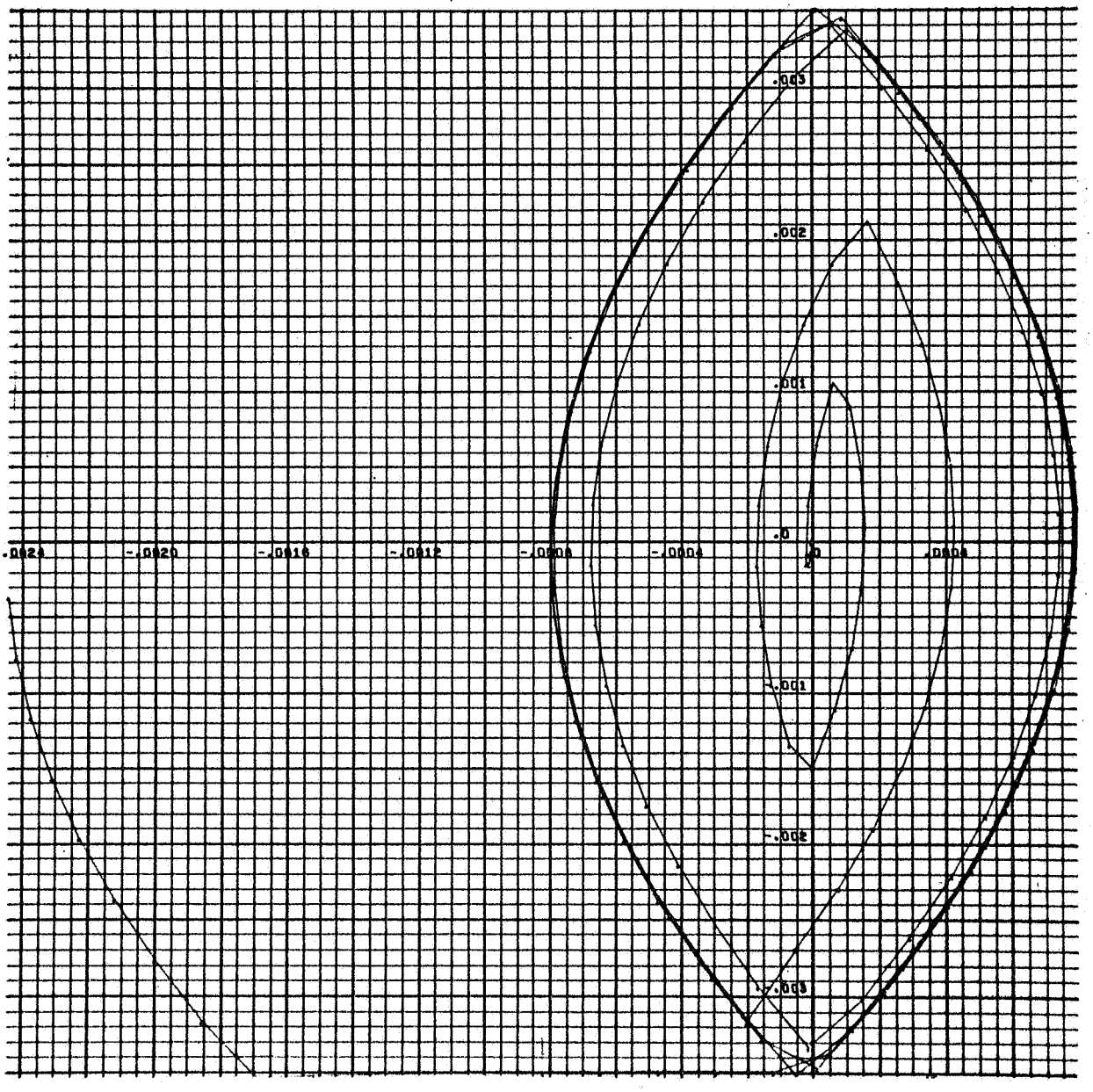

FIGURE 3.2-5 Y CHANNEL PHASE PLANE PLOT

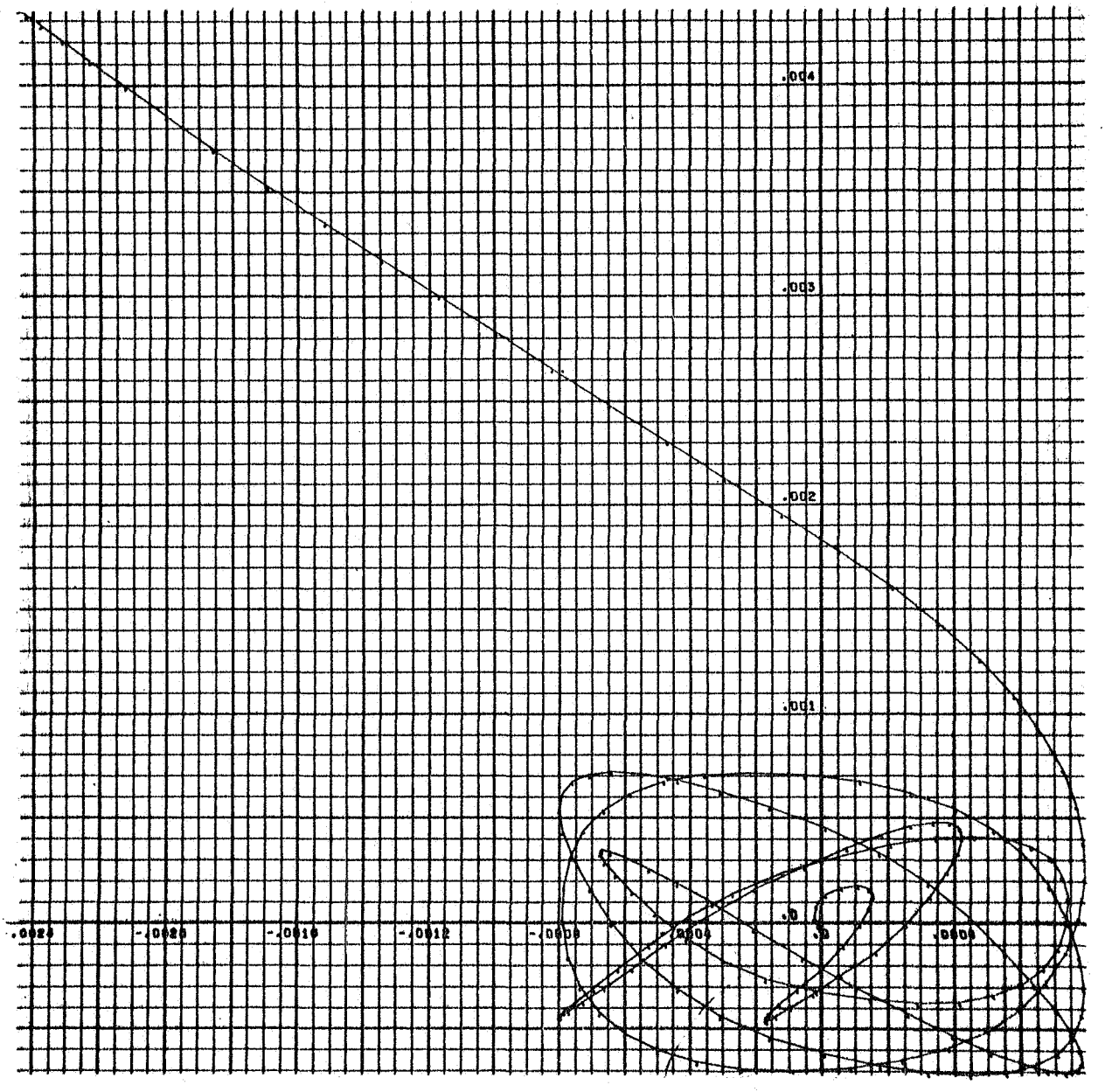

FIGURE 3.2-6 POSITION ERROR TRAJECTORY

Thus, it was deemed necessary to modify the system parameters to produce a more stable telescope control system for the LCSE. In addition to the damping question, consideration was given to the maximum angular rate to which the fine tracking system could respond. The fine tracking system as defined in Paragraph 2.3 is rate limited at an equivalent of approximately 380 arc seconds per second. Since the fine system must lock on the uplink beam to provide the telescope system with a linear region of control, it is necessary that the gimbal system not swing through the fine field-of-view at a rate to which the fine system cannot respond.

It was decided, as a trial design, to set the gimbal system rate limit at 90 arc seconds per second (versus 900 arc seconds per second for the original ATM EPS system). To produce this limiting, the position loop gain of the EPS system was reduced by a factor of 10. These parameter changes are illustrated in parenthesis on Figure 3.2-1. The system response is indicated in Figures 3.2-7 through 3.2-11.

An alternative method for increasing the damping of the original EPS system was tried which amounted to increasing the rate gain K_r by a factor of two to 96 v/°/sec. This action produced increased stability in the non-linear region, but caused a small amplitude oscillation in the linear region. Figures 3.2-12 through 3.2-16 indicate the behavior of the parameters illustrated for the previous cases. Figure 3.2-17 illustrates the angular rates $\dot{\theta}_{tx}$ and $\dot{\theta}_{ty}$ from which the small oscillation in the linear region is observable. This oscillation was not apparent in Figures 3.2-12 through 3.2-16 because of the scale used in the plots shown.

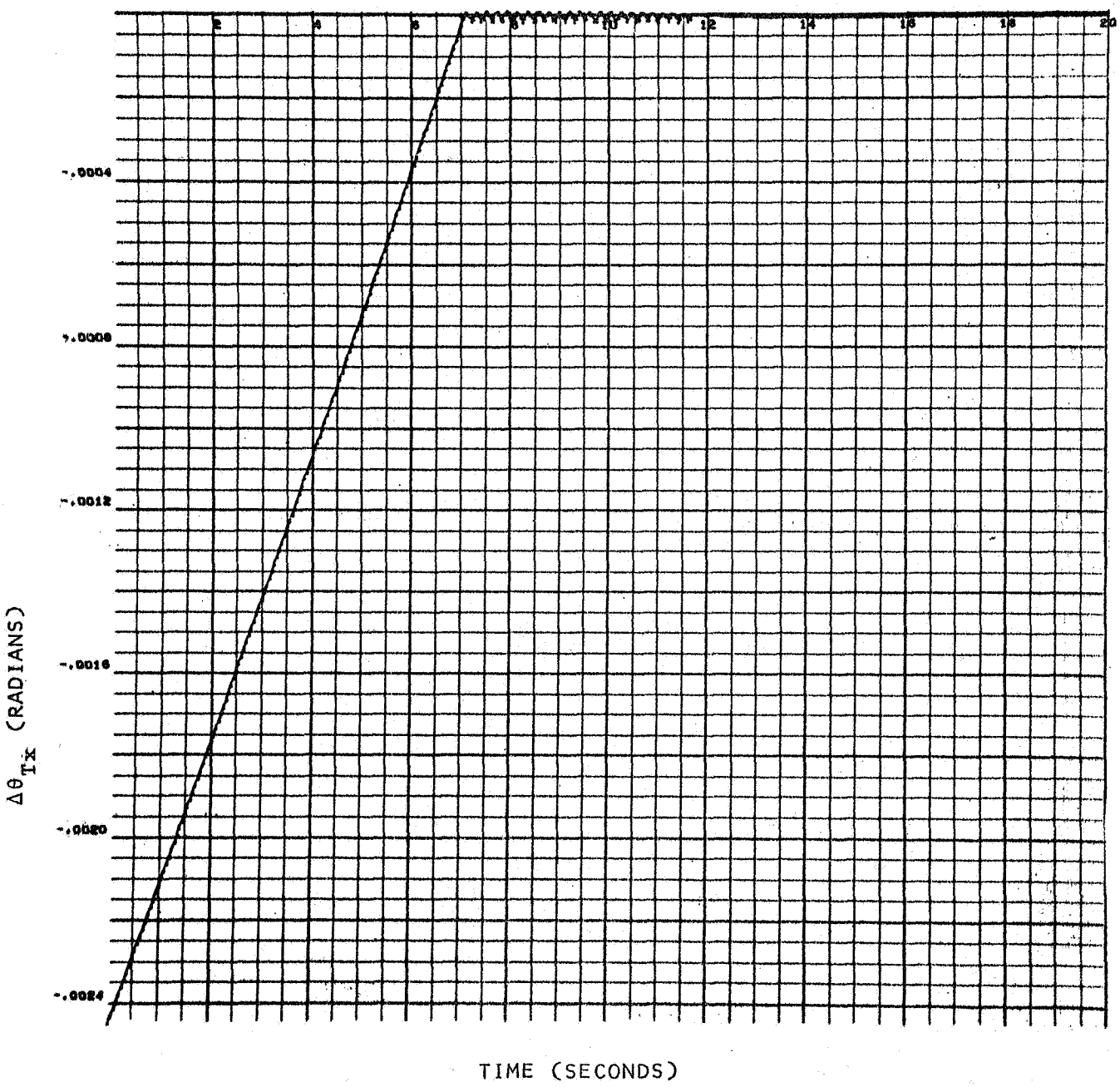

FIGURE 3.2-7 X CHANNEL STEP RESPONSE

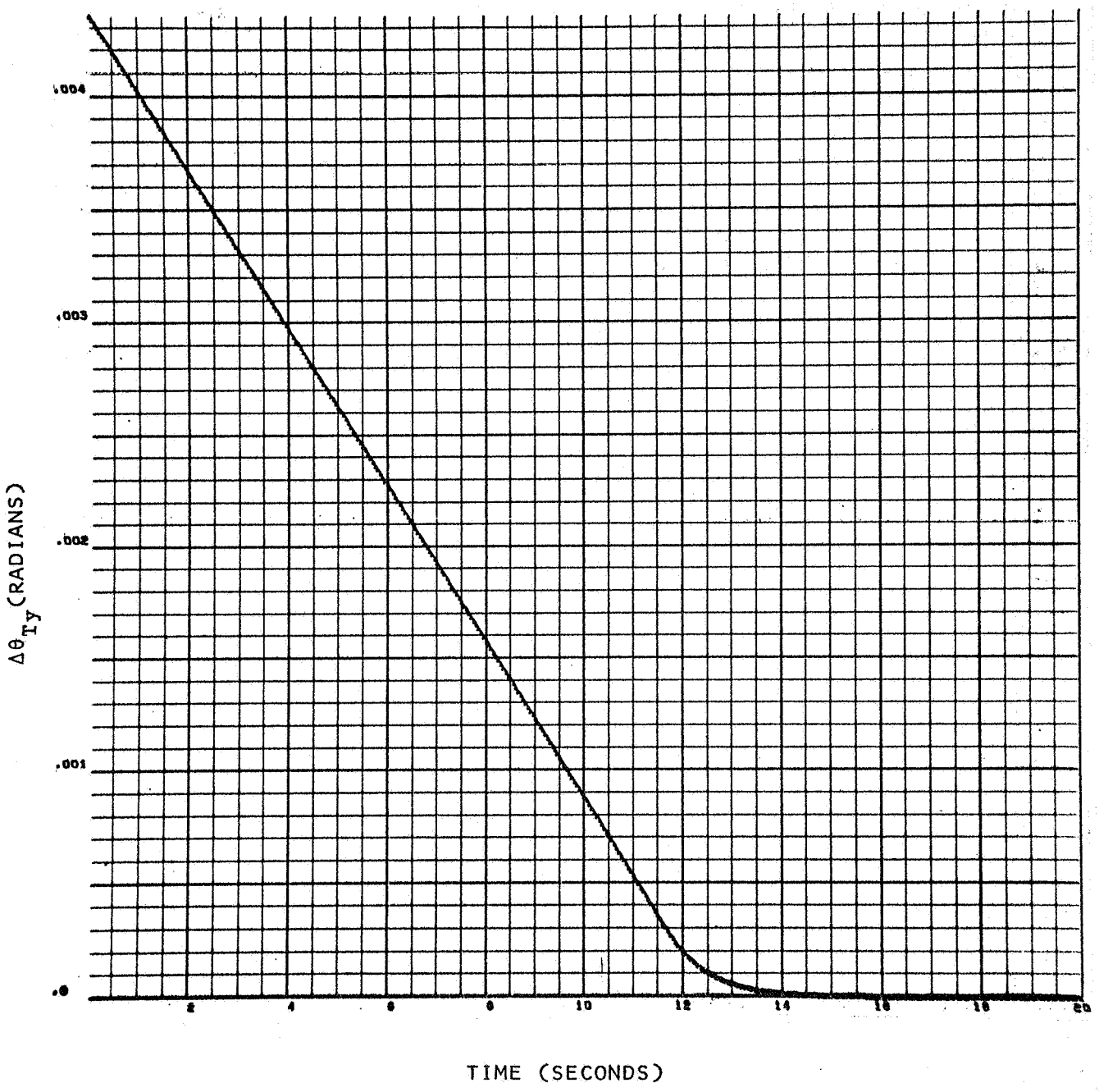

FIGURE 3.2-8 Y CHANNEL STEP RESPONSE

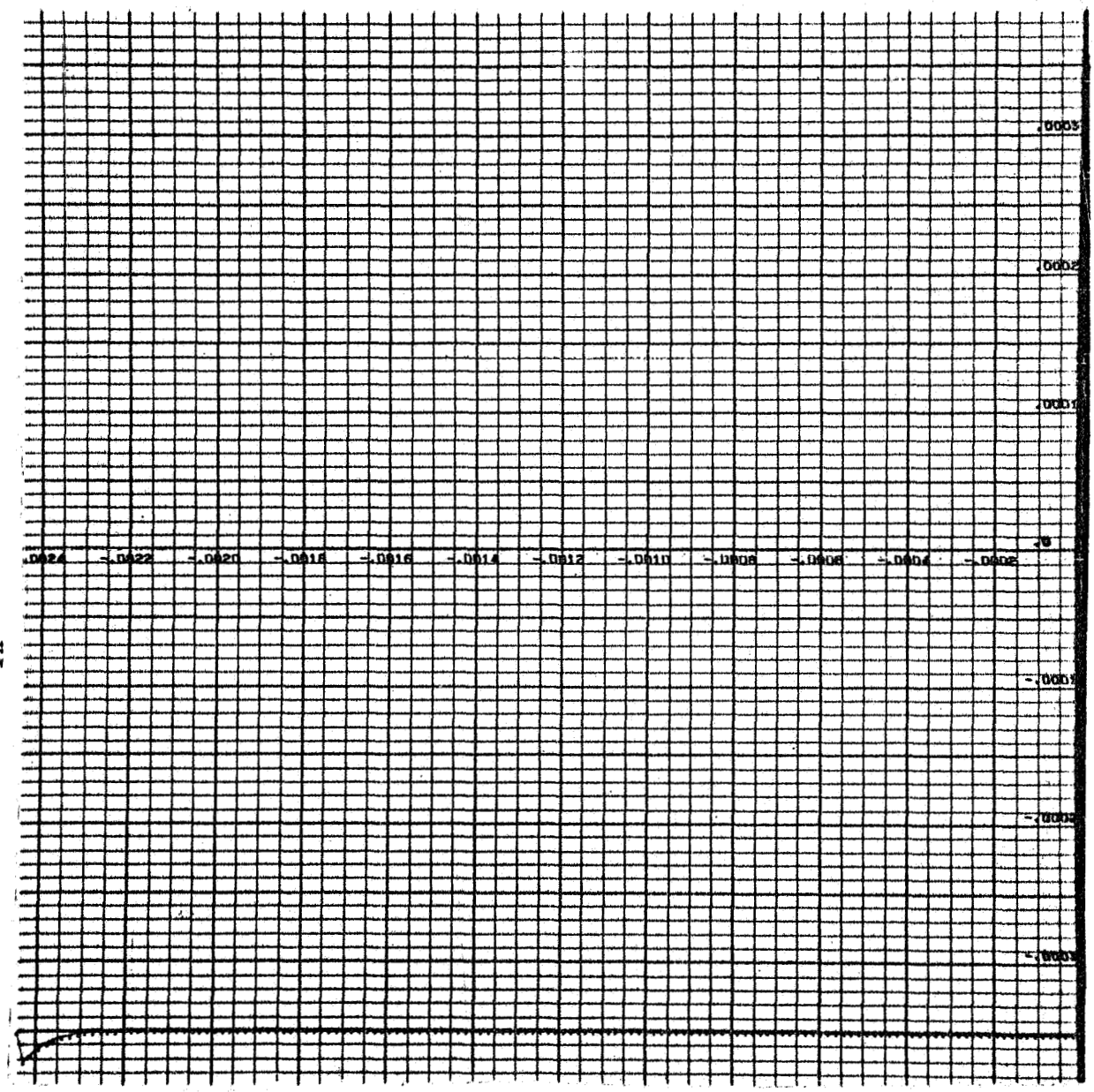

$\dot{\theta}_{Tx}$ (RADIANS)

$\Delta\theta_{Tx}$ (RADIANS)

FIGURE 3.2-9 X CHANNEL PHASE PLANE PLOT

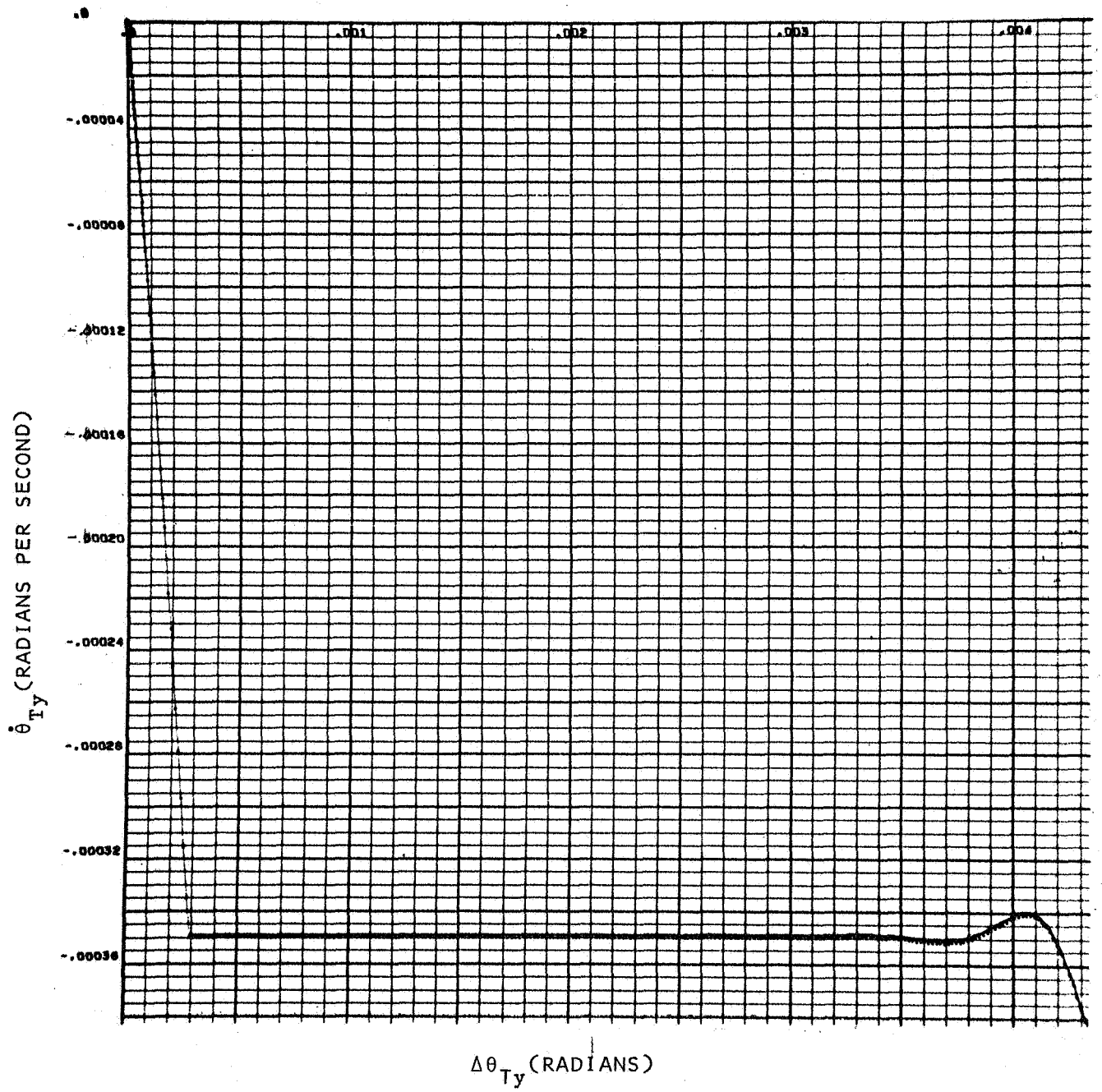

FIGURE 3.2-10 Y CHANNEL PHASE PLANE PLOT

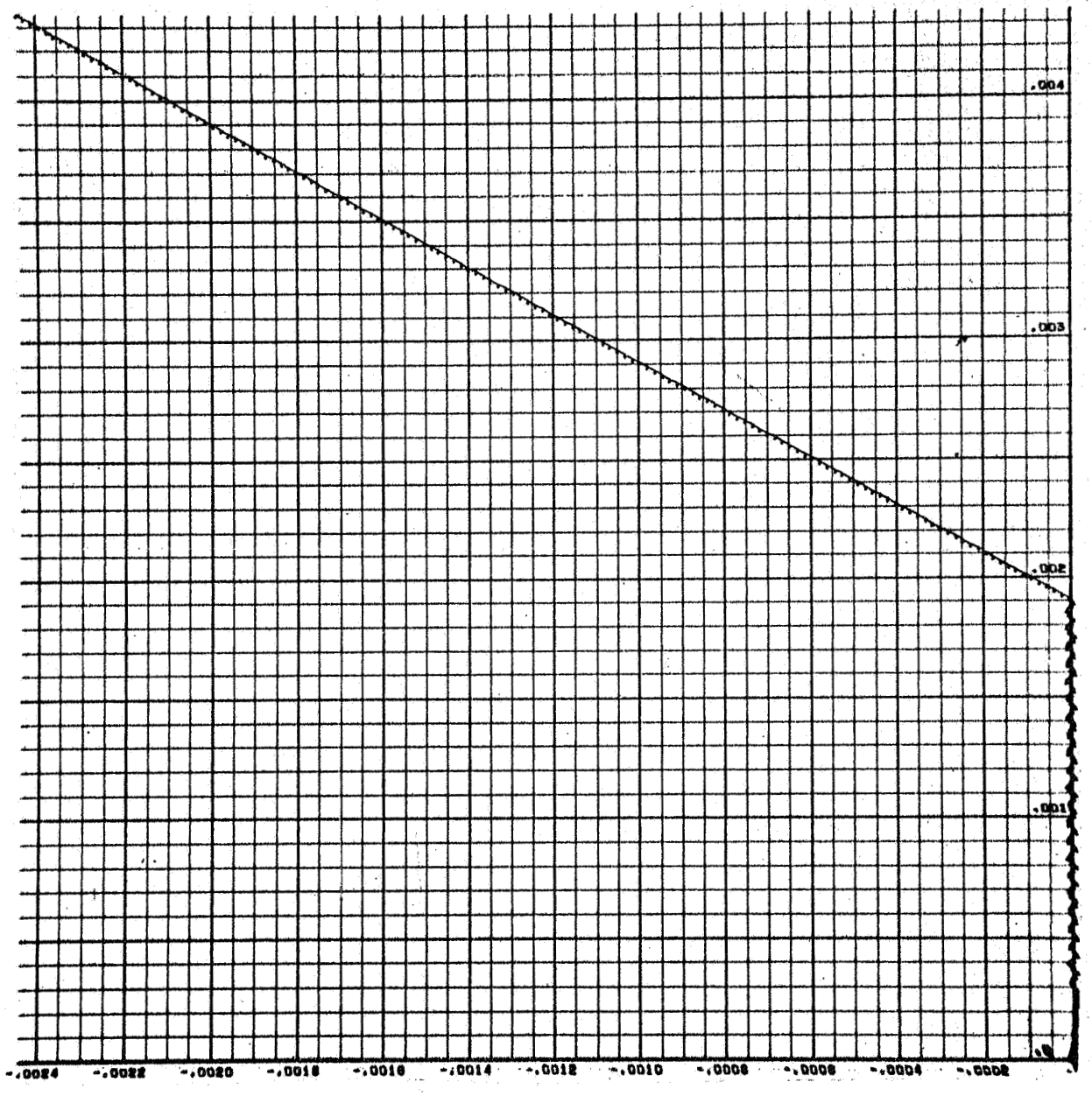

$\Delta\theta_{Ty}$(RADIANS)

$\Delta\theta_{Tx}$(RADIANS)

FIGURE 3.2-11 POSITION ERROR TRAJECTORY

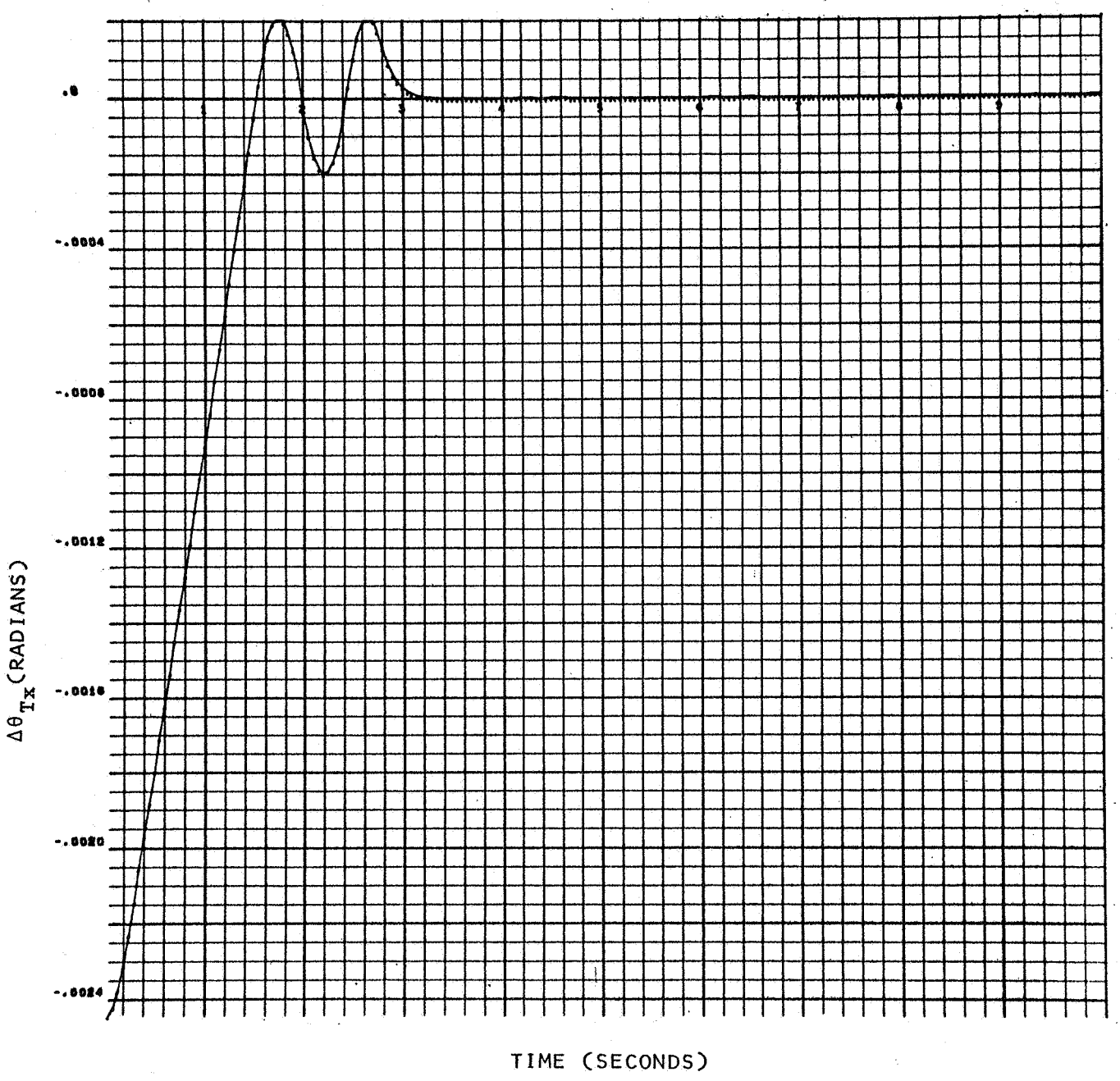

FIGURE 3.2-12 X CHANNEL STEP RESPONSE

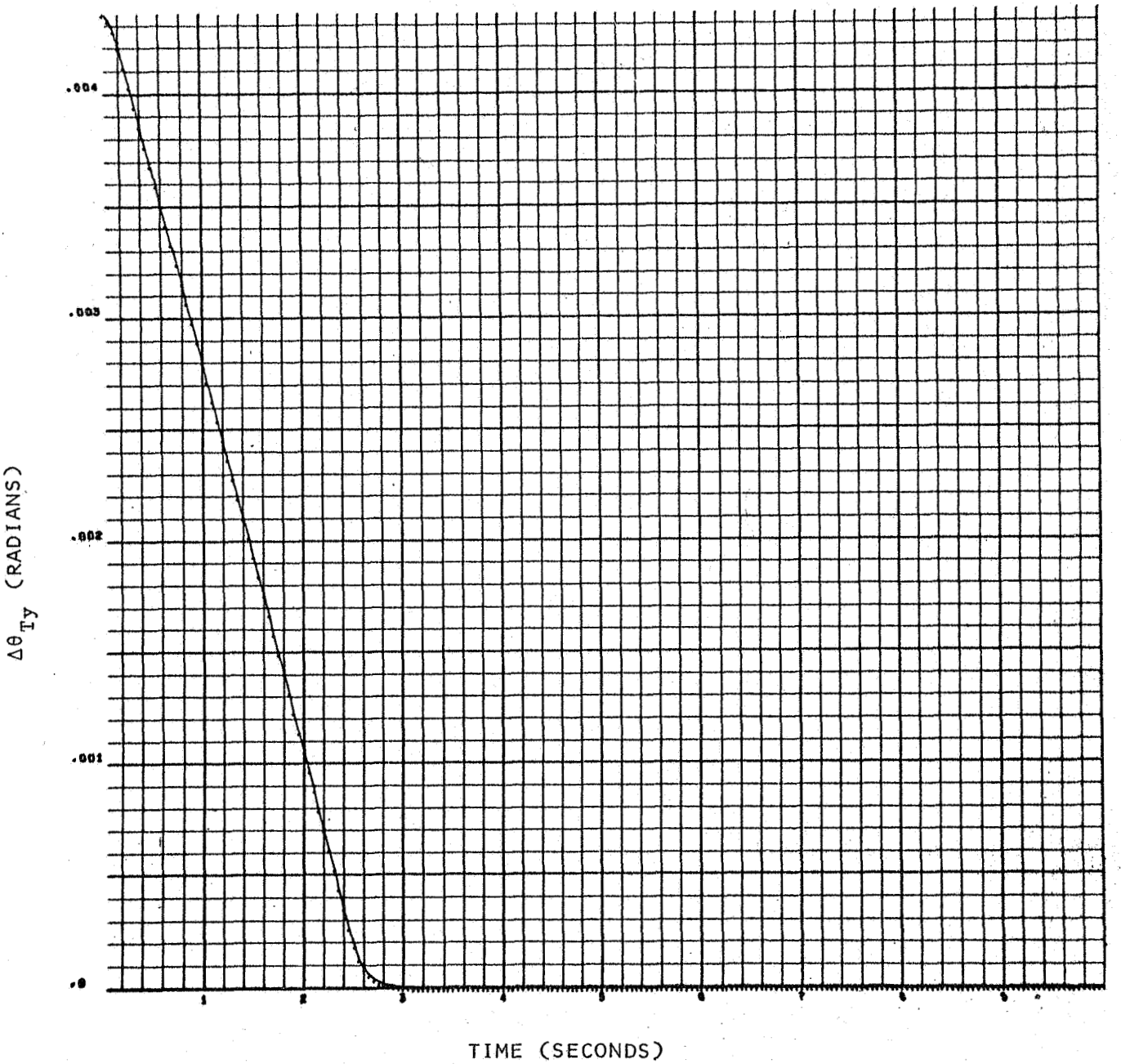

FIGURE 3.2-13 Y CHANNEL STEP RESPONSE

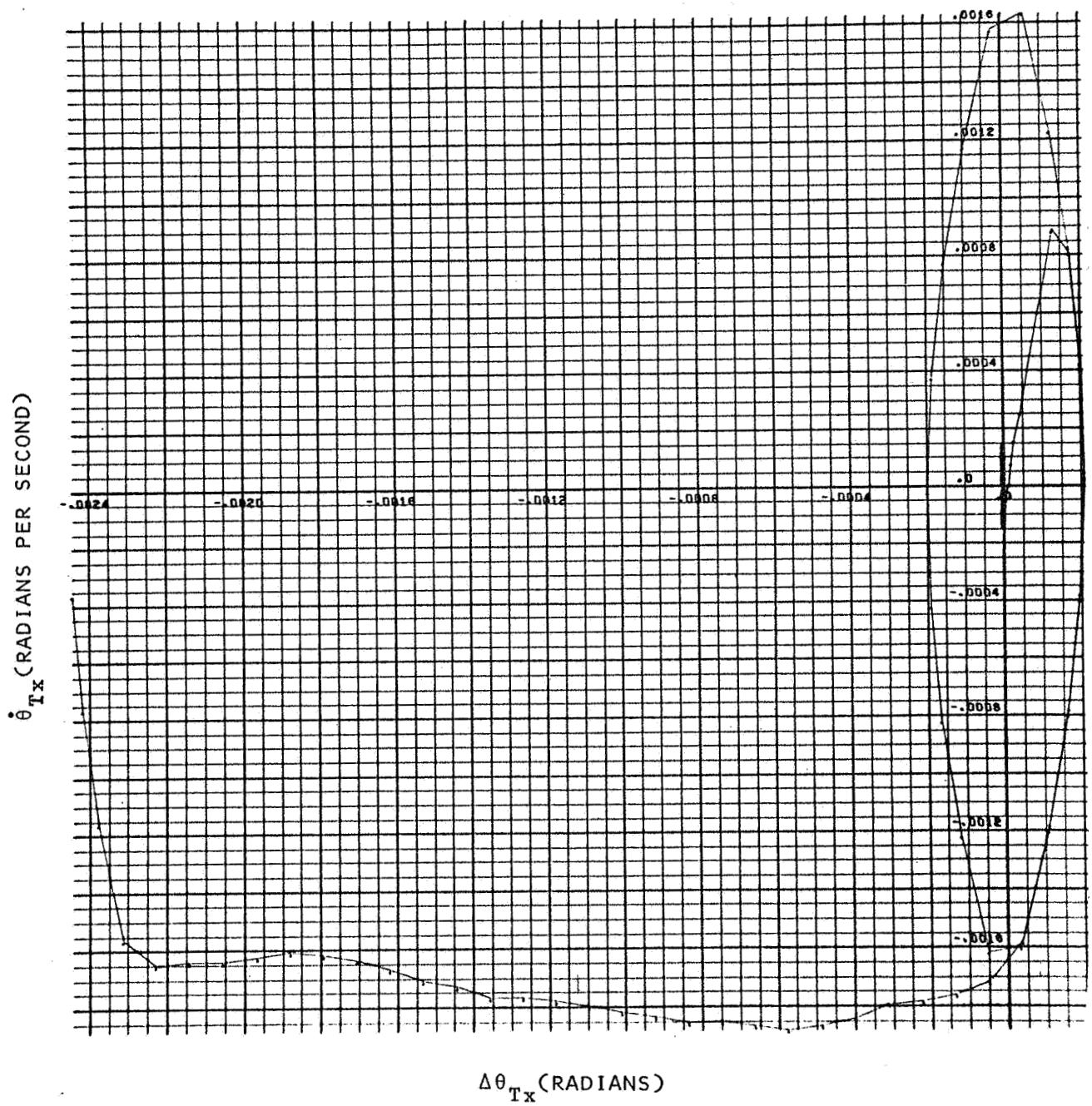

FIGURE 3.2-14 X CHANNEL PHASE PLANE PLOT

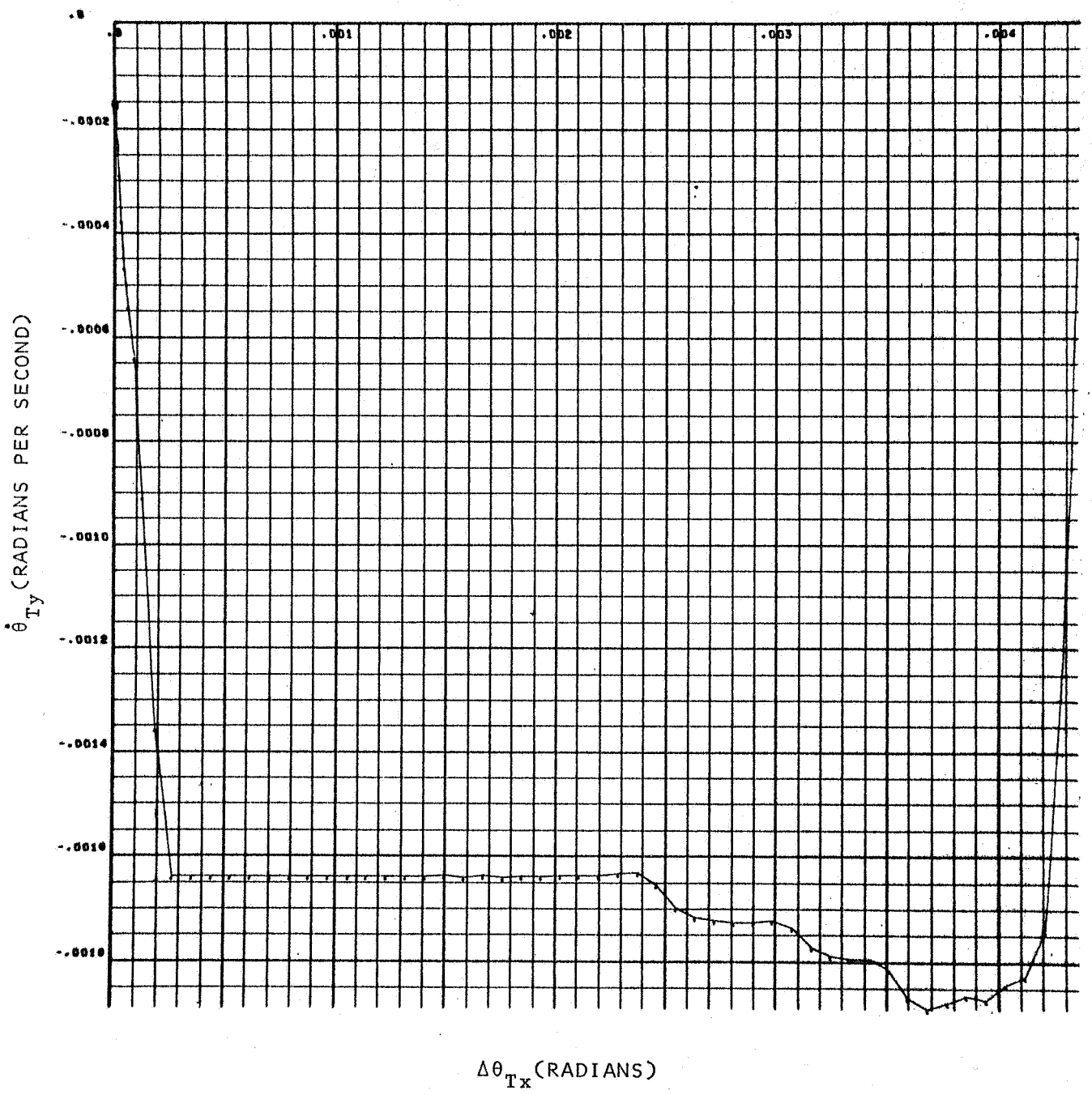

FIGURE 3.2-15 Y CHANNEL PHASE PLANE PLOT

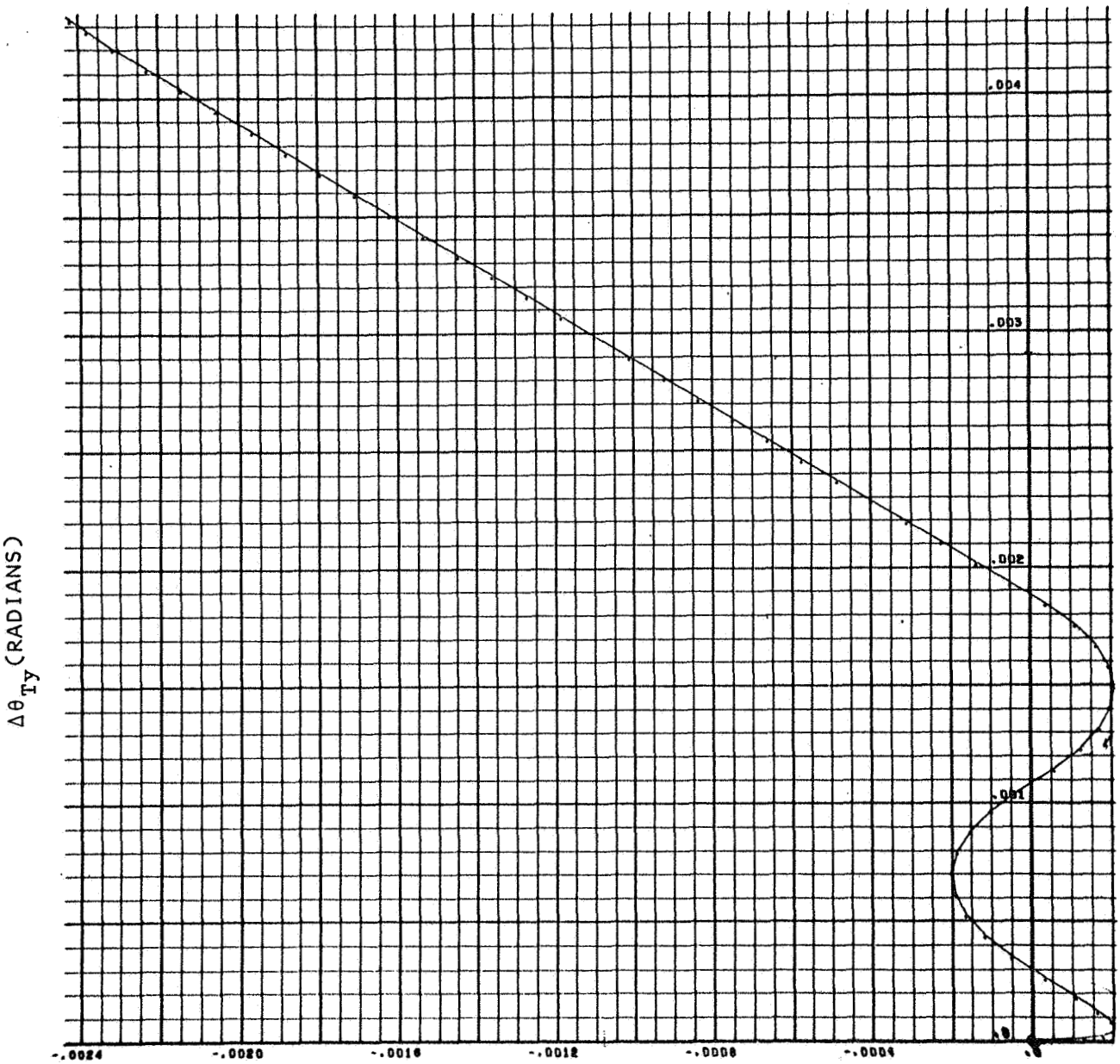

FIGURE 3.2-16 POSITION ERROR TRAJECTORY

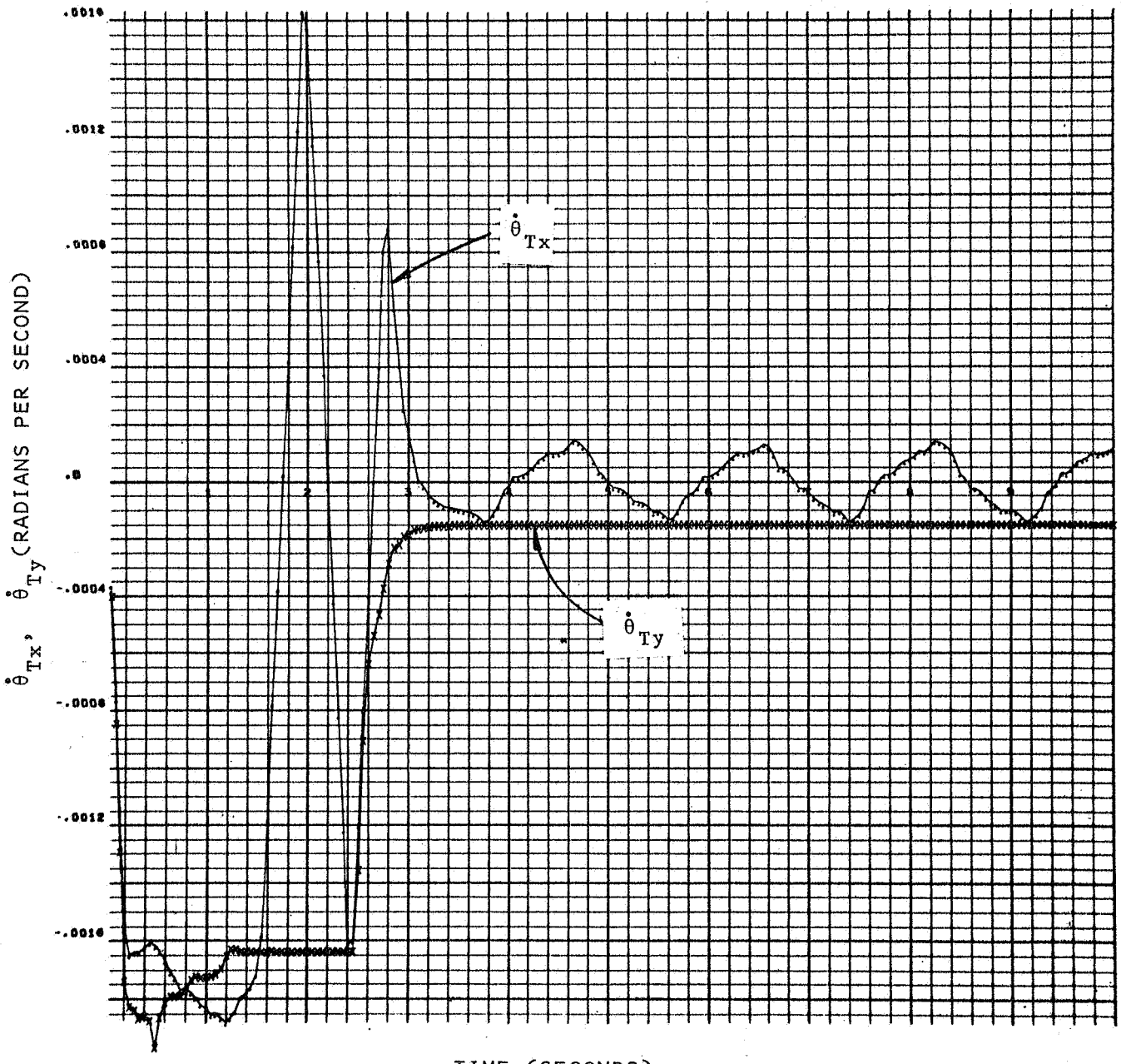

FIGURE 3.2-17 RATE RESPONSES

In summary, simulation of the original ATM EPS (telescope gimbal) control system revealed an incompatibility between this system and the fine tracking system as defined for the LCSE mission. Changes were made to parameters of the telescope gimbal system in order that the system work with the fine tracking system. Paragraph 2.4 enumerates the set of parameters used for the telescope control system which produced a stable and compatible system.

3.3 PERFORMANCE ANALYSIS

The LASIM program has been used to investigate LCSE tracking system operation for several input conditions as part of the program development effort. The following will present the results of these investigations.

3.3.1 Nominal System Performance

The operation of the combined tracking systems in response to an initial position offset between the telescope and the line-of-sight of 30 arc minutes, and between the telescope and spacecraft of 2° is regarded as the nominal case. Figures 3.3-1 through 3.3-6 illustrate the significant system parameters observed. The following describes the parameters shown in the figures.

θ_x, θ_y = Angular misalignment between line-of-sight and optical downlink direction about the x or y telescope axis.

θ_x or θ_y equals the amount the system must be rotated about the Y or X axis to track the uplink beacon exactly. These quantities are driven to zero primarily by the fine tracking subsystem, and it is these quantities which must be controlled such that:

$$\sqrt{\theta_x^2 + \theta_y^2} \leq .1 \text{ arc-second}$$

Because of the range of magnitudes of these quantities which are considered, log plots are shown. This necessitates plotting absolute magnitudes since the quantities take on both positive and negative values.

ψ_x, ψ_y = Telescope gimbal angles; essentially the misalignment existing between telescope and spacecraft about the indicated telescope axis (driven zero by spacecraft attitude control system)

P = Spacecraft inertial angular rate about x axis

Q = Spacecraft inertial angular rate about y axis

θ_z = Angle between telescope geometric longitudinal axis and line-of-sight. This quantity reflects the accuracy with which the telescope gimbal system operates.

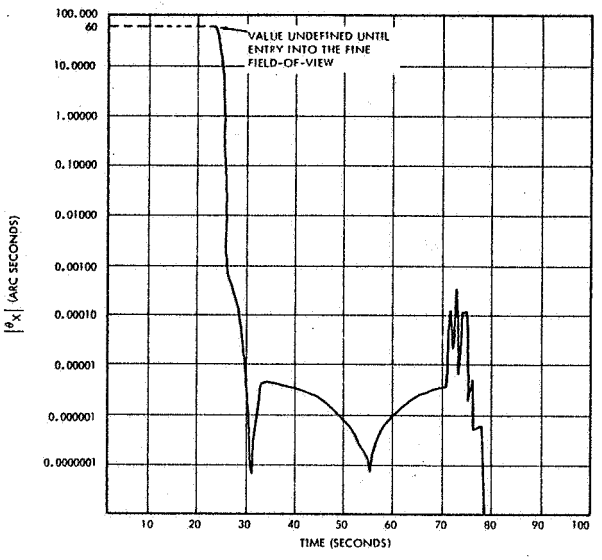

FIGURE 3.3-1 $|\theta_x|$ VERSUS TIME

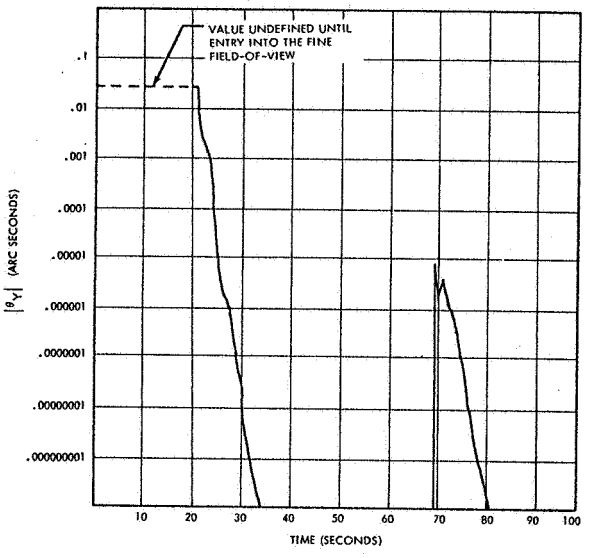

FIGURE 3.3-2 $|\theta_y|$ VERSUS TIME

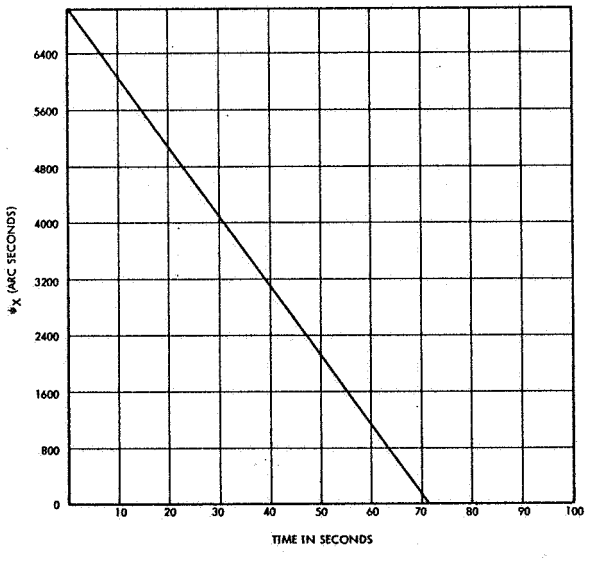

FIGURE 3.3-3 ψ_x VERSUS TIME

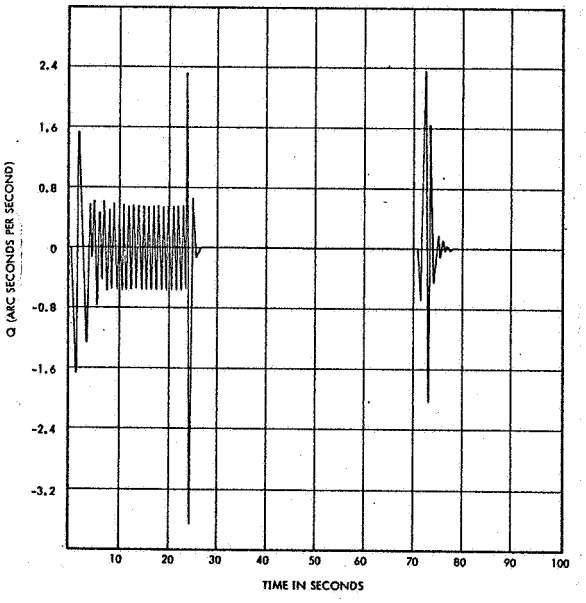

FIGURE 3.3-4 Q VERSUS TIME

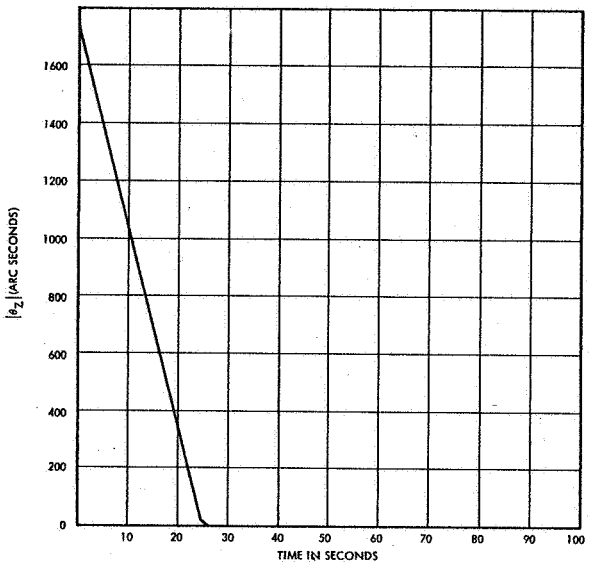

FIGURE 3.3-5 P VERSUS TIME

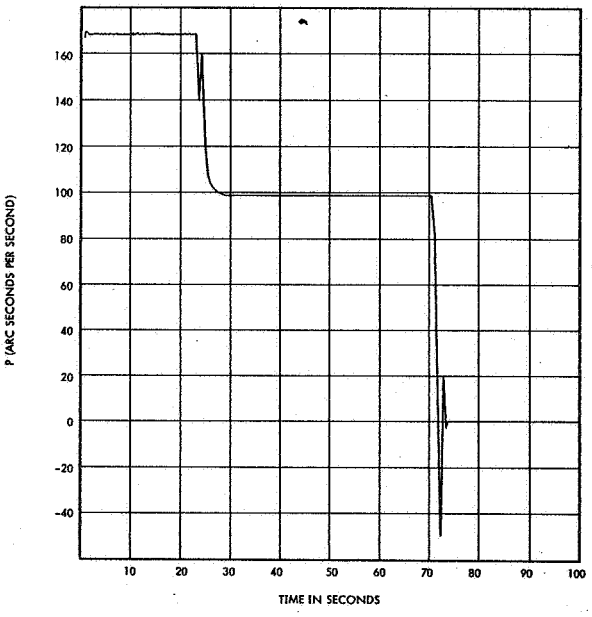

FIGURE 3.3-6 θ_Z VERSUS TIME

It is to be noted that the initial pointing errors are input in the x axis only. The cross coupling into the y axis may be observed from θ_y and Q. The oscillations observed on Q prior to entry into the fine field-of-view (at approximately 22 seconds) are a result of the non-linear position loop in the telescope control system. The y gimbal angle ψ_y, while not illustrated, is oscillating in a manner similar to that shown on Q. This oscillation feeds into the spacecraft control system causing oscillatory torques to be generated in the y channel until the system enters the fine field-of-view. Upon this entry, a linear region of control is provided the telescope control system and the oscillations cease.

3.3.2 Gimbal Angle Resolver Error

The multispeed resolvers used to pick off the experiment package gimbal angles, which serve as position error signals for the spacecraft control system, display certain systematic error characteristics. It was desired to determine the dynamic and steady state tracking errors resulting when the resolver error was introduced. The tracking system was initially misaligned such that the ground beacon was just in the coarse field-of-view (θ_z = 30 arc minutes) and the spacecraft was offset from the telescope by 2° (gimbal angles = 2°). The resolver outputs were modeled as:

$$R_1 = \psi_1 + B_1 + M_1 \, SIN(32\psi_1) \qquad (3.3\text{-}1)$$

$$R_2 = \psi_2 + B_2 + M_2 \, SIN(32\psi_2), \qquad (3.3\text{-}2)$$

where

$R_{1,2}$ = resolver output

$\psi_{1,2}$ = true gimbal angle

$B_{1,2}$ = constant bias error term = 85 arc seconds

$M_{1,2}$ = magnitude of sinusoidal component = 60 arc seconds

The resolver error model is reasonably standard. IBM Report No. 65-208-007H, 1 April 1965, discusses in some detail the systematic error characteristics of multi-speed resolvers.

The resolvers used on the ATM experiment package gimbals are 16:1 resolvers. Using cross-over detectors to sense their output and convert the analog signals into digital words provides an additional 2:1 multiple, so that the resolver system is essentially a 32:1 system. The argument of the sinusoidal error term is equal to the number of electrical degrees through which the resolver has been rotated, or 32 times the mechanical rotation.

In general, tracking system operation is affected only slightly by the resolver errors for the input considered. Operation of the coarse and fine tracking systems is virtually unaffected. The only noticeable effect is that spar gimbal angles are not nulled to zero by the spacecraft control system. This is the expected result, in that there exists a null offset in the gimbal angle equal to the resolver error.

3.3.3 Astronaut Motion and External Disturbance Torques

As has been mentioned previously, astronaut motion in the spacecraft will produce torques on the vehicle which will tend to degrade tracking system performance. The torque profile shown in Figure 2.1-9 was applied to the spacecraft and the resulting tracking errors observed. No other error sources were included for this investigation and the line-of-sight vector was not allowed to move during the simulation. Figures 3.3-7 through 3.3-12 illustrate the significant system parameters observed in this investigation. The quantities illustrated are those defined in Paragraph 3.3.1.

It is seen from the figures that the tracking systems remained "locked on" to the fixed line-of-sight direction to well within the .1 arc second requirement. Also it can be seen that while the spar gimbal angle (ψ_y) moved as much as .8 arc seconds, the telescope remained aligned with the line-of-sight to within about .1 arc second (θ_z).

From these rather encouraging results, it was decided to apply a sinusoidal disturbance torque about the spacecraft y axis, varying the magnitude and frequency of the disturbance. From this, the torque amplitude at the various frequencies at which the system would not maintain tracking accuracies of .1 arc second would be determined.

Time has not permitted this investigation to consider all the combinations of frequencies and amplitudes of disturbance torques which are desirable. (Example: consider frequencies in the range from .01 cps to 5 cps, allowing magnitude to vary from 50 nm to 10^4 nm). However, three frequencies have been considered and the results are quite interesting. Figure 3.3-13 shows a composite plot of:

Maximum fine tracking errors and resulting gimbal angles	VS.	Disturbance torque peak amplitude at the 3 frequencies .1, .5, 1 cps.

In generating the data shown on Figure 3.3-13, the simulation was run for a total of 20 seconds real time for each case. The sinusoidal disturbance torque was applied about the spacecraft axis with the form:

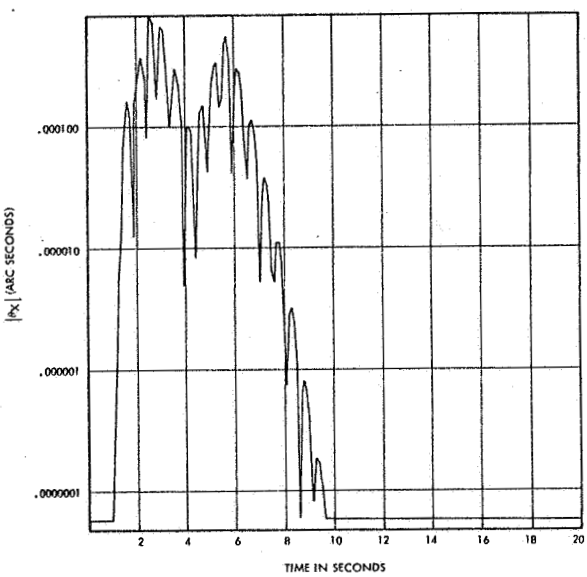

FIGURE 3.3-7 $|\theta_x|$ VERSUS TIME

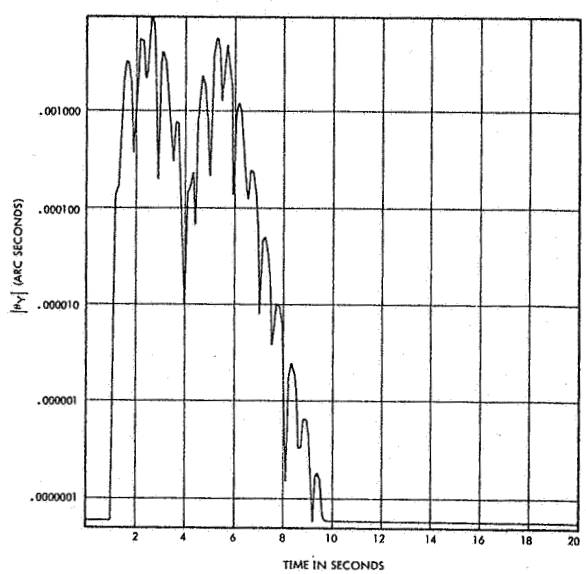

FIGURE 3.3-8 $|\theta_y|$ VERSUS TIME

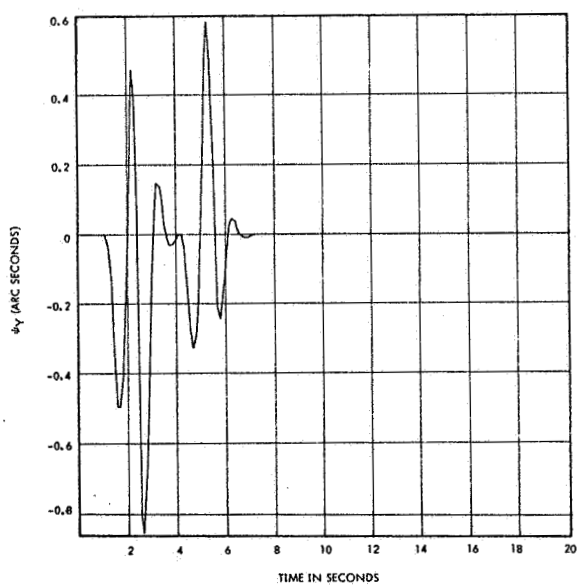

FIGURE 3.3-9 ψ_y VERSUS TIME

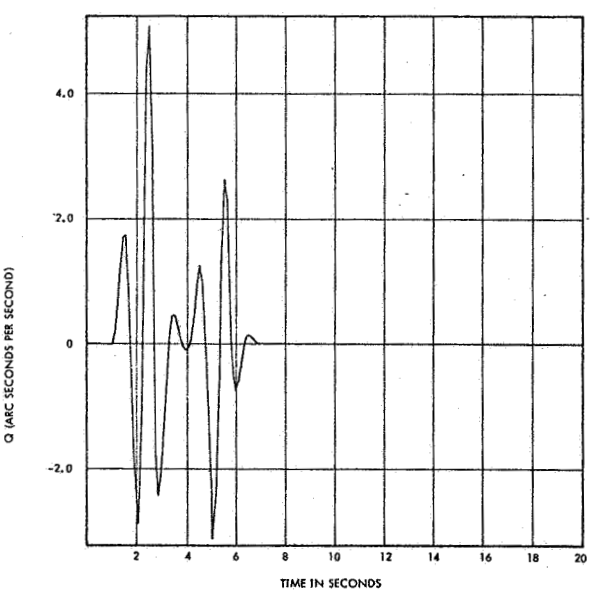

FIGURE 3.3-10 Q VERSUS TIME

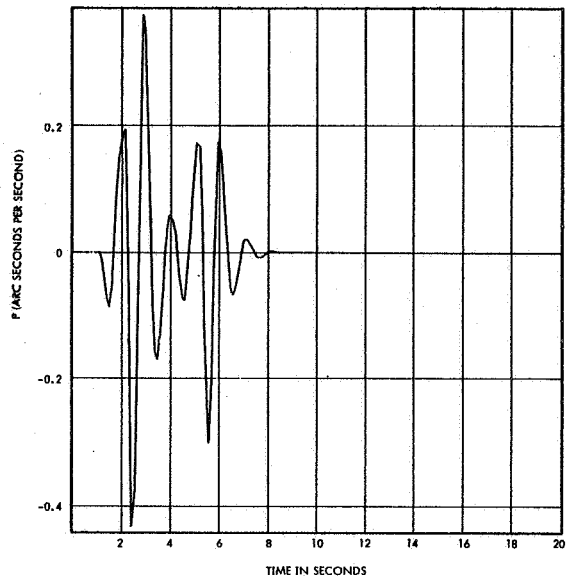

FIGURE 3.3-11 P VERSUS TIME

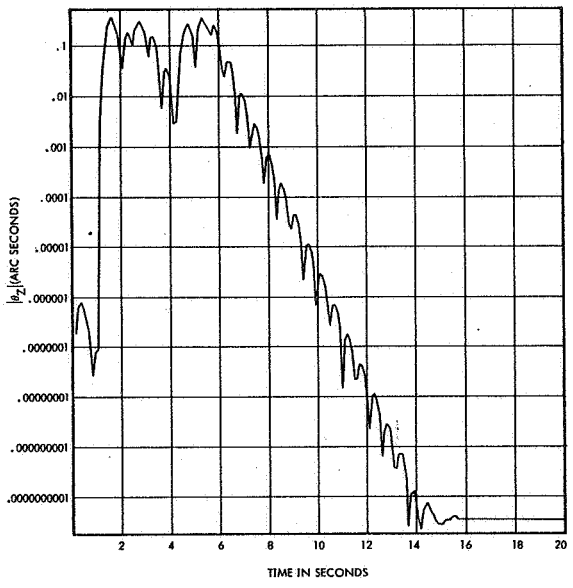

FIGURE 3.3-12 θ_z VERSUS TIME

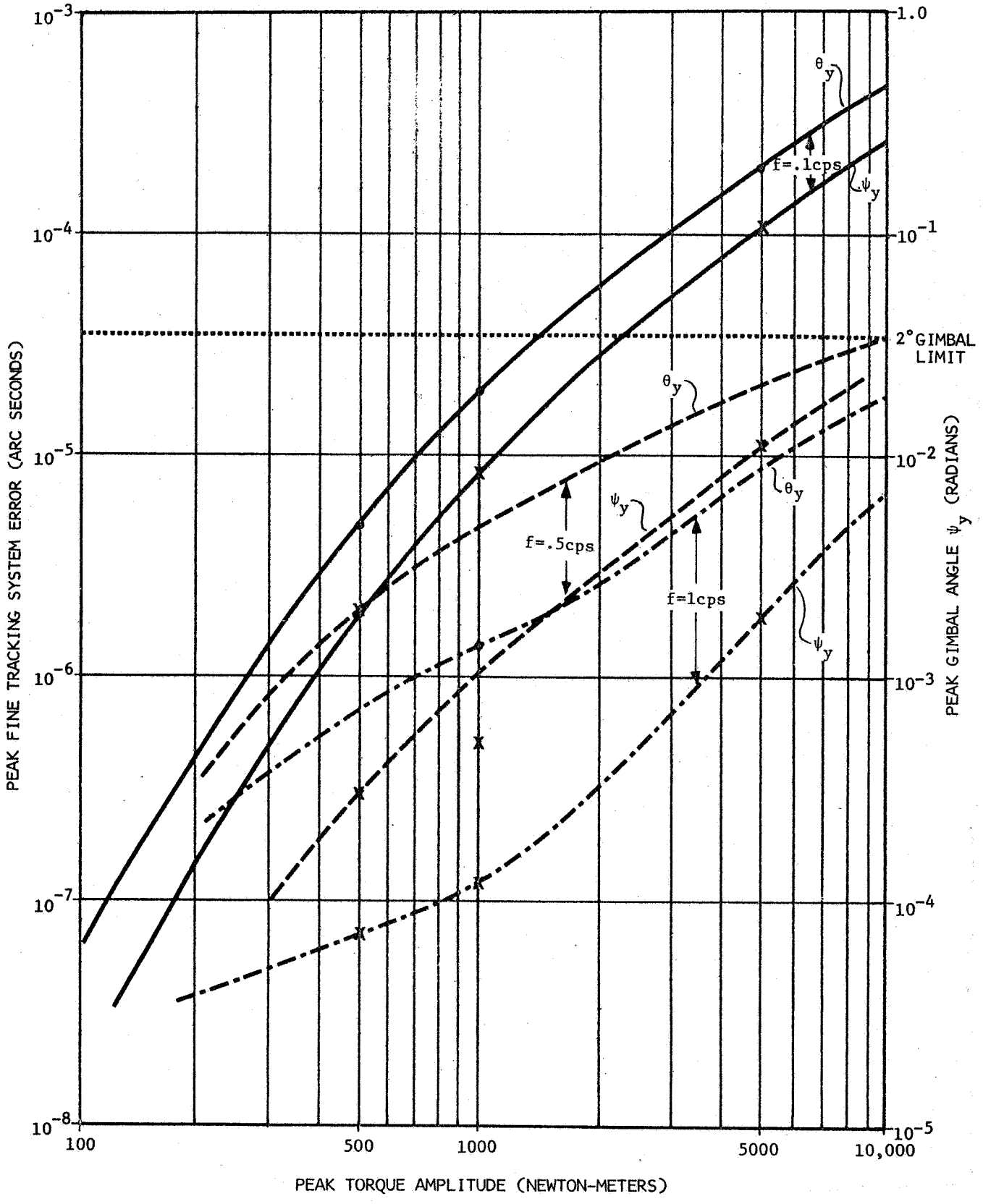

FIGURE 3.3-13 DISTURBANCE TORQUE ANALYSIS

$$T = ASIN(2\pi ft), \qquad (3.3\text{-}3)$$

for the first 10 seconds of the simulation, then removed to allow the system to recover over the last 10 seconds. (It is suggested in the future this exercise be repeated with the disturbance torque applied for the same number of cycles at each frequency.)

To illustrate the system response under the input just discussed, consider the θ_y curve for f = .1 cps on Figure 3.3-13. This curve represents the maximum fine tracking system error observed over the 20 second real time interval for a disturbance torque at frequency f = .1 cps, where the peak amplitude (A in Equation 3.3-3) was allowed to take on values from 100 nm to 10^4 nm. A new run was made for each peak amplitude shown in this range. The ψ_y curve illustrates the y gimbal angle for the same disturbance input.

It may be observed that the tracking system error (θ_y) remained small throughout the range of torque amplitudes. However, it is seen that the gimbal angle reached its maximum of 2° when the torque amplitude was approximately 2500 nm. When this happens the telescope will be turned with the spacecraft and the line-of-sight lost from the field of view of the telescope. As presently modeled in the LASIM program, the gimbal is not limited to a $\pm 2°$ range. Thus, both curves must be observed to determine the effect of the disturbance input.

The other curves in Figure 3.3-13 illustrate the same quantities as above but for disturbance frequencies of .5 cps and 1 cps. It can be seen that the effects are less pronounced at the higher frequencies.

The original purpose in performing the exercise leading to the data shown in Figure 3.3-13 was to establish some threshold values for disturbance torques, above which the tracking systems could not maintain the .1 arc second tracking accuracy. However, rather than providing meaningful values for thresholds, the results obtained raise several questions concerning the manner in which the combined tracking systems operate. For example, it is not altogether clear why the lower frequencies of excitation produce larger tracking errors than the higher frequencies at the same amplitude of disturbance torque. It was found that after several cycles of disturbance input at the large magnitudes (for the case of f = 1 cps), the control torque provided by the CMG system gradually moved in phase with the disturbance torque. The manner in which the position error signal for the CMG control system is related to the spacecraft dynamics and the telescope control system operation is not adequately explained by the single axis diagrams illustrating the hardware coupling.

In summary, results from the exercise described in this paragraph raise some questions concerning the stability of the combined telescope-spacecraft control system combination and point to a continuation of these analyses with the LASIM program to better understand the dynamical coupling involved.

3.4 FUTURE INVESTIGATIONS

The LASIM program as developed constitutes a flexible tool which can be used to investigate various aspects of the LCSE tracking and pointing systems' performance. The program constitutes the very necessary "nominal system" model, from which the effects of innumerable non-nominal conditions and influences may be determined. However, the program, of itself, is no panacea for accomplishing performance analysis. In all cases where particular investigations, not addressed already, are desired, adequate mathematical description of the related external phenomena must be made and incorporated into the program.

The following paragraphs present some illustrative examples of investigations which are relevant to the success of the LCSE mission and which can be made by using the present LASIM program with suitable modifications.

3.4.1 Noise Effects

Because of the extremely accurate operation required of the combined LCSE tracking and pointing systems, low level noise generated within the hardware components and noise resulting from laser beam scintillation and refraction will assume significant importance in determining minimum system error. As shown by the results of Paragraph 3.3, system parameters can be selected such that adequate operation results in the nominal case. Indeed, noise effects along with component non-linearities, such as hysteris in the flexure pivots and possibly the transfer lens motor, will set the minimum errors. These effects are not modeled in the present LASIM simulation.

The following enumerates some of the noise sources or noise-like effects which can be modeled within the LASIM program, once adequate definition of the effects themselves has been accomplished.

1. Photon noise within the photomultiplier detectors -

   Reasonable statistical description of this noise is available.

2. Detector signal noise resulting from beacon intensity scintillation by the earth's atmosphere -

   Comprehensive statistical description of this noise is not readily available but sufficient description may be

deduced from works of Fried, Tatarski and others to allow some analysis.

3. Detector signal fluctuations produced by dynamic refraction of the uplink beacon -

Comprehensive statistical description of this effect is not readily available.

4. Detector noise produced by extraneous objects within the telescope field-of-view -

Analysis of the extent of this occurrence must first be made, then description of the resulting noise formulated. This item includes such things as particle reflectance of sunlight, earthshine, etc; the particles in question being foreign matter ejected from the spacecraft and drifting in the vicinity of the telescope aperture.

5. Gyro noise -

General statistical descriptions of most types of noise associated with rate gyro operation are available.

6. Quantization noise -

In all probability the gimbal resolver output and the lead compensation for the spacecraft control system will be processed in a digital computer within the ATM rack itself. Because of the finite word length operation of the computer and the D→A and A→D conversions attendant to the digital processing, certain random components and quantization noise will be introduced into the spacecraft control system. No quantitative description of these effects for the specific hardware to be used is available at present.

7. Tracking Data Inexactness -

Determination of spacecraft position, the true line-of-sight and the line-of-sight rate in the pointing control ground computations introduce errors in formulating the point-ahead commands. Statistical description of these errors should be obtainable, from which analysis of the resulting pointing errors may be made.

In summary, the effect on laser pointing and tracking produced by noise introduced at various places in the system is a critical factor affecting the success of the LCSE mission. Several of the obvious noise sources have been enumerated, the effects of which should be considered. The LASIM program may be used, with suitable additions, to investigate the effects of the noise sources discussed.

3.4.2 Disturbance Torques

Very little information has been made available to describe the disturbance torques arising from astronaut motion in the LM/CSM/ATM spacecraft. For the one disturbance profile used as a test input (Paragraph 3.3), the tracking system performed within the desired limits. It should be pointed out, however, that the profile used considered only an astronaut raising and lowering his arm in the LM. More energetic movements by the astronauts will produce more severe disturbance torques which will tax the capability of the tracking system.

A comprehensive determination of the torques produced by typical astronaut movements should be obtained. These disturbance torques may be input to the LASIM program and the resulting tracking performance determined. This may be done with very minor program modification.

3.4.3 Structural Dynamics Effects

An extremely important area of investigation, which is not modeled in the present LASIM program and which effects the pointing and tracking performance of the LCSE, is the structural dynamics of the telescope-spar structure and the LM/CSM/ATM spacecraft. Vibratory motion through elastic deformation of the spacecraft and telescope-spar structure affects both control system stability, and pointing and tracking of the laser telescope. Propagation of higher frequency excitations, arising from system noise or astronaut motion, is not completely predicted from the rigid-body model incorporated in the present LASIM program. Consideration of the propagation of disturbances and, in fact, nominal system response should include the contribution of structural dynamics.

A detailed closed-loop simulation of the structural dynamics model of the spacecraft and telescope-spar structures, included with the present model of the control systems, is an extremely complicated simulation problem. This type simulation essentially constitutes a closed loop, elastic body simulation of a multi-part satellite. It would be virtually impossible to construct such a simulation which would not require excessive amounts of computer time to analyze the small scale effects required for the LCSE.

A more realistic approach to consideration of the structural dynamics effects is to consider the natural, structural vibratory motion as a perturbation input to the rigid body model containing the sensor devices and predict the resulting disturbance. This approach assumes that by some means the natural modes and frequencies of structural deformation may be obtained.

The analysis approach envisioned consists of reflecting spacecraft vibration to the experiment package gimbals. This will produce oscillatory motion of the gimbals which will serve as a disturbance input to the coarse and fine control systems. In addition, a structural dynamics analysis of the telescope secondary mirror supports may be undertaken to determine the image motion resulting from vibration of the mirror in response to telescope-spar structure motion.

In summary, structural dynamics effects will impact operation of pointing and tracking of the LCSE. More data on the vehicle and spar elastic deformation characteristics are required in order to formulate a specific approach to detailed analysis and simulation of these effects.

4.0 REFERENCES

1. W. B. Chubb, D. N. Schultz, and S. M. Seltzer, "Attitude Control and Precision Pointing of the Apollo Telescope Mount," AIAA paper number 67-534 presented at the AIAA Guidance, Control, and Flight Dynamics Conference, August, 1967.

2. B. J. O'Conner and L. A. Morine, "The Description of the CMG and Its Application to Space Vehicle Control," AIAA paper number 67-589, presented at the AIAA Guidance, Control, and Flight Dynamics Conference, August, 1967.

3. "Conceptual Design and Analysis of Control System for Apollo Telescope Mount," Lockheed Missiles and Space Company report number LMSC-A842157, March 17, 1967.

4. "Single Axis Hard Mounted ATM Control System Study," Martin-Marietta Corporation report number ED-2002-80, April 6, 1967.

5. "Single Axis Gimbaled ATM Control System Study," Martin-Marietta Corporation report number ED-2002-81, April 6, 1967.

6. "Preliminary Mission Analysis for an Early Synchronous Earth Orbital Mission," MSFC presentation notes, December 15, 1966.

7. Robert E. Roberson, "Attitude Control of Satellites and Space Vehicles," Advances in Space Science, ed. F. I. Ordway, Vol. 2, Academic Press, Inc., New York, 1960.

8. Malcom J. Abzug, "Active Satellite Attitude Control," Guidance and Control of Aerospace Vehicles, ed. C. T. Leondes, McGraw-Hill Book Company, New York, 1963.

9. Robert E. Roberson, "Alternate Form of a Result by Nidley," American Rocket Society Journal, 31 (1961), 1292-1292.

10. W. D. Fryer and W. C. Schultz, "A Survey of Methods for Digital Simulation of Control Systems," Cornell Aeronautical Laboratory Report No. XA-1681-E-1, July, 1964.

11. R. Boxer and S. Thaler, "A Simplified Method of Solving Linear and Non-Linear Systems," Proceedings of the I.R.E., Vol. 44, No. 1, January, 1956, pp. 89-101.

12. C. Heizman, J. Millman and A. Vigants, "Comparison of the X-Transform Method with Other Numerical Methods" Columbia University Electronics Research Laboratories Technical Report No. T-8/c, 4 September 1956. Prepared under Contract DA 30-069-ORD-1725, for Department of Army Ordnance Corps, Redstone Arsenal, Huntsvilla, Alabama.

13. D. C. Baxter and R. Gagne', "Digital Simulation Using Approximate Methods," National Research Council, Division of Mechanical Engineering, Ottawa, Canada, Report No. MK-15, July, 1965.

14. A. Tustin, "A Method of Analyzing the Behavior of Linear Systems in Terms of Time Series," Journal I.E.E. (Proceedings of the Convention on Automatic Regulators and Servomechanisms), Vol. 94, Part II-A, May, 1947.